



Kent Academic Repository

Deimantaviciute, Gintare (2022) *Producing intracellular and extracellular lipid vesicles in E. coli for vaccine development*. Doctor of Philosophy (PhD) thesis, University of Kent,.

Downloaded from

<https://kar.kent.ac.uk/93714/> The University of Kent's Academic Repository KAR

The version of record is available from

<https://doi.org/10.22024/UniKent/01.02.93714>

This document version

UNSPECIFIED

DOI for this version

Licence for this version

CC BY (Attribution)

Additional information

Versions of research works

Versions of Record

If this version is the version of record, it is the same as the published version available on the publisher's web site. Cite as the published version.

Author Accepted Manuscripts

If this document is identified as the Author Accepted Manuscript it is the version after peer review but before type setting, copy editing or publisher branding. Cite as Surname, Initial. (Year) 'Title of article'. To be published in **Title of Journal**, Volume and issue numbers [peer-reviewed accepted version]. Available at: DOI or URL (Accessed: date).

Enquiries

If you have questions about this document contact ResearchSupport@kent.ac.uk. Please include the URL of the record in KAR. If you believe that your, or a third party's rights have been compromised through this document please see our [Take Down policy](https://www.kent.ac.uk/guides/kar-the-kent-academic-repository#policies) (available from <https://www.kent.ac.uk/guides/kar-the-kent-academic-repository#policies>).



**Producing intracellular and extracellular lipid vesicles in
E. coli for vaccine development**

**A PhD Thesis for the Degree of
Doctor of Philosophy
in
Biochemistry**

**Faculty of Sciences, School of Biosciences
University of Kent**

Gintare Deimantaviciute

2021

Declaration

No part of this thesis has been submitted in support of an application for any degree or other qualification to the University of Kent, or any other University in the Institution of learning.

Name: Gintare Deimantaviciute

Date: 08.06.2021

Abstract

Membrane-bound structures such as intracellular compartments and extracellular vesicles appear to play important roles in bacterial biochemistry and survival. Whilst bacterial extracellular vesicles (BEVs) are naturally secreted, intracellular vesicle formation in bacteria has only been observed following the overproduction of some membrane proteins. The proteins of the LemA family have previously been shown to have membrane restructuring capabilities when recombinantly expressed in *Escherichia coli*. Consequently, this project set out to investigate the potential of utilising LemA proteins together with protein engineering approaches to produce intracellular and extracellular vesicles in *E. coli*.

Initial studies focussed on two distinct LemA proteins from *Pseudomonas aeruginosa* (Pa) LemA1 and LemA2, which were predicted to be targeted to the inner and the outer membranes, respectively. Transmission electron microscopy (TEM) analysis revealed the formation of intracellular membrane vesicles in both samples, while scanning electron microscopy (SEM) studies showed increased outer membrane vesiculation in the cells overexpressing *PaLemA2*; findings that were consistent with the predicted localisation of these proteins. Moreover, the purification and structural studies of PaLemA1 provided a solid basis for future structural work on this protein.

The construction and overproduction of the transmembrane and soluble domains of MamQ, LemA.153, LemA.159, LemA.501 and PaLemA1 proteins individually resulted in inclusion body formation in the majority of samples. However, the expression of the transmembrane domain (TMD) of *PaLemA1* alone was sufficient to induce intracellular vesicle production. A 'mix-and-match' approach of the different TMDs and soluble domains further yielded a wide range of novel membranous phenotypes in *E. coli*.

Together, these results provide good evidence for the recombinant production of membranous compartments following LemA protein overproduction in *E. coli*. Furthermore, such membranous structures hold a lot of potential for targeted protein engineering approaches in the generation of a novel vaccine delivery platform.

Acknowledgements

I am extremely grateful to Professor Martin Warren and Professor Mark Smales for giving me the opportunity to work on this project and providing great guidance, support and encouragement throughout the years. I would also like to thank Gary Rogerson for funding my PhD and for always taking an interest in my progress.

I have been exceptionally lucky to be able to work with such a wide range of individuals who have all shaped me into the scientist I am today. I would like to thank Dr Rokas Juodeikis (aka Rokky) for imparting perhaps a small fraction of his wisdom onto me and for guiding me during the infancy of my PhD, your help has been invaluable.

To Ian Brown, thank you for taking your time to train me in all aspects of electron microscopy, putting up with my Disney playlist and for always giving great advice. Your love for science has truly been inspiring and I can only hope I feel the same way in 35 years!

I want to thank Dr James Budge who provided his time, help and support during my work on CHO cells and the rest of the Smales lab for being accommodating and helpful. To Dr Matt Lee, thank you for introducing me to the confocal microscopy world and for sending all the puppy photos.

I would like to thank Dr Jose Ortega-Roldan for dedicating his time and effort in helping me with the structural work of my project. I would also like to thank Dr Jose Borrero de Acuna and Dr Gabriella Molinari for being accommodating and helpful during my fellowship in Germany and for sharing the enthusiasm for this project.

To the current and past Warren lab members, thank you all for creating an enjoyable work environment and all the support and advice that you have provided during my PhD, my experience would have not been the same without you!

I would like also to give my thanks to Jake, your friendship and support has got me through the challenging times of this PhD. Finally, I would like to thank my family, in particular my mother Ale, without whom I would not be where I am today, you have always pushed me to do my best. To James and Lina, thank you for always taking an interest in what I do and for your support!

Table of Contents

Declaration	2
Abstract	3
Acknowledgements	4
Table of Contents	5
List of Figures	9
List of Tables	12
List of Abbreviations	13
Chapter 1	15
1. Introduction	16
1.1 Cell envelope composition of Gram-negative bacteria	17
1.1.1 Outer membrane	18
1.1.2 Periplasm.....	24
1.1.3 Inner membrane	26
1.1.4 The biophysical properties of <i>E. coli</i> membranes	29
1.2 Introduction of prokaryotic organelles	30
1.2.1 Protein-bounded organelles	31
1.2.2 Lipid-bounded organelles	33
1.2.3 Membrane remodelling proteins.....	37
1.2.4 Overexpression of membrane proteins alters bacterial ultrastructure.....	41
1.3 Vaccines	45
1.3.1 Vaccines play an important role in public health.....	45
1.3.2 Vaccine discovery and development	46
1.3.3 Types of vaccines	47
1.3.4 The current threat to public health – SARS-CoV-2.....	50
1.3.5 Membrane vesicle-derived vaccines.....	53
1.4 Aims of the project.....	57
Chapter 2:	59
2.1 Chemicals	60
2.2 Bacterial strains.....	62
2.3 Plasmids	62
2.4 Primers	69
2.5 Media and solutions for bacterial work	70
2.5.1 Sterilisation	70
2.5.1.2 Autoclaving	70
2.5.2 Antibiotics	70

2.5.3 Growth media	70
2.5.4 Media and solutions for protein work	72
2.6 Microbiological methods	75
2.6.1 Plate cultures	75
2.6.2 LB liquid cultures.....	75
2.6.3 Preparation of competent cells	75
2.6.4 Transformation of competent cells	75
2.6.5 Production of recombinant proteins	75
2.6.6 Generation of TEV protease.....	76
2.7 Molecular biology	76
2.7.1 Gene synthesis	76
2.7.2 Polymerase Chain Reaction (PCR).....	76
2.7.3 Plasmid purification	77
2.7.4 Restriction digests.....	77
2.7.5 Ligations	77
2.7.6 DNA electrophoresis	78
2.7.7 Extraction from DNA gels.....	78
2.7.8 DNA sequencing.....	78
2.8 Membrane protein purification, NMR and crystallisation.....	78
2.8.1 Production of ¹⁵ N labelled protein.....	78
2.8.2 Protein solubilisation	79
2.8.3 Purification of membrane proteins using IMAC	79
2.8.4 C-terminal tag cleavage	79
2.8.5 SDS-PAGE	80
2.8.6 Size exclusion chromatography	80
2.8.7 A ₂₈₀ protein concentration estimation	80
2.8.8 Nuclear magnetic resonance (NMR).....	80
2.8.9 Lipidic cubic phase (LCP) crystallography	80
2.9 Confocal microscopy	81
2.9.1 Sample preparation	81
2.9.2 Immunofluorescence staining.....	81
2.10 Electron microscopy.....	82
2.10.1 Preparation of whole cells	82
2.10.2 Fixing and embedding bacteria in resin	82
2.10.3 Ultra-thin sectioning and staining of embedded samples.....	82
2.10.4 Visualisation of samples.....	83
2.11 Field Emission Scanning Electron Microscopy	83

2.12 Mammalian cell experiments.....	83
2.12.1 Generating <i>PalemA1</i> harbouring pcDNA3.1/V5-His-TOPO vector	83
2.12.2 Routine cell culture of Chinese Hamster Ovary-S (CHO-S) cells	84
2.12.3 Transient transfection of CHO-S cells	84
2.12.4 Generation of stable CHO-S cell lines	85
2.12.5 Immunofluorescence analysis.....	85
2.12.6 Western blot	86
2.12.7 Fixing and embedding CHO-S cells in LV resin	86
2.12.8 Embedding cells in LR white resin for immunolabelling.....	87
2.12.9 Immunolabelling of LR white resin embedded samples.....	87
Chapter 3	89
3.1 Introduction	90
3.2 Results.....	92
3.2.1 Expression of <i>PalemA1</i> and <i>PalemA2</i> in <i>E. coli</i>	92
3.3. Discussion.....	130
Chapter 4	134
4.1 Introduction	135
4.2 Results.....	137
4.2.1 Expression and SDS-PAGE analysis of individual LemA proteins	137
4.2.2 Expressing the transmembrane and the soluble domains of LemA proteins individually	142
4.2.3 Generation and expression of LemA hybrid protein.....	149
4.3 Discussion.....	161
Chapter 5	166
Structural investigations into the <i>Pseudomonas aeruginosa</i> PA14 PaLemA1 protein	166
5.1 Introduction	167
5.2 Results.....	169
5.2.1 Cloning of PaLemA1 with a polyhistidine tag	169
5.2.2 Electron microscopy analysis of PaLemA1 with a polyhistidine tag	169
5.2.3 Initial PaLemA1 purification experiments.....	171
5.2.4 Generation and TEM analysis of PaLemA1-sfGFP fusion protein	180
5.2.5 Purification and crystallisation of PaLemA1 using a sfGFP fusion tag	182
5.2.6 Purification of ¹⁵ N-labelled PaLemA1-His protein for NMR analysis	186
5.2.7 Preliminary NMR analysis of ¹⁵ N-labelled PaLemA1-His protein	189
5.3 Discussion.....	191
Chapter 6	194
Discussion	194

6.1 Discussion.....	195
References	203
Supplementary data	220

List of Figures

Figure 1.1. Depiction of the cell envelope of Gram-negative bacteria.....	17
Figure 1.2. Outer membrane protein assembly pathway in <i>E. coli</i>	21
Figure 1.3 Lipoprotein maturation and translocation pathway.	24
Figure 1.4. A schematic diagram representing the major pathways of protein trafficking in Gram-negative bacteria.	27
Figure 1.5. Electron micrographs of <i>Halothiobacillus neapolitanus</i> carboxysomes.	33
Figure 1.6. Transmission electron micrographs of <i>Pirellula marina</i> and <i>Pirellula staleyi</i> cells displaying the pirellosome.	34
Figure 1.7. Transmission electron micrographs of <i>Magnetospirillum gryphiswaldense</i> cells containing magnetosomes.....	36
Figure 1.8. Transmission electron micrographs of thin-sectioned <i>E. coli</i> cells producing LemA proteins from different organisms.....	41
Figure 1.9. Transmission electron micrographs of <i>E. coli</i> HB101 cells overproducing fumarate reductase.	43
Figure 1.10. Freeze fracture electron micrographs of <i>E. coli</i> BL21(DE3)/plysS cells.....	44
Figure 1.11. A flowchart presenting the traditional route to vaccine development.....	47
Figure 3.1. TEM of <i>E. coli</i> expressing PaLemA1 and PaLemA2.....	93
Figure 3.2. Scanning electron micrographs of recombinant <i>E. coli</i> cells expressing <i>PalemA1</i> and <i>PalemA2</i>	95
Figure 3.3. SDS-PAGE analysis of <i>E. coli</i> cells overexpressing <i>PalemA1</i> and <i>PalemA2</i>	96
Figure 3.4. Imaging of <i>E. coli</i> cells expressing PaLemA1- and PaLemA2-sfGFP fusion proteins.	98
Figure 3.5. TEM of <i>E. coli</i> expressing an empty pET3a vector control over a time-course of eight hours.	101
Figure 3.6. TEM of <i>E. coli</i> expressing <i>PalemA1</i> over a time-course of eight hours.....	102
Figure 3.7. TEM of <i>E. coli</i> expressing <i>PalemA2</i> over a time-course of eight hours.....	103
Figure 3.8. Average percentage of <i>E. coli</i> cells displaying a membranous phenotype following <i>PalemA1</i> and <i>PalemA2</i> expression over a time-course of 8 hours.....	104
Figure 3.9. The average number of intracellular vesicles found in <i>E. coli</i> cells expressing <i>PalemA1</i> over a time-course.	106
Figure 3.10. SDS-PAGE analysis of <i>E. coli</i> expressing an empty vector control, PaLemA1 and PaLemA2 over the time-course of 8 hours.	107
Figure 3.11. TEM of <i>E. coli</i> expressing genes of the <i>PalemA1</i> and <i>PalemA2</i> operons.....	110
Figure 3.12. SDS-PAGE analysis of <i>E. coli</i> cells producing proteins of the PaLemA1 and PaLemA2 operons.	111

Figure 3.13. TEM of <i>E. coli</i> expressing <i>PalemA2</i> operon proteins.	113
Figure 3.14. Immunostaining analysis of CHO-S transiently transfected cells with an empty vector control.....	116
Figure 3.15. Immunostaining analysis of CHO-S transiently transfected cells with the pcDNA3.1/V5-His-TOPO vector encoding PaLemA1.....	117
Figure 3.16. SDS-PAGE analysis of CHO-S cells transiently producing PaLemA1.....	118
Figure 3.17. Immunostaining analysis of CHO-S cells stably expressing the pcDNA3.1/V5-His-TOPO empty vector.....	120
Figure 3.18. Immunostaining analysis of CHO-S cells stably expressing the pcDNA3.1/V5-His-TOPO empty vector.....	121
Figure 3.19. Immunostaining analysis of CHO-S cells stably expressing the pcDNA3.1/V5-His-TOPO empty vector.....	122
Figure 3.20. Analysis of <i>PalemA1</i> expression in stably transfected CHO-S cells.	123
Figure 3.21. TEM of recombinant <i>E. coli</i> cells expressing <i>PalemA1-V5</i>	124
Figure 3.22. Electron micrographs of CHO-S cells transfected with the empty pcDNA3.1/V5-His-TOPO vector.....	125
Figure 3.23. Electron micrographs of CHO-S cells producing PaLemA1.	126
Figure 3.24. Analysis of CHO-S stable cells harbouring the pcDNA3.1/V5-His-TOPO vector using the anti-V5 primary antibody.....	128
Figure 3.25. Analysis of CHO-S stable cells expressing <i>PalemA1</i> using the anti-V5 primary antibody.	129
Figure 4.1. TEM of <i>E. coli</i> expressing an empty vector control or <i>MamQ</i>	139
Figure 4.2. TEM of <i>E. coli</i> expressing <i>LemA.153</i> or <i>LemA.159</i>	140
Figure 4.3. TEM of <i>E. coli</i> expressing <i>LemA.501</i> or <i>PaLemA1</i>	141
Figure 4.4. SDS-PAGE analysis of <i>E. coli</i> producing the chosen LemA proteins.....	142
Figure 4.5. TEM of <i>E. coli</i> expressing the transmembrane or the soluble domain of MamQ.....	144
Figure 4.6. TEM of <i>E. coli</i> expressing the soluble domain of LemA.153.	145
Figure 4.7. TEM of <i>E. coli</i> expressing the transmembrane or the soluble domain of LemA.159. ...	145
Figure 4.8. TEM of <i>E. coli</i> expressing the transmembrane or the soluble domain of LemA.501...	146
Figure 4.9. TEM of <i>E. coli</i> expressing the transmembrane or the soluble domain of PaLemA1.....	147
Figure 4.10. SDS-PAGE analysis of <i>E. coli</i> expressing the transmembrane domain or the soluble domain of either MamQ, LemA.153, LemA.159, LemA.501 or PaLemA1 proteins.	148
Figure 4.11. TEM of <i>E. coli</i> producing LemA hybrid proteins.....	153
Figure 4.12. TEM of <i>E. coli</i> producing LemA hybrid proteins.....	154
Figure 4.13. TEM of <i>E. coli</i> producing LemA hybrid proteins.....	155
Figure 4.14. TEM of <i>E. coli</i> producing LemA hybrid proteins.....	156

Figure 4.15. TEM of <i>E. coli</i> producing LemA hybrid proteins.....	157
Figure 4.16. TEM of <i>E. coli</i> producing LemA hybrid proteins.....	158
Figure 4.17. SDS-PAGE analysis of <i>E. coli</i> expressing the LemA hybrid proteins.	159
Figure 4.18. SDS-PAGE analysis of <i>E. coli</i> expressing the LemA hybrid proteins.	160
Figure 5.1. TEM of <i>E. coli</i> expressing an empty pET23b vector control and <i>PaLemA1</i>	170
Figure 5.2. SDS-PAGE analysis of <i>E. coli</i> overproducing PaLemA1-His tagged protein.....	172
Figure 5.3. SDS-PAGE analysis of the detergent purified PaLemA1-His tagged protein from <i>E. coli</i> cells initially grown at 28 °C.	175
Figure 5.4. SDS-PAGE analysis of the detergent purified PaLemA1-His tagged protein from <i>E. coli</i> cells initially grown at 37 °C.	176
Figure 5.5. SDS-PAGE analysis of the detergent purified PaLemA1-His protein from <i>E. coli</i> cells..	178
Figure 5.6. SDS-PAGE analysis of the detergent purified PaLemA1-His tagged protein from <i>E. coli</i> cells.	179
Figure 5.7. TEM of <i>E. coli</i> expressing sfGFP and <i>PaLemA1-sfGFP constructs</i>	181
Figure 5.8. SDS-PAGE analysis of the detergent purified PaLemA1-sfGFP fusion protein from <i>E. coli</i> cells.	183
Figure 5.9. SDS-PAGE analysis of the TEV protease cleaved PaLemA1-sfGFP protein and the resulting size exclusion chromatography fractions.	184
Figure 5.10. PaLemA1 protein crystals formed during LCP crystallisation screening.	185
Figure 5.11. SDS-PAGE analysis of the detergent purified PaLemA1-His protein from <i>E. coli</i> cells for NMR analysis.....	186
Figure 5.12. SDS-PAGE analysis of the eluted fractions from the purification of PaLemA1-His protein from <i>E. coli</i> cells.	187
Figure 5.13. SDS-PAGE analysis of the PaLemA1-His protein size exclusion fractions.	188
Figure 5.14. ¹⁵ N/ ¹ H SOFAST-HSQC spectrum of PaLemA1-His protein at 25 °C.....	189
Figure 5.15. ¹⁵ N/ ¹ H BEST-TROSY-HSQC spectrum of PaLemA1-His protein at 40 °C.....	190

List of Tables

Table 3.1. <i>Pseudomonas aeruginosa</i> LemA proteins chosen for analysis.	94
Table 3.2. Analysis of PaLemA1 and PaLemA2 operon proteins of <i>Pseudomonas aeruginosa</i> PA14.....	108
Table 4.1. LemA proteins chosen for analysis.....	138
Table 4.2. Quantitative electron microscopy analysis of LemA hybrid proteins.	152

List of Abbreviations

ATP	Adenosine triphosphate
BEV	Bacterial extracellular vesicle
BMC	Bacterial microcompartment
CHO	Chinese hamster ovary
CL	Cardiolipin
DDM	n-dodecyl β -d-maltoside
DNA	Deoxyribonucleic acid
EDTA	Ethylenediaminetetraacetic acid
ICM	Intracytoplasmic membrane
IM	Inner membrane
IMAC	Immobilised metal affinity chromatography
IPTG	Isopropyl β - d-1-thiogalactopyranoside
LB	Luria broth
LCP	Lipidic cubic phase
LPS	Lipopolysaccharides
MAI	Magnetosome island
MALDI-TOF	Matrix-assisted laser desorption/ionisation-mass spectrometry
MM	Magnetosome membrane
MTB	Magnetotactic bacteria
MV	Membrane vesicle
NADPH	Nicotinamide adenine dinucleotide phosphate
NAG	N-acetylglucosamine

NAM	N-acetylmuramic acid
OM	Outer membrane
OMP	Outer membrane protein
PCR	Polymerase chain reaction
PE	Phosphatidylethanolamine
PG	Phosphatidylglycerol
PNAG	β -(1 \rightarrow 6)-linked poly-N-acetyl-D-glucosamine
RNA	Ribonucleic acid
SARS-CoV-2	Severe acute respiratory syndrome coronavirus 2
SDS-PAGE	Sodium dodecyl sulphate-polyacrylamide gel electrophoresis
SEM	Scanning electron microscopy
TEM	Transmission electron microscopy
TEV	Tobacco etch virus
TM	Transmembrane
TMD	Transmembrane domain
WHO	World Health Organisation

Chapter 1

Introduction

1. Introduction

Vaccines remain one of the most cost-effective healthcare interventions, greatly reducing the burden of infectious disease, disability, and death. However, current vaccine manufacturing approaches have high costs, which can translate into expensive vaccines that may be unaffordable for those in the developing world. Additionally, the traditional route to developing a novel vaccine candidate from concept to licensure can take between 10 and 15 years, making it hard to manage newly emerging pathogens (Han, 2015). Due to the growing threat of antibiotic resistance and the increased emergence of novel pathogens capable of causing global pandemics, there is a real need for the development of universal vaccine delivery platforms that are less capital-intensive and have shorter production times.

While initial vaccine manufacturing platforms utilised live-attenuated or inactivated pathogens, advances in synthetic biology and the development of reverse genetics systems revolutionised the vaccinology field (Nunes *et al.*, 2014). Recent efforts utilising genetic engineering approaches have yielded recombinant vaccines that allow the targeting of immune responses against a few protective antigens from the pathogen of interest (Price *et al.*, 2016). However, despite this success, developing such vaccines still takes at least 10 years.

When considering the current SARS-CoV2 pandemic, being able to produce an effective vaccine on a more rapid scale proved essential. The utilisation of DNA and RNA encoded antigens for the coronavirus-based vaccines became a success story, and while this vaccine delivery approach may be applied to a wide range of different pathogens, it also presents some drawbacks. The stringent cold-chain requirements may make it harder to deliver these vaccines to those in the less developed world, and the emerging side effects associated with the DNA-based vaccines are likely to result in their reevaluation for use in a non-emergency setting (Crommelin *et al.*, 2021; MHRA, 2021).

As a result, there remains a requirement for the development of more universal vaccine manufacturing platforms. One such option, could be bacterial extracellular vesicles (BEVs), which are naturally produced by Gram-negative and Gram-positive bacteria (Kim *et al.*, 2015). In recent years, with breakthroughs in synthetic biology, research into the therapeutic potential of BEVs has gained momentum. The exploitation of bacterial cell

factories for the production of intracellular and extracellular lipid vesicles will be discussed later.

1.1 Cell envelope composition of Gram-negative bacteria

To survive in unpredictable and often hostile environments, bacteria have evolved a complex multi-layered structure known as the cell envelope. In Gram-negative bacteria, the cell envelope consists of the outer membrane, inner membrane and the periplasm (**Figure 1.1**). The general function of the envelope is to act as a protective barrier, as well as the conduit through which the bacteria can communicate with the surrounding environment. It also plays a role in maintaining the structural integrity of the cell and helps facilitate the selective passage of nutrients from the external environment (Madigan *et al.*, 2008).

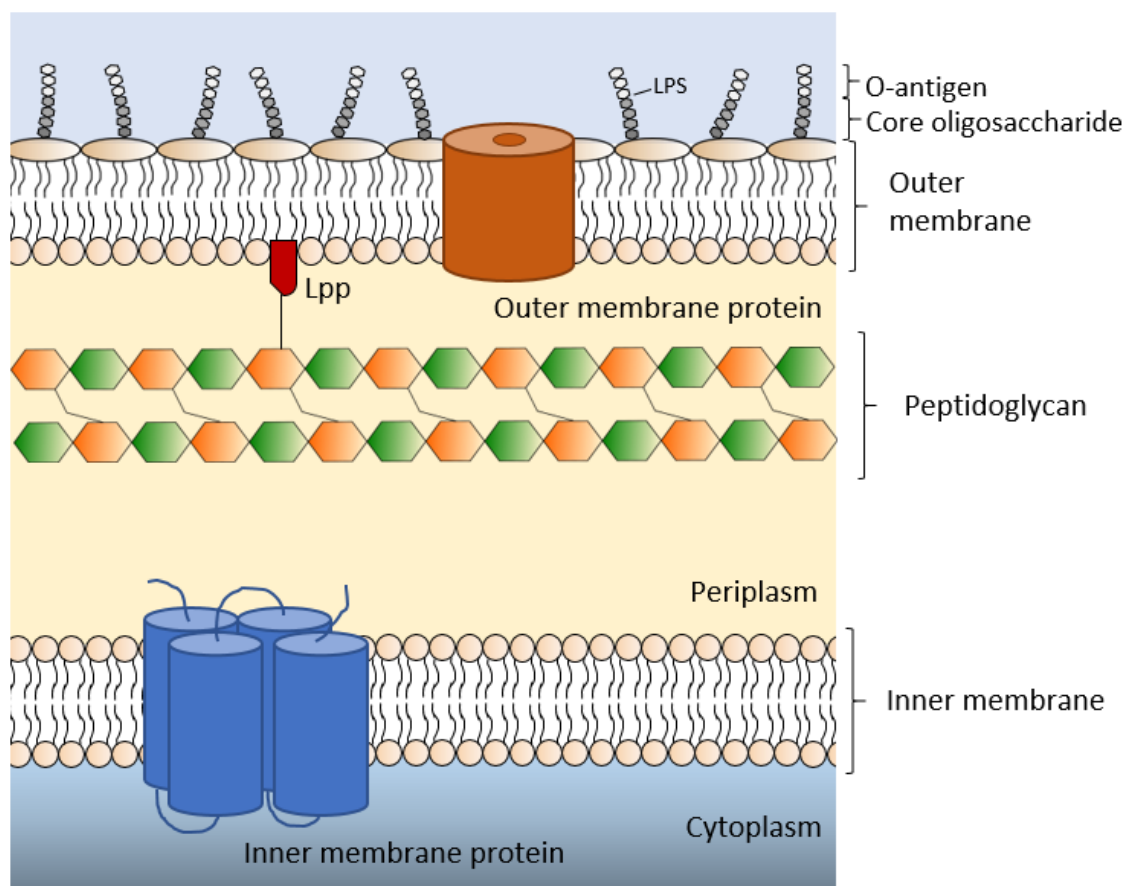


Figure 1.1. Depiction of the cell envelope of Gram-negative bacteria.

The cell envelope of Gram-negative bacteria consists of the outer and the inner lipid membranes which house a variety of membrane proteins. A thin layer of peptidoglycan is found in the periplasmic space, which is anchored to the inner leaflet of the outer membrane by Braun's lipoprotein (Lpp). The outer leaflet of the outer membrane contains lipopolysaccharides.

1.1.1 Outer membrane

The outer membrane (OM) serves as the protective barrier and is distinctly different in composition to the inner membrane. Its main constituents are lipoproteins and β -barrel proteins, and it can be divided into an inner and an outer leaflet. In *E. coli*, phospholipids, particularly phosphatidylethanolamine (PE), which constitutes about 75% of the total lipid content of the OM, phosphatidylglycerol (PG), and cardiolipin (CL), are only found in the inner leaflet (Raetz and Dowhan, 1990; Teissié and Zerbib, 2018). On the other hand, the outer leaflet contains glycolipids, principally lipopolysaccharide (LPS), which consists of lipid A, a core oligosaccharide, and an O-antigen polysaccharide.

1.1.1.1 Lipopolysaccharide

LPS is a unique structure to Gram-negative bacteria, present in the outer leaflet of the OM (**Figure 1.1**). It constitutes approximately 75% of the bacterial surface area and contributes to the structural properties of the cell envelope (Lerouge and Vanderleyden, 2002). The permeability barrier created by LPS prevents large hydrophobic and/or negatively charged molecules from entering the bacterial cell, making Gram-negative bacteria innately resistant to many antimicrobial compounds. LPS also plays a vital role in microbe-host interactions as it is a potent immuno-stimulatory molecule, known as endotoxin. It can modulate responses from the host immune system, and induce a pyrogenic response in mammalian hosts that can ultimately lead to endotoxic shock observed in septicaemia (Raetz and Whitfield, 2002).

1.1.1.2 O-antigen

The O-antigen is a polymer with a highly diverse structure. It provides antigenic specificity and is thus the main component used for serogroup designation in Gram-negative bacteria. In *E. coli*, there are more than 170 serogroups alone (Orskov and Orskov, 1992). It is composed of a varying number of repeating oligosaccharide units that are attached to the core oligosaccharide, and comprises the outermost region of the LPS molecule. Due to this, O-antigens play a key role in protecting the bacterium against cell lysis, as their long chains can prevent the antibody-mediated deposition of complement at the bacterial cell surface in host cells (Goebel *et al.*, 2008). Moreover, the antigenic specificity related to the O-antigen component in bacteria have made them a basis for vaccine development against several human pathogens (Levine *et al.*, 2007).

1.1.1.3 Core oligosaccharide

The core oligosaccharide region is a vital part of the LPS which attaches Lipid A to the O-antigen and is usually built of several different monosaccharides. It can be divided into the inner and outer core regions. The outer core region tends to be more variable and contains more common hexose sugars such as glucose, N-acetyl glucosamine N-acetyl galactosamine and galactose. Whereas, the inner core tends to be much more conserved and contain less common sugars such as heptose and 3-Deoxy-D-manno-oct-2-ulosonic acid (Heinrichs, Yethon and Whitfield, 1998). The core region of the LPS contains negatively charged groups such as anionic phosphate groups, which, through electrostatic interactions with divalent cations (Ca^{2+} and Mg^{2+}), help to stabilise the LPS molecules. It is the formation of these intermolecular cationic cross-links that contributes to the cell rigidity in Gram-negative bacteria (Clifton *et al.*, 2015).

1.1.1.4 Lipid A

The lipid A moiety is a highly hydrophobic region of the LPS and anchors the core oligosaccharide into the outer leaflet of the bacterial OM via electrostatic and hydrophobic interactions. It is a glucosamine-based saccharolipid, consisting of glucosamine units attached to acyl chains (Raetz *et al.*, 2009). This membrane-anchoring region of the LPS is responsible for much of the toxicity associated with Gram-negative bacteria. The lipid A component is a potent elicitor of the host immune system and has been shown to activate mammalian cells via the Toll-like receptor 4/MD-2 (TLR4/MD2) receptor complex (Molinaro *et al.*, 2015). The bioactivity of Lipid A seems to depend on its primary structure, with major contributing factors being the lengths of acyl chains and the phosphorylation status of the disaccharide backbone (Erridge, Bennett-Guerrero and Poxton, 2002).

1.1.1.5 Outer membrane proteins (OMPs)

OMPs can be lipid-linked or integral membrane proteins that are present on the OM of Gram-negative bacteria. The majority of integral OMPs follow a β -barrel conformation. These include porins, which are membrane-embedded proteins that form a hydrophilic channel and allow passive diffusion of solutes up to ~600 Da, across the OM, although porins that display a higher degree of selectivity for particular solutes have been reported (Benz *et al.*, 1986; Hardesty, Ferran and DiRienzo, 1991). Some OMPs have been shown to be expressed in high copy numbers, as is evidenced with OmpA, whose levels in *E. coli* can increase up to 10^6 copies per cell (Molloy *et al.*, 2000). OmpA acts as a porin with low

permeability for small hydrophilic solutes, where the size selective channel makes the OM less permeable, thereby contributing to resistance against environmental stress and antibiotics. Furthermore, its high abundance in *E. coli* could also perhaps be attributed to the probable role it plays in forming non-covalent interactions with the peptidoglycan polymer in the periplasm, thus stabilising the bacterial envelope further (Koebnik, 1995; Koebnik, Locher and Van Gelder, 2000).

1.1.1.6 β -barrel assembly machinery (BAM)

The OMs of Gram-negative bacteria contain integral membrane proteins, the majority of which possess a β -barrel conformation. These OMPs are synthesised in the cytoplasm with an N-terminal signal peptide, which targets these pre-proteins to the SecYEG translocon. This protein-conducting channel is located in the inner membrane, and translocates proteins that are in an unfolded state to the periplasm (Driessen and Nouwen, 2008). Nascent OMPs are prone to aggregation in an aqueous environment and as a result, require the help of chaperones for their transportation across the periplasm. Periplasmic chaperones, such as SurA, Skp and DegP, keep OMPs in a translocation-competent conformation until they reach the OM. Here, β -barrel proteins are integrated into the inner leaflet of the OM as a folded species by the β -barrel assembly machinery (BAM) (**Figure 1.2**) (Rizzitello, Harper and Silhavy, 2001).

In *E. coli* the BAM is a five-component complex, comprised of BamA, an essential intergral OMP, and four peripheral lipoprotein partner subunits: BamB, BamC, BamD and BamE. BamA together with BamD form a complex that is vital for the insertion of β -barrel proteins into the OM (**Figure 1.2**). Deletion of either proteins leads to stalling of OMP assembly and results in cell death. It is noteworthy that all components of the BAM have been shown to be necessary for efficient OMP folding and insertion, as genetic deletions of BamB/C/E, although non-lethal, result in noticeable defects in OMP biogenesis (Kim *et al.*, 2007; Sklar *et al.*, 2007; Hagan, Kim and Kahne, 2010).

In addition to the β -barrel domain, BamA contains an N-terminal region that extends into the periplasm and is comprised of 5 polypeptide translocation association (POTRA) domains (**Figure 1.2**). Although several functions have been ascribed to the POTRA domains, their exact roles are not well understood (Webb, Heinz and Lithgow, 2012; Heinz and Lithgow, 2014). Experimental evidence suggests that they have a chaperone-like function for the nascent OMPs and play an essential role in the docking of the accessory

Bam B/C/D/E lipoproteins, thus facilitating the formation of a functional BAM complex (Kim *et al.*, 2007). Despite the overall function of the BAM complex being well established, the mechanistic contribution of each individual component remains to be elucidated.

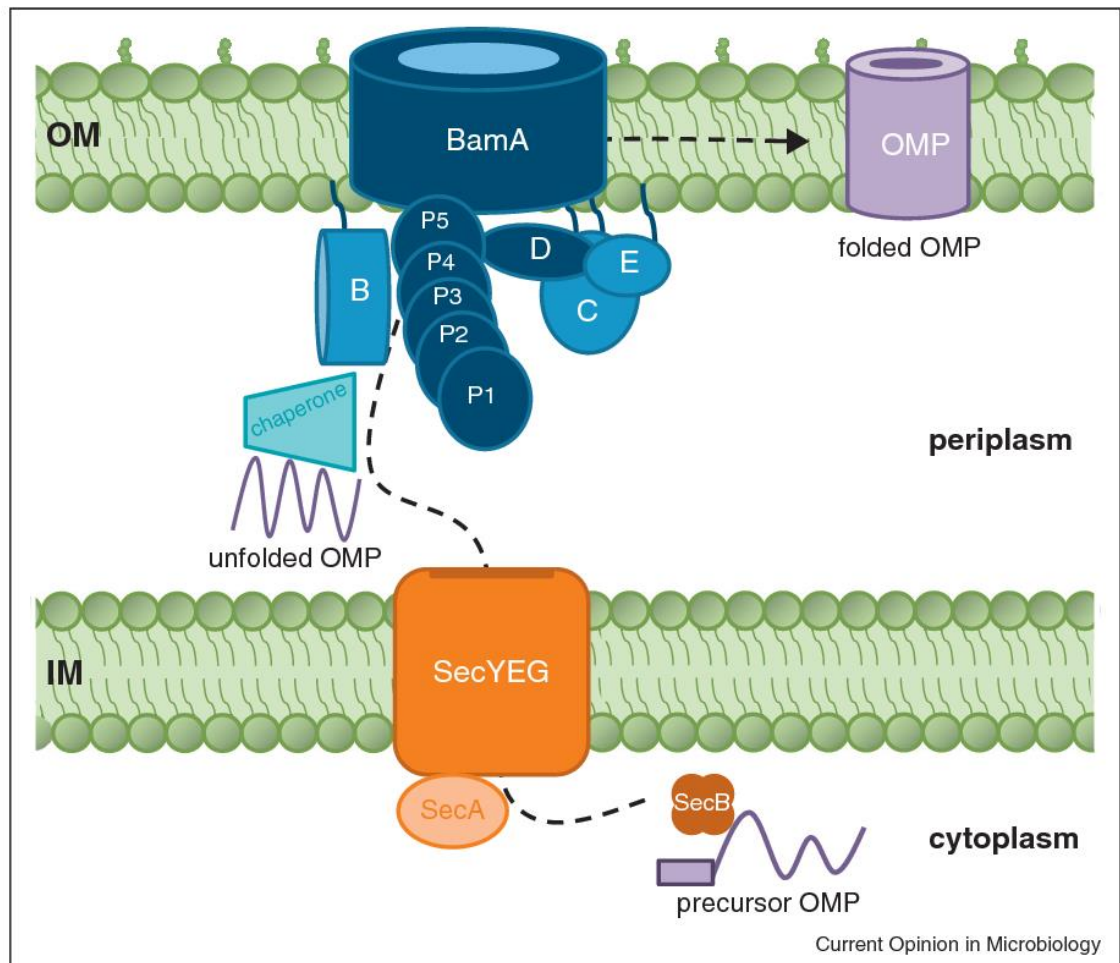


Figure 1.2. Outer membrane protein assembly pathway in *E. coli*.

Precursor outer membrane proteins (OMPs) are synthesised with an N-terminal signal peptide (represented by the purple rectangle), which is recognised by the SecB chaperone. SecB delivers pre-proteins in an unfolded state to SecA, which has the functional properties of an ATPase, facilitating pre-protein translocation across the SecYEG translocase. In the periplasm, the unfolded OMPs are carried by a chaperone to the multi-subunit β -barrel assembly complex where they are folded and inserted into the outer membrane. P1, P2, P3, P4 and P5 refer to the five POTRA domains found associated with the integral OMP BamA (from Rigel & Silhavy, 2012).

1.1.1.7 Lipoprotein (Lol) translocation pathway

Bacterial lipoproteins are proteins that are lipid-anchored to the IM or OM as a result of a series of post-translational modifications, and are important components of the Gram-negative cell envelope. In *E. coli*, lipoproteins are synthesised as prolipoproteins with an N-terminal signal sequence that harbours a characteristic consensus sequence [LVI][ASTVI][GAS]C, known as the lipobox. This directs prolipoprotein translocation across the Sec machinery, after which it undergoes processing and maturation before being transported to its intended target by the lipoprotein (Lol) translocation pathway. The protein components of the Lol pathway are found on the inner membrane, periplasm and the outer membrane (Von Heijne, 1989; Hayashi and Wu, 1990).

Following the translocation of the lipoprotein precursor, the maturation and processing steps take place on the outer leaflet of the IM. There, the conserved lipobox consensus motif is recognised by three lipoprotein-processing membrane-bound enzymes: Lgt, LspA and Lnt. Lgt is a phosphatidylglycerol-prolipoprotein diacylglyceryl transferase that adds a diacylglycerol to the sulfhydryl group of the conserved cysteine residue (Sankaran and Wu, 1994). This modification is required for the cleavage of the signal peptide from the prolipoprotein, which is carried out by LspA, a lipoprotein signal peptidase, creating a new N-terminus with the cysteine residue being at the +1 position (Tokunaga, Tokunaga and Wu, 1982; Dev and Ray, 1984). Lastly, the apolipoprotein N-acyltransferase (Lnt), modifies the amino group of the cysteine residue through N-acylation, thus generating a mature triacylated lipoprotein that remains anchored to the IM (**Figure 1.3**). Lipoproteins are then sorted according to the amino acid following the cysteine residue at position +2. Aspartate results in the retention of the lipoprotein in the IM, whereas most other amino acids lead to the trafficking of the lipoprotein to the OM (Yamaguchi, Yu and Inouye, 1988). If the OM is the intended target, the lipoproteins will be transported there by the Lol pathway and inserted into the inner leaflet (Inouye *et al.*, 1983).

In *E. coli* the Lol machinery is composed of five essential proteins, LolABCDE (Okuda and Tokuda, 2011). During the initial step of lipoprotein trafficking, a membrane-embedded LolCDE complex releases the lipoprotein into the periplasm in the form of a soluble complex with the chaperone LolA; this is an ATP-driven reaction (Heinrichs *et al.*, 1998; Matsuyama *et al.*, 1995; T. Yakushi *et al.*, 2000; Toshiharu Yakushi *et al.*, 1998). The highly hydrophobic acyl chains of the lipoprotein are shielded from the aqueous periplasm in the large

hydrophobic cavity of this chaperone. Next, LolA delivers the lipoprotein to the OM, where LolB, a lipoprotein insertion apparatus, resides (**Figure 1.3**). It contains a large hydrophobic cavity that has an even higher affinity for the acyl chains, in comparison to LolA. This facilitates a unidirectional transfer of the substrate (Matsuyama, Yokota and Tokuda, 1997; Takeda *et al.*, 2003). Lastly, LolB catalyses the insertion of the lipoprotein into the OM (Matsuyama, Yokota and Tokuda, 1997).

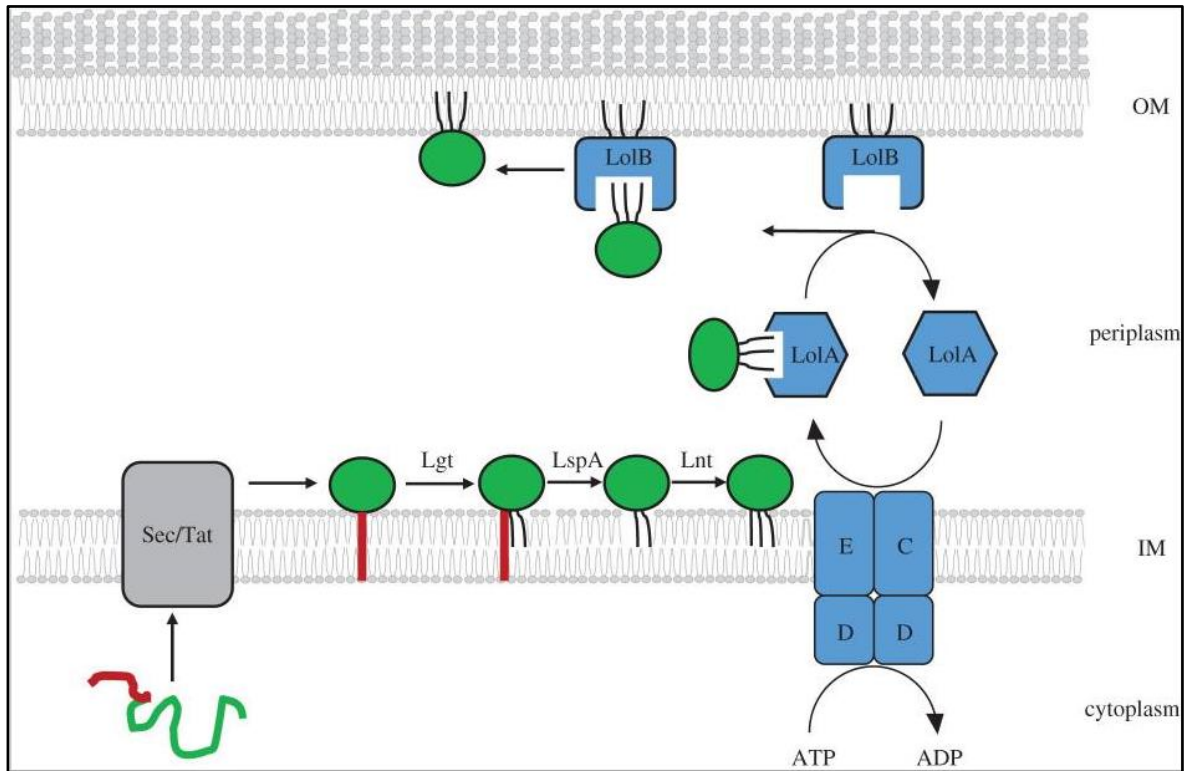


Figure 1.3 Lipoprotein maturation and translocation pathway.

Lipoproteins (green) are synthesised in the cytoplasm with an N-terminal signal peptide (red) which directs lipoprotein translocation across the Sec or Tat translocon. Following its translocation the prolipoprotein remains anchored to the inner membrane (IM) by the signal peptide where it undergoes maturation. This is carried out by the membrane bound enzymes: Lgt, LspA and Lnt. Firstly, Lgt adds a diacylglyceryl moiety to the Cys residue, then the single peptide is cleaved by LspA and lastly, Lnt adds another acyl chain to the newly formed N-terminus. Subsequently, the lipoprotein is recognised by the LolCDE complex which is found embedded in the inner membrane, which releases the lipoprotein into the periplasm in the form of a soluble complex with the periplasmic chaperone LolA. This process is ATP driven. LolA then delivers the lipoprotein to the outer membrane (OM), where LolB catalyses the insertion of the lipoprotein into the OM (image sourced from Konovalova & Silhavy, 2015).

1.1.2 Periplasm

The periplasm is located between the inner and outer membranes, and in *E. coli* can make up to 40% of the cell volume (Stock, Rauch and Roseman, 1977). It is a multipurpose compartment that is osmotically active and contains over 60 known proteins, providing the periplasm with the ability to carry out functions in protein transport, disulphide bond

formation, folding and quality control. Moreover, the periplasm plays a key role in cellular stability, as it contains a rigid peptidoglycan layer that is anchored to the OM via covalent interactions to the major membrane lipoprotein, and non-covalent links to porins (Liu, 2019).

The oxidising microenvironment of the periplasmic space facilitates disulphide bond formation in periplasmic and secretory proteins, a process that cannot take place in the more reducing location of the cytoplasm. However, the periplasm lacks any known source of energy-providing molecules, for instance, NADPH and ATP, which in itself creates a unique and challenging environment for protein folding and stabilisation. To overcome these difficulties, organisms such as *E. coli* utilise a number of general and specialised chaperones (Allen, Phan and Waksman, 2009).

1.1.2.1 Peptidoglycan

A peptidoglycan monomer is composed of sugars and amino acids. In particular, it consists of two joined amino sugars, N-acetylglucosamine (NAG) and N-acetylmuramic acid (NAM), and a peptide chain of three to five amino acids attached to NAM. These monomers are linked via glycosidic bonds into growing chains of peptidoglycan, which can join to one another by means of peptide cross-links between the peptides attached to the NAMs (**Figure 1.1**). Cross-linking the chains of sugars in this manner provides tremendous rigidity to the cell, enabling it to function similarly to a molecular chain link fence (Silhavy, Kahne and Walker, 2010; Que and Moreillon, 2014).

Although the primary function of the peptidoglycan is to preserve cell integrity by withstanding mechanical and osmotic stresses, it also acts as a scaffold for anchoring other cell envelope components. In *E. coli*, the OM and the peptidoglycan are covalently-linked by the Braun's lipoprotein (Ipp) and, together with OmpA, maintain cellular rigidity (Braun and Rehn, 1969; Koebnik, Locher and Van Gelder, 2000).

1.1.2.2 Periplasmic chaperones

Molecular chaperones play a crucial role in maintaining cellular homeostasis through their interactions with unfolded or partially folded proteins. They can aid in protein folding, assembly and stabilisation, with some chaperones also having proteolytic activity, thus allowing the degradation of irretrievably mis-folded proteins. Periplasmic chaperones can be broadly separated into two basic functions, carrier chaperones and folding chaperones.

However, a certain amount of functional overlap between the two does occur. Due to the lack of energy equivalents in the periplasm, it is thought that these chaperones are able to obtain energy from substrate binding and utilise it for transportation or specific reactivity.

1.1.3 Inner membrane

The inner membrane (IM) is a dynamic substructure that surrounds the cytoplasm, segregating it from the remainder of the bacterial cell. Unlike the OM, the IM has a lipid bilayer that is composed of phospholipids, lipoproteins and integral transmembrane (TM) proteins, with the latter possessing an α -helical conformation. Similarly to the inner leaflet of the OM, the IM of *E. coli* contains three main phospholipids: PE, PG and CL, with PE constituting approximately 50% of the total IM phospholipid content (Langley, Hawrot and Kennedy, 1982).

The IM harbours a wide diversity of proteins, and in *E. coli* more than 650 different integral proteins associated with the IM have been discovered, though computational approaches suggest there may be well over a 1000 (Bernsel and Daley, 2009; Díaz-Mejía, Babu and Emili, 2009). They play vital roles in cellular processes such as trafficking of ions, molecules and macromolecules; environmental sensing; synthesis of lipids, polysaccharides, and peptidoglycan; cell division; and metabolism (Papanastasiou *et al.*, 2013).

1.1.3.1 Protein trafficking in Gram-negative bacteria

All proteins in *E. coli* are synthesised in the cytoplasm, but they may need to travel across the IM to reach their final destinations. Some proteins may be destined for the periplasm, OM or secretion out of the cell. In order to accurately and efficiently move proteins from one location to another, bacteria have evolved a number of different translocation pathways to achieve this.

There are two major secretory pathways in bacteria that transport proteins across the inner membrane (IM): the general secretory (Sec) pathway (previously mentioned in **Section 1.1.1.6**) and the twin-arginine translocation (Tat) pathway (**Figure 1.4**). In bacteria, the vast majority of extracytoplasmic proteins are transported across the IM by the Sec apparatus (Lycklama A Nijeholt and Driessen, 2012).

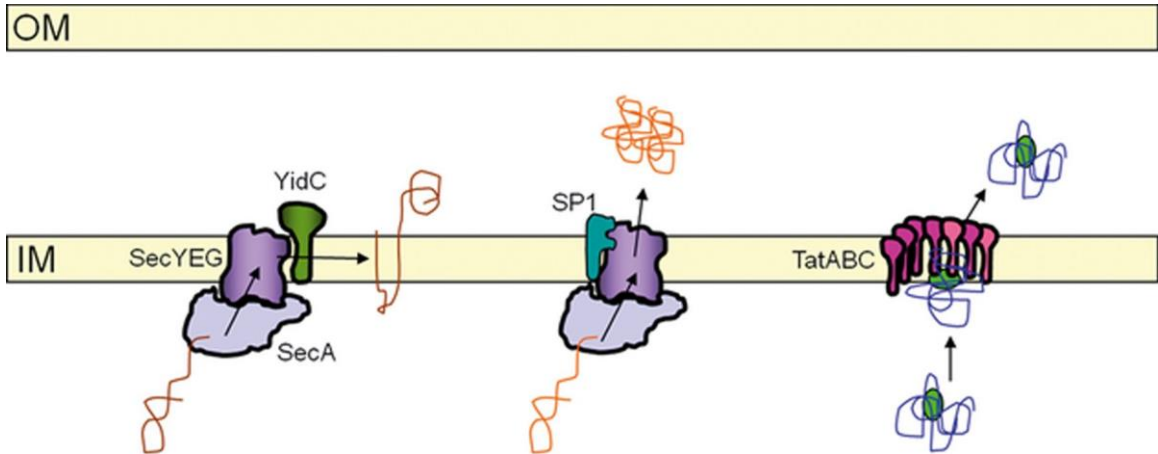


Figure 1.4. A schematic diagram representing the major pathways of protein trafficking in Gram-negative bacteria.

The SecYEG translocase (purple) plays a central role in exporting unfolded proteins across the inner membrane (IM) to the periplasmic space, while TatABC complex (pink) translocates folded proteins. **1.** Unfolded proteins destined for integration into the IM are translocated across the SecYEG translocase with the help of SecA (light blue), which functions as an ATP driven molecular motor. During this process, YidC (green) ushers the transmembrane helices of the protein through a lateral gate of SecY into the IM, where the protein remains attached. **2.** Unfolded proteins destined for translocation into the periplasm are transported across the IM through the SecYEG channel with the help of SecA, where upon translocation they are folded by periplasmic chaperones. **3.** The TatABC complex contains an oligomeric pore through which folded substrates can be translocated across (from (Dalbey and Kuhn, 2012)).

1.1.3.2 The Sec translocon

The Sec pathway primarily catalyses the translocation of unfolded proteins across the IM, but it is also known to play a role in the integration of some membrane proteins into the IM. Secretory proteins are commonly referred to as pre-proteins since they possess a cleavable N-terminal signal peptide (Rusch & Kendall, 2007). The signal peptide usually consists of 17-24 residues and contains a positively charged N-terminal region, a hydrophobic core of 8-12 amino acids followed by a short polar C-terminal region with a cleavage site (Kipping et al., 2003). The role of these 'address tags' is to sort secretory proteins from cytoplasmic proteins. Proteins intended for secretion into the periplasm or out of the cell have a SecB specific signal sequence, whilst those destined to be embedded

into the IM have a signal-recognition particle (SRP) specific signal peptide (Kim & Kendall, 2000).

All pre-proteins reach the Sec translocase, which is a membrane embedded protein conducting channel with a subset of partner proteins. It is predominantly composed of the membrane bound heterotrimer SecYEG and a peripherally associated ATPase, SecA, which functions as a molecular motor and provides energy for the translocation of secretory proteins (Douville et al., 1995).

Pre-proteins with an N-terminal SecB specific signal peptide are recognised by the chaperone, SecB. This chaperone binds to the secretory protein, preventing it from folding, and delivers it to SecA. Prior to being transported through the channel, the N-terminal signal peptide is cleaved off by a protease and the protein is folded upon delivery to the periplasm (Fekkes et al., 1997).

Conversely, pre-proteins with an N-terminal SRP specific signal peptide often contain hydrophobic domains and as such are unstable in the cytoplasm. Thus, the SRP pathway utilises a co-translational targeting mechanism which combines protein translation from the ribosome with secretion across the SecYEG channel. During translation the SRP recognises and binds to the signal peptide when the nascent protein emerges from the ribosome (Connolly & Gilmore, 1989). The SRP recruits FtsY, a docking protein, which binds and delivers the ribosome-protein complex to SecYEG, where the translation of the protein drives it through the channel. It is proposed that during translocation, YidC, a membrane protein 'insertase', ushers transmembrane helices through a lateral gate of SecY into the IM, where the signal peptide is proteolytically cleaved, and the mature protein remains attached (Petriman et al., 2018).

1.1.3.3 Twin-arginine translocation (Tat) pathway

The Tat pathway primarily translocates folded proteins across the cytoplasmic membrane. Secretory proteins utilising the Tat pathway possess an N-terminal signal sequence which has the canonical twin-arginine motif. The motif has the S/T-R-R-x-F-L-K consensus sequence, whereby x is any polar residue. Although the N-terminal signal peptides of Tat protein substrates resemble the organisation of the Sec signal sequences, they typically possess a larger positively charged N-terminal (Palmer & Berks, 2012).

Tat cargo proteins require the aid of dedicated chaperones that can bind the twin-arginine motif, facilitate its folding and deliver the protein to the Tat translocon. In *E. coli* there are three main components of the Tat translocon: TatA, TatB and TatC. Unlike the Sec translocon, the Tat machinery does not pre-exist in the IM as a stable protein complex, but is thought to assemble on demand. TatB and TatC are able to recognise and bind the N-terminal signal peptide that contains the twin-arginine motif on folded Tat secretory proteins. The TatBC complex is then able to recruit TatA to the cytoplasmic membrane where it is believed to form an oligomeric pore through which proteins can be translocated across. Once the substrate has been translocated, the signal peptide is cleaved and the mature protein is released into the periplasm (Mangels et al., 2005).

1.1.4 The biophysical properties of *E. coli* membranes

Biological membranes serve a vital function in defining a cell in respect to its environment, and play an important role in maintaining the internal turgor pressure in prokaryotes. The viability of bacteria is directly dependant on the adaptation and maintenance of electrochemical gradients and membrane homeostasis in different environmental conditions.

E. coli membranes consist of three main phospholipids, the zwitterionic PE which constitutes about 75% of total lipid content, and the anionic PG and CL, whose relative abundance varies depending on the physiological state of the cell (log- or stationary-phase). Generally, the membrane lipid content of PG and CL tends to be around 20% and 5%, respectively, although the levels of CL are known to rise during the stationary phase (Raetz and Dowhan, 1990; Hiraoka, Matsuzaki and Shibuya, 1993). The presence of these anionic lipids consequently gives the membrane a net negative charge (Lin and Weibel, 2016).

Additionally, in the rod-shaped *E. coli* CL seems to be preferentially located in regions with the largest curvature, such as at the septa and the poles of the cell. This is not unexpected, as CL is known to have an intrinsic curvature due to its conical shape, making it favourable for this lipid to be positioned in negatively curved regions of the bacterial membrane (Mileykovskaya and Dowhan, 2000; Huang and Ramamurthi, 2010).

Furthermore, CL is known to interact with a large number of membrane proteins. As it is negatively charged, it has been shown to form electrostatic interactions with basic residues

of the neighbouring membrane proteins (Erand et al., 2007; Palsdottir & Hunte, 2004; Schlame et al., 1991). This further promotes the development of local regions with high curvature. In cases where membrane protein overexpression led to the formation of intracytoplasmic membranes (ICMs), mutations in any of the enzymes involved in CL biosynthesis in *E. coli* affected the morphology of the ICMs, highlighting the importance of this lipid in membrane remodelling (Carranza *et al.*, 2017).

Phospholipid synthesis and membrane remodelling are energy intensive processes, so it is not surprising that lipid metabolism is tightly regulated, both enzymatically and transcriptionally (Cronan, Jr. and Rock, 2008). Two different cross-regulated enzymes, phosphatidylserine synthase (gene product of *PssA*) and phosphatidylglycerophosphate synthase (gene product of *PgsA*), are part of a feedback mechanism that controls PE and PG/CL synthesis, respectively. Phosphatidylserine synthase is a membrane protein that acts as a sensor. It detects alterations in the relative phospholipid composition and becomes active when it is associated with the anionic phospholipids PG and CL, catalysing the synthesis of PE. Conversely, when there is a decrease in anionic phospholipids, the enzyme phosphatidylserine synthase is deactivated, and the synthesis of PG and CL is accelerated through the phosphatidylglycerophosphate synthase metabolic pathway (Louie, Chen and Dowhan, 1986; Kumar Saha *et al.*, 1996; Royes *et al.*, 2020).

In addition to the aforementioned enzymatic regulation, phospholipid homeostasis is also subject to transcriptional regulation. Any changes detected in the membrane phospholipid composition can activate several stress response pathways. These work to ensure the integrity of the bacterial envelope. In *E. coli* the Cpx system is of particular interest (Bury-Moné *et al.*, 2009; Rowlett *et al.*, 2017). It can activate the transcription of 100+ genes, especially those involved in phospholipid metabolism and membrane protein production. When modifications in the relative amounts of anionic phospholipids are detected in the lipid bilayer by the transmembrane protein kinase CpxA, this pathway is activated (Price and Raivio, 2009; Raivio, Leblanc and Price, 2013; Keller *et al.*, 2015).

1.2 Introduction of prokaryotic organelles

The presence of specialised membranous structures that compartmentalise biochemical reactions was traditionally seen as one of the hallmarks of a eukaryotic cell plan. However, since the discovery of chromatophores in photosynthetic bacteria over 60 years ago, the belief that all prokaryotes are simple organisms devoid of any organised subcellular

architecture has become obsolete (Pardee, Schachman and Stanier, 1952). Recent breakthroughs in revolutionary imaging technologies such as super-resolution imaging and cryo-electron tomography, coupled with developments in comparative genomics and systems biology, have allowed us to make more robust assessments of bacterial cell ultrastructure.

Although distinct from eukaryotic organelles, decades of research have uncovered a multitude of functionally sophisticated protein- and lipid-bounded organelles in prokaryotes. Traditionally, an organelle is defined as a subcellular structure that contains a proteomically distinct interior and a defined boundary layer. These structures allow for a more sophisticated spatiotemporal regulation of cellular processes and depending on the organelle can have a range of specific functions. For instance, by increasing local concentrations of enzymes and metabolites they can enhance the efficiency of metabolic processes, sequester volatile or toxic intermediates from other cellular components, and provide microenvironments with distinct pH and/or redox states (Cornejo *et al.*, 2016; Stoeger, Battich and Pelkmans, 2016; Grommet, Feller and Klajn, 2020).

More recently, with the advent of recombinant protein expression and the high practicality of using *E. coli* as the host system, multiple reports have described the formation of various intracellular membranous structures resulting from the overexpression of several membrane proteins (Weiner *et al.*, 1984; Wilkison *et al.*, 1986; Voorhout *et al.*, 1988; Armour and Brewer, 1990; Van Weeghel, Keck and Robillard, 1990; Lefman *et al.*, 2004; Eriksson *et al.*, 2009). As *E. coli* is a well-studied organism that does not contain any intracellular compartments, it provides a relatively simplified landscape through which we can study and better understand the processes involved in intracellular compartment formation. Interestingly, the resultant membranous structures have been shown to have a different composition to the IM. In particular, they contain high amounts of the overexpressed protein in the membrane of the compartment and have altered lipid-protein ratios (Arechaga *et al.*, 2000; Jamin *et al.*, 2018).

1.2.1 Protein-bounded organelles

In the absence of a phospholipid-bilayer, protein-bounded organelle synthesis seems to depend upon two steps, which can occur simultaneously or sequentially. Firstly, the proteinaceous boundary is formed by multimerisation of protein units and is followed by the targeting of organelle-specific proteome to the compartment (Kerfeld *et al.*, 2005).

Well-known examples of protein-bounded organelles in bacteria include bacterial microcompartments (BMCs) and gas vacuoles.

1.2.1.1 The gas vacuole

The gas vacuole is a compound organelle containing a variable number of gas vesicles. The hollow gas-filled interiors of these organelles are defined by a protein membrane, which in turn provide buoyancy to a diverse range of planktonic bacteria (Blaurock and Wober, 1976; Yeates *et al.*, 2008).

1.2.1.2 Bacterial microcompartments

Conversely, BMCs contain a selectively semi-permeable protein shell that encapsulates an enzymatic core. While the basic architecture of the protein shell is conserved across a whole range of anabolic and catabolic BMCs in different bacteria, they are functionally diverse (Kerfeld *et al.*, 2018).

The carboxysome, a type of anabolic BMC, is the best-studied example of this type of organelle and can be found in all cyanobacteria and some chemoautotrophs (**Figure 1.5**). They are self-assembling compartments containing the metabolic enzymes: ribulose-1,5-bisphosphate carboxylase/oxygenase (RuBisCO) and carbonic anhydrase. Their function is to fix carbon dioxide as part of the Calvin-Benson–Bassham cycle (Shively *et al.*, 1973; Price, Coleman and Badger, 1992). The selectively permeable nature of the protein shell retards the diffusion of CO₂ out of the organelle, thus generating an elevated steady-state concentration of CO₂ inside the BMC, a condition which favours the carboxylation reaction (Dou *et al.*, 2008).

On the other hand, metabolosomes are catabolic BMCs that are responsible for the breakdown of mainly mucosal-derived substrates such as propanediol, ethanolamine and choline. These catabolic BMCs are inherently more complex than carboxysomes and contain more enzymes. Metabolosomes have shown themselves to be amenable to remodelling in synthetic biology applications (Lee *et al.*, 2018; Lee, Palmer and Warren, 2019; Juodeikis *et al.*, 2020).

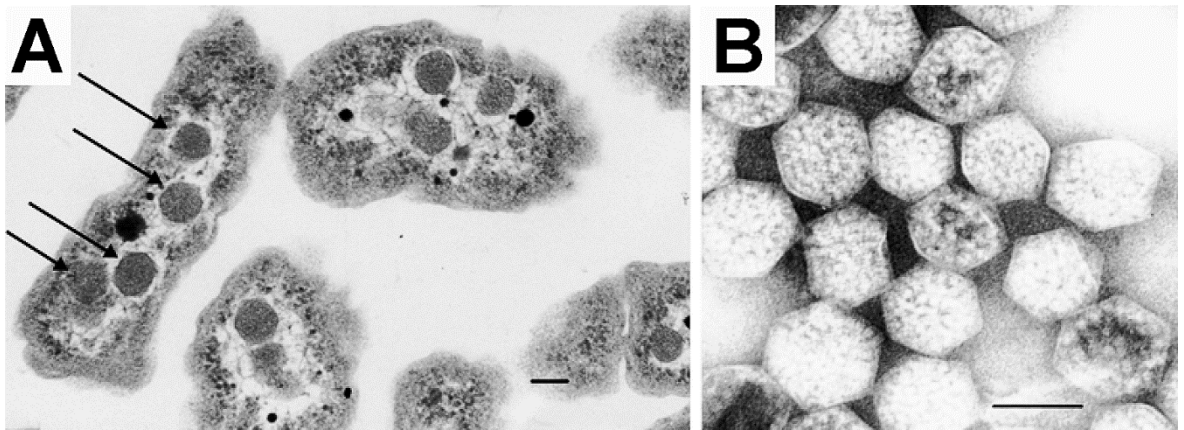


Figure 1.5. Electron micrographs of *Halothiobacillus neapolitanus* carboxysomes.

(A) Transmission electron micrographs of thin-sectioned *H. neapolitanus* cells containing carboxysomes. The arrows highlight the visible carboxysomes. (B) A negatively stained electron micrograph featuring isolated carboxysomes from *H. neapolitanus*. Scale bars indicate 100 nm (from Tsai et al., 2007).

1.2.2 Lipid-bounded organelles

Mature bacterial organelles have a diverse range of structures and functions, there are some common steps that may take place during their formation. A fundamental requirement for lipid-bounded organelle formation is the remodelling of the inner membrane during the compartmentalisation process. Although in most cases it is poorly understood, this process is believed to be driven by the incorporation of curvature-inducing proteins which encourage the budding of the membrane towards the cytoplasm. Secondly, the luminal space needs to be populated with cargo that is specific to the function of the organelle (Rahn-Lee *et al.*, 2015). Some of the membranous organelles include intracytoplasmic membranes (ICMs), magnetosomes and bacterial extracellular vesicles (BEVs), to name a few. Depending on the organelle, protein targeting can occur during membrane invagination or after organelle abscission, however, for the most part, the mechanisms underlying selective protein targeting remain to be elucidated (Zak *et al.*, 2001).

1.2.2.1 Intracytoplasmic membranes

Intricate ICM invaginations have been found in *Planctomycetes*, a deep branching phylum of bacteria. A large proportion of this phylum has been characterised by the extensive and truly remarkable compartmentalisation of their cytoplasmic space (Lindsay *et al.*, 2001). In organisms of the *Pirellula* genus, the ICMs induce the compartmentalisation of the

cytoplasmic region into a pirellosome and paryphoplasm, the latter being the peripheral ribosome-free region of the cell. The internal compartment of a pirellosome possesses an organelle composed of a large lipid-bilayer which houses the ribosomes and the chromosome, separating them from other cellular components. Moreover, these bacteria often possess a membrane-bound nucleoid region within the pirellosome, analogous in some respects to the nuclei of eukaryotic cells (**Figure 1.6**) (Lindsay, Webb and Fuerst, 1997). As is the case for many prokaryotic organelles, the function and evolution of such a cell plan is still subject to debate, but in this case could play a role in protecting the bacterial DNA, particularly against horizontal gene transfer (Pinos *et al.*, 2016).

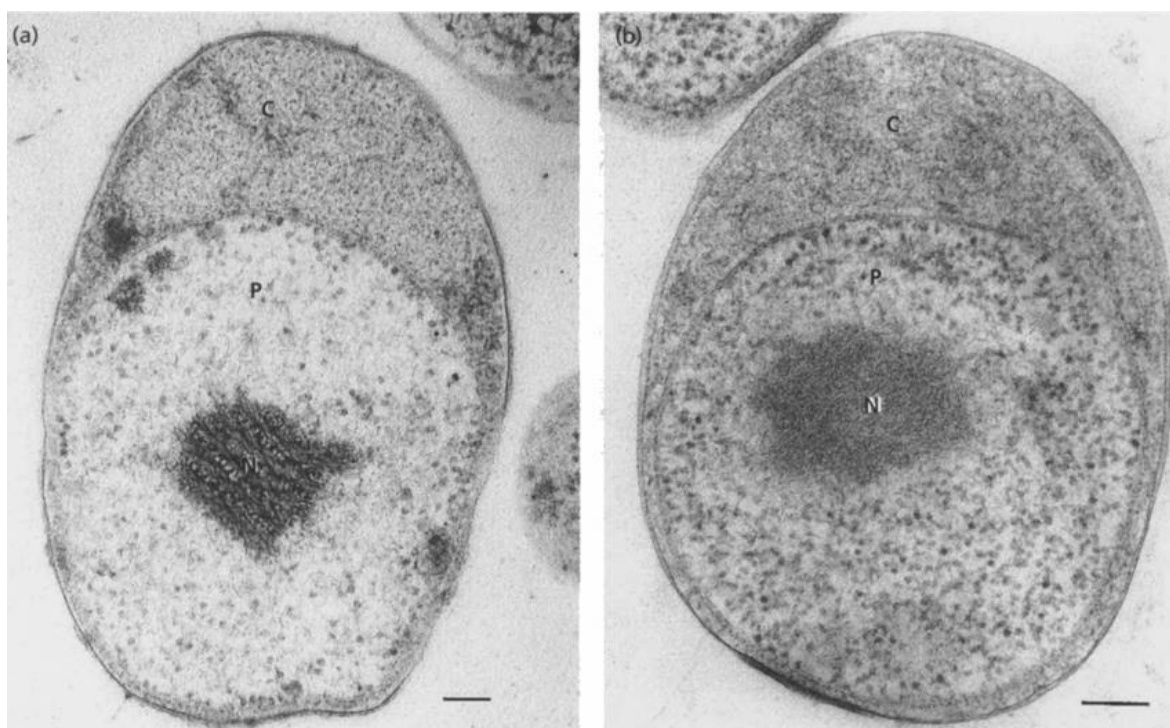


Figure 1.6. Transmission electron micrographs of *Pirellula marina* and *Pirellula staleyii* cells displaying the pirellosome.

Transmission electron micrographs of thin-sectioned cryosubstituted cells displaying intracellular compartmentalisation in (a) *P. marina* and (b) *P. staleyii* cells. The presence of the pirellosome (P) organelle can be observed in these samples, with the *P. staleyii* cell containing a fibrillary nucleoid (N). Polar cap region is depicted by (C). Scale bars: 0.1 μ m (from Lindsay *et al.*, 1997).

More complex ICMs have also been found in ammonia-oxidising *Planctomycetes*, which have been shown to possess an energy producing mitochondrion-like organelle known as an anammoxosome (**Figure 1.7**). The membrane of the anammoxosome is enriched with a

unique component, a ladderane phospholipid (Sinninghe Damsté *et al.*, 2002). These concatenated ladderane lipids are thought to increase membrane density, and as such create a more impermeable barrier, preventing the escape of toxic intermediates while retaining the components of the anammox reaction within the organelle. The ICMs of anammox bacteria play a crucial role in the energy metabolism by generating a proton motive force for the synthesis of ATP (Van Niftrik *et al.*, 2004). Interestingly, studies have shown that the central enzymes involved in the bioenergetic reactions carried out by some ICM organelles can be densely packed into the membranes, constituting upwards of 50% of the total membrane protein content (Brantner *et al.*, 2002; Muñoz-Gómez *et al.*, 2017; LaSarre *et al.*, 2018).

1.2.2.2 Magnetosomes

Magnetotactic bacteria (MTB), such as the alphaproteobacterium *Magnetospirillum gryphiswaldense*, produce a well-studied example of a lipid-bounded organelle that is called the magnetosome (**Figure 1.8**). A magnetosome contains membrane-bound and luminal proteins that mediate iron transport and regulate crystal nucleation as well as a crystalline magnetic mineral enclosed within a lipid-bilayer. The magnetic crystal is nano-sized and cubo-octahedral in shape and can be composed of either iron oxide (Fe_3O_4) or iron sulphide (Fe_3S_4). Actin-like filaments align magnetosomes into chains in the cytoplasm, enabling magnetotactic cells to orient themselves within magnetic fields. This allows MTB, through magneto-aerotaxis, to move towards environments with a desirable oxygen tension, as they prefer micro-anaerobic conditions (Komeili *et al.*, 2006).

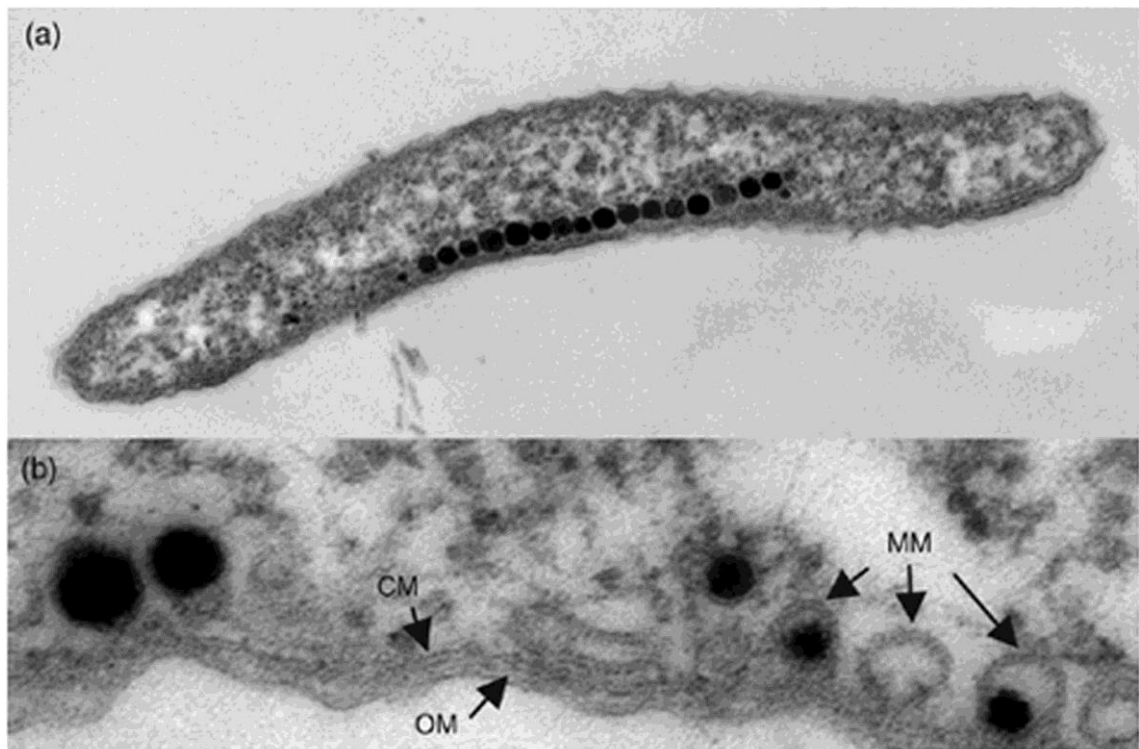


Figure 1.7. Transmission electron micrographs of *Magnetospirillum gryphiswaldense* cells containing magnetosomes.

Electron micrographs of thin-sectioned *Magnetospirillum gryphiswaldense* cells displaying (a) magnetosomes, which are chains of membrane enveloped magnetite crystals present in the cytoplasm of the cell; (b) empty and partially filled magnetosome membrane (MM) vesicles. OM refers to outer membrane, while CM refers to cytoplasmic membrane (from Schüler, 2008).

1.2.2.3 Bacterial extracellular vesicles

A fascinating example of membrane-bound organelles are BEVs of Gram-negative and Gram-positive bacteria, which are spherical particles ranging in size from 10-300 nm. The formation of these organelles seems to be a regulated process that occurs throughout the life cycle of the bacterium. A simplistic model of vesicle formation in the Gram-negative bacteria involves the liberation of the outer membrane (OM) from the underlying peptidoglycan layer in patches across the OM. Subsequently, this allows for the OM to bulge outwards until the budding vesicle undergoes fission and detaches, encapsulating some periplasmic luminal contents (Yashroy, 1999). The membrane and lumen of BEVs are known to be enriched with a wide range of cargo, including but not limited to: lipopolysaccharides (LPS), outer membrane proteins (OMPs), nucleic acids (DNA and RNA),

cytoplasmic and periplasmic proteins, as well as virulence factors (Ellis and Kuehn, 2010; Kaparakis-Liaskos and Ferrero, 2015). However, often the composition of the BEV membrane and lumen differ to that of the bacterial OM and periplasm, meaning that a selective mechanism for BEV cargo inclusion likely exists (Bonnington and Kuehn, 2014). Recent studies have shown that accumulation of phospholipids in the outer leaflet of the OM and/or lipid A deacylation can each play a role in the formation of BEVs (Elhenawy et al., 2016; Roier et al., 2016).

Furthermore, explosive cell lysis has also been shown to play a role in membrane vesicle formation, particularly in a bacterial biofilm setting. The process of explosive cell lysis has been highly attributed to the exposure of the bacteria to various exogenous stresses such as antibiotics or DNA damaging agents. In *Pseudomonas aeruginosa*, the presence of unfavourable environmental conditions has been shown to lead to the upregulation of the endolysin-encoding gene (*lys*), resulting in enhanced permeability of the cell membranes and autolysis (Turnbull et al., 2016). The resulting membrane fragments have been shown to curl up and form membrane vesicles, encapsulating some of the cellular components released during the explosion. In this capacity, the membrane vesicles are thought to contribute towards the protection and structural integrity of the bacterial biofilm since they can act as decoys for antibiotics and interact with extracellular DNA (Schooling et al., 2009).

BEVs have been shown to contribute to diverse biological processes and play important roles in bacterial survival through the following roles: 1) DNA and protein transfer between bacterial cells, 2) removal of harmful misfolded proteins, 3) delivery of toxins to eukaryotic cells, 4) tracking of cell-cell signals and 5) delivering proteases and antibiotic-degrading enzymes (Mashburn and Whiteley, 2005). Although the biogenesis of BEVs has been well documented, the mechanisms underlying their formation are still poorly characterised.

1.2.3 Membrane remodelling proteins

Although some genetic components required for prokaryotic organelle formation have been uncovered, the molecular processes underpinning membrane restructuring in lipid-bounded organelles remains poorly understood. Uncovering the processes involved in membrane remodelling would certainly have many biotechnological applications, such as bacterial cell restructuring and recombinant membrane vesicle (MV) production.

1.2.3.1 Magnetosome membrane vesicle formation

The formation of a magnetosome organelle is believed to be a step-wise process that begins with vesicle formation and is followed by crystal nucleation, organelle alignment and crystal maturation (Komeili, 2007).

The magnetosome membrane (MM) forms a distinct vesicular compartment that acts as a nanoreactor, within which the conditions for magnetite precipitation can be tightly regulated. In several *Magnetospirillum* species, the MM has been shown to be similar in composition to the IM, and is comprised of phospholipids, notably PE and PG, fatty acids, and is often enriched with a particular subset of proteins, some of which appear to be unique to the MM. Due to the similarity in composition between the MM and the IM, the current belief is that the magnetosome organelle formation is driven by the invagination and the subsequent 'pinching off' of the IM (Gorby, Beveridge and Blakemore, 1988; Grünberg *et al.*, 2001).

Magnetosome synthesis is a genetically complex process, including a rather large set of candidate genes that are largely located within the magnetosome island (MAI) (Ullrich *et al.*, 2005; Fukuda *et al.*, 2006). Genetic dissection studies have revealed a number of proteins, which are encoded within the MAI, are implicated in MM invagination. The deletion of all or some of the genes including *MamB*, *I*, *L* and *Q*, in several *Magnetospirillum* species, resulted in the complete abolishment of magnetosome vesicle formation, suggesting these proteins play key roles in the first step of magnetosome production (Murat *et al.*, 2010; Uebe *et al.*, 2011).

MamB is classified as a cation diffusion facilitator and is thought to play a dual role in magnetosome assembly. It is an integral membrane protein that is present in the MM, and is suspected of containing metal-ion binding sites at its transmembrane (TM) and soluble domains, playing a key role in iron transportation (Grass *et al.*, 2005; Jogler *et al.*, 2009; Nudelman and Zarivach, 2014). Studies into the bi-functional nature of *MamB* revealed that although the disruption of the metal-ion binding sites lead to the termination of magnetite biomineralisation, it did not abolish magnetosome vesicle formation. The deletion of the gene was required to completely abolish membrane vesiculation in *Magnetospirillum gryphiswaldense*, although in *Magnetospirillum magneticum* the deletion of the four genes, *MamB*, *I*, *L* and *Q*, was necessary to achieve the same outcome (Uebe *et al.*, 2011; Raschdorf *et al.*, 2016).

MamI and MamL are unique to MTB, are small in size, and are predicted to have two integral membrane α -helices. Secondary structure prediction suggests the presence of a short loop of amino acids between the transmembrane helices, which may contribute to creating the intimal curvature needed to form the MM (Murat *et al.*, 2010; Komeili, 2012).

MamQ is predicted to be an integral membrane protein, and is homologous to the LemA protein family (Komeili, 2012). Secondary structure prediction shows that MamQ has one integral N-terminal helix that is followed by a soluble C-terminal domain, which is presumably located inside the magnetosome lumen (Arnold *et al.*, 2006). Deletion of MamQ in *Magnetospirillum magneticum* results in the complete loss of magnetosome formation, signifying its key role in the vesiculation of the MM (Murat *et al.*, 2010). Due to its weak similarity to Bin/Amphiphysin/Rvs (BAR) proteins, which participate in membrane deformation, MamQ is believed to take part in membrane bending during magnetosome invagination (Komeili, 2012; Lohße *et al.*, 2014). Although genetic studies have shed a light on some components that contribute to magnetosome formation, and particularly MM invagination, the precise mechanisms and the proteins involved remain to be elucidated.

1.2.3.2 LemA protein family

LemA proteins are predicted to be a family of integral membrane proteins that have an N-terminal membrane spanning domain followed by a C-terminal soluble domain (Lenz, Dere and Bevan, 1996). To date, there is a single unpublished crystal structure of the soluble domain of *Thermatoga maritima* LemA protein, TM0961, which is available on PDB (2ETD). It shows a coiled-coil structure; however, no further structural analysis has been carried out.

Currently, there are approximately 29,000 LemA proteins according to Interpro (Blum *et al.*, 2021), the majority of which appear to be in bacterial genomes. Members of the LemA family are present in both Gram-negative and Gram-positive bacteria and although some studies have shed some light on their possible roles, their exact molecular function remains uncertain.

A LemA protein was first identified in 1996 as a H2-M3-restricted *Listeria monocytogenes* epitope, although further work revealed the protein was not necessary for intracellular infection or T-cell activation (Lenz, Dere and Bevan, 1996; D’Orazio *et al.*, 2003). More recently, using a reverse vaccinology approach, a putative LemA protein with an M3

epitope similar to that of *Listeria* was found in several pathogenic strains of *Leptospira* (Hartwig *et al.*, 2013). In *Leptospira interrogans*, the amino terminus of this protein is predicted to be oriented towards the outside of the bacterium, where the protein has been shown to bind a number of host extracellular matrix proteins, particularly fibrinogen, laminin and collagen type IV. As a result, the protein is believed to play a role in host-cell adhesion during the infection process (Oliveira *et al.*, 2018). Interestingly, a combination of the recombinant LemA protein coupled with the adjuvant AddaVax™, induced protective immunity of up to 87.5% in Golden Syrian hamsters against a lethal *Leptospira interrogans* challenge. Additionally, it is worth noting that the LemA protein did not exhibit any cytotoxic effects, and thus presents itself as a good candidate for a recombinant subunit vaccine against leptospirosis (Oliveira *et al.*, 2020).

Lastly, MamQ, a member of the LemA family which has been implicated in the MM invagination in *Magnetospirillum gryphiswaldense*, was further investigated for its membrane restructuring properties through recombinant expression in *E. coli*. Multiple IM invaginations and the formation of poly-membrane bodies were observed following the expression of the full-length protein. However, the removal of the N-terminal transmembrane region of MamQ resulted in inclusion body formation and the loss of the membranous phenotype. These findings indicate that the putative transmembrane region plays a role in targeting the protein to the membrane, and may cause membrane invagination through the induction of membrane curvature (Juodeikis, 2016).

In light of these results, further work was undertaken to gain a better understanding of the membrane restructuring effects of LemA proteins. As a starting point four different LemA proteins from *Bacillus megaterium* (LemA.153), *Clostridium kluyveri* (LemA.159), *Brucella melitensis* (LemA.501) and *Pseudomonas aeruginosa* PA14 strain (PaLemA1) were individually overexpressed in *E. coli* (**Figure 1.9**). A range of phenotypes were observed, which included the production of intracellular vesicles, poly-membrane bodies and inclusion bodies, in each case exhibiting a strong effect on the IM of the bacterium (Juodeikis, 2016).

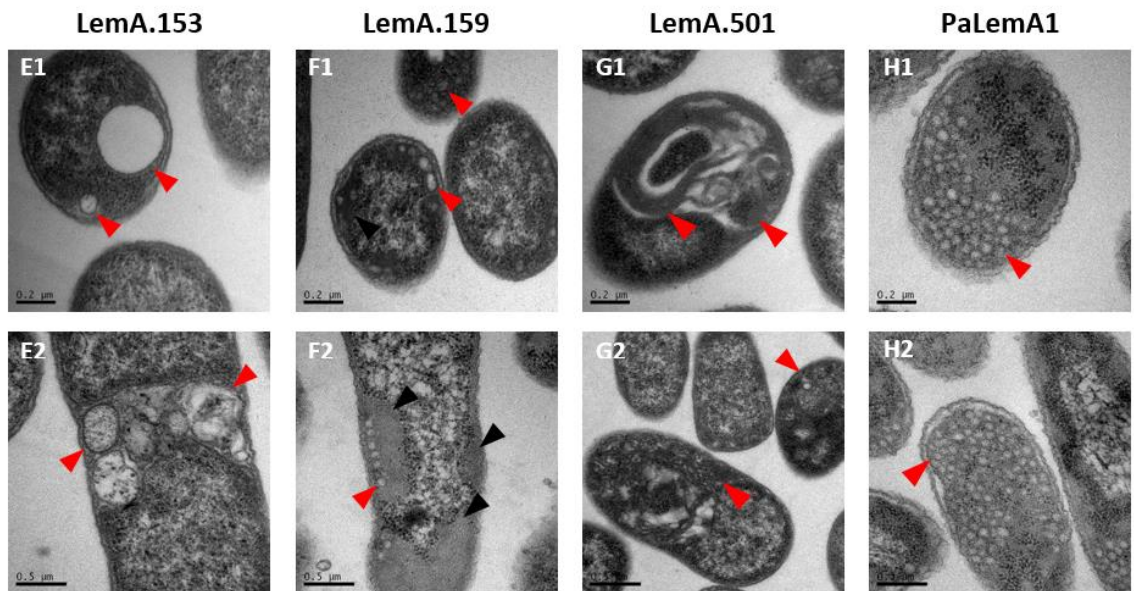


Figure 1.8. Transmission electron micrographs of thin-sectioned *E. coli* cells producing LemA proteins from different organisms.

E. coli BL21 (DE3) Star cells overproducing different LemA proteins from the following organisms: LemA.153 – *Bacillus megaterium*; LemA.159 – *Clostridium kluyveri*; LemA.501 – *Brucella melitensis*; PaLemA1 – *Pseudomonas aeruginosa* (PA14 strain). **Red arrows** indicate membranous structures observed, while the **black arrows** indicate the presence of inclusion bodies. LemA.153 leads to formation of large and small membranous vesicles and membrane invaginations; LemA.159 results in small intracellular vesicle formation and large inclusion body formation; LemA.501 leads to membranous ruffle formation and PaLemA1 results in small intracellular vesicle formation and inclusion body formation. Scale bars: 200 nm (E1-H1); 500nm (E2-H2) (from Juodeikis, 2016).

1.2.4 Overexpression of membrane proteins alters bacterial ultrastructure

On average, membrane proteins constitute 20-30% of most organisms' proteomes, yet there remain to be very few solved protein structures (Krogh *et al.*, 2001). They are challenging targets in structural biology due to their partially hydrophobic surfaces, flexible nature and lack of stability. In addition, matters are complicated further by the fact that the natural abundance of membrane proteins in eukaryotic and prokaryotic cells are usually not adequate enough to provide sufficient amounts for functional and structural studies (Bernaudat *et al.*, 2011).

Membrane protein overexpression is common practise and has been successfully achieved in a number of expression systems, with one of the most commonly used hosts being the gram-negative bacterium, *E. coli*. It has relatively short generation times, inexpensive culture media, high yield of overexpression and well characterised genetics, making it a popular expression platform. However, overexpressing membrane proteins does not come without its challenges. Often, high concentrations of membrane proteins can lead to cellular toxicity and protein aggregation within inclusion bodies in the host (Makrides, 1996; Stevens, 2000).

Interestingly, in a few cases membrane protein overexpression has led to the formation of ectopic neo-formed intracellular membranes. Several morphologies of these intracellular membranous structures have been reported in the literature and include cylindrically shaped tubules, spherical vesicles, as well as a range of undefined, ordered and disordered cytoplasmic structures, the majority of which were found to be enriched with the overexpressed protein (Jamin *et al.*, 2018).

Several mechanisms are thought to be responsible for the formation of intracellular membranous structures. These include the over-concentration of membrane proteins which induce local membrane curvature in the IM, and possibly, through electrostatic interactions with CL provide the necessary forces to bend the membrane (Renner and Weibel, 2011; Ge *et al.*, 2014; Royes *et al.*, 2020). Furthermore, the general membrane stress response triggered by the high level of membrane protein overexpression activates the phospholipid homeostasis pathways (Cronan, Jr. and Rock, 2008). These respond by synthesising new phospholipids in order to maintain the lipid-protein ratio of the IM, resulting in continuous membrane expansion which leads to the bending of the IM inwards to the cytoplasm (Raivio, Leblanc and Price, 2013; Keller *et al.*, 2015; Rowlett *et al.*, 2017; Royes *et al.*, 2020).

Strains of *E. coli* overexpressing the transmembrane enzyme, *sn*-glycerol-3-P acyltransferase, have been shown to form intracellular tubular structures, with initial characterisation revealing them to be helical arrays of the enzyme itself (Wilkison and Bell, 1997). Similarly, overproducing the integral membrane enzyme, fumarate reductase, also results in the formation of tubules (**Figure 1.10**), although unlike the *sn*-glycerol-3-P acyltransferase, changes in lipid composition were reported. Increased amounts of membrane material were produced to maintain the lipid-protein ratio, and in particular a

large increase in CL content was observed. Quantification studies revealed the total content of fumarate reductase in the tubules to be approximately 50% (Weiner *et al.*, 1984; Elmes, Scraba and Weiner, 1986).

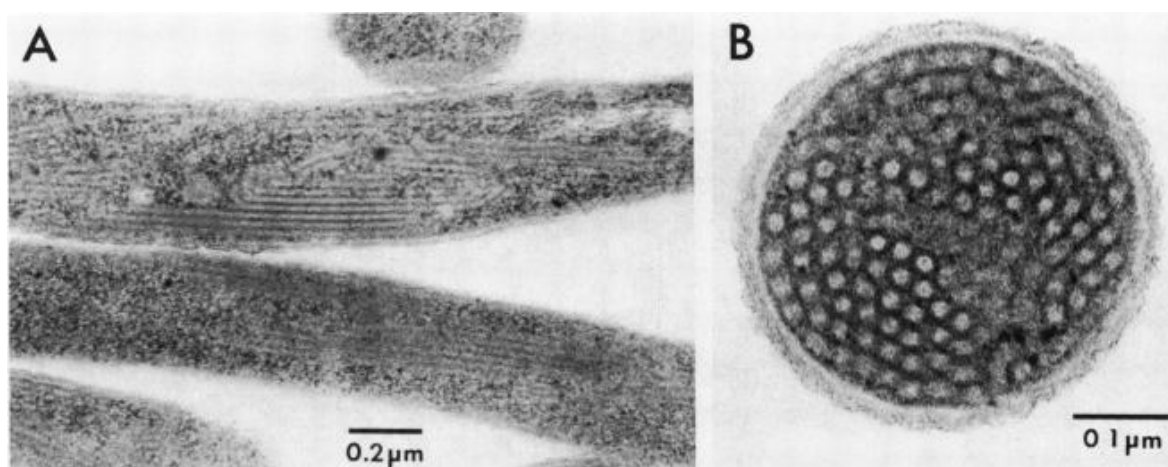


Figure 1.9. Transmission electron micrographs of *E. coli* HB101 cells overproducing fumarate reductase.

TEM analysis of longitudinal (A) and transverse (B) sections of *E. coli* cells overproducing the fumarate reductase protein. Longitudinal sections reveal the presence of thin tubular structures in the cytoplasm of the cell, which seem to run along the length of the cell. On the other hand, the transverse section shows the presence of rings, the diameter of which can be approximated to be 25 nm (from Weiner *et al.*, 1984).

One of the key transmembrane enzymes implicated in the biosynthesis of peptidoglycan is the glycosyltransferase MurG, which when overexpressed in *E. coli* results in the formation of spherical vesicles (**Figure 1.11**). The over-produced protein appears to preferentially localise to the cell poles and induce membrane accumulation through increased phospholipid synthesis, particularly CL (Van den Brink-van der Laan *et al.*, 2003). Since the polar regions of the cell tend to be metabolically silent after their formation, they may contain more free cytosolic space, possibly offering an explanation for the vesicle localisation (Vollmer and Höltje, 2001). Having a better understanding of the molecular mechanisms underlying the formation of such recombinant membranous structures could provide a strong basis for their exploitation for a number of biotechnological applications. In particular, directed production coupled with the selective enrichment of these structures with specific antigens could serve as a novel vaccine production platform.

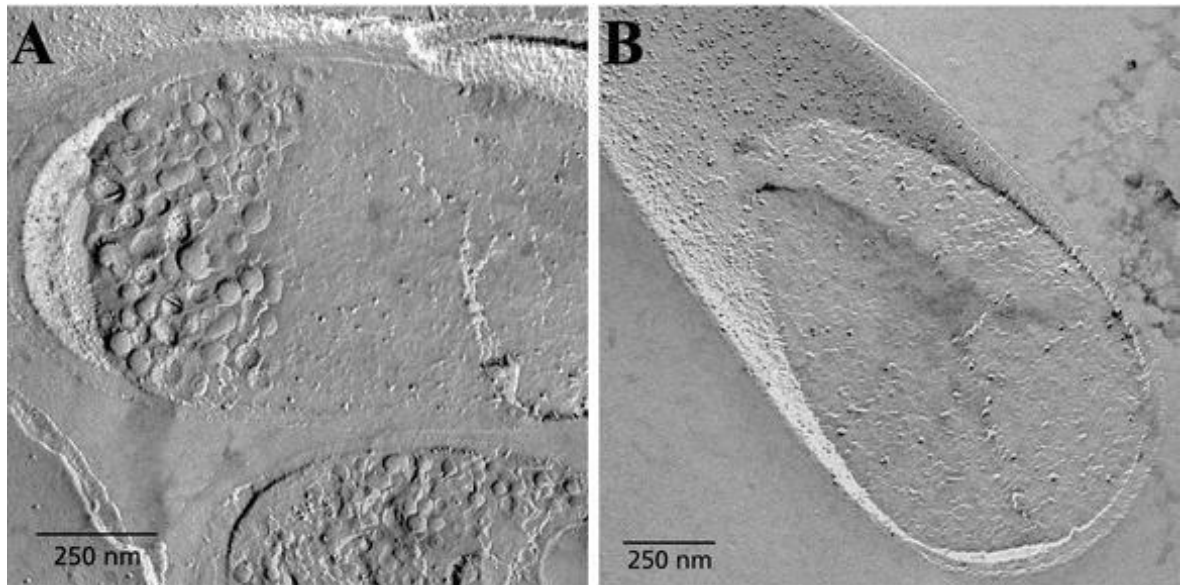


Figure 1.10. Freeze fracture electron micrographs of *E. coli* BL21(DE3)/plysS cells.

Electron micrographs of freeze fractured *E. coli* BL21(DE3)/plysS cells: (A) overproducing the glycosyltransferase MurG, following IPTG induction, (B) harbouring the construct for glycosyltransferase MurG, without IPTG induction. Formation of intracellular vesicles can be observed at the poles of the cells (A) (from Van den Brink-van der Laan et al., 2003).

It is now well known that the membrane domains of integral proteins can be involved in membrane remodelling, vesiculation, as well as cellular shape alterations. The formation of internal membrane systems in *E. coli* has been observed following the overexpression of several membrane embedded proteins. However, more work is required to understand the molecular mechanisms underlying the production of intracellular tubules and vesicles, as they could be exploited for multiple biotechnological applications.

1.3 Vaccines

Vaccines are biological preparations that elicit an adaptive immune response and stimulate the production of antibodies, providing long-term immunity against a causative agent of infectious disease. Estimates show that global vaccination programmes annually prevent 6 million deaths, on average saving approximately 386 million years of life (Ehreth, 2003).

1.3.1 Vaccines play an important role in public health

Immunisation remains to be one of the most cost-effective healthcare interventions, greatly reducing the burden of infectious disease, disability, death and inequity on both individuals and the wider society. Efficacious vaccines protect individuals prior to exposure to a particular pathogen, and this preventative approach has shown huge success against a cluster of childhood diseases (World Health Organization (WHO), 2012; Benn *et al.*, 2013). Prompt vaccination can also take place following a potential exposure and has been shown to reduce the risk of illness in the case of hepatitis A, rabies, hepatitis B, varicella and measles (Succi and Farhat, 2006).

In the wider context, vaccines have the potential to eradicate or locally eliminate the causative microorganism through herd protection. This is possible because the vaccinated individuals cease to be reservoirs of infection for other individuals. Two of the most notable accomplishments resulting from mass vaccination programmes include the reduction in polio cases by more than 99% since 1988, and the eradication of smallpox (Fenner, 1982; Garon, Cochi and Orenstein, 2015).

Some of the societal benefits include economic growth, enhanced equity, extended life expectancy and the prevention of antibiotic resistance. The health of any particular nation is fundamental to its economic growth and studies have suggested that vaccines can increase lifetime productivity through improved physical health, cognitive function and educational outcomes by increasing school attendance (Loeppke *et al.*, 2008; Deogaonkar *et al.*, 2012; Bärnighausen *et al.*, 2014). The establishment of vaccination programmes by leading global health organisations, allows the vaccines to reach vulnerable communities and individuals at the highest risk of suffering from a particular disease, thereby reducing inequity (Bishai, Koenig and Ali Khan, 2003; Flannery *et al.*, 2004). Furthermore, vaccines reduce antibiotic usage by preventing disease development, thus help to limit the spread of antibiotic resistance (Laufer, Sanchez-Vegas and Ramos, 2006).

1.3.2 Vaccine discovery and development

Under normal circumstance, the development of a novel vaccine, from concept to licensure, can take between 10 and 15 years. This is due to the elaborate and stringent development process that takes place after the initial discovery stage of a vaccine candidate (Han, 2015). Regulatory authorities such as the World Health Organisation (WHO), European Medicines Agency (EMA) and United States Food and Drug Administration (USFDA) provide guidelines which outline the steps that need to be taken to get a vaccine approved (WHO, 2004; European Medicines Agency, 2007; United States Food and Drug Administration, 2011). Once the proof-of-concept for a selected vaccine candidate is validated during the explanatory phase, it has to be tested to establish its safety, immunogenicity, efficacy and stability in preclinical and clinical trials.

In a preclinical setting, *in vitro* and *in vivo* testing in animal models takes place. It evaluates the vaccine's safety, potency and immunogenicity, which can aid the adjuvant selection process, if applicable. During Phase I trials, which are the first studies performed in man, the main objective is to assess the reactogenicity and safety profile of the vaccine and to collect the relevant immune response data. Frequently, the dosage, immunisation schedules and vaccine administration routes are also assessed (Authorities, Introduction and Remarks, 2003; Goetz, Pfleiderer and Schneider, 2010). Only following a satisfactory outcome in Phase I, demonstrating both safety and immunogenicity, can a vaccine candidate proceed to Phase II clinical evaluation. Phase II trials incur a much larger capital investment as they are usually bigger field studies, and therefore only take place after a stringent assessment of preclinical and clinical Phase I trial data. The primary aim of Phase II trials is to identify the optimal dose, immunisation schedule and the final vaccine formulation for Phase III trials. The Phase III clinical trials are pivotal for vaccine registration and approval to market, and generally assess the efficacy and safety of the final formulation, in turn providing relevant data about the potential impact of the vaccine on public health (**Figure 1.12**) (Artaud, Kara and Launay, 2019).

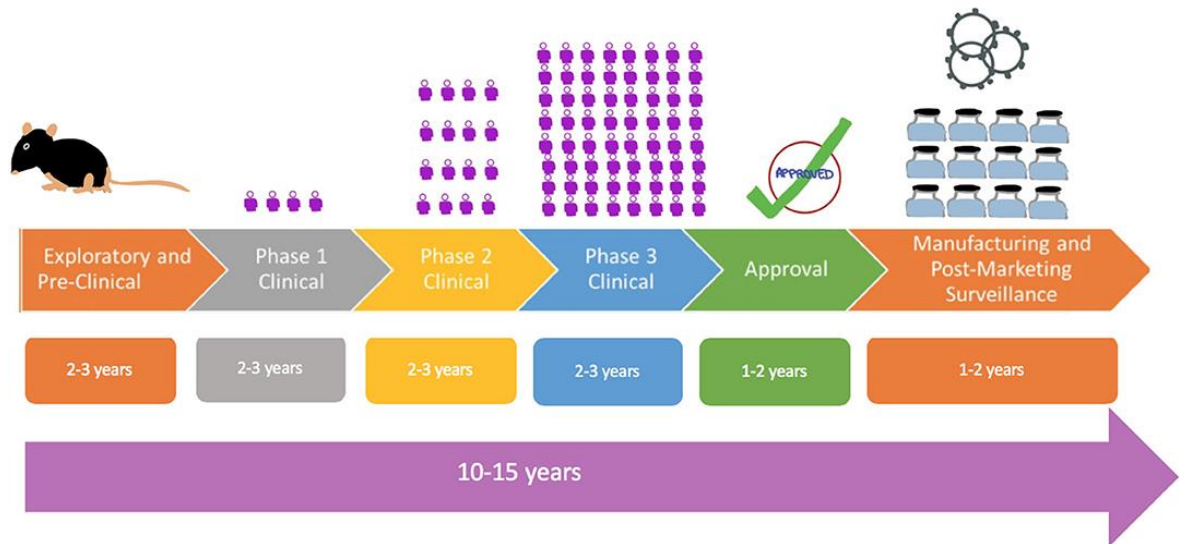



Figure 1.11. A flowchart presenting the traditional route to vaccine development.

The traditional route of vaccine development starts at the explanatory phase and goes through to Phase 1 clinical studies where a relatively small number of volunteers receive the vaccine, onto the larger Phase 2 and 3 clinical studies. The  represents the relative size of the clinical trial (from Sharma et al., 2020).

Vaccine development is a complex and a costly endeavour, which is one of the primary reasons why the number of vaccine manufacturers remains low despite the unmet demand for many vaccines globally (Plotkin *et al.*, 2017). As a result, while currently available vaccines contribute tremendous value to public health, there is a need for the development of cheaper and more universal vaccine delivery technologies, which could not only improve global vaccine accessibility but also allow nations to respond to local epidemics or pandemics faster. Ideally, such delivery platforms would use a base carrier for antigenic components of a pathogen, for instance, a viral vector, liposomes or BEVs (Watson, Endsley and Huang, 2012; van der Pol, Stork and van der Ley, 2015; de Vries and Rimmelzwaan, 2016). Once designed and licensed, the development of future vaccines would only require a substitution with the desired antigen, enabling faster and cheaper development, regulatory approval and mass production.

1.3.3 Types of vaccines

Vaccines contain immunogenic antigens specific to a pathogen, and can be monovalent, designed to provide immunity against a single organism, or multivalent, designed to protect an individual against two or more strains/microorganisms (Bartlett, Pellicane and Tying,

2009). Multiple different types of vaccine formulations are currently in use, and there are more in the process of being developed.

While traditional vaccine formulations are often comprised of attenuated or inactivated versions of microorganisms, they can pose a certain degree of unpredictability raising some stability and safety concerns. Although very rare, attenuated pathogens in vaccine preparations have the potential to revert back to a pathogenic form, causing disease in their recipients. In addition, they may be harmful if given to immunocompromised and pregnant individuals, leaving this vulnerable demographic of people unprotected (Pirofski and Casadevall, 1998; Kamboj and Sepkowitz, 2007; Pliaka, Kyriakopoulou and Markoulatos, 2012). Conversely, while inactivated vaccines do not pose a risk of infection, even to immunodeficient individuals, multiple doses may be needed to evoke a sufficient immune response, and in some cases immunity may not be long-lasting (Kang and Compans, 2009).

Due to the safety concerns associated with live-attenuated vaccines and the inconvenience of requiring multiple doses of the inactivated vaccine to maintain long-lasting immunity, research efforts have focussed more on creating vaccines based on individual pathogen antigens. As a result, in recent years we have witnessed the emergence of more refined methods of vaccine preparation, including toxoid- or subunit-based vaccines, as well as conjugate, heterotypic and RNA vaccines (Koff *et al.*, 2013; Nabel, 2013). While these seem to be safer alternatives to traditional vaccines, they appear have a lower capacity to induce long lasting immunity, and in a lot of cases require the addition of adjuvants, which are immunological agents that enhance the body's response to an antigen (Josefsberg and Buckland, 2012).

1.3.3.1 Current and emerging vaccine technologies

There are different methods for vaccine production and these include the use of traditional egg-based approaches, cell-based systems utilising mammalian cell cultures, as well as other investigational methodologies exploiting plant, insect and bacterial cells.

1.3.3.2 Egg-based approaches to vaccine production

Fertilised embryonic chicken eggs have been the most popular choice for the production of the seasonal influenza vaccine for the last 70 years (Barberis *et al.*, 2016). It is a well-established process, however, it has a long time-frame of production, taking approximately

6 months every year. This means that the influenza virus candidates must be selected based on *in silico* approaches ahead of the flu season (World Health Organization, 2007; Ampofo *et al.*, 2012). Often this results in less efficacious vaccines since the influenza virus frequently undergoes antigenic drift in its surface glycoproteins (Fitch *et al.*, 1997). This can mean that the vaccine formulation which has been designed for particular strains of influenza is different to the strains that are currently circulating, thus providing a greatly reduced protection against illness that season (Centers for Disease Control and Prevention, 2018).

Moreover, the effectiveness of the vaccine can be further compromised when the virus acquires egg-adaptive mutations in the influenza hemagglutinin (HA) glycoprotein during production, which can modify the antigenic profile of the virus (Both *et al.*, 1983; Steinhauer, Domingo and Holland, 1992). As a result, depending on the year, the effectiveness of the influenza vaccine can vary between 40-60% (Dawood *et al.*, 2020). It is worth noting that annually this approach relies on the availability of more than a 100 million embryonated eggs from flocks of chickens that must be pathogen free, rendering this vaccine delivery platform unsustainable in the management of a public health crisis (Rajaram *et al.*, 2020).

In addition, due to the nature of the egg-based production approach, individuals with an egg allergy cannot receive the influenza vaccine. However, in recent years an insect derived recombinant subunit vaccine and a cell-based vaccine containing the antigenic HA glycoproteins, have been approved for market use (Cox and Hollister, 2009; Manini *et al.*, 2015). These new generation vaccines have been promising and were shown to induce a stronger and longer-lasting immune response in comparison to the egg-based influenza vaccines (Dunkle *et al.*, 2017). Nevertheless, these still face the challenges of high manufacturing costs, and the rapid antigenic evolution of the virus (Wei *et al.*, 2010, 2020; Medina *et al.*, 2013).

1.3.3.3 Cell-based approaches to vaccine production

With the advent of recombinant DNA technology, cell-based methods utilising mammalian cell systems for vaccine manufacturing became well established in the mid-1990s (Rubio and Eiros, 2018). A number of vaccines are currently successfully produced this way with some of these including the rabies, hepatitis A and influenza vaccines (Peetermans, 1992; Wu, Smith and Rupprecht, 2011). Using this approach has a number of advantages which

include the ease of scalability and shorter production times in comparison to egg-based methods. This allows vaccine manufacturers to respond to increased market demands faster, which is particularly important in pandemic situations (Buckland, 2005; Josefsberg and Buckland, 2012).

Recombinant subunit vaccines that can be composed of a single or multiple antigenic proteins, eliminate the risks associated with handling a live pathogen, meaning that these vaccines can be produced at lower biosafety level facilities. Additionally, utilising mammalian cell culture allows the preservation of the proteins' biological activity, as it permits for correct folding and post-translational modifications to take place (Josefsberg and Buckland, 2012).

Present-day vaccine manufacturing practises have begun to exploit the baculovirus expression vector system (BEVS) for recombinant antigen expression in insect cells. The use of this expression platform has many advantages, which include the high capacity to simultaneously express multiple genes or large inserts, post-translational modifications similar to mammalian cell-processing and a strong promoter system resulting in high protein yields (Mena and Kamen, 2011). To date, this approach has produced a number of vaccines that are currently licensed for human use, including Flublok[®], CERVARIX[®] and PROVENGE[®] (Kirnbauer *et al.*, 1992; Small *et al.*, 2000; Cox and Hollister, 2009). However, the glycosylation patterns in insect cells differs in many respects to those in mammalian cells, and the relatively slow growth rate and high costs associated with the production, limits this platform's use to the developed world (Tripathi and Shrivastava, 2019).

In general, mammalian- and insect-based systems offer greater process control and provide a more reliable and well-characterised product than the egg-based approaches. However, they both utilise a relatively new technology and the high costs associated with the development and manufacturing processes can translate into expensive vaccines that may be unaffordable for those in the developing world (Hegde, 2015; Plotkin *et al.*, 2017).

1.3.4 The current threat to public health – SARS-CoV-2

We are fast approaching a post-antibiotic era due to the global dissemination of multi-drug resistant strains, favoured by the misuse/overuse of antibiotics. As a result, the infections that once could be successfully treated are becoming a serious threat to global public health. This coupled with the increased incidence of pandemic outbreaks in recent decades,

such as the Ebola virus that devastated Central African countries, the Zika crisis in 2016, and the current SARS-CoV-2 pandemic, has reinforced the need for the development of novel vaccine production platforms that would allow a rapid global response.

Since the emergence of the severe acute respiratory syndrome coronavirus 2 (SARS-CoV-2) in December, 2019, and its worldwide spread, culminating in the declaration of a global pandemic by the WHO in March, 2020, the world landscape has dramatically changed (Sohrabi *et al.*, 2020). Over 100 million people have been infected with SARS-CoV-2 worldwide, which has a mortality rate of 2-3% (Palacios Cruz *et al.*, 2021).

Currently, there are no licensed pharmacotherapies that are able to treat SARS-CoV-2 infection effectively. Efforts to date have focused on the discovery of novel vaccine candidates to aid the management of this global health crisis. In the advent of such unprecedented times, international cooperation and the open sharing of resources has enabled the scientific community to develop safe and effective vaccines against SARS-CoV-2 in less than a year. This represents an astoundingly monumental task that has hopefully paved the way for future vaccine development (Kaur and Gupta, 2020).

The Pfizer-BioNTech BNT162b2 SARS-CoV-2 mRNA-based vaccine was the first to be approved for emergency use by the Medicines and Healthcare products Regulatory Agency (MHRA) in the United Kingdom (UK), in December, 2020 (GOV.UK, 2020). It was closely followed by the approval of the Oxford-AstraZeneca DNA-based vaccine and the Moderna mRNA-based vaccine, a few weeks later. The Pfizer-BioNTech and the Moderna vaccines are both composed of a lipid nanoparticle that encapsulates a nucleoside-modified mRNA. The mRNA encodes for the spike glycoprotein, a major structural component that is embedded on the viral surface envelope of SARS-CoV-2, and has been shown to induce a strong immune response when combined with an adjuvant (Wørzner *et al.*, 2021).

On the other hand, although the Oxford-AstraZeneca vaccine is similar in design, it utilises a modified adenoviral vector as the base carrier for DNA that supplies the genetic information for the SARS-CoV-2 spike protein. All three of the aforementioned vaccines were shown to generate a sufficient immunogenic response and have acceptable safety profiles that warranted the MHRA to grant their emergency use in the current pandemic (Polack *et al.*, 2020; Wang *et al.*, 2021). However, it is worth noting that there are disadvantages to utilising a vaccine platform that has not undergone a stringent

assessment process. Presently, many questions remain unanswered, including how long immunity lasts after vaccination, does the vaccine stop the transmission of the virus and whether it is safe for use in pregnant women and children.

While no RNA- or DNA-based vaccines had been licensed for human use previously, their therapeutic potential has been extensively studied for over three decades, with many promising candidates entering the clinical trial stage (Tang, Devit and Johnston, 1992; Pardi *et al.*, 2018; Lopes, Vandermeulen and Pr eat, 2019; Xu *et al.*, 2020). The simplicity of such vaccine systems, since they are composed of readily available materials, makes the manufacturing process relatively cheap and easily scalable. Furthermore, the sequence of RNA or DNA can be easily modified to encode for a disease specific antigen, thus allowing for a faster response to a public health crisis than the traditional production methods would otherwise allow.

However, the RNA- and DNA-based vaccines also present some challenges. RNA and DNA fragments alone may not generate a sufficient immune response to induce long-lasting protective immunity, and may therefore require multiple doses and the addition of adjuvants into the final formulation (Martinon *et al.*, 1993; Scheel *et al.*, 2005; Kim *et al.*, 2010; Fotin-Mleczek *et al.*, 2011). Another hurdle of the single-stranded RNA fragments is their inherent instability, which makes them prone to enzymatic degradation above freezing temperatures (Tsui, Ng and Lo, 2002; Probst *et al.*, 2006). This is further complicated by the temperature-sensitive lipid nanoparticles that are utilised in the Pfizer-BioNTech and Moderna vaccines as base carriers for the RNA. This could not only lead to difficulties when scaling up the production, but also during the cold chain distribution of the vaccine product (Corey *et al.*, 2020). Consequently, vaccines that employ the use of RNA-based technology present challenges to their widespread distribution in rural communities and developing countries, which do not have the infrastructure required for their cold storage.

On the other hand, DNA-based vaccines, although more stable, pose a possible risk of integration into the host genome that could result in insertional mutagenesis (Fahim Halim Khan, 2009). Also, the use of a modified adenovirus as a base carrier for the immunogenic DNA fragment in the case of the Oxford-AstraZeneca vaccine, may limit the efficacy of the vaccine, as people may have pre-existing levels of immunity against the viral vector (Fausther-Bovendo and Kobinger, 2014; Kremer, 2020).

The aforementioned SARS-CoV-2 vaccines provide the first hope in impeding the progress of this devastating pandemic. However, further research is essential to generate more stable vaccine platforms that do not have such stringent cold chain requirements, to allow life-saving immunisations to reach vulnerable communities in low- and middle-income countries. In addition, novel production methods should focus on developing universal vaccine platforms that are highly adaptable, cheap and fast to produce and elicit a strong immune response with limited side effects. The innovation of such technologies could provide solutions to current and emerging challenging targets, reducing the burden of disease and allowing us to respond to local and global outbreaks faster.

1.3.5 Membrane vesicle-derived vaccines

In recent years, research into the therapeutic potential of membrane vesicles (MVs) as vaccine candidates has gained momentum. Bacterial extracellular vesicles (BEVs) which are released during the growth of Gram-negative bacteria, contain a range of antigens that have natural properties such as immunogenicity and self-adjuvantivity. Additionally, as they are naturally non-replicating spherical nanoparticles, they do not carry the risk of infecting the host, which makes BEVs particularly attractive vaccine delivery platforms (Acevedo *et al.*, 2014; Kaparakis-Liaskos and Ferrero, 2015).

Advances in synthetic biology, genetic engineering and reverse vaccinology have paved the way for new MV platforms that can be manipulated and engineered to contain specific antigens on their surface or within their lumen. Using the BEV structure for antigen presentation has numerous advantages, the most important of which is the preservation of the physico-chemical stability of the surface-exposed antigen. BEV vaccines have been shown to be thermostable, lasting for years if stored at 5 °C, a property that could be of particular importance to low- and middle-income nations (Fredriksen *et al.*, 1991; Gerritzen *et al.*, 2017). In addition, BEV-based vaccine technologies can be easily scalable, present low technological complexity and are relatively cheap to manufacture, while having the potential to produce a wide variety of vaccines.

The production of BEVs can be achieved in several ways: wild-type bacteria can be cultured to secrete native BEVs, genetic modifications can be used to enhance the vesiculation of the bacterial OM, and detergent extraction methods can be exploited to chemically disrupt cellular membranes and release vesicles of heterogeneous size. Moreover, BEVs have been shown to be readily taken up by host immune cells, and stimulate humoral and cell-

mediated immune responses against a number of pathogenic bacteria, which makes them attractive targets for vaccine development (Kuehn and Kesty, 2005; Ellis, Leiman and Kuehn, 2010; Parker *et al.*, 2010). However, it is worth noting that pathogen-associated molecular patterns (PAMPs), especially lipid A, can be found on the surface of BEVs and trigger strong innate immune responses and the release of inflammatory cytokines in humans (Zariri *et al.*, 2016). Due to the high inherent toxicity of lipid A, which is associated with the integrity of its chemical structure, genetic deletions of *msbA* in *E. coli* and *lpxL1* in *N. meningitidis* have previously been shown to modify the reactogenicity of LPS. These genetic alterations modify the acylation pattern of lipid A and thus reduce the activation of TLR4/MD2 by LPS, decreasing its toxicity (Zhou *et al.*, 1998; Van Der Ley *et al.*, 2001). Further fine-tuning of the LPS immunogenicity can be achieved through recombinant expression of lipid A modifying enzymes, LpxE or PagL, and has been demonstrated to allow for a balanced activation of the human immune system (Pupo *et al.*, 2014).

Additionally, by utilising detergent extraction protocols for vesicle production, LPS content in BEVs can also be largely reduced, though there are several disadvantages to using this method. The immunogenicity of the BEVs can be largely decreased due to the loss of membrane associated surface antigens, possibly requiring the addition of adjuvants in the final vaccine formulation. BEVs can also become prone to aggregation, which can affect the yield of the final product, and contamination of BEVs with cytoplasmic proteins can occur from the resulting bacterial cell lysis (Koeberling, Seubert and Granoff, 2008; Van De Waterbeemd *et al.*, 2013; Kis *et al.*, 2019). Due to this, BEV preparations utilising genetic detoxification methods present the most promising technology for the generation of BEVs with sufficient adjuvant activity and limited side effects (van de Waterbeemd *et al.*, 2010).

Interestingly, recent efforts in generating a universal BEV-based vaccine platform have even turned to membrane vesicles produced by Gram-positive bacteria. In one study, *Bacteroides thetaiotaomicron*, which is a human commensal gut bacterium, was engineered to express the stalk region of the influenza A hemagglutinin viral protein in its membrane vesicles. Following inoculation with these engineered BEVs, mice were protected from lethal challenge and showed the production of the relevant IgG and IgA antibodies (Bentley *et al.*, 2019).

1.3.5.1 Vaccines against meningococcal disease

Over the last 20 years, the development and licensure of BEV-based vaccines (MenBvac[®], MeNZB[®], VA-MENGOCC-BC[®], and BexSero[®]) against bacterial meningococcal disease has successfully taken place in a number of countries across the world (Bjune *et al.*, 1991; Sierra *et al.*, 1991; Arnold *et al.*, 2011; Norheim *et al.*, 2012). *Neisseria meningitidis* is a Gram-negative bacterium and is one of the causal agents responsible for invasive meningococcal disease. It poses a significant global health burden, with an estimated 500,000 cases occurring annually (Jafri *et al.*, 2013). The lethality of this disease can range between 5-10%, with an approximated 20% of infections leading to permanent sequelae in survivors, and these can include visual or hearing loss, loss of limbs and neurological damage (Pace and Pollard, 2012).

There are 12 different serogroups of *N. meningitidis*, which are characterised based on their capsular polysaccharide. Conjugate polysaccharide vaccines against the strains, A, C, W-135 and Y, have been in use since the 1970s (Gotschlich, Goldschneider and Artenstein, 1969; Milligan and Barrett, 2014). However, for serogroup B, which happens to be one of the most prevalent strains in Europe, Americas and Australia, the polysaccharide vaccine approach was deemed unsuitable (Wyle *et al.*, 1972; Bruge *et al.*, 2004; Harrison, Trotter and Ramsay, 2009; Sadarangani and Pollard, 2010). The polysaccharide of serogroup B was shown to have very poor immunogenicity. This was attributed to its shared structural homology with a human neural cell adhesion molecule, PSA-NCAM, that is expressed in the foetal brain and various host tissues, resulting in its immunological tolerance (Devi *et al.*, 1997; Zollinger *et al.*, 1997). This has led to concerns about the potential production of autoantibodies against the host PSA-NCAM molecule, which could lead to an autoimmune response and tissue damage in the recipients (Finne, Leinonen and Mäkelä, 1983). As a result, vaccine efforts for serogroup B meningococci have largely focused on BEVs that display the major immunogenic OMPs found on the surface of *N. meningitidis* (Claassen *et al.*, 1996).

The first vaccine formulations utilising monovalent wild-type BEVs were generally strain specific, which was due to the fact that immunity was primarily initiated against the immuno-dominant OMP, PorA, a highly variable protein among different meningococci strains (Sacchi *et al.*, 2000; Wong *et al.*, 2007). As a result, they did not induce broad protective immunity against the wide array of *N. meningitidis* B serogroups circulating

worldwide (Tappero *et al.*, 1999; Holst *et al.*, 2009, 2013). Recent approaches have focused on multivalent BEV vaccines that display multiple versions of the PorA protein and consequently provide cross-protection against most group B strains (Claassen *et al.*, 1996; Cartwright *et al.*, 1999; Giuliani *et al.*, 2006).

1.3.5.2 Towards a universal membrane vesicle vaccine platform

Due to the success of BEV-based meningococcal vaccines, other BEV candidates have been tested for their efficacy in preventing infections from various pathogenic bacteria, such as *Streptococcus pneumoniae*, *Acinetobacter baumannii* and *Bordetella pertussis* (Roberts *et al.*, 2008; McConnell *et al.*, 2011; Price *et al.*, 2016). While for the most part BEVs were produced by the pathogenic organisms of interest, recombinant BEV production systems are emerging as alternative strategies to creating a highly adaptable universal vaccine delivery platform.

Recent work on the laboratory workhorse *E. coli* has shown great promise for recombinant BEV production. *E. coli* is a well-characterised host for the expression of recombinant proteins, offering short generation times, low-cost media and easy genetic manipulation. Particularly, it is our extensive understanding and knowledge of *E. coli* genetics that makes this organism an attractive target for genetic engineering.

Initial studies highlighted that immunisation with BEVs purified from pathogenic *E. coli* can induce immunity in mice challenged with a lethal dose of this bacteria (Kim *et al.*, 2013). Furthermore, glycoengineered BEVs produced in *E. coli* expressing glycans from *Streptococcus pneumoniae*, a causative agent of pneumococcal disease, were shown to induce an immune response in mice, similar to that generated by the commercially available conjugate vaccine (Price *et al.*, 2016).

Other approaches have focused on creating a more broadly protective *E. coli* derived BEV vaccine by employing recombinant expression of a conserved surface polysaccharide, β -(1 \rightarrow 6)-linked poly-N-acetyl-D-glucosamine (PNAG), found on the surface of many eukaryotic pathogens. It is able to induce broad protective immunity in animals, but only in its deacetylated PNAG glycoform, a process that using conventional vaccine approaches is technically demanding and expensive. Through the utilisation of genetic engineering, BEVs decorated with the PNAG glycopolymer induced high titres of PNAG-specific IgG antibodies in mice following immunisation. *In vitro* studies confirmed the ability of these

antibodies to mediate the killing of two distinct PNAG expressing bacterial species, namely *S. aureus* and *Francisella tularensis* (Stevenson *et al.*, 2018). Building upon these findings could potentially lead to the development of a universal membrane vesicle-derived vaccine against PNAG containing pathogens.

Lastly, Kim *et al.* have demonstrated a promising BEV expression platform that utilises a heterologous fusion construct encoding for the transmembrane protein ClyA followed by an antigen of interest (Kim *et al.*, 2008; Chen *et al.*, 2010). When expressed in hypervesiculating strains of *E. coli*, these constructs are efficiently translocated across the IM where integration of the fusion protein into the OM takes place. In this manner, the resulting BEVs are decorated with an antigen of interest. Recently, this system was exploited to express an M2e ectodomain of the influenza A matrix protein (M2), a promising antigenic target for a universal flu vaccine. Vaccinated mice showed antibody-mediated immunity against a lethal influenza A challenge, a response largely enhanced by the adjuvant qualities of BEVs (Rappazzo *et al.*, 2016). The aforementioned studies detail encouraging results in the use of *E. coli* derived BEVs for a universal vaccine delivery platform, however, further work is needed to refine these methodologies.

To conclude, while the currently licensed BEV vaccines emphasise the enormous potential of this innovative vaccine delivery platform, it is clear that further work is required to take this technology forward. Future studies should focus on increasing our understanding of the BEV cargo carrying abilities, the mechanisms involved in membrane vesiculation, as well as BEV interactions with the host immune system. The accumulation of such findings could facilitate the widespread use of BEVs in future vaccine development and enable scientists to work towards a universal BEV-based vaccine with multiple applications.

1.4 Aims of the project

In the current global climate, where antibiotic resistance is becoming commonplace and the threat from newly emerging pathogens is only increasing, the development of novel vaccine delivery platforms that are cheaper and have shorter production times has never been more necessary. The microorganism *Escherichia coli* presents one of the most cost-efficient hosts used for the production of recombinant proteins. While *E. coli* usually lacks any cellular compartmentalisation, recent studies have demonstrated that this host can produce recombinant membranous compartments following the overproduction of some

membrane proteins (Jamin *et al.*, 2018). In particular, when members of the LemA protein family have been previously overexpressed in this host, a range of different membrane phenotypes was observed (**Figure 1.9**) (Juodeikis, 2016). The broad aim of the project was to investigate the possibility of utilising different LemA proteins for the recombinant production of intracellular and extracellular lipid vesicles in *E. coli* for vaccine development. The objectives set out within this broad aim included the production of different LemA hybrid proteins, comprising of 'mix-and-matched' transmembrane and soluble domains. As the production of recombinant membranous structures was previously seen with the expression of chimeric proteins harbouring a membrane embedded domain, it was imperative to explore if membrane restructuring could be directed with the use of these constructs (Voorhout *et al.*, 1988). Furthermore, the effects of the *Pseudomonas aeruginosa* (PA14 strain) PaLemA1 protein were of particular interest, as its overproduction in *E. coli* has previously been shown to result in the formation of small intracellular lipid vesicles. If by employing protein engineering approaches these PaLemA1-derived vesicles could selectively be decorated with a specific antigen, it could present a novel recombinant vaccine production platform.

Chapter 2:

Materials and methods

2.1 Chemicals

Chemical	Supplier
2-Mercaptoethanol	Sigma-Aldrich
5-Bromo-4-chloro-3-indolyl phosphate	Sigma-Aldrich
Acetic acid	Fischer Scientific
Agar (bacteriological)	Oxoid
Agar low viscosity (LV) epoxy resin	Agar Scientific
Agarose	Alpha Laboratories
Ampicillin sodium salt	Melford
BCIP/NBT	Sigma-Aldrich
Bovine serum albumin	Sigma-Aldrich
Bromophenol Blue	Sigma-Aldrich
CaCl ₂ ·2H ₂ O	Sigma-Aldrich
Chelating Sepharose Fast Flow	GE Healthcare
Coomassie brilliant blue	Sigma-Aldrich
Deuterium oxide	Sigma-Aldrich
Dimethyl sulfoxide (DMSO)	New England Biolabs
Ethanol	Fischer Scientific
Ethidium Bromide	Fischer Scientific
Ethylenediaminetetraacetic acid (EDTA)	Sigma-Aldrich
Formaldehyde	Agar Scientific
Gentamicin	Sigma-Aldrich
Glucose	Fisher Scientific
Glutaraldehyde	Agar Scientific
Glycerol	Fischer Scientific
Glycine	Sigma-Aldrich
HCl	Fisher Scientific
Hepes free acid	Melford Biolaboratories
Hygromycin B	Fisher Scientific
Imidazole	Sigma-Aldrich
Isopropanol	Fisher Scientific
Isopropyl β-D-1-thiogalactopyranoside	Melford Biolaboratories
KCl	Sigma-Aldrich
K ₂ HPO ₄	Sigma-Aldrich

KH ₂ PO ₄	Sigma-Aldrich
KOH	Fisher Scientific
l-Oleoyl-rac-glycerol	Sigma-Aldrich
Lead citrate	Agar Scientific
LR white resin	Agar Scientific
Methanol	Fisher Scientific
MgSO ₄	Sigma-Aldrich
Na ₂ HPO ₄	Sigma-Aldrich
NaCl	Fisher Scientific
NaOH	Sigma-Aldrich
NH ₄ Cl	Sigma-Aldrich
¹⁵ NH ₄ Cl	Cambridge Isotope Laboratories
NiSO ₄	Sigma-Aldrich
n-Dodecyl β-maltoside	Glycon Biochemicals GmbH
Osmium tetroxide	Agar Scientific
Poly-L-lysine	Sigma-Aldrich
Propylene oxide	Agar Scientific
Skimmed milk powder	Oxoid
Sodium cacodylate	Agar Scientific
Sodium dodecyl sulphate	Fisher Scientific
Tris-acetate-EDTA (TAE) buffer	Fisher Scientific
Thiamine-HCl.2H ₂ O	Sigma-Aldrich
Trichloroacetic acid	Sigma-Aldrich
Tris	Fisher Scientific
Triton X-100	Sigma-Aldrich
Tryptone	Fisher Scientific
Tween 20	Sigma-Aldrich
Uranyl acetate	Agar Scientific
Yeast Extract	Fisher Scientific

2.2 Bacterial strains

Strain	Genotype	Use	Reference
<i>E. coli</i> BL21 (DE3) Star™	F ⁻ <i>ompT hsdSB</i> (rB-mB-) <i>gal dcm rne131</i> (DE3)	Protein production	Novagen
<i>E. coli</i> DH10β	F ⁻ <i>mcrA</i> Δ(<i>mrr-hsdRMS-mcrBC</i>) φ80 <i>lacZ</i> ΔM15 Δ <i>lacX74 recA1 endA1 araD139</i> Δ(<i>ara-leu</i>)7697 <i>galU galK</i> λ ⁻ <i>rpsL</i> (Str ^R) <i>nupG</i>	Cloning	New England Biolabs

2.3 Plasmids

Name	Resistance	Description
pET3a	Ampicillin	pET3a vector plasmid obtained from Dr. Rokas Juodeikis, University of Kent.
pET3a (-T7 tag)	Ampicillin	pET3a vector plasmid digested with BamHI and BglII restriction enzymes to remove the T7 tag.
pET14b	Ampicillin	pET3a vector plasmid obtained from Dr. Rokas Juodeikis, University of Kent.
pET23b	Ampicillin	pET3a vector plasmid obtained from Dr. Rokas Juodeikis, University of Kent.
pSEVA634-PaLemA2	Gentamicin	pSEVA634 vector plasmid harbouring the PaLemA2 gene obtained from Dr Jose Borrero de Acuna at the Technical University of Braunschweig, Germany.
pcDNA3.1/V5-His-TOPO	Hygromycin B	pcDNA3.1/V5-His-TOPO vector plasmid obtained from Dr James Budge, University of Kent.
pET3a LemA 153	Ampicillin	pET3a vector plasmid harbouring the LemA 153 gene obtained from Dr. Rokas Juodeikis, University of Kent.
pET3a LemA 159	Ampicillin	pET3a vector plasmid harbouring the LemA 159 gene obtained from Dr. Rokas Juodeikis, University of Kent.
pET3a LemA 501	Ampicillin	pET3a vector plasmid harbouring the LemA 501 gene obtained from Dr. Rokas Juodeikis, University of Kent.

pET3a PaLemA1	Ampicillin	pET3a vector plasmid harbouring the <i>PaLemA1</i> gene obtained from Dr. Rokas Juodeikis, University of Kent.
pET3a PaLemA2	Ampicillin	A restriction digest of pSEVA634-PaLemA2 vector digested with NdeI and XbaI restrictions enzymes, generating the <i>PaLemA2</i> harbouring insert, ligated into a NdeI and SpeI digested pET3a vector.
pET3a MamQ	Ampicillin	pET3a vector plasmid harbouring the MamQ gene obtained from Dr. Rokas Juodeikis, University of Kent.
pET14b MamQs	Ampicillin	pET14b vector plasmid encoding the soluble domain of the MamQ protein obtained from Dr. Rokas Juodeikis, University of Kent.
pET14b LemA 153s	Ampicillin	pET14b vector plasmid encoding the soluble domain of the LemA 153 protein obtained from Dr. Rokas Juodeikis, University of Kent.
pET14b LemA 159s	Ampicillin	pET14b vector plasmid encoding the soluble domain of the LemA 159 protein obtained from Dr. Rokas Juodeikis, University of Kent.
pET14b LemA 501s	Ampicillin	pET14b vector plasmid encoding the soluble domain of the LemA 501 protein obtained from Dr. Rokas Juodeikis, University of Kent.
pET14b PaLemA1s	Ampicillin	pET14b vector plasmid encoding the soluble domain of the <i>PaLemA1</i> protein obtained from Dr. Rokas Juodeikis, University of Kent.
pET3a MamQ TMD	Ampicillin	pET3a vector plasmid encoding the transmembrane domain of the MamQ protein obtained from Dr. Rokas Juodeikis, University of Kent.
pET3a LemA 153 TMD	Ampicillin	pET3a vector plasmid encoding the transmembrane domain of the LemA 153 protein obtained from Dr. Rokas Juodeikis, University of Kent.
pET3a LemA 159 TMD	Ampicillin	pET3a vector plasmid encoding the transmembrane domain of the LemA 159 protein obtained from Dr. Rokas Juodeikis, University of Kent.

pET3a LemA 501 TMD	Ampicillin	pET3a vector plasmid encoding the transmembrane domain of the LemA 501 protein obtained from Dr. Rokas Juodeikis, University of Kent.
pET3a PaLemA1 TMD	Ampicillin	pET3a vector plasmid encoding the transmembrane domain of the <i>PaLemA1</i> protein obtained from Dr. Rokas Juodeikis, University of Kent.
pET3a MamQ TMD MamQs	Ampicillin	pET3a vector plasmid encoding the hybrid LemA protein composed of the transmembrane domain of MamQ and the soluble domain of LemA MamQ, obtained from Dr. Rokas Juodeikis, University of Kent.
pET3a MamQ TMD 153s	Ampicillin	pET3a vector plasmid encoding the hybrid LemA protein composed of the transmembrane domain of MamQ and the soluble domain of LemA 153, obtained from Dr. Rokas Juodeikis, University of Kent.
pET3a MamQ TMD 159s	Ampicillin	pET3a vector plasmid encoding the hybrid LemA protein composed of the transmembrane domain of MamQ and the soluble domain of LemA 159, obtained from Dr. Rokas Juodeikis, University of Kent.
pET3a MamQ TMD 501s	Ampicillin	pET3a vector plasmid encoding the hybrid LemA protein composed of the transmembrane domain of MamQ and the soluble domain of LemA 501, obtained from Dr. Rokas Juodeikis, University of Kent.
pET3a MamQ TMD PaLemA1s	Ampicillin	pET3a vector plasmid encoding the hybrid LemA protein composed of the transmembrane domain of MamQ and the soluble domain of LemA PaLemA1, obtained from Dr. Rokas Juodeikis, University of Kent.
pET3a LemA 153 TMD 153s	Ampicillin	pET3a vector plasmid encoding the hybrid LemA protein composed of the transmembrane domain of LemA 153 and the soluble domain of LemA 153, obtained from Dr. Rokas Juodeikis, University of Kent.
pET3a LemA 153 TMD 159s	Ampicillin	pET3a vector plasmid encoding the hybrid LemA protein composed of the transmembrane domain of

		LemA 153 and the soluble domain of LemA 159, obtained from Dr. Rokas Juodeikis, University of Kent.
pET3a LemA 153 TMD 501s	Ampicillin	pET3a vector plasmid encoding the hybrid LemA protein composed of the transmembrane domain of LemA 153 and the soluble domain of LemA 501, obtained from Dr. Rokas Juodeikis, University of Kent.
pET3a LemA 153 TMD PaLemA1s	Ampicillin	pET3a vector plasmid encoding the hybrid LemA protein composed of the transmembrane domain of LemA 153 and the soluble domain of PaLemA1, obtained from Dr. Rokas Juodeikis, University of Kent.
pET3a LemA 153 TMD MamQs	Ampicillin	pET3a vector plasmid encoding the hybrid LemA protein composed of the transmembrane domain of LemA 153 and the soluble domain of MamQ, obtained from Dr. Rokas Juodeikis, University of Kent.
pET3a LemA 159 TMD 153s	Ampicillin	pET3a vector plasmid encoding the hybrid LemA protein composed of the transmembrane domain of LemA 159 and the soluble domain of LemA 153. obtained from Dr. Rokas Juodeikis, University of Kent.
pET3a LemA 159 TMD 159s	Ampicillin	pET3a vector plasmid encoding the hybrid LemA protein composed of the transmembrane domain of LemA 159 and the soluble domain of LemA 159, obtained from Dr. Rokas Juodeikis, University of Kent.
pET3a LemA 159 TMD 501s	Ampicillin	pET3a vector plasmid encoding the hybrid LemA protein composed of the transmembrane domain of LemA 159 and the soluble domain of LemA 501, obtained from Dr. Rokas Juodeikis, University of Kent.
pET3a LemA 159 TMD PaLemA1s	Ampicillin	pET3a vector plasmid encoding the hybrid LemA protein composed of the transmembrane domain of LemA 159 and the soluble domain of PaLemA1, obtained from Dr. Rokas Juodeikis, University of Kent.

pET3a LemA 159 TMD MamQs	Ampicillin	pET3a vector plasmid encoding the hybrid LemA protein composed of the transmembrane domain of LemA 159 and the soluble domain of MamQ, obtained from Dr. Rokas Juodeikis, University of Kent.
pET3a LemA 501 TMD 153s	Ampicillin	pET3a vector plasmid encoding the hybrid LemA protein composed of the transmembrane domain of LemA 501 and the soluble domain of LemA 153, obtained from Dr. Rokas Juodeikis, University of Kent.
pET3a LemA 501 TMD 159s	Ampicillin	pET3a vector plasmid encoding the hybrid LemA protein composed of the transmembrane domain of LemA 501 and the soluble domain of LemA 159, obtained from Dr. Rokas Juodeikis, University of Kent.
pET3a LemA 501 TMD 501s	Ampicillin	pET3a vector plasmid encoding the hybrid LemA protein composed of the transmembrane domain of LemA 501 and the soluble domain of LemA 501, obtained from Dr. Rokas Juodeikis, University of Kent.
pET3a LemA 501 TMD PaLemA1s	Ampicillin	pET3a vector plasmid encoding the hybrid LemA protein composed of the transmembrane domain of LemA 501 and the soluble domain of PaLemA1, obtained from Dr. Rokas Juodeikis, University of Kent.
pET3a LemA 501 TMD MamQs	Ampicillin	pET3a vector plasmid encoding the hybrid LemA protein composed of the transmembrane domain of LemA 501 and the soluble domain of MamQ, obtained from Dr. Rokas Juodeikis, University of Kent.
pET3a PaLemA1 TMD 153s	Ampicillin	pET3a vector plasmid encoding the hybrid LemA protein composed of the transmembrane domain of PaLemA1 and the soluble domain of LemA 153 obtained from Dr. Rokas Juodeikis, University of Kent.
pET3a PaLemA1 TMD 159s	Ampicillin	pET3a vector plasmid encoding the hybrid LemA protein composed of the transmembrane domain of PaLemA1 and the soluble domain of LemA 153. Both

		pET3a PaLemA1 TMD and pET14b 159s plasmids were digested with NdeI and SpeI prior to ligation.
pET3a PaLemA1 TMD 501s	Ampicillin	pET3a vector plasmid encoding the hybrid LemA protein composed of the transmembrane domain of PaLemA1 and the soluble domain of LemA 501, obtained from Dr. Rokas Juodeikis, University of Kent.
pET3a PaLemA1 TMD PaLemA1s	Ampicillin	pET3a vector plasmid encoding the hybrid LemA protein composed of the transmembrane domain of PaLemA1 and the soluble domain of PaLemA1, obtained from Dr. Rokas Juodeikis, University of Kent.
pET3a PaLemA1 TMD MamQs	Ampicillin	pET3a vector plasmid encoding the hybrid LemA protein composed of the transmembrane domain of PaLemA1 and the soluble domain of MamQ, obtained from Dr. Rokas Juodeikis, University of Kent.
pET3a PA0538	Ampicillin	PA0538 expressed from a T7 promoter with the ribosome binding site from the pET3a vector.
pET3a PA0536	Ampicillin	PA0536 expressed from a T7 promoter with the ribosome binding site from the pET3a vector.
pET3a PA4368	Ampicillin	PA4368 expressed from a T7 promoter with the ribosome binding site from the pET3a vector.
pET3a PA0538 PaLemA2	Ampicillin	PA0538-PaLemA2 expressed from a T7 promoter with the ribosome binding site from the pET3a vector.
pET3a PA0538 PaLemA2 PA0536	Ampicillin	PA0538-PaLemA2-PA0536 expressed from a T7 promoter with the ribosome binding site from the pET3a vector.
pET3a PaLemA2 PA0536	Ampicillin	PaLemA2-PA0536 expressed from a T7 promoter with the ribosome binding site from the pET3a vector.
pET3a PaLemA1 PA4368	Ampicillin	PaLemA1-PA4368 expressed from a T7 promoter with the ribosome binding site from the pET3a vector.
pET3a CTERM sfGFP	Ampicillin	A sfGFP construct made for protein purification, including a TEV protease cleavage site followed by a sfGFP followed by a His tag, expressed from a T7

		promoter with the ribosome binding site in the pET3a vector.
pET3a PaLemA1 CTERM sfGFP	Ampicillin	PaLemA1 with a C-terminal sfGFP purification construct cloned in-frame with the sequence. C-terminal sfGFP construct including a TEV protease cleavage site, sfGFP followed by a His tag, expressed from a T7 promoter with the ribosome binding site from the pET3a vector.
pET3a PaLemA2 CTERM sfGFP	Ampicillin	PaLemA2 with a C-terminal sfGFP purification construct cloned in-frame with the sequence. C-terminal sfGFP construct including a TEV protease cleavage site, sfGFP followed by a His tag, expressed from a T7 promoter with the ribosome binding site from the pET3a vector.
pET23b PaLemA1	Ampicillin	<i>PaLemA1</i> gene was sub-cloned into the pET23b vector by digesting the pET3a PaLemA1 construct with NdeI and SpeI restriction enzymes and the pET23b with NdeI and XhoI restriction enzymes and ligating the insert with the digested vector. Had the ribosome binding site from the pET14b vector.
pET23b PaLemA2	Ampicillin	<i>PaLemA2</i> gene was sub-cloned into the pET23b vector by digesting the pET3a PaLemA1 construct with NdeI and SpeI restriction enzymes and the pET23b with NdeI and XhoI restriction enzymes and ligating the insert with the digested vector.
pET3a PaLemA1 V5	Ampicillin	<i>PaLemA1</i> with a V5 tag expressed from a T7 promoter with the ribosome binding site from the pET3a vector.
pcDNA3.1/V5- His-TOPO PaLemA1	Hygromycin B	<i>PaLemA1</i> expressed in the pcDNA3.1/V5-His-TOPO vector, compatible for expression in CHO-S cells.

2.4 Primers

All primers were ordered and supplied by Eurofins™.

Name (Restriction site)	Primer sequence
PaLemA1 (XhoI) Rev	GT <u>ACTCGAG</u> GCCGAACAGGGCCTTGAG
PaLemA1 (NdeI) For	GATATAC <u>CATATG</u> AGTCTGACCGCTATCGCTTCTGGGTTGTCCTGCTG
PaLemA1 V5 Extra (SpeI) Rev	GAC <u>ACTAGT</u> TCAAGTAGAGTCTAATCCCAGCAAAGGGTTAGGGATGG GCTTCCC GCCGAACAGGGCCTTGAGATCGACGTCGGCCTTC
PaLemA2 (NdeI) For	GTAC <u>CATATG</u> CCTCGATTCTCAG
PaLemA2 (SpeI) Rev	GAT <u>ACTAGT</u> TTACTGCGCCGGTTGC
PA0538 (NdeI) For	GTAC <u>CATATG</u> TTGAGCGCTCTCCTC
PA0538 (SpeI) Rev	GAT <u>ACTAGT</u> TCAGGCGGTGC
PA0536 (NdeI) For	GTAC <u>CATATG</u> CGCCGGCTGCTACTG
PA0536 (SpeI) Rev	GAT <u>ACTAGT</u> TCACCAGCGTC
PA4368 (NdeI) For	GTAC <u>CATATG</u> GACTTCGACCTGC
PA4368 (SpeI) Rev	GAT <u>ACTAGT</u> TCAGAACAGGCGGC
Vec1WALDO Rev	GCGATAGCGGTCAGACTCATATGTATATCTCCTTCTTAAAGTTAAAC
Vec1WALDO For	TCAAGGCCCTGTTCCGGCTGAGAAAACCTGTACTTCCAGGGTC
Frag1WALDO Rev	CCCTGGAAGTACAGTTTTTCTCAGCCGAACAGGGCCTTG
Frag1WALDO For	AGAAGGAGATATACATATGAGTCTGACCGC
Sco3484 Rev	CTAGTATCATATGTGAACATCCGGCCAGCAACACGGCACCCGCCAC GCCTAAGCTGCCTCCAGGAATCCACGACGGGAAACACCGCTAGG GACGACGACTGGTTTAGTCATAT
Sco3484 For	TAATATGACTAAACCAGTCGTCCTAGCGGTGTTTCCCGTCGTGGAT TCCTGGGAGGCAGCTTAGGCGTGGCGGGTGCCGTGTTGCTGGCCG GATGTTACATATGATA

2.5 Media and solutions for bacterial work

2.5.1 Sterilisation

2.5.1.2 Autoclaving

Materials were sterilised at 121 °C and 15 psi pressure for 15 minutes.

2.5.1.3 Filter sterilisation

Sterilisation achieved by filtration through a 0.2 µm filter next to a Bunsen burner.

2.5.2 Antibiotics

Antibiotic	Concentration		Solution
	Stock	Working	
Ampicillin (Sodium salt)	100 mg/mL	0.1 mg/mL	ddH ₂ O : EtOH (1 : 1)
Gentamicin	50 mg/mL	0.01 mg/mL	ddH ₂ O
Hygromycin B	50 mg/mL	0.5-0.75 mg/mL	ddH ₂ O

Ampicillin and Gentamicin were filter sterilised and stored at -20 °C. Hygromycin B was stored in the fridge at 4 °C.

2.5.3 Growth media

2.5.3.1 Lysogeny broth (LB)

Chemical	Concentration in dH ₂ O
NaCl	5 g/L
Yeast extract	5 g/L
Tryptone	10 g/L

Sterilised by autoclaving.

2.5.3.2 LB agar

LB media with 15 g/L of bacteriological agar added prior to sterilisation by autoclaving.

2.5.3.3 M9 minimal media for isotope labelling

10X M9 salts solution:

Chemical	Concentration in dH ₂ O
Na ₂ HPO ₄ ·2H ₂ O	66 g/L
KH ₂ PO ₄	33 g/L
NaCl	5.5 g/L

The pH was adjusted to 7.2 prior to sterilisation by autoclaving.

10X Trace metal stock solution:

Chemical	Concentration in dH ₂ O
Na ₂ EDTA·2H ₂ O	48.4 g/L
ZnSO ₄ ·7H ₂ O	23.0 g/L
H ₃ BO ₃	11.1 g/L
MnCl ₂ ·4H ₂ O	5.1 g/L
CoCl ₂ ·6H ₂ O	1.7 g/L
CuSO ₄ ·5H ₂ O	1.5 g/L
(NH ₄) ₆ Mo ₇ O ₂₄ ·4H ₂ O	1.0 g/L

Sterilised by autoclaving.

Complete M9 minimal media broth:

Chemical	Concentration in D ₂ O	Sterilisation
10X M9 salts	100 mL/L	Autoclaving
1M MgSO ₄	1 mL/L	Autoclaving
0.1 M CaCl ₂	1 mL/L	Autoclaving
Thiamine HCl	3 mM	Filter sterilisation
Trace metal stock	10 mL/L	Autoclaving
Glucose	4 g/L	Filter sterilisation
¹⁵ NH ₄ Cl	1 g/L	-

All solutions were made separately prior to being combined. Ammonium-¹⁵N chloride was weighed and directly added to the broth. Antibiotics were added to the correct concentration and the solution was made up to 1 L with sterile D₂O.

2.5.4 Media and solutions for protein work

2.5.4.1 Solutions for polyacrylamide gels

2X Laemmli buffer:

Chemical	Concentration in dH ₂ O
2-Mercaptoethanol	10% (v/v)
Bromophenol Blue	0.004% (v/v)
Glycerol	20% (v/v)
Sodium dodecyl sulfate	4% (w/v)
Tris-HCl (pH 6.8)	125 mM

10X running buffer for SDS-PAGE:

Chemical	Concentration in dH ₂ O
Tris	250 mM
Glycine	1.92 M
SDS	1% (w/v)

Coomassie blue stain:

Chemical	Concentration in dH ₂ O
Trichloroacetic acid	250 mL/L
Coomassie brilliant blue	0.6 g/L
Sodium dodecyl sulfate	0.1 g/L
Tris	0.25 g/L
Glycine	0.15 g/L

Molecular mass marker:

The Blue Prestained Protein Standard, Broad Range (11-190 kDa) (NEB™) was used to quantitate the observed protein sizes until it was decommissioned, after which the Blue Prestained Protein Standard, Broad Range (11-250 kDa) (NEB™) was used.

Composition of 12.5% (v/v) polyacrylamide gels:

Solutions	Stacking gel (5% v/v)	Running gel (12.5% v/v)
1.5 M Tris-HCl pH 8.8	-	3.8 mL
0.5 M Tris-HCl pH 6.8	1.9 mL	-
30% (v/v) Acrylamide/bis	1.5 mL	6.3 mL
10% SDS (v/v)	0.75 mL	1.5 mL
10% APS (/v)	0.075 mL	0.15 mL
Water	3.4 mL	3.4 mL
TEMED	0.01 mL	0.01 mL

2.5.4.2 Western blotting solutions

Transfer buffer:

Chemical	Concentration in dH₂O
Tris	3.03 g/L
Glycine	14.41 g/L
Methanol	200 mL/L

Phosphate buffered saline:

Chemical	Concentration in dH₂O
NaCl	140 mM
KCl	3 mM
Na ₂ HPO ₄	10 mM
KH ₂ PO ₄	2 mM

Phosphate-free solution:

Chemical	Concentration in dH₂O
NaCl	150 mM
Tris	50 mM

The pH of the solution was adjusted to 7.5 with HCl.

2.5.4.3 Immobilised metal ion affinity chromatography solutions

Buffer	Concentration in dH ₂ O					
	NiSO ₄	Hepes (pH 8.0)	NaCl	Imidazole	DDM	Triton X-100
Charge	0.1% (w/v)	-	-	-	-	-
Binding	-	50 mM	300 mM	-	0.25% (w/v)	0.25% (v/v)
Wash 1	-	50 mM	300 mM	-	0.2% (w/v)	-
Wash 2	-	50 mM	300 mM	-	0.1% (w/v)	-
Wash 3	-	50 mM	300 mM	50 mM	0.075% (w/v)	-
Elution	-	50 mM	300 mM	400 mM	0.05% (w/v)	-

Strip buffer consisting of 20 mM Tris-HCl (pH 8.0), 100 mM NaCl and 100 mM EDTA was used to remove the nickel, so the resin could be re-used.

2.5.4.4 Lysis buffer for TEV protease purification

Chemical	Concentration in dH ₂ O
Tris pH 8.0	50 mM
NaCl	500 mM
Glycerol	10% (v/v)
Imidazole	20 mM

EDTA-free protease inhibitor (Sigma Aldrich) was added to the Lysis buffer prior to cell disruption.

2.6 Microbiological methods

2.6.1 Plate cultures

Bacteria were spread on LB agar plates, containing appropriate antibiotics, next to the Bunsen burner and incubated overnight at 37 °C.

2.6.2 LB liquid cultures

Liquid cultures were inoculated to starting OD₆₀₀ of 0.01 using overnight starter cultures and grown at 37 °C at 160 rpm.

2.6.3 Preparation of competent cells

The desired strain was streaked out on an LB-agar plate and grown overnight at 37 °C. 3-4 colonies were used to inoculate 50 mL of LB and grown at 37 °C with shaking until the OD₆₀₀ reached ~0.3-0.5. The cells were then incubated on ice for 1 hour and centrifuged at 4000 rpm for 10 minutes at 4 °C. The cell pellet was gently resuspended in 10 mL of 0.1 M CaCl₂ (filter sterilised and pre-cooled) and incubated on ice for 30 minutes. Subsequently, the cells were pelleted 4000 rpm for 10 minutes at 4 °C, and gently resuspended in 1 mL of 0.1 M CaCl₂ containing 10% (v/v) glycerol (filter sterilised and pre-cooled). Competent cells were divided into 100 µL aliquots in sterile 1.5 mL tubes (pre-chilled), flash frozen on dry-ice and stored at -80 °C.

2.6.4 Transformation of competent cells

Competent cells were thawed on ice for 15 minutes prior to addition of exogenous DNA. For single transformations, 0.2 µL of purified plasmid DNA was mixed with 50 µL competent cells. For transformation of ligated vectors, 5 µL of the ligation mixture was added to 50 µL competent cells. The cells were then incubated on ice for 15 minutes, heat shocked at 42 °C for 1 minute and incubated on ice for further 2 minutes. After the addition of 150 µL of sterile LB, the cells were incubated at 37 °C for 30 minutes. The mixture was then spread on an LB plate containing appropriate antibiotics and incubated overnight at 37 °C.

2.6.5 Production of recombinant proteins

E. coli strain BL21 (DE3) Star competent cells were transformed with a vector containing the gene(s) of interest. The recombinant strain was grown in LB with ampicillin at 37 °C with shaking (160 rpm). When the OD₆₀₀ reached 0.4-0.8, protein expression was induced

with 100 μ M IPTG overnight at 19 °C. The following day cells were sedimented by centrifugation at 4000 rpm for 10 minutes at 4 °C.

2.6.6 Generation of TEV protease

E. coli BL21 (DE3) competent cells were transformed with a pRK793 vector encoding for the TEV protease. The cells were grown at 37 °C until the OD₆₀₀ reached 0.6-0.8, at which point protein production was induced with 50 μ M IPTG and left overnight at 19 °C. Cells were pelleted, resuspended in Lysis buffer (refer to **section 2.5.4.4**) and disrupted using a homogeniser. The soluble and the insoluble cell fractions were separated via centrifugation, with the soluble fraction loaded onto an equilibrated Ni-NTA column, as the TEV-protease is His-tagged. The protein was eluted in linear gradients of imidazole up to 600 mM, with the protein eluting around 250-300 mM imidazole, although SDS-PAGE analysis should be carried out to confirm this each time. To greatly reduce imidazole concentration, the correct fractions were pooled together and dialysed in 20 mM phosphate buffer pH 6.0, 250 mM and 10% (v/v) glycerol. Aliquots were stored at -20 °C.

2.7 Molecular biology

2.7.1 Gene synthesis

The synthesis of the *PA4368* gene and the C-terminal sfGFP construct was carried out by Eurofins™.

2.7.2 Polymerase Chain Reaction (PCR)

The FastStart High Fidelity PCR System from Roche™ was used to amplify genes of interest according to the standard protocol. The amount of DMSO used for each reaction was between 0-5 μ L. The annealing temperature was dependant on the primers used and varied between 58-68 °C. The typical PCR reaction is summarised on the following page.

Reagent	Volume (μL)
FastStart High Fidelity Reaction Buffer 10X	5
200 μM dNTP	5
Forward primer (0.2 μM)	5
Reverse primer (0.2 μM)	5
Template DNA	1
FastStart High Fidelity Enzyme Blend	0.5
DMSO	0 - 5
ddH ₂ O	Adjusted to 50
Total Volume	50
Thermocycler programme	
(1X cycle) 95 °C	2 minutes
(35X cycle) 95 °C	30 seconds
61/62 °C (primer dependant)	30 seconds
72 °C	1 min/1000 bp
72 °C	7 minutes
4 °C	Hold

2.7.3 Plasmid purification

QIAprep Spin Miniprep and Midiprep Kits from Qiagen™ were used to purify plasmids using the standard protocol provided using a microcentrifuge. Plasmids were eluted in 30 μL and 1 mL of elution buffer for Miniprep and Midiprep, respectively.

2.7.4 Restriction digests

Restriction enzymes from Promega™ and/or NEB were used for digestion of plasmids or DNA fragments, according to manufacturer's instructions. Buffers that had less than 50% activity for each enzyme, were not used. Briefly, a typical restriction reaction included 5 μL of Miniprep DNA, 1 μL of 10X Buffer, 0.5 μL of each restriction enzymes and made up to 10 μL with sterile ddH₂O. The reaction was incubated at 37 °C for 1-2 hours.

2.7.5 Ligations

Vector and insert were digested with the relevant restriction enzymes, as described above. The ligation reaction was carried out at room temperature for 2 hours or at 4°C overnight.

A typical ligation reaction:

Reagent	Volume (μL)
Insert	3.5
Vector	1
2X Ligation buffer	5
T4 DNA Ligase (Promega)	0.5

2.7.6 DNA electrophoresis

Agarose-TAE gels (0.8% (w/v)) were used to separate DNA fragments according to size. Ethidium bromide, at a final concentration of 0.5 $\mu\text{g}/\text{mL}$, was used to visualise the DNA. Prior to loading of sample, DNA was diluted using the 5X DNA loading buffer (Bioline). HyperLadder™ 1kb (Bioline) was used to estimate fragment sizes. The gel was placed onto a UV transilluminator (UVITEC) for visualisation.

2.7.7 Extraction from DNA gels

The DNA fragment corresponding to the expected size was excised out of the agarose gel with a scalpel. The QIAquick Gel Extraction Kit was used according to manufacturer's instructions to extract the DNA. The DNA was eluted into 30 μL of Elution Buffer.

2.7.8 DNA sequencing

Samples were shipped to Genewiz™ for Sanger Sequencing to confirm the correct sequence identity. Plasmids and the appropriate primers were diluted to 100 $\text{ng}/\mu\text{L}$ and 5 $\text{pmol}/\mu\text{L}$ using sterile MilliQ water, respectively.

2.8 Membrane protein purification, NMR and crystallisation

2.8.1 Production of ^{15}N labelled protein

E. coli BL21 (DE3) Star competent cells were transformed with a vector containing the gene of interest. A single colony was used to prepare a 10 mL LB overnight starter culture. 4X 1L of LB containing ampicillin was inoculated to a starting OD_{600} of 0.01 using the starter culture and grown at 37 °C with shaking (160 rpm) until OD_{600} reached approximately 0.7. The cells were pelleted at 4000 rpm for 20 minutes, resuspended in 200 mL of 1X M9 salt solution. Following this wash step, the cells were pelleted at 4000 rpm for 20 minutes and resuspended in 1 L of the minimal media broth (refer to Section 2.5.3.3). The culture was

incubated at 37 °C for 45 minutes prior to being induced with 100 µM IPTG and moved to a 19 °C room with shaking (160 rpm) overnight.

2.8.2 Protein solubilisation

Biomass was harvested at 4000 rpm for 20 minutes and resuspended in lysis buffer (HEPES 50 mM pH 8, 300 mM NaCl and EDTA-free protease inhibitor). Cells were lysed using a sonicator for 10 minutes with a 30 second on 30 second off cycle at an amplitude of 55%. Cell membranes were pelleted at 18,000 rpm for 20 minutes, resuspended in lysis buffer and homogenised. The lysis buffer was supplemented with 1% (w/v) DDM and 1% (v/v) Triton X-100 and left overnight on a rotary spinner at 4 °C.

2.8.3 Purification of membrane proteins using IMAC

The solubilised mixture was pelleted at 18,000 rpm for 20 minutes and the cell debris was removed. 20 mL of Chelating Sepharose Fast Flow resin was loaded into a column, washed with 100 mL of dH₂O and subsequently charged with 50 mL of Charge buffer. The column was equilibrated with 50 mL of Binding buffer, after which the supernatant was applied to the column. The column was then washed with decreasing concentrations of DDM using 100 mL of Wash 1 buffer, followed by 100 mL of Wash 2 buffer. A final wash using 50 mL of Wash 3 buffer was allowed to equilibrate in the column prior to elution. Protein of interest was eluted with 25 mL of elution buffer and 1 mL elution fractions were collected. Nickel was removed from the column using 50 mL of strip buffer and the column was washed with 50 mL of dH₂O and stored in 20% (v/v) ethanol solution at 4 °C.

2.8.4 C-terminal tag cleavage

The expression of the *PaLemA1-sfGFP* construct that harbours a TEV protease cleavage site between PaLemA1 and sfGFP-His tag, required the removal of the sfGFP tag since the PaLemA1 protein was intended for structural analysis. Following the purification of this fusion protein using the IMAC column, the eluted fractions were pooled and together with the TEV protease placed into dialysis tubing (10,000 kDa cut-off). The dialysis tube was placed in 50 mM HEPES buffer pH 8.0 with 1 mM DTT and the cleavage reaction was carried out at 4 °C overnight. Subsequently, to reduce the DTT concentration, the dialysis tube was transferred into 50 mM HEPES buffer pH 8.0 only for 3-4 hours at room temperature. The dialysed contents were then collected and centrifuged to remove the aggregated protein and the supernatant was loaded onto a pre-equilibrated Ni-NTA column. The eluted protein was collected, concentrated and separated on a size exclusion chromatography column.

2.8.5 SDS-PAGE

The composition of the gel, buffers and stain were as described in Section **2.5.4.1**. Prior to analysis, the sample was denatured by addition of 2X Laemmli buffer in a 1:1 ratio (sample:buffer) and boiled for 10 minutes. 10-20 μ L of each denatured sample and a single 5 μ L of molecular mass marker were loaded onto each gel. Electrophoresis was performed using the Atto Dual Mini Slab AE6450 apparatus, at a constant voltage of 200 V for ~1.5 hours. The gels were stained with the Coomassie Blue stain for 10-30 minutes and de-stained in dH₂O overnight.

2.8.6 Size exclusion chromatography

Eluted fractions were concentrated using the Amicon® Ultra-15 10 kDa cut-off centrifugal filter columns and applied to a pre-equilibrated Superdex™ S200 Increase 10/300 column (GE Healthcare), in buffer (50 mM Hepes pH 7.4, 20 mM NaCl, 0.03% (w/v) DDM). The protein was eluted at 0.35 mL/min into 0.5 mL fractions. Fractions were analysed using SDS-PAGE and the purest fractions were pooled together.

2.8.7 A₂₈₀ protein concentration estimation

Purified PaLemA1 protein concentrations were estimated using the NanoDrop™ One/OneC Microvolume UV-Vis Spectrophotometer (Thermo Fisher) by recording the OD₂₈₀ and using the molecular mass of the protein and the predicted extinction coefficient for the protein. Concentrations were provided in mg/mL.

2.8.8 Nuclear magnetic resonance (NMR)

¹H-¹⁵N Best TROSY HSQC spectra were acquired on a Bruker Avance III spectrometer at a proton frequency of 600MHz using a QCIP cryoprobe. Time domain data of 1048 and 128 complex points were used in the direct and indirect domains respectively. The sweep widths used in the ¹H and ¹⁵N dimensions were 8403.361 and 1824.291 Hz respectively. The inter scan delay was set to 200 ms and 128 scans were acquired per increment with 32 dummy scans at the start of each experiment. 2D spectra were processed with NMRPipe5 and analysed using NMRView.

2.8.9 Lipidic cubic phase (LCP) crystallography

Following size exclusion chromatography protein fractions of interest were concentrated until the protein concentration reached ~10-25 mg/mL. The purified protein was reconstituted into LCP by mixing protein solution with molten monoolein in a volume ratio

2:3 (protein:lipid), using a syringe mixer. Crystallisation screens were performed using the mosquito[®] crystal robot (SPTLabtech) dispensing 50 nL of protein-laden LCP and overlaying it with 800 nL of precipitant solution in each well of a 96-well Laminex™ plastic sandwich plate (Molecular Dimensions). Plates were stored in a 19 °C incubator and checked periodically for crystal formation using a light microscope.

2.9 Confocal microscopy

2.9.1 Sample preparation

Following growth and induction of fluorescent protein expression, 1 mL of cell culture was fixed using 3% (w/v) paraformaldehyde in PBS solution for 20 minutes at room temperature. The cells were pelleted at 4000 rpm for 3 minutes then washed with 0.3 M glycine in PBS and once with PBS alone. The cells were pelleted, resuspended in 10 µL of PBS and 10 µL of the ProLong Gold mountant, pipetted onto a 1.5 mm thickness coverslip before being inverted on a glass slide. Slides were incubated overnight at room temperature in the dark to cure.

2.9.2 Immunofluorescence staining

50 mL of sterile LB was inoculated with 3-4 colonies from a fresh overnight LB agar plate and incubated at 37 °C until OD₆₀₀ was 0.6-0.8. The culture was induced with 100 µM of IPTG and incubated overnight at 19 °C at 160 rpm. To adhere cells onto a surface, sterile coverslips were prepared by incubation in 0.01% (w/v) Poly-L-Lysine solution (Sigma P8920) at room temperature for 10 minutes, and subsequently dried. Following the overnight induction, the cells were fixed with 3% (w/v) paraformaldehyde in PBS for 20 minutes at room temperature. 1 mL of fixed cells were centrifuged at 4000 rpm for 3 minutes and the pellet was washed with 1 mL of PBS, pelleted and resuspended in 100 µL of PBS. Each Poly-L-Lysine coated coverslip was incubated with 50 µL of the cell solution for 15 minutes at room temperature. The supernatant was aspirated and the coverslip was washed once with 0.3 M glycine in PBS and once with PBS alone. The cells were permeabilised using 0.1% (v/v) Triton X-100 in PBS solution for 5 minutes at room temperature, then washed twice with PBS. The coverslip was incubated for 45 minutes in the blocking solution: 10% (v/v) inactivated FCS in PBS. Primary antibody (1 mg/mL) was diluted to a ratio of 1:1000 (antibody:blocking solution) and the cells were incubated for 1 hour, before being washed twice with PBS and placed in blocking solution for a further 15 minutes. Secondary antibody

(1 mg/mL) was diluted to a ratio of 1:100 (antibody:blocking solution) and the cells were incubated in the dark for 45 minutes, washed and the coverslips were mounted onto clean glass slides using 5 μ L of ProLong Gold DAPI. Samples were visualised using the Zeiss LSM 880 confocal microscope with Airyscan.

2.10 Electron microscopy

2.10.1 Preparation of whole cells

Multiple colonies from a freshly grown LB agar plate were used to inoculate 50 mL of LB. The cells were grown at 30 °C and incubated with shaking at 160 rpm until the OD₆₀₀ reached 0.6-0.8. Protein production was induced with 100 μ M IPTG and the cells were incubated overnight at 19 °C and 160 rpm.

2.10.2 Fixing and embedding bacteria in resin

Cells were harvested at 4000 rpm for 10 minutes. The cell pellet was resuspended in 2.5% (v/v) glutaraldehyde, 100 mM sodium cacodylate pH 7.2 in dH₂O and incubated with gentle spinning at room temperature for 2 hours. Cells were pelleted at 10,000 rpm for 2 minutes and washed twice with 100 mM sodium cacodylate pH 7.2 in dH₂O. Cells were stained with 1% (v/v) osmium tetroxide in 100 mM sodium cacodylate pH 7.2 in dH₂O for 1 hour, and were subsequently washed twice with dH₂O. Dehydration was achieved by incubation of the cells in an ethanol gradient, 50% (v/v) ethanol for 10 minutes, 70% (v/v) ethanol overnight, 90% (v/v) ethanol for 10 minutes followed by three 10 minute 100% (v/v) ethanol washes. The samples were further dehydrated by two 10 minute propylene oxide (PO) washes. Pelleted cells were resuspended in 1 mL of a 1:1 mix of propylene oxide and Agar LV Resin and incubated for 30 minutes with spinning. Cells were harvested via centrifugation and incubated in 100% (v/v) Agar LV Resin for 1.5 hours twice. The cell pellet was resuspended in fresh resin and transferred to a 0.5 mL embedding mould, centrifuged for 1100 rpm for 5 minutes and incubated for 18 hours and 60 °C.

2.10.3 Ultra-thin sectioning and staining of embedded samples

The samples were thin sectioned using the Leica EM UC7 ultramicrotome with a diamond knife (diatome 45°). Sections were placed on 300 mesh copper grids (Agar Scientific™) and left to dry.

Grids were stained by incubation in 4.5% (w/v) uranyl acetate in 1% (v/v) acetic acid solution for 45 minutes, followed by 2 washes in dH₂O. The grids were then transferred to 0.1% (w/v) lead citrate solution for 8 minutes and lastly washed in dH₂O.

2.10.4 Visualisation of samples

Samples were imaged using the JEOL-1230 TEM.

2.11 Field Emission Scanning Electron Microscopy

E. coli BL21 (DE3) Star cells harbouring a plasmid of interest were used to inoculate 50 ml LB supplemented with 0.1 mg/mL ampicillin in baffled flasks. Cells were incubated at 37 °C with shaking until OD₆₀₀ reached approximately 0.4-0.6, and protein production was induced with 100 µM IPTG. Cultures were incubated overnight at 19 °C with shaking. Subsequently, the cells were fixed with 2% (v/v) glutaraldehyde for 30 minutes, after which formaldehyde was added to a final concentration of 5% (v/v). After 1 hour on ice, the fixed bacteria were washed twice in TE buffer (20 mM TRIS pH 6.9, 1 mM EDTA) for 10 minutes, then dehydrated for 15 minutes in a series of graded acetone concentrations (10% (v/v), 30% (v/v), 50% (v/v), 70% (v/v) and 90% (v/v)) on ice. Samples in the 100% (v/v) acetone step were allowed to reach room temperature before another change to 100% (v/v) acetone was carried out. The samples were then subjected to critical-point drying with liquid CO₂ (CPD 30, Bal-Tec, Liechtenstein). Dried samples were fixed onto aluminium stubs with a conductive adhesive tape and covered with a gold/palladium film by sputter coating (SCD 500 Bal-Tec, Liechtenstein) before examination in a field emission scanning electron microscope Zeiss Merlin (Zeiss, Oberkochen) using the Everhart Thornley HESE2 detector and the inlens SE detector in a 25:75 ratio with an acceleration voltage of 5 kV using the SEM software 5.5.

2.12 Mammalian cell experiments

2.12.1 Generating *PalemA1* harbouring pcDNA3.1/V5-His-TOPO vector

Following unsuccessful attempts at sub-cloning the *PalemA1* gene from the pET3a PaLemA1 vector using primers with a V5 tag overhang, a gene fragment including the *PalemA1* with an in-frame V5 tag was synthesised with KpnI and NheI restriction sites by Eurofins™. Subsequently, the empty pcDNA3.1/V5-His-TOPO vector and the PaLemA1-V5 gene fragments were both digested with KpnI and NheI restriction endonucleases. The

generated PaLemA V5 insert and the cut vector were ligated together. Positive clones were identified using test digests and confirmed via sequencing.

2.12.2 Routine cell culture of Chinese Hamster Ovary-S (CHO-S) cells

Cryopreserved CHO-S cells were recovered by thawing the vial of cells at room temperature. The thawed cells were transferred to 10 mL of warm medium (37 °C) and sedimented at 1,000 rpm for 5 minutes. The supernatant was discarded and the cell pellet was resuspended in 20 mL of 37 °C warm medium supplemented with 8 mM of L-glutamine and transferred to a 125 mL Erlenmeyer flask (Corning®) and incubated in a 5% CO₂ environment with shaking (140 rpm) for three days.

The CHO-S host cell line was cultured in CD-CHO medium (ThermoFisher Scientific) supplemented with 8 mM of L-glutamine at 37 °C in a 5% CO₂ environment and shaking at 140 rpm. The ViCell (Beckman Coulter) instrument was used for routine cell counts by using 1 mL of cell culture sample to determine total as well as viable cell concentrations. Cell viability was determined as the number of viable cells present as a proportion of total cell population. Cells were sub-cultured every 3-4 days, seeding new cultures at 0.2X 10⁶ viable cells per mL in 20 mL of culture volume in a 125 mL Erlenmeyer flask (Corning®).

2.12.3 Transient transfection of CHO-S cells

For every single transfection 1X 10⁷ of cells were taken from the culture medium, sedimented using centrifugation (1000 rpm for 5 minutes), at which point the supernatant was removed and the cells were resuspended in 0.7 mL of 37 °C CD-CHO media supplemented with 8mM L-glutamine. 20 µg of the vector pcDNA3.1/V5-His-TOPO LemA1 in 100 µL of TE buffer was added to the cells, and the solution was transferred to a 4 mm transfection cuvette. Electroporation of cells was achieved by delivering a voltage via the Gene Pulser Xcell™ (Bio-Rad) at 250 V and 900 µF. The electroporated mixture was added to 18.5 mL of warm CD-CHO and 8mM L-glutamine media in 125 mL Erlenmeyer flask. The cuvette was washed with 0.7 mL of warm culture medium and added to the culture vessel. Each experiment was done in triplicate and a control was run in parallel whereby the empty pcDNA 3.1 Hygro (+) V5 vector was used as the control. The cells were grown at 37 °C in a 5% CO₂ environment and shaking at 140 rpm for 48 hours.

2.12.4 Generation of stable CHO-S cell lines

The PaLemA gene was cloned into the pcDNA3.1/V5-His-TOPO vector and the CHO-S cells were transfected as described in section 2.11.1, apart from the final culturing step. Following the electroporation, the cells were grown at 37 °C in a 5% CO₂ environment and shaking at 140 rpm for 24 hours. Subsequently, the selection marker, Hygromycin B, at a concentration of 500 µg/mL was added to the culture media to select for cells producing PaLemA.

2.12.5 Immunofluorescence analysis

Due to the fact CHO-S cells are adapted for growth in suspension, sterile 13 mm round coverslips coated in poly-L-lysine solution were used to adhere cells onto a surface. The coverslips were placed inside a 24 well plate and the cells were seeded at 2×10^5 cells/well in 1 mL of medium and incubated overnight in a static incubator at 37 °C and 5% CO₂, to ensure adhering. The following day the medium was aspirated and the cells were rinsed with 1 mL of warmed (37 °C) phosphate buffered saline. Cells were fixed and permeabilised with ice cold methanol (100% (v/v)) for 5 minutes, after which the methanol was removed and the cells were washed four times in 1 mL of PBS. The cells were incubated for 20 minutes at room temperature in the blocking solution containing 3% (w/v) BSA in PBS. During this time the primary antibodies were prepared by diluting the mouse anti-V5 antibody 1:500 and rabbit anti-calnexin antibody in the blocking solution. The coverslips were then directly transferred into the primary antibody containing blocking solution and left to incubate at 4 °C overnight in a damp box. The coverslips were then incubated four times in 0.1% (v/v) Tween in PBS for 5 minutes. Ensuring limited light was present from this step onwards, the secondary antibodies, goat anti-TRITC and mouse anti-FITC, were diluted 1:100 in 3% (w/v) BSA in PBS. This preparation was centrifuged at 13,000 rpm for 10 minutes to remove any antibody aggregates. Coverslips were placed into the secondary antibody solution and left to incubate in the dark at room temperature for 2 hours. Subsequently, the coverslips were washed in 0.1% (v/v) Tween in PBS 4 times before being incubated in 50 µL of DAPI for 1 minute at room temperature. The coverslips were then washed as mentioned prior to being placed into a small amount of mounting reagent (ProLong Diamond) on a glass slide and allowed to cure overnight at 4 °C in a light protected box. The cells were visualised on the Zeiss LSM 880 confocal microscope with Airyscan.

2.12.6 Western blot

Prior to SDS-PAGE gels analysis (as described previously in section **2.8.5**), the total amount of protein present in the sample was determined using a Bradford assay and Jenway 6705 UV/Vis spectrophotometer at 595 nm. The nitrocellulose membrane was equilibrated in methanol for 10 seconds, washed with dH₂O and equilibrated in transfer buffer, together with the SDS-PAGE gel. The proteins were electrophoretically transferred onto the nitrocellulose membrane in a cooled gel tank at the constant voltage of 100 V for 1 hour. The membrane was incubated in blocking solution composed of 5% (w/v) skimmed milk powder in phosphate buffered saline (PBS), at 4 °C overnight. Subsequently, the membrane was incubated with the primary antibody diluted to an appropriate concentration in PBS for 2 hours with gentle agitation. The membrane was rinsed 3 times in PBS and equilibrated in phosphate-free solution for 10 minutes at room temperature. An alkaline phosphate-coupled secondary antibody (at a dilution of 1:5000) was added to the phosphate-free solution containing 5% (w/v) skimmed milk powder, the membrane was incubated in this solution for 1 hour with gentle agitation. The solution was then discarded, and the membrane was washed in phosphate-free solution 3 times for 10 minutes at room temperature. The membrane was equilibrated in distilled water after a single tablet of the chromogenic substrate, 5-Bromo-4-chloro-3-indolyl phosphate/Nitro blue tetrazolium (BCIP/NBT), was dissolved in 10 mL of distilled water. The membrane was placed in the BCIP/NBT solution. After sufficient colour had developed the membrane was removed, rinsed with distilled water, dried, and visualised using a camera.

2.12.7 Fixing and embedding CHO-S cells in LV resin

To perform conventional electron microscopy studies of CHO-S cells, 2X 10⁵ cells/well were seeded onto sterile 13 mm round coverslips coated in poly-L-lysine solution inside a 24 well plate. The cells were incubated in 1 mL of medium overnight in a static incubator at 37 °C and 5% CO₂, to ensure adhering. To begin, the cells were fixed with 2.5% (v/v) glutaraldehyde in 100 mM sodium cacodylate buffer for 2 hours, followed by an incubation in 1% (v/v) OsO₄ for 1 hour. The cells were washed twice in 100 mM sodium cacodylate buffer, followed by an incubation in 1% (v/v) OsO₄ for 1 hour. The cells were then dehydrated in an ethanol gradient, 50% (v/v) EtOH for 10 min, 70% (v/v) EtOH for 10 min, 90% (v/v) EtOH for 10 min, followed by three 15 min washes in 100% (v/v) EtOH. Subsequently, the cells were further dehydrated in propylene oxide prior to being

incubated in 1:1, LV Resin:propylene oxide solution for 30 minutes. The cells were then incubated in 100% (v/v) LV Resin for 2 hours twice, before being placed into moulds and polymerised at 60 °C for 18 hours.

The blocks containing cells were sectioned using the Leica EM UC7 ultramicrotome with a diamond knife (diatome 45°) and the 70 nm cell sections were collected onto copper-coated grids (Agar Scientific). Cell sections were stained using 4.5% (w/v) uranyl acetate in 1% (v/v) acetic acid solution for 45 minutes followed by 2 washes in ddH₂O, after which the grids were incubated in 0.1% (w/v) lead citrate for 8 minutes followed by a wash in ddH₂O. Samples were imaged using the JEOL-1230 TEM.

2.12.8 Embedding cells in LR white resin for immunolabelling

CHO-S cells were seeded at 2×10^5 cells/well onto sterilised aclar coverslips in a 24 well plate and incubated for 24 hours at 37 °C and 5% CO₂. Subsequently the cells were fixed with 2% (v/v) formaldehyde and 0.5% (v/v) glutaraldehyde in 100 mM sodium cacodylate buffer. The cells were dehydrated in an increasing ethanol gradient, 50% (v/v) EtOH for 10 min, 70% (v/v) EtOH for 10 min, 90% (v/v) EtOH for 10 min, followed by three 15 min washes in 100% (v/v) EtOH. Following this step, the cells were incubated in 100% (v/v) LR white resin for 12 hours, 3 times. The aclar discs were then cut in half and inserted into a gelatine capsule size 00 (Agar Scientific) and filled up to the top with LR white resin. A lid was placed on top as LR white resin does not polymerise well in the presence of oxygen. The sample was incubated at 60 °C for 20 hours.

The cells were sectioned using the Leica EM UC7 ultramicrotome with a diamond knife (diatome 45°) and the 80 nm cell sections were collected onto copper-coated grids.

2.12.9 Immunolabelling of LR white resin embedded samples

The grids containing cell sections of CHO-S cells embedded in LR white resin were first hydrated in Tris-buffered saline with Tween (TBST) buffer (20 mM Tris pH 7.4, 500 mM NaCl, 0.1% (w/v) BSA, 0.05% (v/v) Tween 20), before being transferred into the blocking solution. The sectioned cells were incubated in the blocking solution, composed of 2% (w/v) BSA in TBST buffer, for 30 minutes at room temperature. In the meantime, primary antibody (mouse anti-V5) dilutions (1:25, 1:50, 1:100, 1:250 and 1:500) were prepared in TBST buffer. The grids were then incubated with the primary antibody for 1 hour and subsequently washed in TBST buffer alone 6 times. The secondary antibody, goat anti-

rabbit gold IgG containing a 15 nm gold particle, was diluted 1:50 in TBST buffer. Two lines of drops containing the secondary antibody were deposited onto Parafilm™. Excess moisture was removed from the grids and they were firstly placed into the first drop containing secondary antibody before being moved into the second drop. This was done to ensure the secondary antibody was not diluted from the wash steps. The grids were incubated in secondary antibody for 30 minutes at room temperature and washed in TBST 6 times and ddH₂O before allowing the grids to dry. To ensure no unspecific cross-reactivity of the antibodies or contamination of the TBST buffer occurred, grids that were only incubated in TBST buffer, primary or secondary antibodies alone were used as control samples.

Cell sections were stained in 4.5% (w/v) uranyl acetate in 1% (v/v) acetic acid solution for 15 minutes followed by 2 washes in ddH₂O, after which the grids were incubated in 0.1% (w/v) lead citrate for 3 minutes followed by 2 washes in ddH₂O. Samples were imaged using the JEOL-1230 TEM.

Chapter 3

Analysis of *Pseudomonas aeruginosa* PA14 PaLemA1 and PaLemA2 proteins

3.1 Introduction

For many years, prokaryotic organisms were distinguished from eukaryotic cells based on their lack of cytoplasmic membrane-bounded organelles. However, recent advances in analytical methods, such as super resolution imaging, have led us to the discovery of multiple prokaryotic organelles, changing this view. These organelles include anammoxosomes, magnetosomes, bacterial extracellular vesicles (BEVs), and others.

Magnetosomes are membranous organelles which are composed of a ferromagnetic crystal enclosed within a lipid bilayer, which allow MTBs to orientate themselves within magnetic fields (Komeili *et al.*, 2006). Previously conducted work on magnetosomes revealed that deletion of MamQ in *Magnetospirillum magneticum* leads to the complete abolishment of membrane vesicle formation, a key step required for the synthesis of this organelle (Murat *et al.*, 2010). MamQ is homologous to an integral membrane protein family known as LemA, which are predicted to have an N-terminal membrane spanning domain, and a C-terminal soluble domain, though their function remains uncharacterised.

To investigate the membrane restructuring properties of the LemA protein family, some of these proteins were overproduced in our model organism, *E. coli*, and analysed using transmission electron microscopy (TEM). *E. coli* was chosen as the model bacterium as it has been extensively studied and utilised for a multitude of biotechnological applications. Also, this bacterium does not normally produce any intracellular compartments, providing a relatively simplified landscape to work with.

Previously, four different LemA proteins were overproduced in *E. coli* and analysed using TEM. One of the most interesting phenotypes discovered was that of the PaLemA1 protein from *Pseudomonas aeruginosa* PA14 strain, which led to the formation of spherical intracellular vesicles that appeared uniform in shape and size (Juodeikis, 2016). As BEVs have been a popular target for vaccine development in recent decades, it was our imperative to investigate the membrane restructuring effects of *P. aeruginosa* LemA proteins. The work conducted as part of this chapter will contribute towards our understanding of LemA protein induced vesiculation and help us to assess the feasibility of these *E. coli* derived vesicles as potential future vaccine delivery platforms.

To gain a better understanding of the biogenesis of these vesicles, a number of studies were performed. In addition to PaLemA1, a second LemA protein, PaLemA2, was found in

the *P. aeruginosa* (PA14 strain) genome. It was overproduced in *E. coli* and assessed for a membranous phenotype using TEM. Also LemA fusion proteins which consisted of PaLemA1 or PaLemA2 with a fluorescent protein were generated. These fusion constructs were used to study the localisation of the LemA proteins and assess their ability in delivering proteins of interest to the membranes.

Moreover, to confirm the relationship between *PalemA1* and *PalemA2* overexpression and vesicle formation, time-course studies were completed and analysed using TEM. Scanning electron microscopy (SEM) was utilised to assess the OM vesiculation in the case of both PaLemA1 and PaLemA2. Lastly, to examine the effects of *PalemA1* expression in a mammalian cell host, this protein was cloned into a Chinese Hamster Ovary (CHO) cell compatible vector and produced in a CHO-S cell line.

3.2 Results

3.2.1 Expression of *PalemA1* and *PalemA2* in *E. coli*

To investigate the membrane restructuring properties of PaLemA1 and PaLemA2, pET3a vectors encoding each of the respective genes were overexpressed in *E. coli* BL21 (DE3) Star cells overnight, with an empty pET3a vector being used as a control (**Table 3.1**). The cells were then harvested, fixed, embedded, sectioned, stained and imaged as described in materials and methods. A combination of both TEM and SEM was utilised to assess the morphological changes in bacterial cell structure.

Electron microscopy analysis of *E. coli* cells producing PaLemA1 revealed the formation of intracellular vesicles (**Figure 3.1**), which appear to be relatively small, having an approximate diameter of 50 nm. Longitudinal sections of these cells did not reveal any tubular structures, supporting the finding that the vesicles must be spherically shaped. The vesicles appeared to predominantly localise to areas with protein aggregation, which are indicated by the denser regions of the cytoplasm lacking ribosomes in the transmission electron micrographs (**Figure 3.1**, panels **D** and **E**). Additionally, some cellular lysis was observed however, the vesicles appeared to remain intact and hold their spherical shape (**Figure 3.1**, panel **F**). In these lysed cells an identifiable lipid bilayer was distinguishable from the lumen of the vesicles due to differential negative staining, further supporting the theory that these vesicles originate from the cellular membrane. These findings are in accordance with previously obtained data (**Figure 1.9**) and confirm the reproducibility of the PaLemA1-driven phenotype in the *E. coli* host.

Overexpression of *PalemA2* in *E. coli* also revealed the formation of intracellular vesicles but of varying sizes, with the majority ranging from 50 nm - 300 nm in diameter (**Figure 3.1**, panels **G**, **H** and **I**). The electron micrographs also showed some inclusion body formation, as well as an increase in membrane production, as intracellular ectopic membranes were observed.

To quantify the proportion of cells displaying a membranous phenotype following PaLemA1 and PaLemA2 overproduction, 600 cells were counted for each sample and assessed for intracellular vesicles and ectopic membrane production (**Table 3.1**). Overall, a membranous phenotype was observed in 86% of PaLemA1, and 73% of PaLemA2 overproducing cells. Comparatively, this phenotype was present in 10.8% of the control cell population.

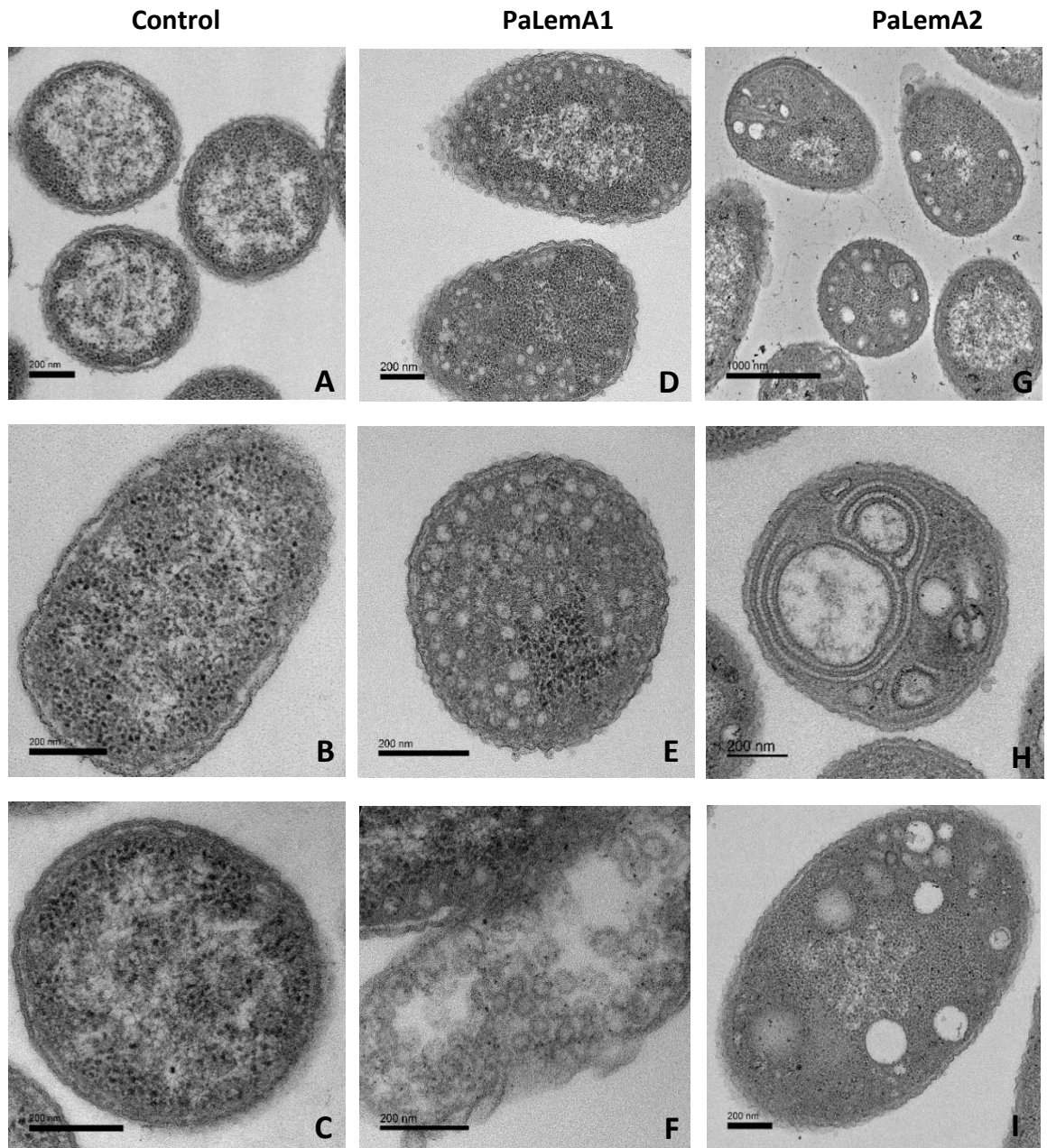


Figure 3.1. TEM of *E. coli* expressing PaLemA1 and PaLemA2.

Transmission electron micrographs of *E. coli* BL21 (DE3) Star cell sections producing PaLemA1 (panels **D**, **E** and **F**) and PaLemA2 (panels **G**, **H** and **I**) proteins overnight. Following PaLemA1 overproduction small intracellular vesicles were observed in the cytoplasm (**D**, **E**), and despite cell lysis these vesicles appeared to remain intact in some cells (**F**). PaLemA2 resulted in the formation of larger intracellular vesicles which displayed a range of different sizes (**G**, **I**), as well as ectopic membrane production (**H**) as excess membrane was seen in the cytoplasm of some cells. An empty pET3a vector was used as the control to show the typical morphology of *E. coli* cells (panels **A**, **B** and **C**).

To assess for morphological changes in cell structure, *E. coli* cells overproducing PaLemA1 and PaLemA2 overnight were analysed using SEM (**Figure 3.2**). The control cells containing an empty pET3a vector had a rather rough appearance, with wrinkles being visible on the cell surface (**Figure 3.2**, panel A). A few cells appeared to be elongated and the production of small vesicles could be observed on the surface of the cell.

The *E. coli* strain producing PaLemA1, which is predicted to localise to the inner membrane, produced smooth looking cells that appeared to be elongated (**Figure 3.2**, panel B). However, no significant differences in extracellular vesiculation could be seen in comparison to the control. On the other hand, the sequence of PaLemA2 contains a putative lipoprotein signal peptide which is predicted to target the protein towards the outer membrane, where it is possibly secreted. It was therefore intriguing to examine whether this would encourage increased extracellular vesiculation. Interestingly, PaLemA2 overproduction in *E. coli* yielded an increase in extracellular vesicle formation (**Figure 3.2**, panel C). Moreover, the expression of *PaLemA2* appeared to favour the formation of larger vesicles on the surface of the cell. SDS-PAGE analysis showed observable overproduction of both PaLemA1 and PaLemA2 (**Figure 3.3**).

Name	Organism	UniProt ID	Molecular weight (kDa)	TMDs	Predicted localisation
PaLemA1	<i>Pseudomonas aeruginosa</i> PA14	AOA0H2ZF10	21.05	1	Inner membrane
PaLemA2	<i>Pseudomonas aeruginosa</i> PA14	AOA0H2ZKG2	22.19	0	Outer membrane

Table 3.1. *Pseudomonas aeruginosa* PA14 LemA proteins chosen for analysis.

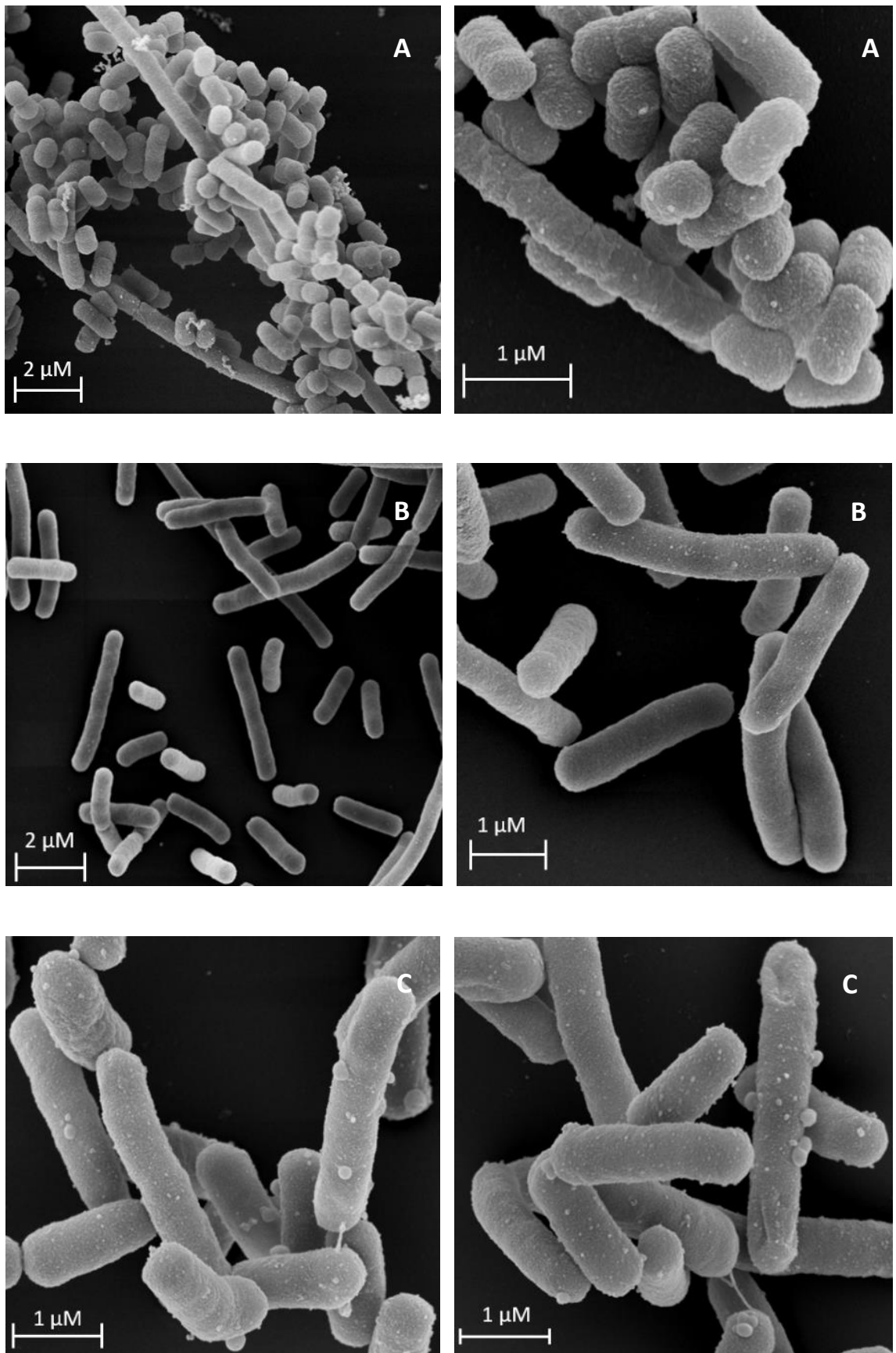


Figure 3.2. Scanning electron micrographs of recombinant *E. coli* cells expressing *PaLemA1* and *PaLemA2*.

SEM of *E. coli* BL21 (DE3) Star cells producing PaLemA1 (B) or PaLemA2 (C) following an overnight induction with IPTG. An empty pET3a vector was used as the control (A).

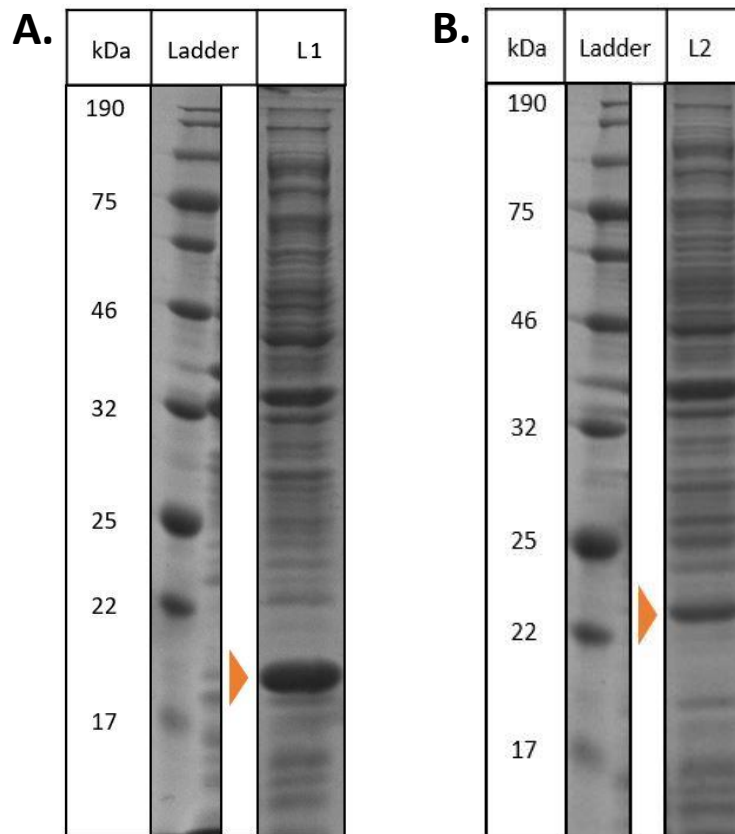


Figure 3.3. SDS-PAGE analysis of *E. coli* cells overexpressing *PaLemA1* and *PaLemA2*.

A) PaLemA1 overproduction (L1). **B)** PaLemA2 overproduction (L2). **Arrows** indicate bands of interest for PaLemA1 and PaLemA2.

3.2.2 Localisation studies for PaLemA1 and PaLemA2 in *E. coli*

In order to determine the cellular localisation of PaLemA1 and PaLemA2 a variety of *E. coli* constructs were made. Initial studies focused on immunofluorescent approaches which utilise antibodies to target fluorophores to specific protein targets, thus allowing the visualisation of the distribution of the target molecule. As part of this *E. coli* cells were grown and induced with IPTG, with samples being collected over a course of 3 hours. The cells were fixed in paraformaldehyde, permeabilised and stained with either anti-PaLemA1 or anti-PaLemA2 primary antibodies. Specific secondary antibodies conjugated to a fluorophore were used to visualise the location of the two LemA protein variants. However, this method relies on the capability of the antibodies to effectively penetrate the bacterial cells to reach their intended target. The results of this study, (**supplementary Figure 4 and 5**) confirmed poor infusion of the cells by the antibodies, as only a few cells were positive for fluorescence despite the utilisation of different permeabilisation agents.

A different approach involved the construction of PaLemA1 and PaLemA2 fusion proteins that contained a C-terminal sfGFP cloned in-frame with each gene of interest. *E. coli* harbouring each of these fusion constructs were grown and induced, with samples collected at 0, 1, 2 and 3 hours after IPTG induction. The cells were fixed and mounted directly onto microscope slides and imaged (**Figure 3.4**).

The control sample, expressing sfGFP alone, had low levels of protein production immediately prior to induction (0 hours), which was not surprising bearing in mind the fact that the T7 expression system is not very tightly regulated (**Figure 3.4**, panel A). The protein localisation appeared to be homogenous across the cell population, up until 2 hours after protein production. At this point, distinct punctate bodies can be seen forming in the poles of the cells and, taken together with TEM results, suggest that these regions most likely represent inclusion bodies. Following 3 hours of induction larger polar inclusion bodies can be seen, with the cells appearing to have higher amounts of protein production as an increase in the positive signal was observed.

The PaLemA1-sfGFP fusion protein prior to induction appeared to preferentially localise around the membrane, with the majority of the signal being detected there (**Figure 3.4**, panel B). However, when assessing protein localisation at 2- and 3-hours post-induction, although the membranes of the cells remained highly populated with the protein, the cells developed polar as well as punctate regions of PaLemA1-sfGFP localisation.

On the other hand, the PaLemA2-sfGFP protein fusion prior to induction (0h) seemed to localise to the membranes in the highly curved regions of the cell (**Figure 3.4**, panel C). While this polar membranous localisation remained to be the case after 2 and 3 hours of induction, some cells had punctate bodies of localised protein across the whole body of the cell. After 3 hours of protein production, the majority of the signal seemed to be concentrated in and around the cell membranes, however, due to the short distance between the two membranes it was not possible to discern whether the protein localised to the inner or the outer membrane.

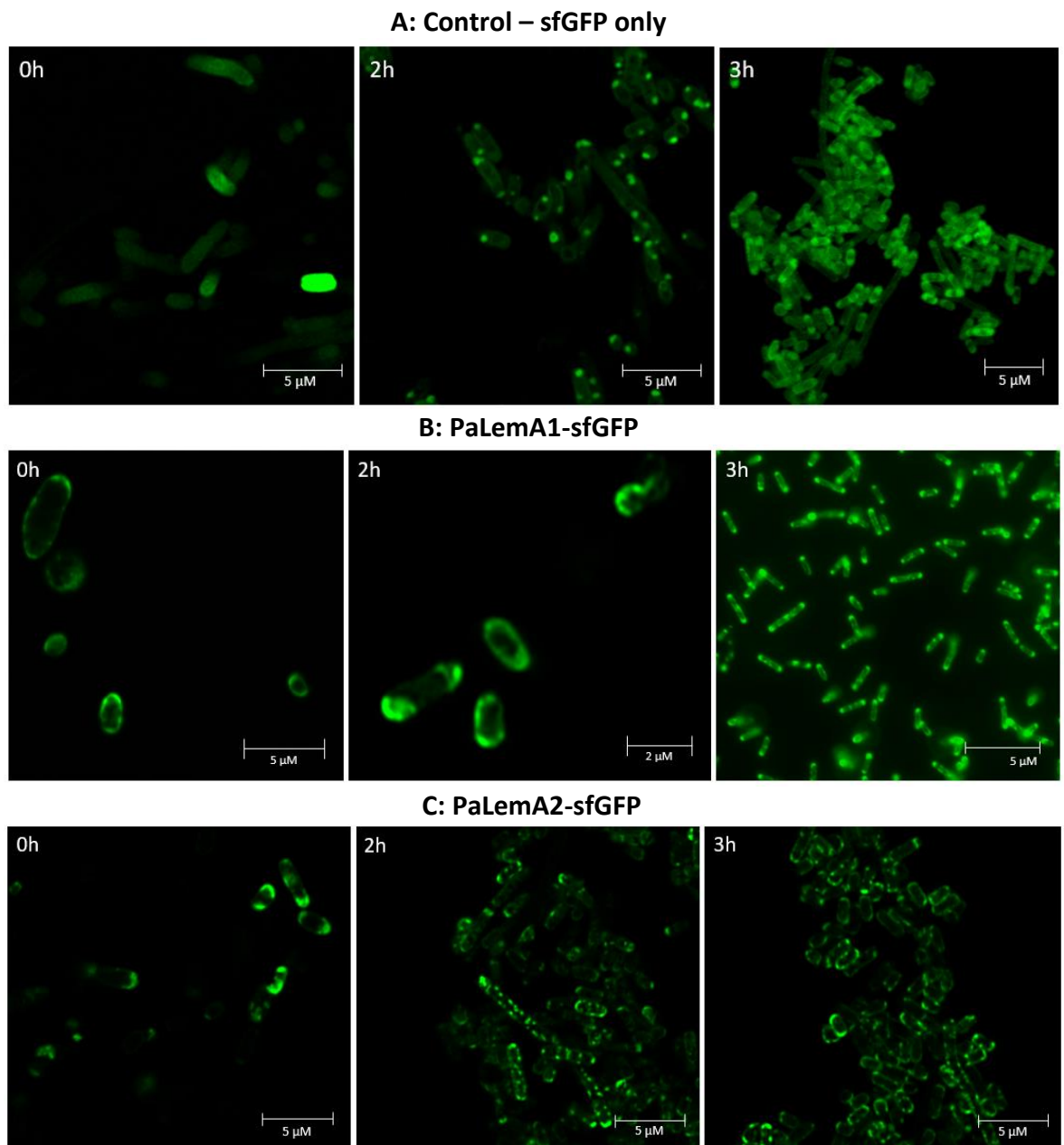


Figure 3.4. Imaging of *E. coli* cells expressing PaLemA1- and PaLemA2-sfGFP fusion proteins.

Images of *E. coli* BL21 (DE3) Star cells producing either sfGFP alone (**A**), PaLemA1-sfGFP (**B**) or PaLemA2-sfGFP (**C**) over a time-course of 3 hours. 0h refers to cell sample taken prior to protein induction, whereas 2h and 3h refers to samples being collected 2- and 3-hours following protein induction, respectively.

3.2.3 Time-course studies on PaLemA1 and PaLemA2 production in *E. coli*

While the analysis of *PalemA* and *PalemA2* following an overnight expression confirmed the presence of vesicles and the production of ectopic membranes inside *E. coli* cells, time-course studies were performed to gain a better understanding of the temporal appearance of this membranous phenotype. *E. coli* BL21 (DE3) Star cells producing PaLemA1, PaLemA2 or an empty vector control, were grown and induced with IPTG. Samples were collected at 0, 1, 2-, 4-, 6- and 8-hours post-induction, fixed overnight, embedded and analysed using TEM. Time-point 0 was taken promptly before the addition of IPTG. To monitor the cells for a membranous phenotype over time, 300 cells were counted for each biological repeat at each time point.

The control cells had a mostly unremarkable cellular morphology, although they did display some intracellular vesicle formation following IPTG induction (**Figure 3.5**, panels **B**, **C** and **D**). These vesicles appeared to be approximately 50 nm in diameter and localised to the inner membrane region where they appeared to be closely associated with the membrane. The proportion of cells harbouring these vesicles peaked around 2 hours post-induction (**Figure 3.5**, panel **C**), where approximately 54% of cells displayed this phenotype. It is worth noting that on average these cells did not seem to have more than 1-2 vesicles inside them. Over the course of the study, the number of cells containing vesicles steadily decreased to approximately 19% after 8 hours of induction.

In the case of PaLemA1, the characteristic intracellular vesicle formation could be observed from time-point 0, which is not surprising when taking into account the 'leaky' nature of the T7 promoter (**Figure 3.6**, panel **A**). The formation of these vesicles seemed to be driven by protein induction, with the number of vesicles inside each cell increasing as the study progressed. This suggested that PaLemA1 may be directly responsible for induction of membrane curvature and blebbing. The number of cells displaying a membranous phenotype peaked at 2 hours after the addition of IPTG, remaining relatively steady thereafter (**Figure 3.6**, panel **C**). Similarly to cells embedded following an overnight induction (**Figure 3.1**, panels **D** and **E**), the vesicles appeared to form in regions with protein aggregation, and unlike the control cells, did not only localise along the inner membrane. Instead they appeared to be distributed in the poles of the cell as well as in the periphery of the cytoplasm (**Figure 3.6**, panels **C**, **D**, **E** and **F**).

On the other hand, the expression of *PaLemA2* in *E. coli* seemed to trigger ectopic membrane formation, vesicle production and protein aggregation (**Figure 3.7**). The proportion of cells exhibiting a membranous phenotype increased overtime, with 83% of cells displaying this phenotype 8 hours post-induction (**Figure 3.8**). Interestingly, the formation of ectopic membranes appeared to be the dominating phenotype up until 6 hours post-induction (**Figure 3.7**, panels **B**, **C** and **D**), when vesicle production was beginning to be seen in a larger cohort of cells (**Figure 3.7**, panels **E** and **F**). The vesicles seemed to vary in size and localisation, and even seemed to appear in the periplasmic space. Additionally, in a large number of cells, the periplasmic space appeared to be obscured by ectopic membranes in the periplasm, following 6+ hours of PaLemA2 production.

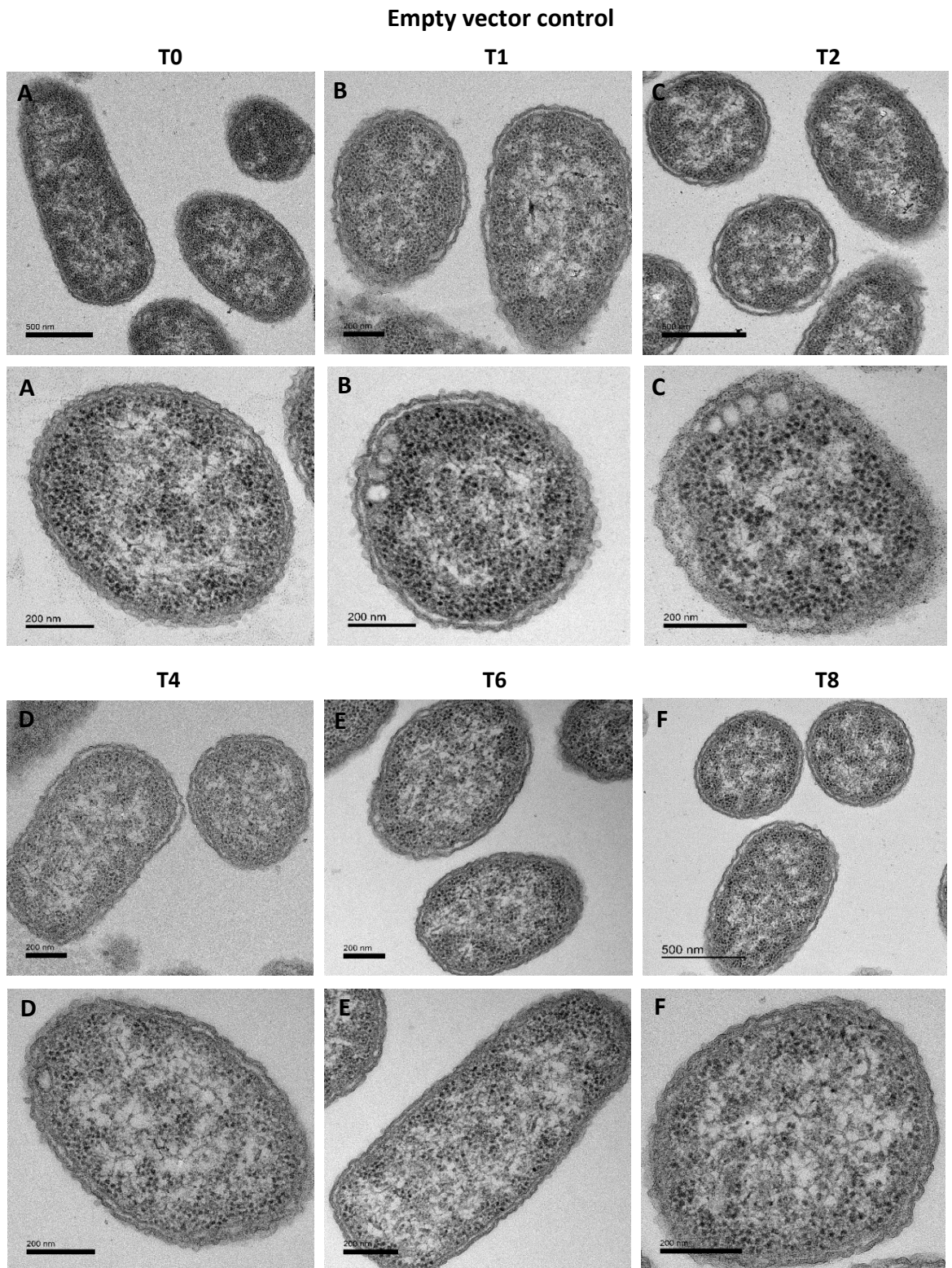


Figure 3.5. TEM of *E. coli* expressing an empty pET3a vector control over a time-course of eight hours.

Transmission electron micrographs of *E. coli* BL21 (DE3) Star cell sections expressing an empty pET3a vector over a course of 8 hours. **A)** Time point 0 (T0) was taken prior to protein induction with IPTG. Following **B)** 1 hour (T1), **C)** 2 hours (T2), **D)** 4 hours (T4), **E)** 6 hours (T6) and **F)** 8 hours (T8) after protein induction cell samples were collected.

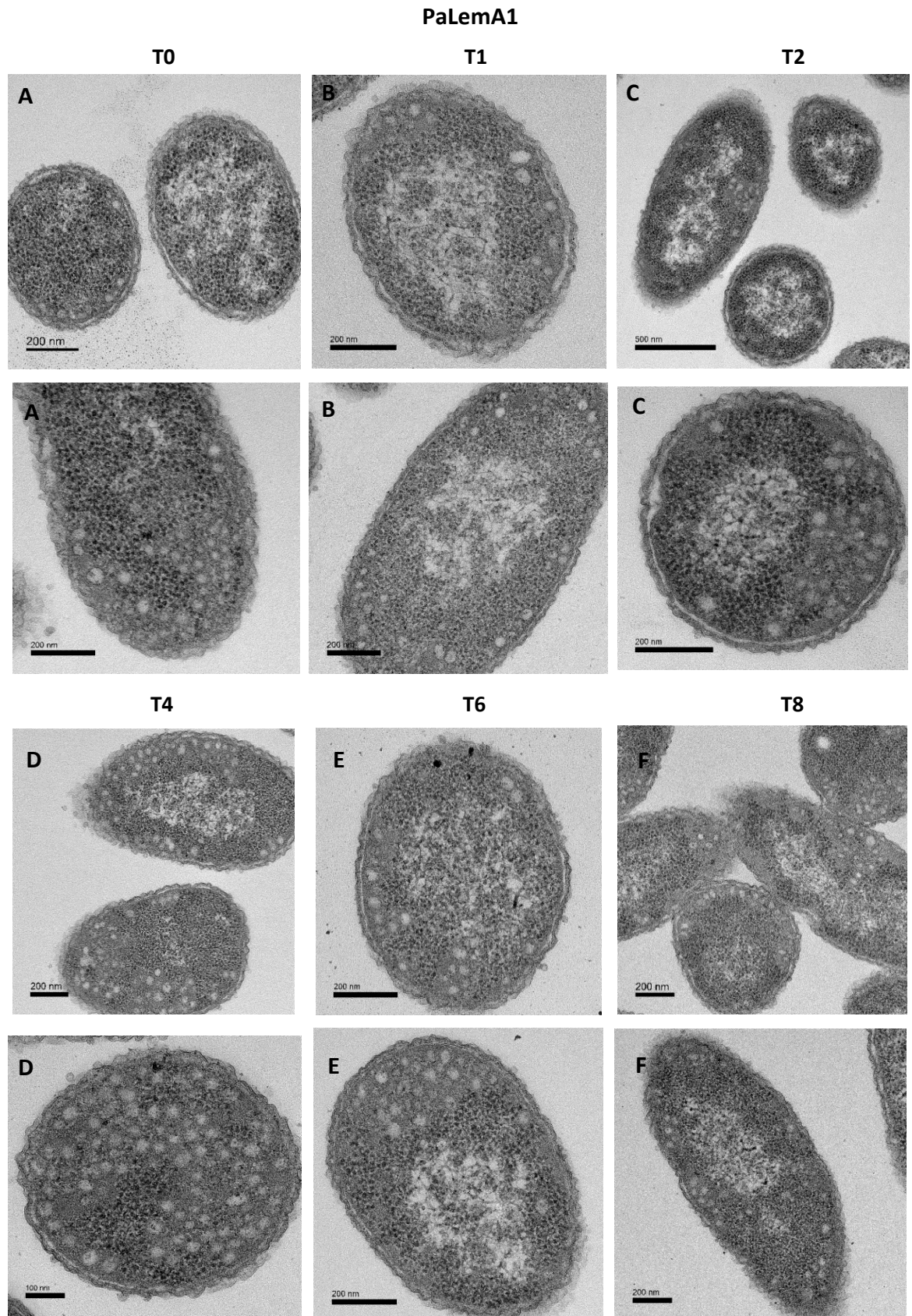


Figure 3.6. TEM of *E. coli* expressing *PaLemA1* over a time-course of eight hours.

Transmission electron micrographs of *E. coli* BL21 (DE3) Star cell sections producing PaLemA2 over a course of 8 hours. **A)** Time point 0 (T0) was taken prior to protein induction with IPTG. Following **B)** 1 hour (T1), **C)** 2 hours (T2), **D)** 4 hours (T4), **E)** 6 hours (T6) and **F)** 8 hours (T8) after protein induction cell samples were collected.

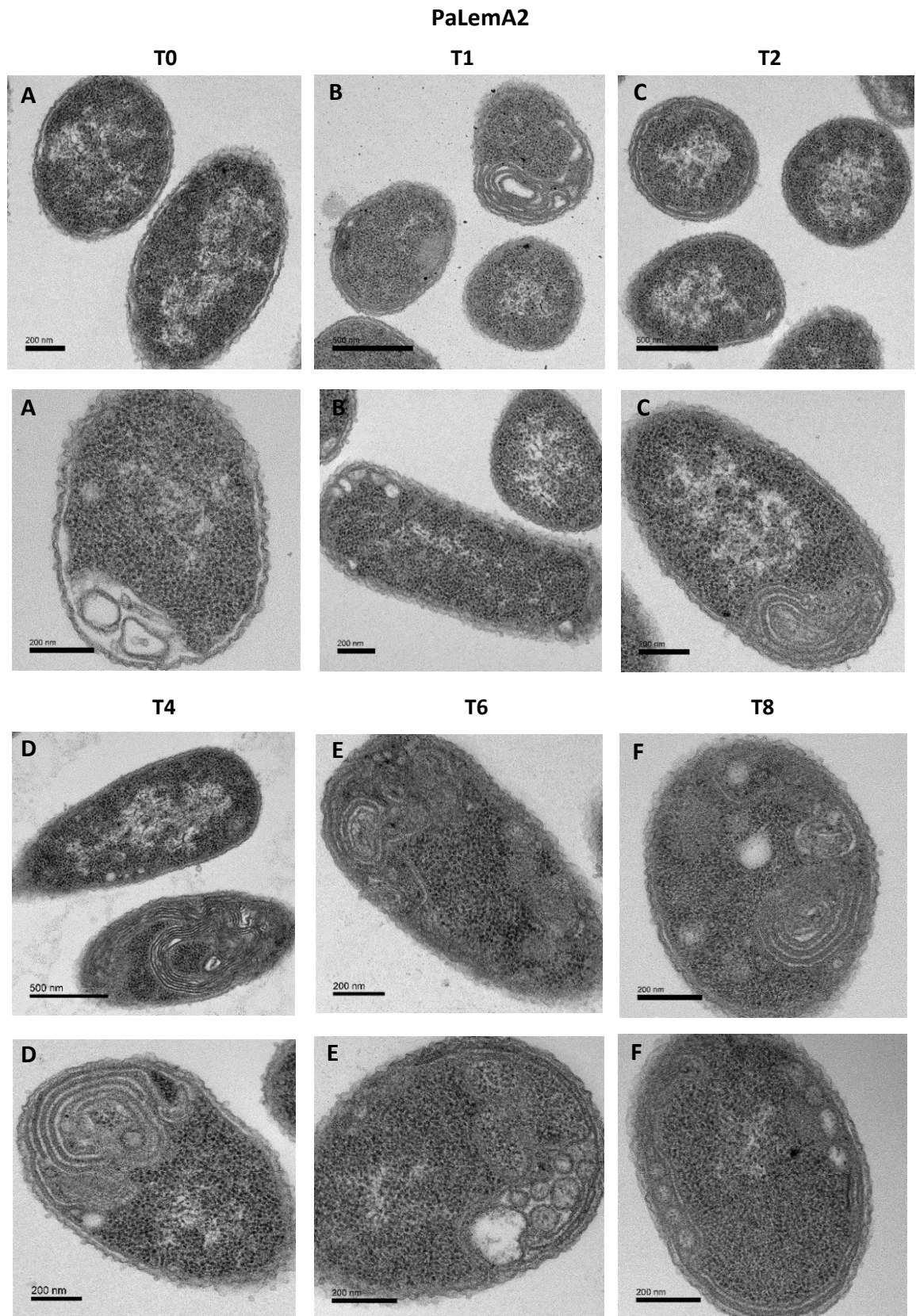


Figure 3.7. TEM of *E. coli* expressing *PaLemA2* over a time-course of eight hours.

Transmission electron micrographs of *E. coli* BL21 (DE3) Star cell sections producing PaLemA2 over a course of 8 hours. **A)** Time point 0 (T0) was taken prior to protein induction with IPTG. Following **B)** 1 hour (T1), **C)** 2 hours (T2), **D)** 4 hours (T4), **E)** 6 hours (T6) and **F)** 8 hours (T8) after protein induction cell samples were collected.

Counting the number of cells with a membranous phenotype provided a good insight into the intracellular morphological changes that accompanied the expression of PaLemA1 and PaLemA2 (**Figure 3.8**). During the analysis of the control and PaLemA1 samples, the difference between the vesicles formed in both samples was evident. Following PaLemA1 production (**Figure 3.6**), the intracellular vesicles were smaller, present in regions with inclusion bodies and, in comparison to the control sample (**Figure 3.5**), did not only localise along the inner membrane. Also, while the percentage of control cells containing vesicles was high, on observation a very small number of vesicles seemed to be present inside each cell. To confirm this, the number of vesicles present inside each cell were counted.

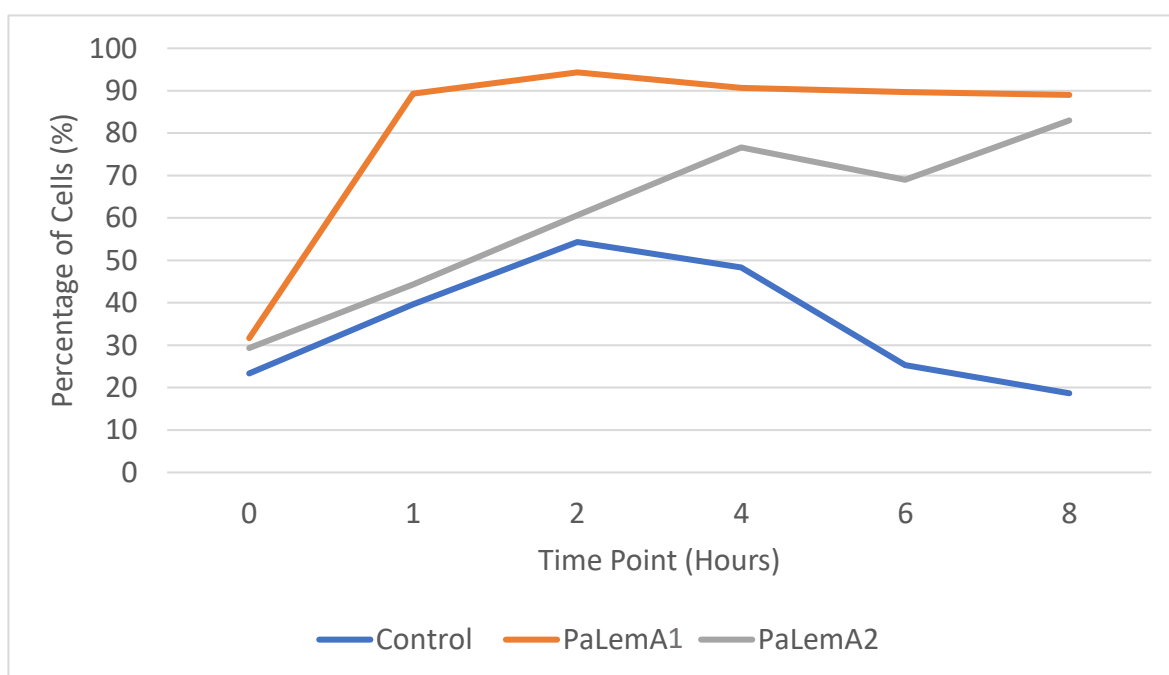


Figure 3.8. Average percentage of *E. coli* cells displaying a membranous phenotype following *PalemA1* and *PalemA2* expression over a time-course of 8 hours.

E. coli BL21 (DE3) Star cells expressing either an empty pET3a control vector or a pET3a plasmid harbouring *PalemA1* or *PalemA2* genes, were assessed for a membranous phenotype, 0, 1, 2, 4, 6 and 8 hours after the induction of protein production. The data shown is the average result of two independent biological repeats.

In total, 50 cells were selected at random and the number of intracellular vesicles were quantified for both the control and PaLemA1 sample at each time-point (**Figure 3.9**). Since there were two biological repeats performed, the analysis was done for each individual replicate. By combining the results of the two repeats for both the control and PaLemA1 samples, an average number of vesicles across the two sample cohorts was calculated.

Moreover, the error bars were calculated by dividing the standard deviation by the square root of the number of measurements that make up the mean (in this case N=100). Both the mean and the error bars were plotted on a graph to illustrate the findings (**Figure 3.9**).

Overall, when comparing the average number of vesicles present in the control sample to PaLemA1, it is evident that there is a significant difference between the two samples. The control sample had a maximum of 1.3 vesicles per cell 1-hour post induction, however, on average the number of intracellular vesicles present was around 0.7 per cell (**Figure 3.9**). Both of the control repeats (CTRL 1 and CTRL 2) followed an almost identical trend. Likewise, the two biological replicates of PaLemA1 followed a similar trend and had a varying number of vesicles during the time-course, though in comparison to the second repeat (PaLemA1 2), the first repeat (PaLemA1 1) had a lower mean number of vesicles inside the cell.

Together, these results demonstrate the clear difference between the control and the PaLemA 1+2 samples in regards to intracellular vesicle numbers. Over the course of the study, the mean number of vesicles for the PaLemA 1+2 samples post-induction ranged between 14-20, in contrast to the control samples (CTRL 1+2) which ranged between 0.6-1.3. It is also worth noting that there is more variation in the PaLemA sample than in the control, as indicated by the error bars (**Figure 3.9**).

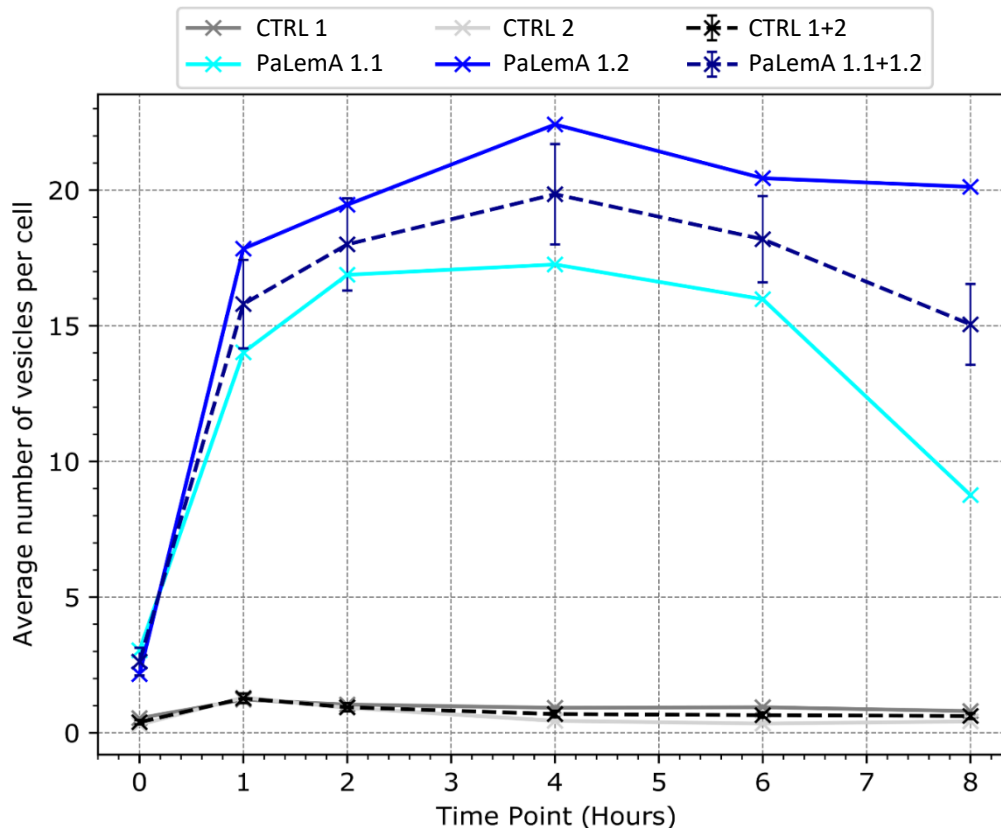


Figure 3.9. The average number of intracellular vesicles found in *E. coli* cells expressing *PaLemA1* over a time-course.

The number of intracellular vesicles inside the control and PaLemA1 producing cells was counted for each time point (0, 1, 2-, 4-, 6-, and 8-hours post-induction), averaged and summarised in the graph. CTRL 1 and PaLemA1 1 refer to the data collected from the initial study, whereas CTRL 2 and PaLemA1 2 show the data collected from a biological repeat. Both biological replicates for each sample were combined to study the variation in data.

To evaluate the expression levels of PaLemA1 and PaLemA2 during the time-course study, whole cells were harvested at 0, 1, 2-, 4-, 6- and 8-hours post-induction and analysed via SDS-PAGE (**Figure 3.10**). There was a clear overproduction of PaLemA1, with a strong band appearing around 21 kDa 1-hour post-induction and thereafter (**Figure 3.10**, lanes LT1-LT8). However, no clear overproduction of PaLemA2 was seen (**Figure 3.10**, lanes L2T0-L2T8).

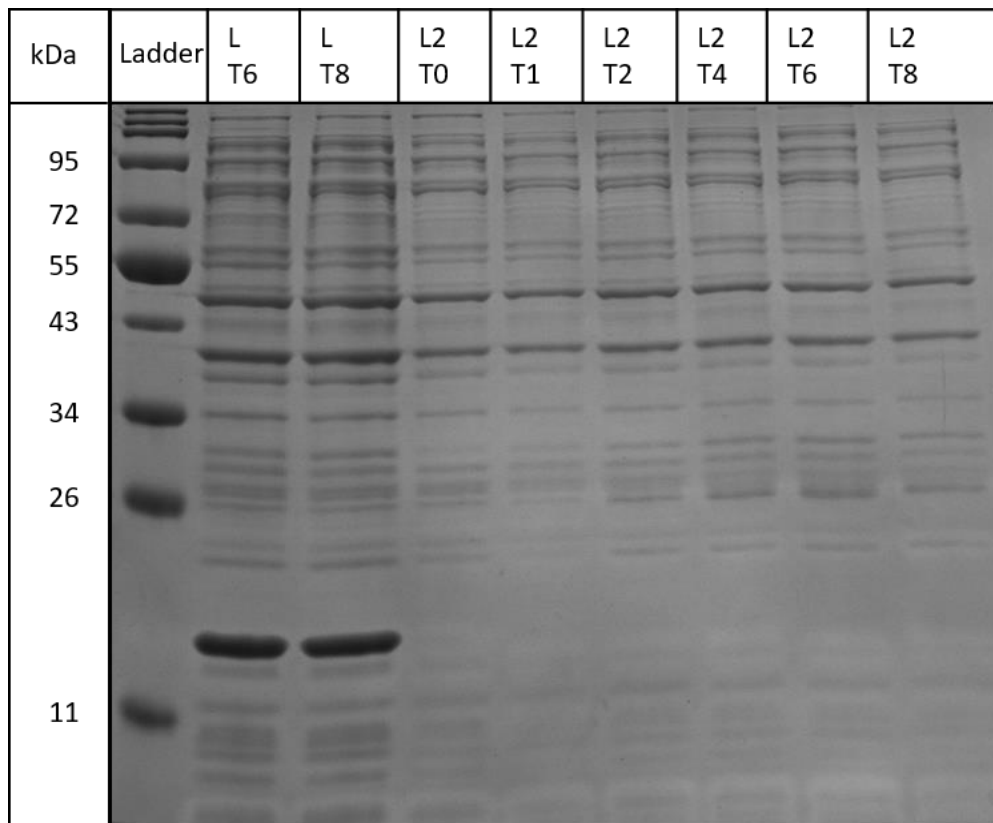
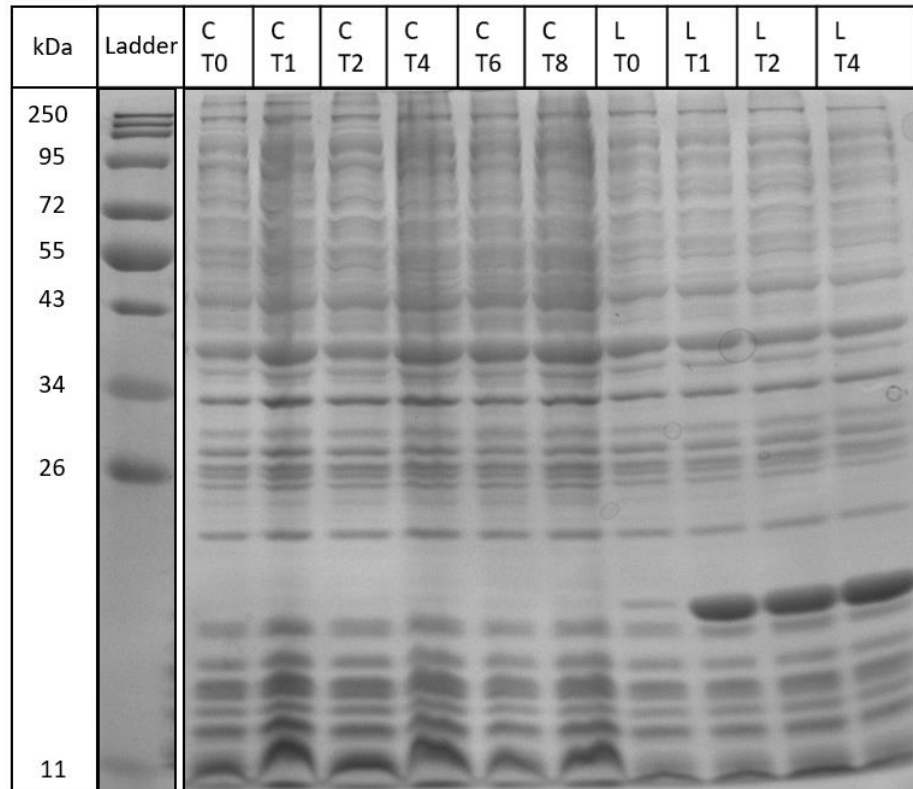


Figure 3.10. SDS-PAGE analysis of *E. coli* expressing an empty vector control, PaLemA1 and PaLemA2 over the time-course of 8 hours.

E. coli BL21 DE3 Star cells expressing PaLemA1 (L), PaLemA2 (L2) or an empty pET3a vector control (C). Samples were collected 0, 1, 2-, 4-, 6- and 8-hours post-induction, and represent T0, T1, T2, T4, T6 and T8, respectively.

3.2.4 Analysing the effects of expressing the operons of *PalemA1* and *PalemA2* in *E. coli*

Studying the effects of PaLemA1 and PaLemA2 production in *E. coli* provided an insight into the membrane restructuring properties of these proteins. However, the precise molecular function of this protein family is uncertain, and it is not possible to understand more about the nature of these proteins without performing further bioinformatics and/or structural analysis studies.

In order to gather more information about the *Pseudomonas aeruginosa* LemA proteins a bioinformatics analysis was carried out (**Table 3.2**). Sequence alignment of PaLemA1 and PaLemA2 revealed approximately 31% sequence identity between the two proteins. Further to this, PaLemA1 and PaLemA2 were found to be located in two distinct operons (**supplementary Figure 1 and 2**). The PaLemA1 operon consisted of one other protein, PA4368, while the PaLemA2 operon contained two other proteins, PA0538 and PA0536.

Protein	Uniprot ID	Molecular weight (kDa)	TMHs	Predicted localisation of soluble domain	Predicted motif/function
PaLemA1	AAG07757	21.05	1	Cytoplasmic	N/A
PA4368	AAG07756	33.58	2	Periplasmic	RING-type E3 ubiquitin transferase
PA0538	AAG03927	18.13	4	Periplasmic	Protein disulphide isomerase*
PaLemA2	AAG03926	22.19	0	N/A	N/A
PA0536	AAG03925	35.56	3	Periplasmic	TPM phosphatase motif

Table 3.2. Analysis of PaLemA1 and PaLemA2 operon proteins of *Pseudomonas aeruginosa* PA14.

*The characterised function of this protein.

In order to gain some insights into the effects of the genes found in the *PalemA1* and *PalemA2* operons, the genes were cloned and expressed individually (**Figure 3.11**) and in combination (**Figure 3.13**) in *E. coli*. Following overnight protein production, the cells were

fixed and processed for TEM analysis. The overproduction of PA4368 appeared to promote the formation of unstructured membranous invaginations that were present around the inner membrane, which can be seen in both transverse and longitudinal cell sections (**Figure 3.11**, column A). Protein overproduction was observed following SDS-PAGE analysis, although it appeared a few kDa below the expected molecular weight of the protein (**Figure 3.12**, lane 3).

Conversely, the production of PA0538 seemed to result in the lysis of a large proportion of cells, as there was significant cellular debris present in the cell sections (**Figure 3.11**, column B). In the majority of cases this phenotype was impossible to quantify due to the lysed cells being indistinguishable from one another. While the morphology of the intact cells remained relatively similar to that of control cells, a few intracellular vesicles were observed in a small number of cells. Interestingly, the lysed regions of the sample contained large numbers of vesicles, although the mechanisms behind the biogenesis of these vesicles remain unclear. However, since intracellular vesicles were not observed in the majority of intact *E. coli* cells, it suggests that the vesicles formed during or after cell lysis. In addition, the fact that the overexpression of *PA0538* was not seen following SDS-PAGE analysis (**Figure 3.12**, lane 2) could mean that small quantities of this protein were sufficient for induction of cell lysis. In this case, there would have been a strong selection against the cells producing PA0538, which goes in line with the finding that intact cells remained morphologically similar to the control cells.

Following expression of *PA0536* no distinct phenotype could be observed (**Figure 3.11**, column C). While some intracellular vesicle formation was observed, this only appeared in a small number of cells. Moreover, no protein overproduction was observed following SDS-PAGE analysis (**Figure 3.12**, lane 1).

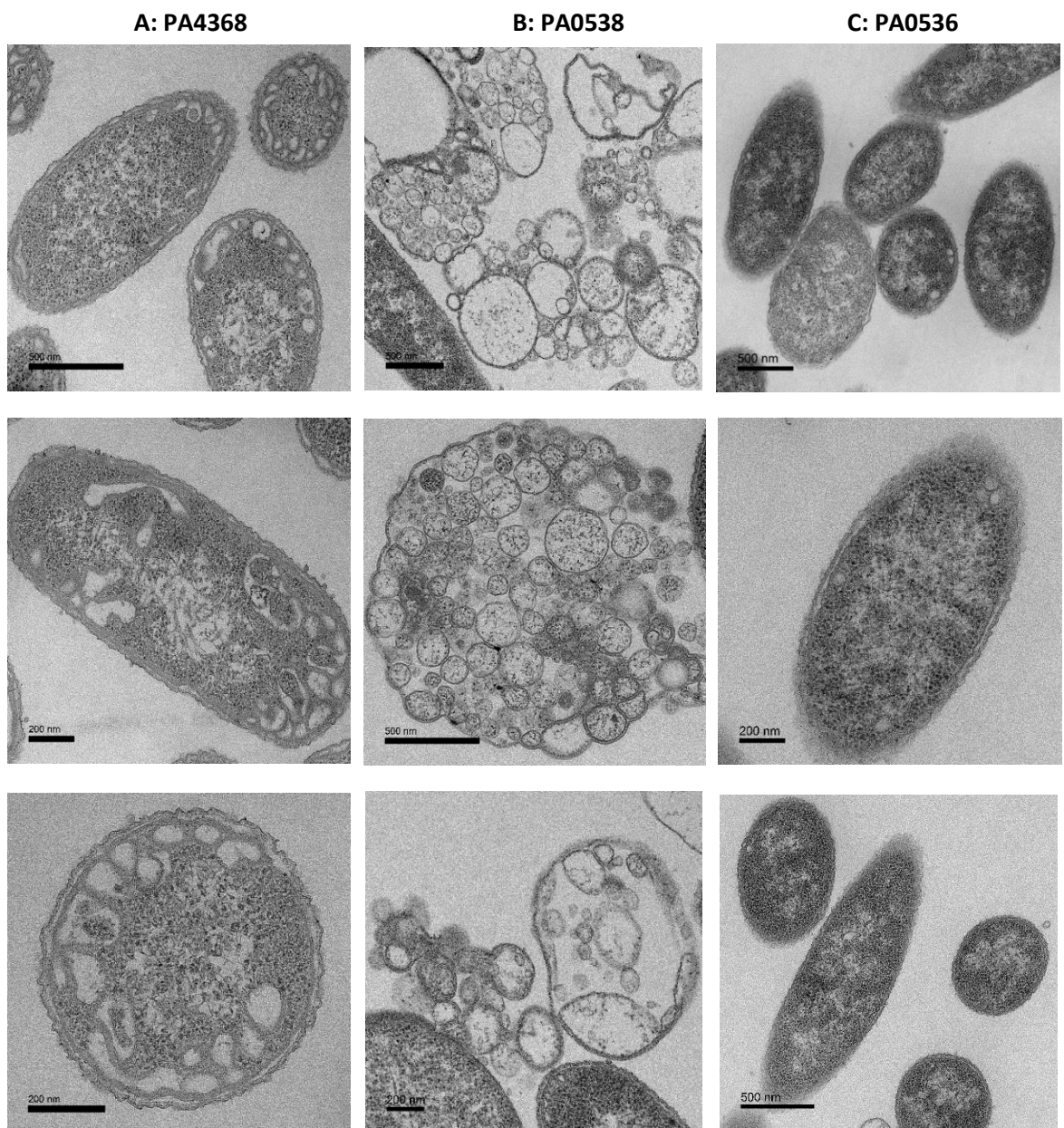


Figure 3.11. TEM of *E. coli* expressing genes of the *PalemA1* and *PalemA2* operons.

Transmission electron micrographs of *E. coli* BL21 (DE3) Star cell sections producing PaLemA1 and PaLemA2 operon proteins individually. **A)** PA4368 production results in membranous invaginations which appear to be originating from the inner membrane; **B)** PA0538 production leads to large amounts of cell lysis and vesicle formation; **C)** PA0536 production does not have a significant effect in *E. coli* cells, as only a few cytoplasmic vesicles are observed in a small number of cells.

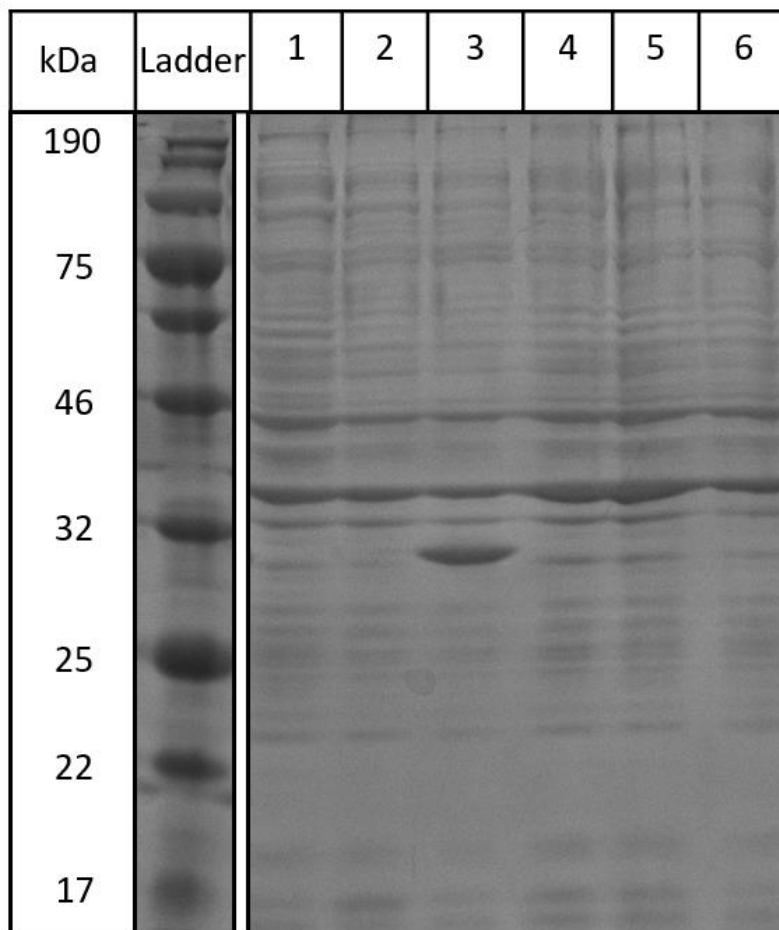


Figure 3.12. SDS-PAGE analysis of *E. coli* cells producing proteins of the PaLemA1 and PaLemA2 operons.

E. coli BL21 DE3 Star cells expressing **1)** PA0536, **2)** PA0538, **3)** PA4368, **4)** PA0538-PaLemA2, **5)** PA0538-PaLemA2-PA0536 and **6)** PaLemA2-PA0536, following overnight induction.

Following the production of PaLemA1 and PaLemA2 operon proteins individually (**Figure 3.11**), the complete operons were assessed for phenotypic changes in *E. coli* (**Figure 3.13**). Initially, the genes were cloned in-frame in a pET3a vector using the Link and Lock method in the order in which they occur in the operons (McGoldrick *et al.*, 2005). The *PalemA1* operon consisted of PaLemA1-PA4368, in this particular order. In the case of the *PalemA2* operon which had a total of three proteins, a combination of cloned constructs was used to assess for any phenotypic changes. These constructs included genes encoding PA0538-PaLemA2, PaLemA2-PA0536 and the full operon, PA0538-PaLemA2-PA0536.

Although successful clones of the *PalemA1* operon were obtained, the operon did not transform in *E. coli* BL21 (DE3) Star cells. On further assessment transformations were successfully achieved in *E. coli* DH10 β cells, which do not have capacity for protein production, most likely suggesting that the overexpression of the two genes in combination is detrimental to cell viability.

When producing the *PalemA2* operon proteins in *E. coli* in different combinations, a range of cellular phenotypic changes were observed. After PA0538-PaLemA2 production a significant level of cellular lysis was observed (**Figure 3.13**, column A). The regions containing cellular debris contained large amounts of differently sized vesicles, which is similar to the findings obtained following PA0538 expression alone (**Figure 3.11**, column B). Some of the unlysed cells also contained what appeared to be distinct cytoplasmic compartments, having a lighter lumen to the rest of the cytoplasm. Furthermore, these compartments were surrounded by what could possibly be disordered ectopic membranes.

Analysis after thin-sectioning and TEM producing of cells of PaLemA2-PA0536, revealed an increase in outer membrane vesiculation and ectopic membrane formation in *E. coli* (**Figure 3.13**, column B). Finally, production of the complete *PalemA2* operon led to the formation of large cytoplasmic compartments. Some ectopic membrane formation was also observed in the cytoplasm (**Figure 3.13**, column C). However, no protein overproduction was observed following SDS-PAGE analysis (**Figure 3.12**, lane 5).

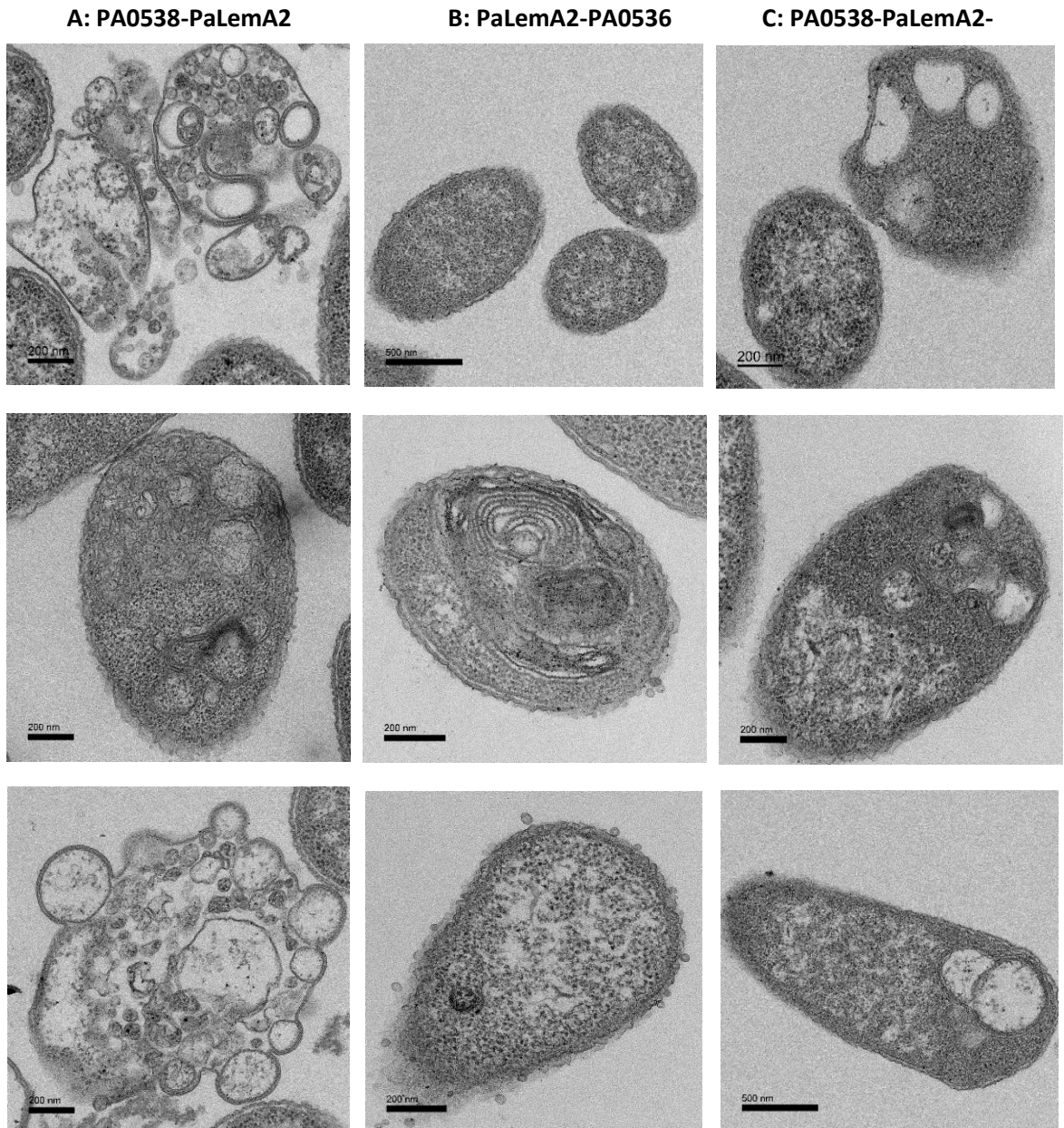


Figure 3.13. TEM of *E. coli* expressing *PaLemA2* operon proteins.

Transmission electron micrographs of *E. coli* BL21 (DE3) Star cell sections producing PaLemA2 operon proteins in various combinations overnight. **A)** PA0538-PaLemA2 production leads to large amounts of cellular lysis, formation of vesicles and excessive membrane overproduction; **B)** PaLemA2-PA0536 production results in polymembrane body formation and an increase in extracellular vesicle formation; **C)** PA0538-PaLemA2-PA0536 production leads to cytoplasmic membrane invaginations and excess production of membranes.

3.2.5 Expression of *PalemA1* in Chinese Hamster Ovary (CHO) cells

While *E. coli* derived vesicles have shown great potential in being exploited as future vaccine delivery platforms, they do present some safety concerns especially with respect to the inclusion of lipopolysaccharide. Due to this, and our continued interest in exploiting PaLemA1 derived intracellular vesicles for vaccine development, it was important to explore if membrane vesiculation could be increased in a mammalian cell system following *PalemA1* expression. As the PaLemA1 protein has an integral membrane domain, it was thought that the production of this protein in CHO cells could increase membrane invagination in and around the endoplasmic reticulum, which should be the first membrane the translated protein would encounter.

The CHO cell line grown in suspension (CHO-S) was chosen as the host system due to its capacity for rapid and high-yield protein expression, especially in the case of difficult to express proteins. To explore if PaLemA1 had any effect on the CHO-S cell vesiculation, a construct harbouring *PalemA1* was at first transiently and later stably transfected into this cell line. Protein expression, localisation and lipid vesicle formation were assessed using a combination of SDS-PAGE, Western blot analysis, immunofluorescent staining and TEM.

Initially, as *PalemA1* was previously cloned into a pET3a vector, by using NheI and KpnI restriction sites, this gene was subcloned into a CHO cell compatible vector, pcDNA3.1/V5-His-TOPO, which harbours a C-terminal V5 tag. It was decided to have the V5 tag on the C-terminus of the protein due to the importance of the N-terminus of PaLemA1, since it is predicted to contain the transmembrane domain. Following this, CHO-S cells were transiently transfected with pcDNA3.1/V5-His-TOPO-PaLemA1 to assess the protein expression profile for PaLemA1 using SDS-PAGE analysis and fluorescent immunostaining.

Although no protein overproduction could be observed following SDS-PAGE analysis (**Figure 3.16**), immunofluorescent staining of CHO-S cells transiently expressing *PalemA1* revealed the production of this protein in a small number of cells (**Figure 3.15**). No PaLemA1 production was seen in any of the control cell population (**Figure 3.14**). Together, this indicates a relatively low level of protein expression across the total cell population, which suggests that only a low percentage of cells were successfully transfected with the pcDNA3.1/V5-His-TOPO-PaLemA1 vector. The localisation of PaLemA1 (green), appears to have some overlap with the endoplasmic reticulum (ER) region of the cell (red), which is not surprising since the ER is the hub for protein production in mammalian cells.

While these initial studies conducted in a transient system allowed us to gather preliminary data on the expression profile of PaLemA1 in mammalian cells, in order to assess if the expression of *PalemA1* results in the formation of any organised structures, particularly vesicles, TEM studies were undertaken. As the production of PaLemA1 in CHO-S cells was low, it was decided to generate stable cell lines where the whole cell population would express *PalemA1*.

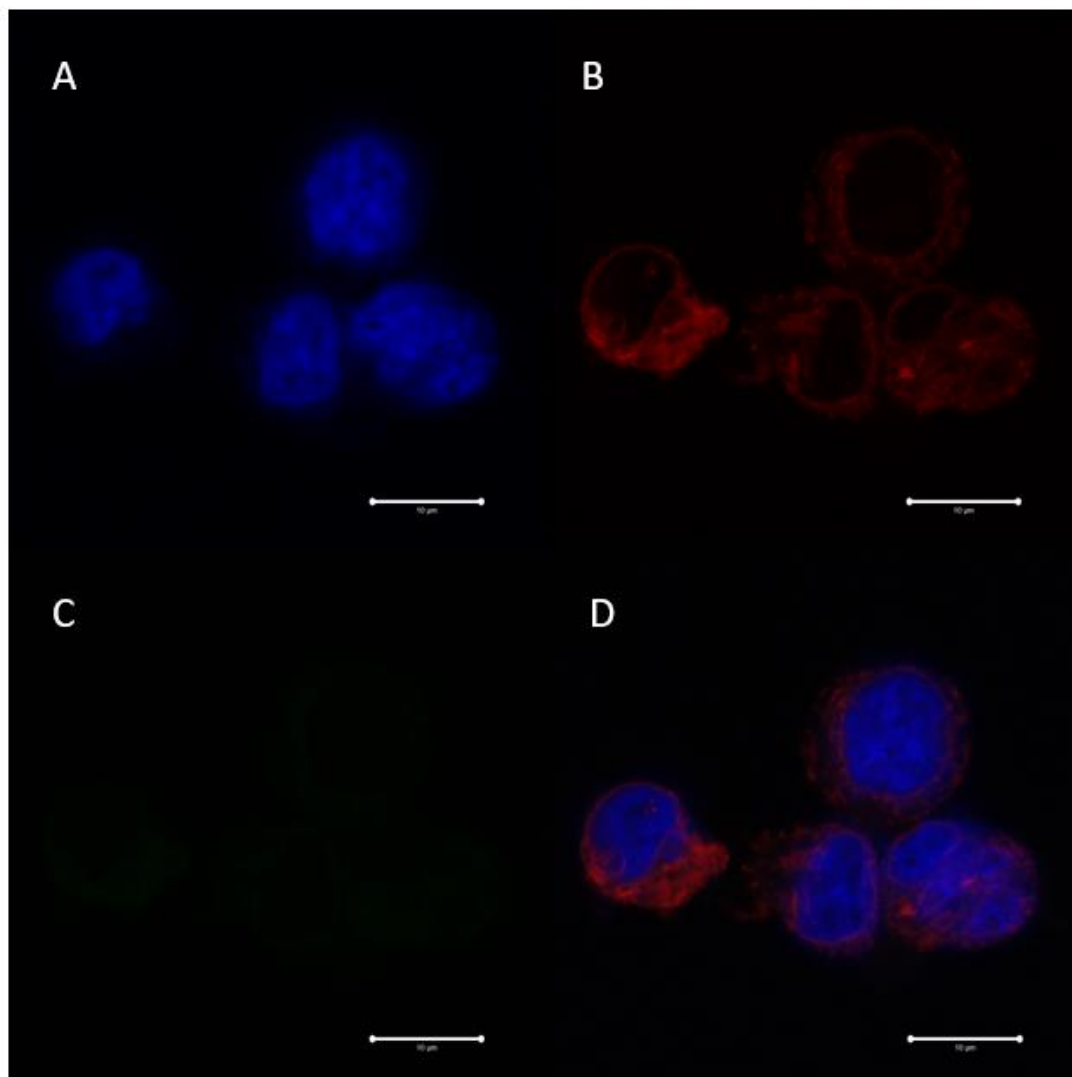


Figure 3.14. Immunostaining analysis of CHO-S transiently transfected cells with an empty vector control.

Confocal microscopy images of CHO-S cells transiently transfected with the empty vector control, pcDNA3.1/V5-His-TOPO, 48 hours after the cells were seeded. Cells were fixed and incubated with anti-V5 and anti-Calnexin primary antibodies. Anti-FITC (green) and anti-TRITC (red) secondary antibodies were used to visualise the anti-V5 and anti-Calnexin antibodies, respectively. The nuclei of the cells were visualised with the DNA stain, DAPI (blue). A. DAPI stained nuclei. B. Anti-Calnexin antibody marker for endoplasmic reticulum. C. Anti-V5 antibody marking PaLemA1 production. D. Composite image of all three channels (A-C). Scale bars: 10 μ M.

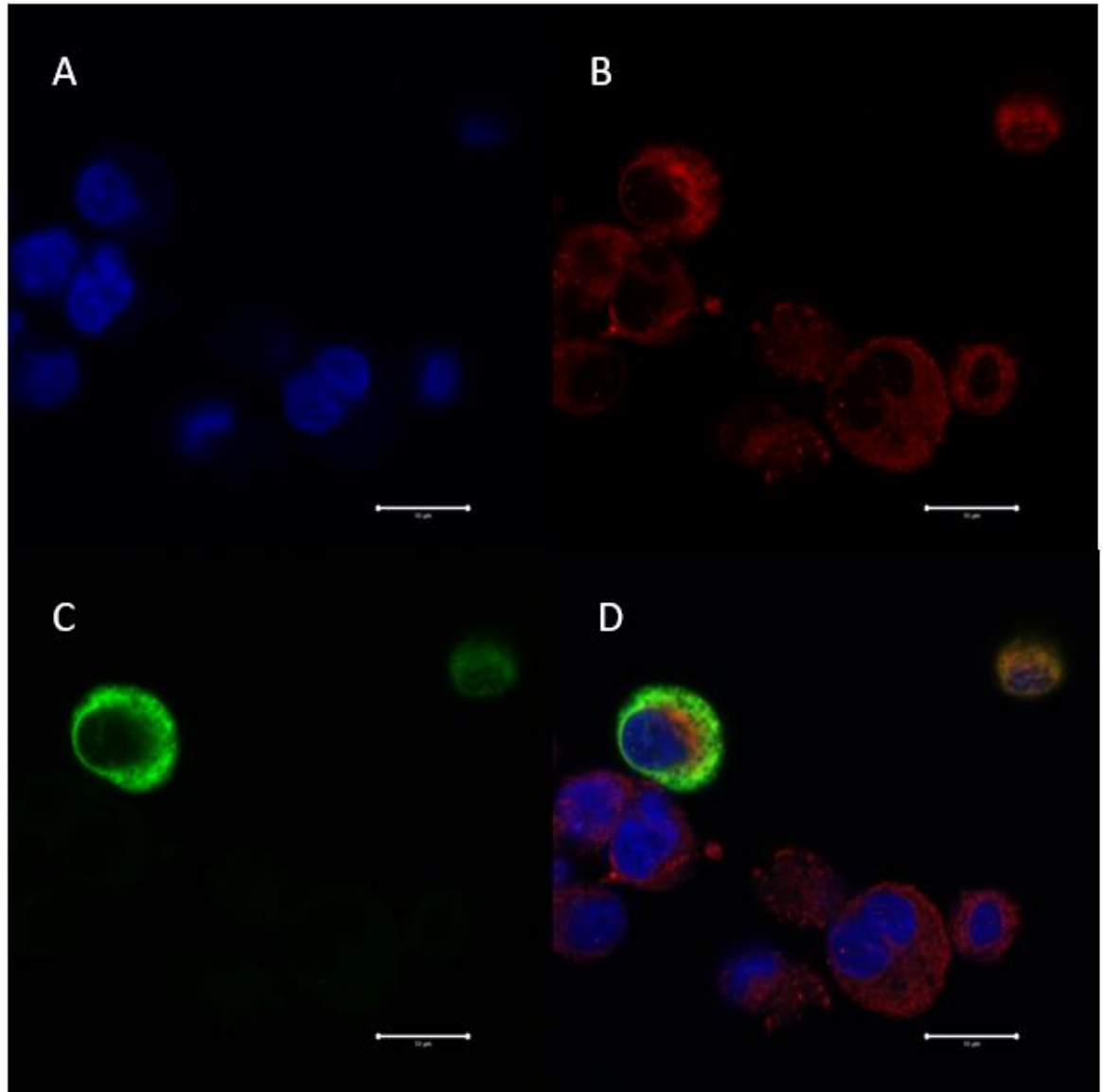


Figure 3.15. Immunostaining analysis of CHO-S transiently transfected cells with the pcDNA3.1/V5-His-TOPO vector encoding PaLemA1.

Confocal microscopy images of CHO-S cells transiently transfected with the pcDNA3.1/V5-His-TOPO-PaLemA1 vector, 48 hours after the cells were seeded. Cells were fixed and incubated with anti-V5 and anti-Calnexin primary antibodies. Anti-FITC (green) and anti-TRITC (red) secondary antibodies were used to visualise the anti-V5 and anti-Calnexin antibodies, respectively. The nuclei of the cells were visualised with the DNA stain, DAPI (blue). A. DAPI stained nuclei. B. Anti-Calnexin antibody marker for endoplasmic reticulum. C. Anti-V5 antibody marking PaLemA1 production. D. Composite image of all three channels (A-C). Scale bars: 10 μ M.

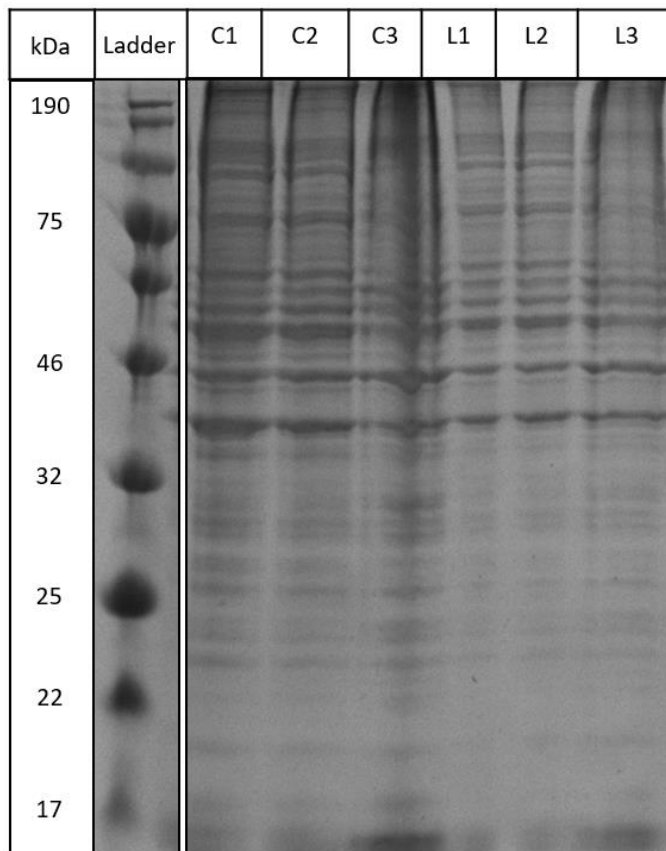


Figure 3.16. SDS-PAGE analysis of CHO-S cells transiently producing PaLemA1.

CHO-S cells transiently expressing an empty vector control (C1, C2 and C3), or PaLemA1 (L1, L2, L3). The expected molecular weight of PaLemA1-V5 was 22.47 kDa.

Following the transfection of CHO-S cells with *PaLemA1*, stable cell lines were generated by maintaining the CHO-S cells in Hygromycin B. To deduce whether a higher concentration of this selection marker would result in increased PaLemA1 production, two different concentrations of Hygromycin B were tested, 500 µg/mL and 750 µg/mL. To ensure the whole cell population was expressing the protein of interest prior to TEM analysis, immunofluorescence and Western blot analysis was carried out to confirm this.

In both, the 500 µg/mL and 750 µg/mL Hygromycin B selection samples, a range of PaLemA production profiles could be seen (**Figures 3.18** and **3.19**). While in the 500 µg/mL Hygromycin B CHO-S cells, approximately 50% of cells appeared to be high producers of PaLemA1 as determined by the intensity of the signal, the remaining cells produced barely detectable amounts of the protein. Although hardly visible, a very faint green outline of the cells could be seen. In the case of 750 µg/mL Hygromycin B challenged CHO-S cells, the overall cell population appeared to have slightly increased basal levels of PaLemA1 production in comparison to the 500 µg/mL Hygromycin B challenged cells. The cells that

appeared to produce smaller amounts of PaLemA1 were more clearly distinguishable from the low producers of the 500 µg/mL Hygromycin B CHO-S cells. As expected, no PaLemA1 production could be seen in the cells expressing the empty vector control (**Figure 3.17**).

Although no PaLemA1 overproduction could be seen following SDS-PAGE analysis, in both the 500 µg/mL and the 750 µg/mL Hygromycin B challenge samples, the Western blot revealed bands around 22.47 kDa, which were indicative of the V5 tagged PaLemA1 protein (**Figure 3.20**). The primary anti-PaLemA1 antibody had unspecific binding to several larger sized protein bands on the blot. These bands appeared in both the control and the PaLemA1 samples, indicating that this interaction was not the result of an oligomerisation or a proteolytic reaction related to the PaLemA1 protein. Moreover, although quantification studies were not carried out to assess whether there was any difference in the levels of PaLemA1 production between the 500 µg/mL or the 750 µg/mL Hygromycin B challenged samples, a marginally larger amount of PaLemA seemed to be present in the cells maintained in 750 µg/mL of Hygromycin B.

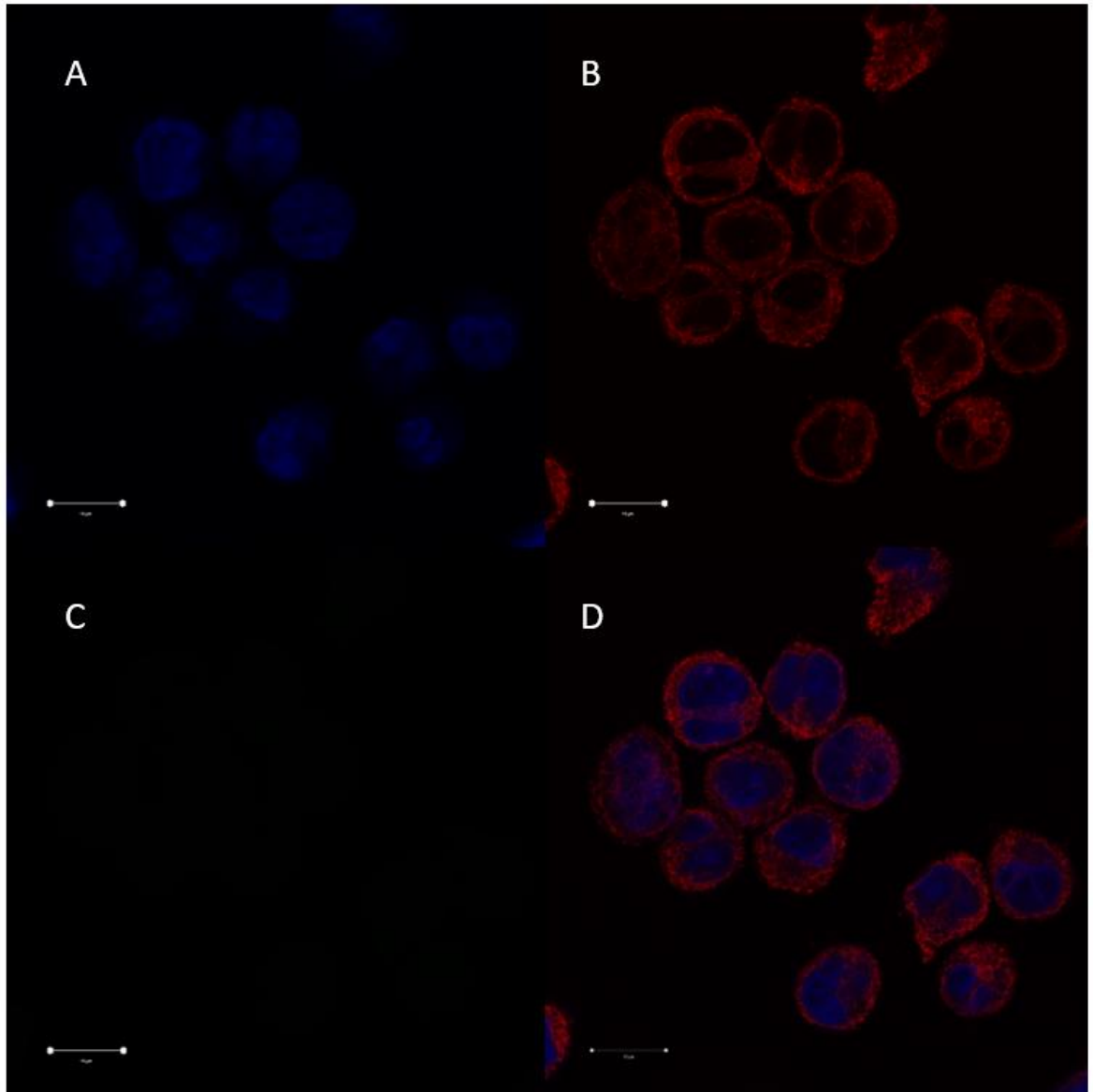


Figure 3.17. Immunostaining analysis of CHO-S cells stably expressing the pcDNA3.1/V5-His-TOPO empty vector.

Imaging of CHO-S cells, maintained in 500 $\mu\text{g/ml}$ of Hygromycin B, stably expressing the pcDNA3.1/V5-His-TOPO empty vector, 24 hours after cells were seeded onto coverslips. Cells were fixed and incubated with anti-V5 and anti-Calnexin primary antibodies. Anti-FITC (green) and anti-TRITC (red) secondary antibodies were used to visualise the anti-V5 and anti-Calnexin antibodies, respectively. The nuclei of the cells were visualised with the DNA stain, DAPI (blue). A. DAPI stained nuclei. B. Anti-Calnexin antibody marker for endoplasmic reticulum. C. Anti-V5 antibody marking PaLemA production. D. Composite image of all three channels (A-C). Scale bars: 10 μM .

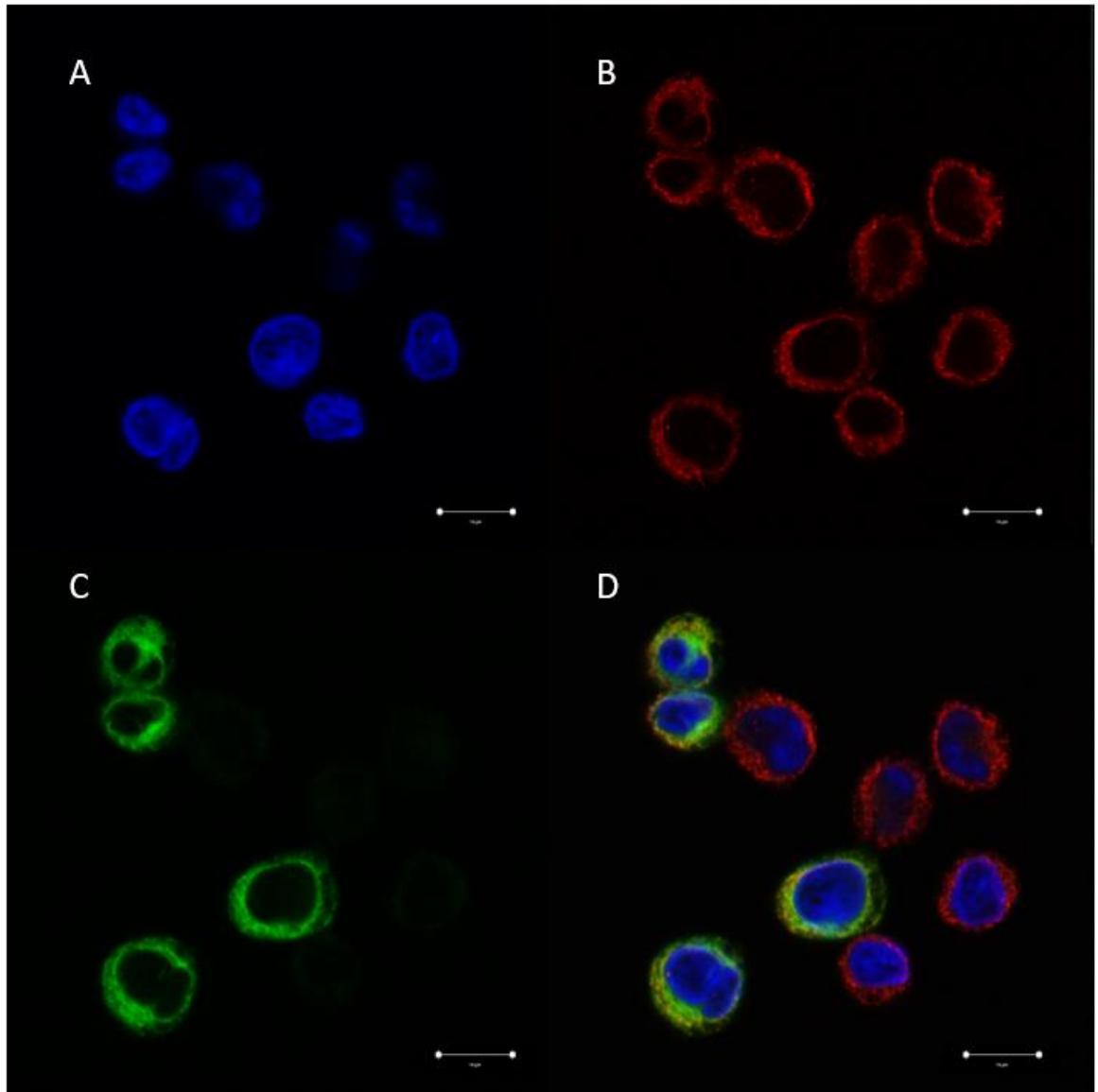


Figure 3.18. Immunostaining analysis of CHO-S cells stably expressing the pcDNA3.1/V5-His-TOPO empty vector.

Imaging of CHO-S cells, maintained in 500 $\mu\text{g}/\text{ml}$ of Hygromycin B, stably expressing the pcDNA3.1/V5-His-TOPO empty vector, 24 hours after cells were seeded onto coverslips. Cells were fixed and incubated with anti-V5 and anti-Calnexin primary antibodies. Anti-FITC (green) and anti-TRITC (red) secondary antibodies were used to visualise the anti-V5 and anti-Calnexin antibodies, respectively. The nuclei of the cells were visualised with the DNA stain, DAPI (blue). A. DAPI stained nuclei. B. Anti-Calnexin antibody marker for endoplasmic reticulum. C. Anti-V5 antibody marking PaLemA1 production. D. Composite image of all three channels (A-C). Scale bars: 10 μM .

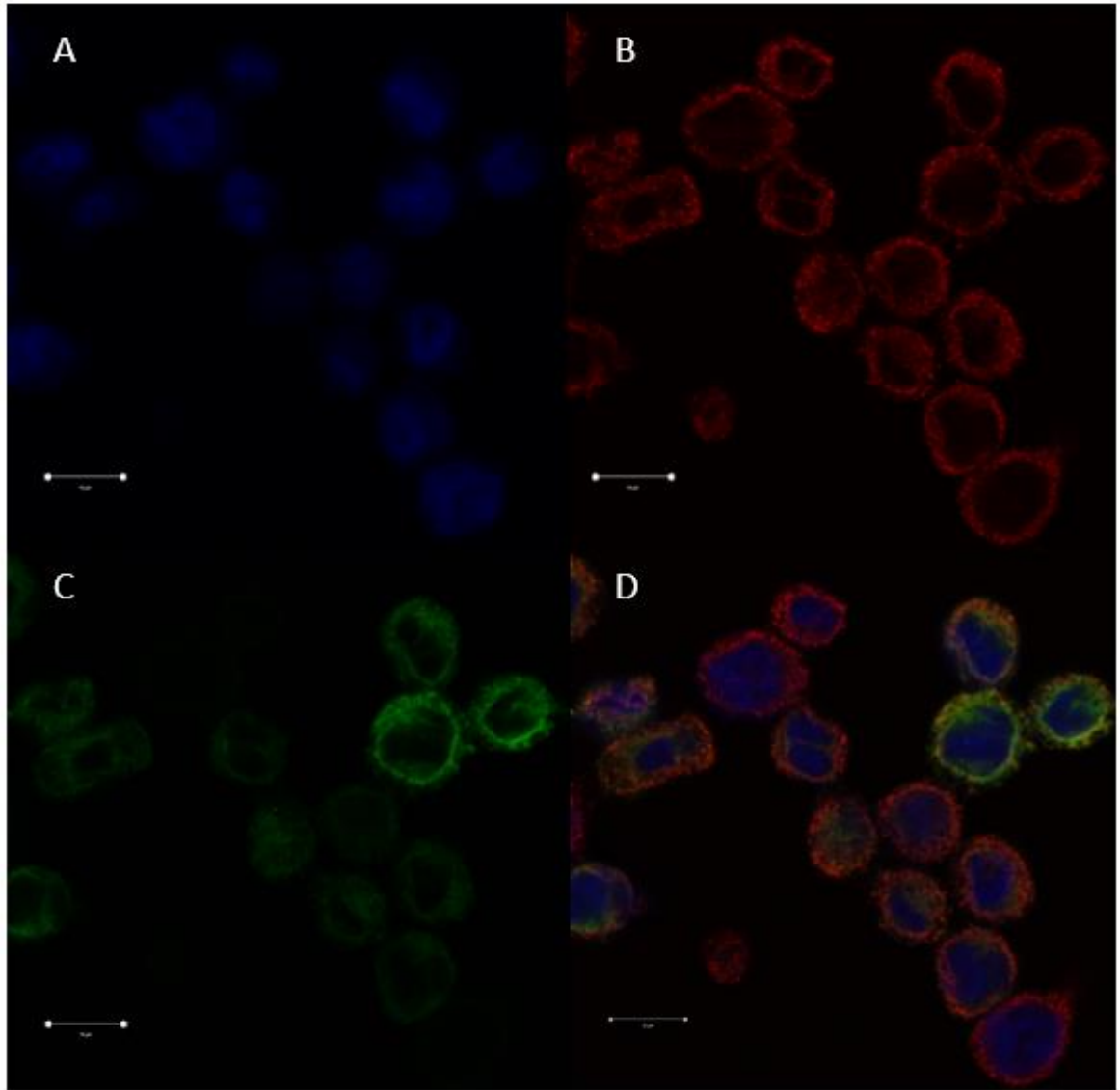


Figure 3.19. Immunostaining analysis of CHO-S cells stably expressing the pcDNA3.1/V5-His-TOPO empty vector.

Imaging of CHO-S cells, maintained in 750 $\mu\text{g}/\text{mL}$ of Hygromycin B, stably expressing the pcDNA3.1/V5-His-TOPO empty vector, 24 hours after cells were seeded onto coverslips. Cells were fixed and incubated with anti-V5 and anti-Calnexin primary antibodies. Anti-FITC (green) and anti-TRITC (red) secondary antibodies were used to visualise the anti-V5 and anti-Calnexin antibodies, respectively. The nuclei of the cells were visualised with the DNA stain, DAPI (blue). A. DAPI stained nuclei. B. Anti-Calnexin antibody marker for endoplasmic reticulum. C. Anti-V5 antibody marking PaLemA1 production. D. Composite image of all three channels (A-C). Scale bars: 10 μM .

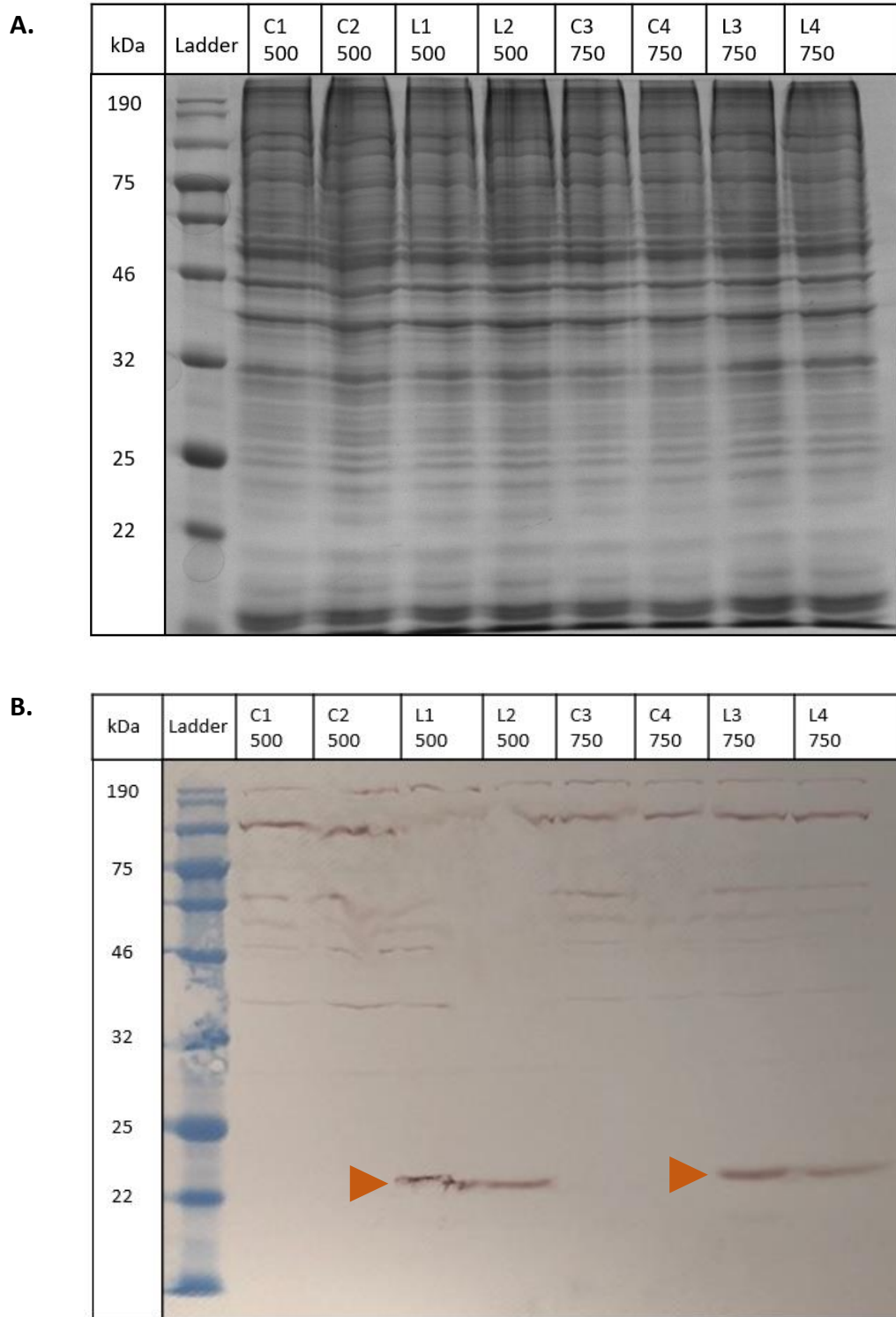


Figure 3.20. Analysis of *PaLemA1* expression in stably transfected CHO-S cells.

A. SDS-PAGE analysis of CHO-S cell lines stably expressing PaLemA1. Samples C1, C2, C3 and C4 are of CHO-S cells expressing the empty vector control and L1, L2, L3 and L4 are of CHO-S cells expressing PaLemA1. 500 and 750 refers to the concentration of Hygromycin, in $\mu\text{g/ml}$, used to select for cells expressing PaLemA1. **B.** Western blot analysis of PaLemA1 stable cell lines. The nitrocellulose membrane was stained with the primary anti-PaLemA antibody. The expected band at 22.47 kDa, indicated by the **arrow**.

Following the confirmation of PaLemA1 production in the stable CHO-S cells, further work was undertaken to examine whether the production of PaLemA1 led to the formation of any intracellular structures in these cells. In particular, TEM studies enabled us to perform more detailed investigations into the cellular localisation of PaLemA1, whilst allowing us to determine whether any organised structures were present in the transfected cells following protein production.

Initially, to ensure that the V5 epitope tag did not have any deleterious effects on the PaLemA1 protein and the resultant intracellular vesicle formation, the PaLemA1-V5 construct was subcloned into a pET3a vector and expressed in *E. coli* BL21 (DE3) Star cells (**Figure 3.21**). The cells were embedded, sectioned and imaged as before. It was evident that the C-terminal V5 tag did not seem to alter the effects of PaLemA1, as the formation of small intracellular vesicles was still clearly visible inside the cells. The vesicles appeared to be identical to those formed after the production of PaLemA1 alone, confirming that the epitope tag most likely did not alter the protein structure.

PaLemA1-V5

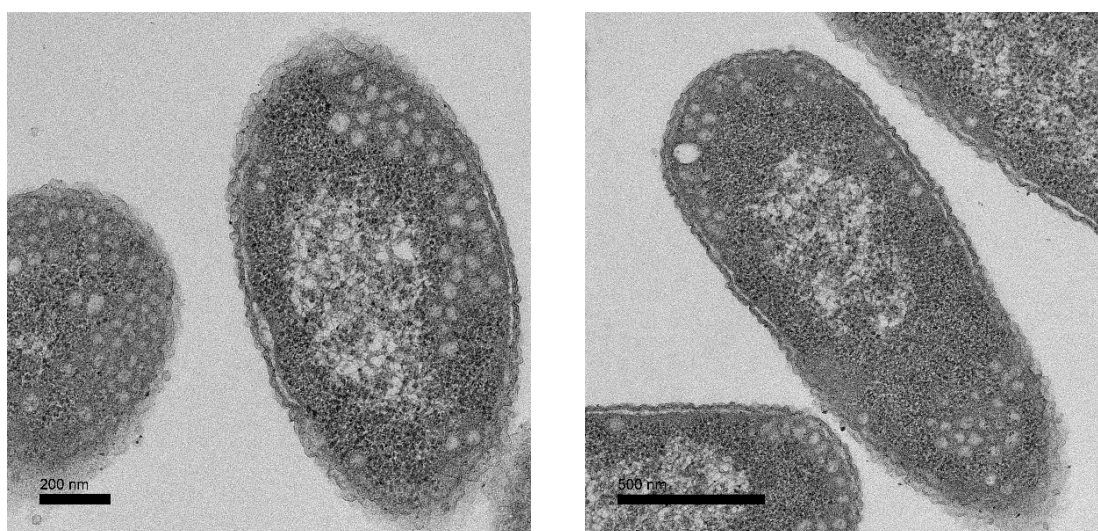


Figure 3.21. TEM of recombinant *E. coli* cells expressing *PaLemA1-V5*.

Transmission electron micrographs of *E. coli* BL21 (DE3) Star cells producing PaLemA1-V5 following an overnight induction with IPTG.

Transmission electron microscopy analysis of stable CHO-S cells producing PaLemA1 revealed the presence of intracellular and extracellular lipid vesicles, which was also the case for the control sample (**Figure 3.22 and 3.23**). In both the PaLemA1 and the control samples, the cellular membranes of the cells had vast amounts of blebbing and vesiculation taking place. While the intracellular vesicles seemed to appear in regions where the Golgi apparatus was present, the extracellular vesicles did not have a localisation pattern. Some notable differences between the two samples included the increased presence of lysosomal bodies and the characteristically darker nuclear regions in the PaLemA1 producing cell line. The lysosomal compartments seemed to have a range of different contents, with the majority of these organelles containing digested membranous material.

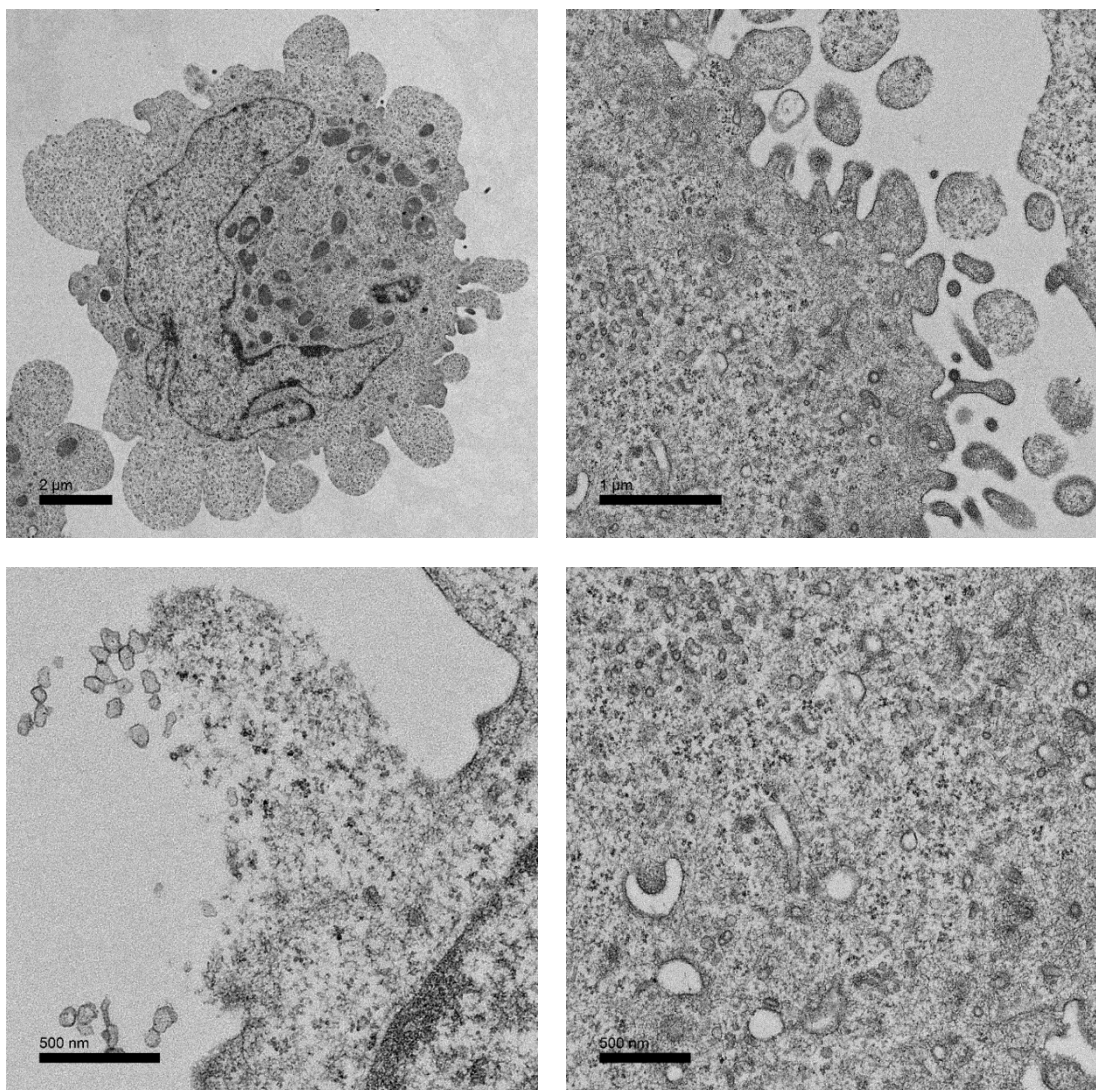


Figure 3.22. Electron micrographs of CHO-S cells transfected with the empty pcDNA3.1/V5-His-TOPO vector.

Representative transmission electron micrographs of stable CHO-S cells containing an empty vector control, pcDNA3.1/V5-His-TOPO empty vector.

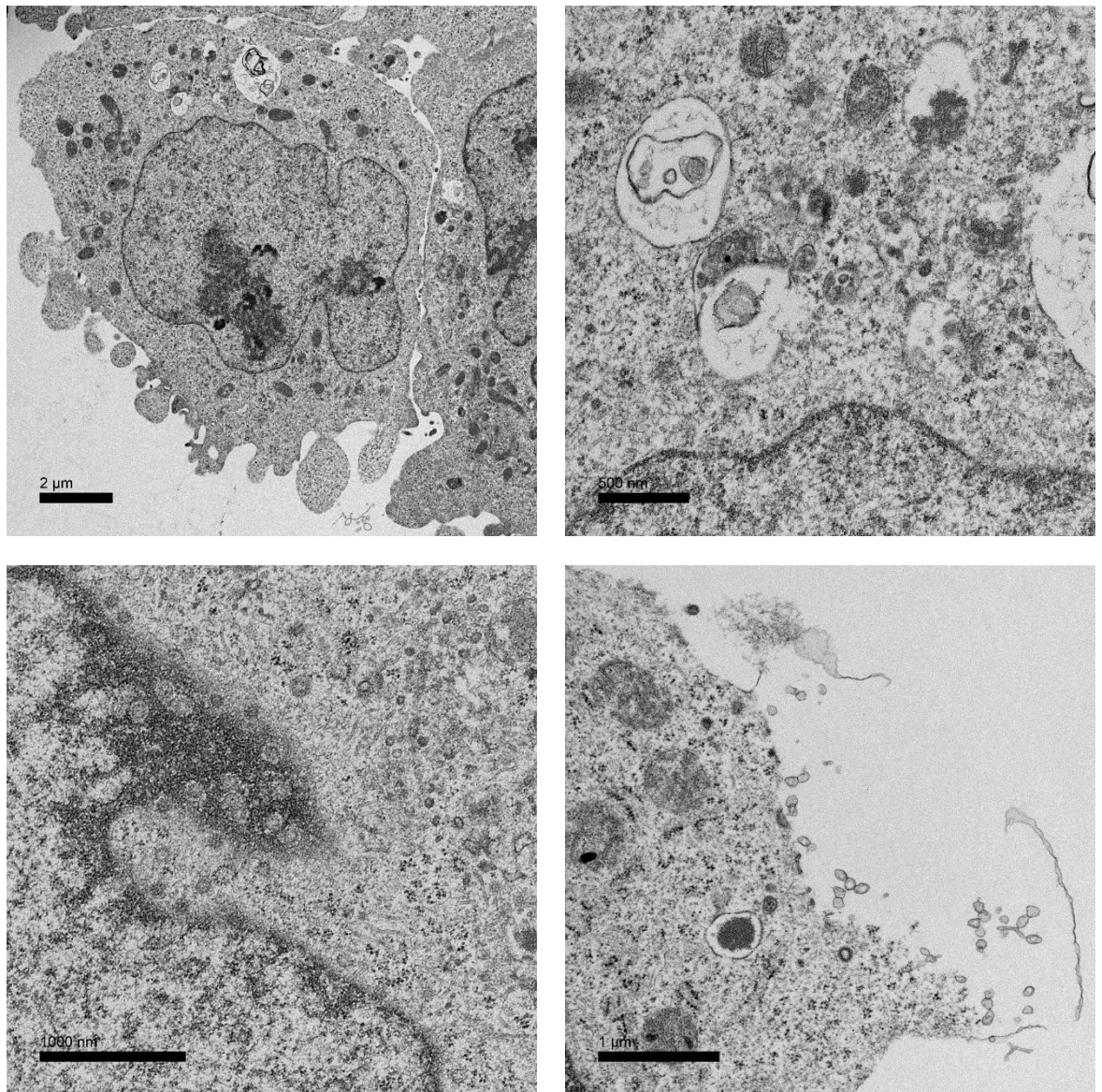


Figure 3.23. Electron micrographs of CHO-S cells producing PaLemA1.

Representative transmission electron micrographs of stable CHO-S cells expressing *PaLemA1*.

Further work was undertaken in an attempt to assess the localisation of the PaLemA1 protein in CHO-S cells. Stable CHO-S cells were seeded onto a clear coverslip and embedded in the LR white resin and sectioned. Immuno-gold labelling, using an anti-V5 primary antibody and a secondary antibody conjugated to gold coated nanoparticle was utilised to determine the localisation of PaLemA1. A range of different primary antibody concentrations were tried until the concentration at which the minimal amount of binding occurred in the control sample was found, while giving a positive signal in the cells expressing *PaLemA1*. The range of dilutions that were tested included 1:50, 1:100, 1:250

and 1:500. The 1:50 (antibody:buffer) dilution was used in the final study, as it showed the highest amount of positive binding in the PaLemA1 sample.

In the control sample a small amount of non-specific binding was observed, with 1-2 gold particles found in each cell section (**Figure 3.24**). In addition, the binding did not seem to localise to any particular cellular location, appearing random in nature. Similarly, in the PaLemA1 sample there was a small amount of gold particles binding to the cell sections (**Figure 3.25**). However, in comparison to the control sample, a lot more gold particles were present. On average 10-15 gold particles were found on each cell, with some appearing around the cell membrane, while others seemed to preferentially bind in and around the lysosome organelle. Taking these results into account, no clear pattern of PaLemA1 localisation could be identified using the control and the PaLemA1 immuno-embedded samples.

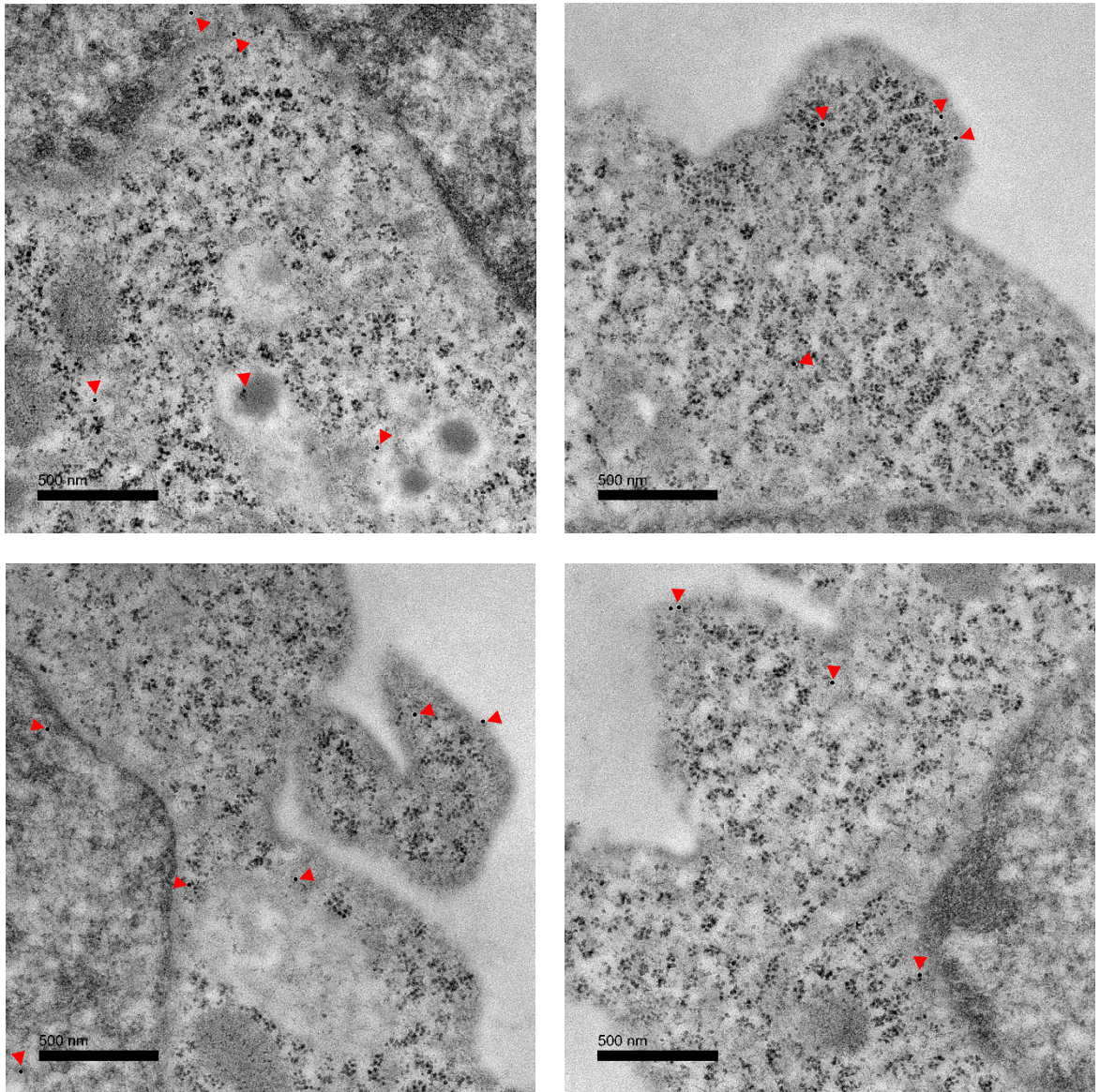


Figure 3.24. Analysis of CHO-S stable cells harbouring the pcDNA3.1/V5-His-TOPO vector using the anti-V5 primary antibody.

Representative electron micrographs of CHO-S cells stably transfected with pcDNA3.1/V5-His-TOPO vector, and labelled with a V5 primary antibody, at a dilution of 1:50, and a specific secondary antibody conjugated to a 15 nm gold particle. **Red arrows** indicate the presence of gold nanoparticles.

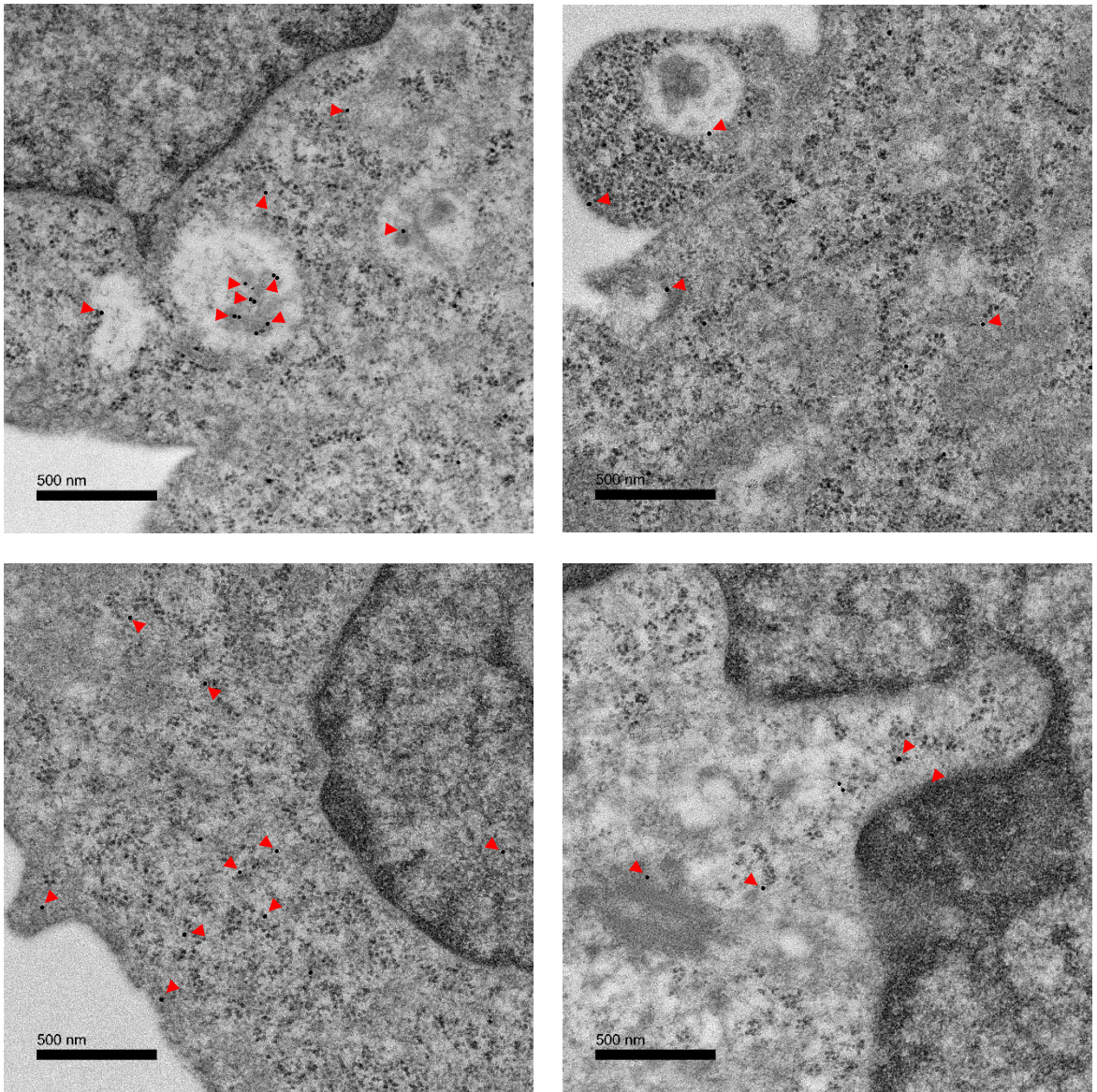


Figure 3.25. Analysis of CHO-S stable cells expressing *PaLemA1* using the anti-V5 primary antibody.

Representative electron micrographs of CHO-S cells stably transfected with PaLemA1, and labelled with a V5 primary antibody, at a dilution of 1:50, and a specific secondary antibody conjugated to a 15 nm gold particle. **Red arrows** indicate the presence of gold nanoparticles.

3.3. Discussion

In this chapter, the morphological effects of overproducing PaLemA1 and PaLemA2 proteins in both *E. coli* and CHO-S cells was explored. Following an overnight induction, *E. coli* cells producing PaLemA1 and PaLemA2 showed a range of phenotypes. While PaLemA1 harboured small intracellular vesicles, PaLemA2 producing cells showed the signs of ectopic membrane formation and contained bigger, diversely sized intracellular vesicles. Since it was clear that these proteins have membrane restructuring capabilities, further work was required to understand the full potential of these proteins for the production of specific membrane vesicles for vaccine development.

Studying of the fusion proteins, PaLemA1-sfGFP and PaLemA2-sfGFP, highlighted that while both PaLemA1 and PaLemA2 appeared to localise to the membranes, after 3 hours of protein induction PaLemA1-sfGFP populated the cytoplasmic space in distinct and punctate spots. This finding taken together with the time-course results may indicate that these regions could likely correlate to cellular areas harbouring the intracellular vesicles. Although no distinction upon which of the membranes the proteins localised to could be determined, previously conducted immuno-gold labelling studies have shed some light on this. Interestingly, following the expression of *PaLemA1* overnight the gold labelling was found co-localised to the inner membrane as well as to the intracellular vesicle structures that have been shown to form in *E. coli*. This indicates that the PaLemA1 protein is directly associated with membrane restructuring and likely plays a role in membrane curvature induction. On the other hand, PaLemA2 was found to be localised to both the inner and the outer membranes. These findings seem to be consistent with the predicted localisation of the proteins.

Furthermore, SEM analysis of PaLemA2 overproducing *E. coli* strains revealed an increased amount of outer membrane vesiculation, with larger vesicles forming on the surface of the cells at a higher frequency than those observed in the control sample. A similar observation was made when both PaLemA1 and PaLemA2 were overproduced in their native strain, *Pseudomonas aeruginosa* PA14. Though no difference in vesiculation was observed following PaLemA1 production, as was the case in *E. coli*, PaLemA2 increased outer membrane vesiculation. In addition, *P. aeruginosa* PaLemA2 knock-out strains had a greatly reduced BEV production when compared to the wild-type strain, adding further evidence

that PaLemA2 is targeted to the outer membrane, where it possibly promotes BEV formation.

Time-course studies demonstrated that the production of intracellular vesicles in *E. coli* was concomitant with *PalemA1* expression, as vesicles were present even prior to protein induction. Also, the increase in the number of vesicles following protein production provided further support to the hypothesis that PaLemA1 is directly responsible for the initiation of the inner membrane vesiculation. Although, a relatively high number of control cells appeared to have the defined membranous phenotype, in practise, the number of intracellular vesicles between the control and the PaLemA1 sample was significantly different. The reason behind the appearance of these vesicles in the control sample remains unclear, but could be due to the cells reaching the stationary stage in their growth cycle, meaning nutrient availability is limited. This can often result in cellular stress and altered phospholipid metabolism, which may lead to membrane invagination. In the case of PaLemA2, the time-course study revealed extensive formation of ectopic membranes, which was a sign of altered cellular phospholipid metabolism. Usually, cells maintain a set protein-lipid ratio in the inner membrane, but a shift in this balance can occur when a protein that localises to a membrane is overproduced. This can result in the initiation of compensatory mechanisms that synthesise additional phospholipids, largely cardiolipin, to maintain the ratio (Jamin *et al.*, 2018). However, in some cases an excess of membrane production contributes to ectopic membrane formation that can be observed in the case of the PaLemA2 time-course.

Due to the fact that in prokaryotes, proteins with related function tend to be grouped into operons, we decided to investigate the *PalemA1* and *PalemA2* operons. Expression of *PA4368*, which is predicted to be a RING type-E3 ubiquitin transferase, led to the formation of inner membrane invaginations that were dynamically shaped. Typically, prokaryotes harbouring the genes for RING type-E3 ubiquitin transferases are pathogenic in nature, utilising this enzyme to evade the eukaryotic hosts' immune response (Lin and Machner, 2017). Therefore, it could be likely that PaLemA1 plays a similar role in aiding the pathogenesis of *P. aeruginosa*.

On the other hand, the protein PA0538 situated in the *PalemA2* operon, induced widespread cell lysis that resulted in vesicle formation. PA0538 is a membrane anchored protein disulphide isomerase DsbB which is responsible for regenerating DsbA, an enzyme

which catalyses the formation of disulphide bonds. Usually this reaction takes place in the oxidative environment of the periplasm, thus it could be possible that DsbB overproduction could lead to a shift in the redox environment of the cytoplasm, which comes at a detriment to cell viability. This would explain the lack of visible overproduction of PA0538, as cells likely lysed prior to detectable quantities of DsbB could accumulate inside the cells. Furthermore, cell lysis was previously seen with DsbB production in a similar expression system in *E. coli*, further supporting the toxicity of overproducing such proteins (Bader *et al.*, 1998). However, further work would be needed to fully understand the negative implications associated with *dsbB* overexpression in *E. coli*.

Despite a few vesicles being seen inside the cells, the overproduction of PA0536 did not seem to result in any distinct phenotype, which goes in line with the lack of visible PA0536 protein production in the SDS-PAGE analysis. When expressing the *PalemA2* operon proteins in various combinations, PA0538-PaLemA2 construct, seemed to result in a lot of cell lysis, likely attributed to the expression of PA0538, since PaLemA2 production alone did not induce this phenotype. However, cell lysis was not observed when the full *PalemA2* operon was produced, which could be due to the lack of effective protein production. Previously conducted work by our German collaborators revealed that when the full *PalemA2* operon was produced in *P. aeruginosa*, it gave rise to a massive production of pyoverdine. Pyoverdines are fluorescent siderophores which play important roles as virulence factors with *P. aeruginosa* infections, indicating that perhaps the *PalemA2* operon could also play a role in pathogenesis. However, due the number of unknown factors associated with the studies, no further conclusions could be drawn from this data.

Lastly, although the stable CHO-S cell lines expressing *PalemA1* were successfully generated, production of PaLemA1 did not appear to result in a distinct phenotype that could be associated with increased cellular vesiculation. In future studies, due to the high incidence of membrane vesiculation in CHO-S cells, a more suitable cell line should be chosen to assess the potential of generating PaLemA1 derived mammalian lipid vesicles.

Overall, PaLemA1 and PaLemA2 both appear to have membrane restructuring abilities in *E. coli*. While PaLemA1 appears to have more effects on the inner membrane, PaLemA2 contributes more to the restructuring of the outer membrane, where it appears to increase BEV formation. PaLemA1 and PaLemA2 operon expression studies provided some

suggestion that these operons may contribute towards the pathogenesis of *P. aeruginosa*, though no definitive conclusions can be drawn from this.

Chapter 4

Restructuring *Escherichia coli* membranes: LemA hybrid protein expression and analysis

4.1 Introduction

Biological membranes are indispensable for life as they carry out numerous functions that include, but are not limited to, providing a permeable barrier to the extracellular environment, compartmentalising biochemical reactions and creating a matrix for insertion of proteins. In *E. coli* there are two membranes, the inner membrane that segregates the cytoplasm from the periplasm and the outer membrane that creates a boundary between the periplasm and the extracellular environment. These membranes are composed of lipids, and in this bacterium are generally comprised of PE, which constitutes about 75% of the total lipid content, PG and CL, which make up about 20% and 5% of the total lipid content, respectively (Raetz and Dowhan, 1990; Hiraoka, Matsuzaki and Shibuya, 1993). CL appears to preferentially localise to negatively curved regions of the membrane, which is not surprising given its conical shape which has intrinsic curvature, which can relax curvature frustration (Mileykovskaya and Dowhan, 2000; Huang and Ramamurthi, 2010). In addition, the lipid and protein constituents of membranes also appear to vary in composition in response to various signals and/or environmental conditions that can lead to membrane remodelling.

While membrane proteins are often overproduced in *E. coli* for the purposes of structural studies, the commonly used high yield expression systems often lead to aggregation of the membrane proteins in the cytoplasm. However, a number of recent studies have demonstrated the formation of cytoplasmic membranous structures, including vesicles, tubules as well as stacks of flat membranes, following membrane protein overproduction (Royes *et al.*, 2020). This protein-induced route of intracellular membrane proliferation presents an exciting opportunity for exploitation. Moreover, establishing control over the production and composition of such membranous structures would hold great potential for biotechnological applications.

A previous study exploring the effects of LemA protein overproduction in *E. coli* yielded some interesting results, showcasing the membrane remodelling potential of these proteins. It was, therefore, of interest to ensure these results were reproducible. Consequently, MamQ, LemA.153, LemA.159, LemA.501 and PaLemA1 were overexpressed in *E. coli*. Secondly, to delve deeper into the predicted functional domains of these proteins, it was decided to express the transmembrane and the soluble domains individually. Finally, LemA hybrid proteins containing 'mix and match' domains were generated and

overproduced in *E. coli* to explore if novel membranous phenotypes could be generated. This is of particular interest to vaccine development, since chimeric proteins containing a membrane-spanning domain capable of inducing intracellular vesicle formation could present a novel vaccine delivery platform. Thus, improving global vaccine accessibility due to the short production times and improving vaccine safety through controlling the composition of the vesicles. This would certainly present an advantage over the currently employed methods, which utilise detergents for the generation of membrane vesicles, granting less control over the composition of the membrane vesicle (Acevedo *et al.*, 2014).

4.2 Results

4.2.1 Expression and SDS-PAGE analysis of individual LemA proteins

Different LemA proteins were previously expressed in *E. coli* BL21 (DE3) Star cells and analysed for a membranous phenotype as discussed in the introduction. To confirm the previous findings, the same proteins, MamQ, LemA.153, LemA159, LemA.501 and PaLemA1 (**Table 4.1**) were expressed in *E. coli*, with an empty vector used as the control. Sequence analysis of the LemA proteins revealed the presence of a hydrophobic stretch of approximately 20 amino acids situated on the N-terminal region of each protein. This indicated the presence of an integral membrane domain, while the rest of the protein was predicted to be soluble. The localisation of the soluble domain would be highly dependent on the insertion and the orientation of the transmembrane domain, meaning the soluble domain of the protein could be positioned either on the cytoplasmic or the periplasmic side following protein expression in the gram-negative *E. coli*. It is worth noting that two of the proteins, LemA.153 and LemA.159, both originate from gram-positive bacteria. As such, the results in **Table 4.1** would suggest these proteins would be predicted to have their soluble domains orientated towards the cell surface in their respective organisms.

Following overnight protein production, the cells were analysed using TEM and SDS-PAGE. The proportion of cells displaying a membranous phenotype were quantified by counting 300 cells for each sample. The presence of a membranous phenotype was defined as any membranous structure that deviated from the control sample.

Similarly to previously obtained results, TEM analysis of MamQ revealed the presence of membranous invaginations in the cells, which appeared to be originating from the inner membrane (**Figure 4.1**, right column). Approximately 46% of cells displayed this phenotype. LemA.153 produced large vesicles that were clearly defined by a membrane and appeared mostly devoid of any luminal contents (**Figure 4.2**, left column), while the production of LemA.159 led to the formation of large inclusion bodies and small intracellular vesicles (**Figure 4.2**, right column); about 55% and 69% of cells exhibited this phenotype, respectively. The expression of *LemA.501* produced membranous ruffles, with some compartmentalisation appearing to take place (**Figure 4.3**, left column), whereas PaLemA1 led to the production of small intracellular vesicles (**Figure 4.3**, right column), with 73% and 81% of cells displaying this phenotype, respectively. SDS-PAGE analysis revealed

overproduction of all LemA proteins apart from LemA.153 (**Figure 4.4**), while in the previously conducted study only overproduction of LemA.159 was observed. This study confirmed the reproducibility of the previous findings, indicating that the membranous structures found inside the cells are likely a direct consequence of each respective protein being produced.

Name	Organism	NCBI accession	Molecular weight (kDa)	TMDs	Putative position of soluble domain in <i>E. coli</i>
MamQ	<i>Magnetospirillum gryphiswaldense</i>	CAE12041.1	30.03	1	Cytoplasm
LemA.153	<i>Bacillus megaterium</i>	ADF40219	21.8	1	Periplasm
LemA.159	<i>Clostridium kluyveri</i>	WP_012102790	21.08	1	Periplasm
LemA.501	<i>Brucella melitensis</i>	WP_006264043	23.25	1	Cytoplasm
PaLemA1	<i>Pseudomonas aeruginosa</i>	NP_253059	21.05	1	Cytoplasm

Table 4.1. LemA proteins chosen for analysis.

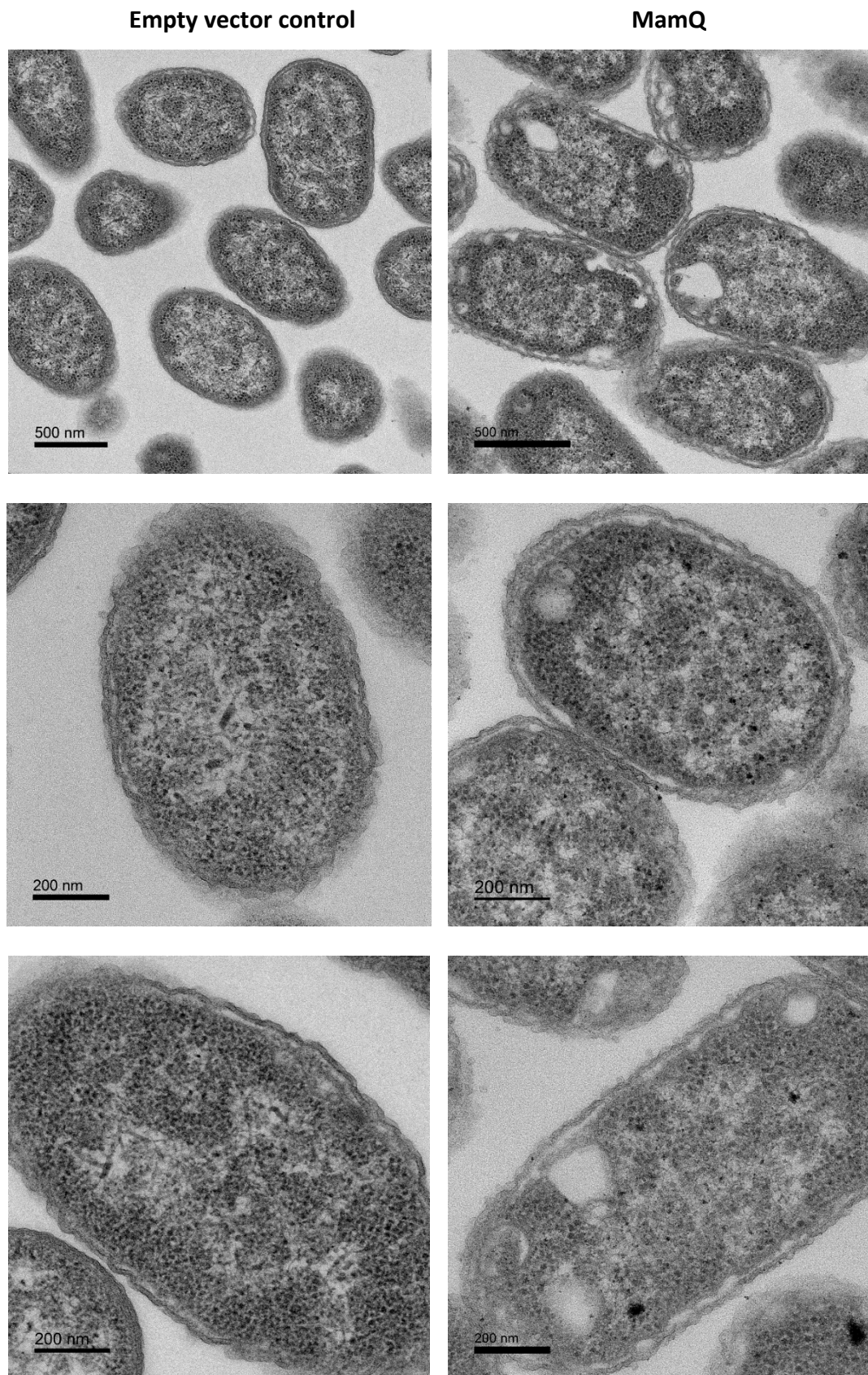
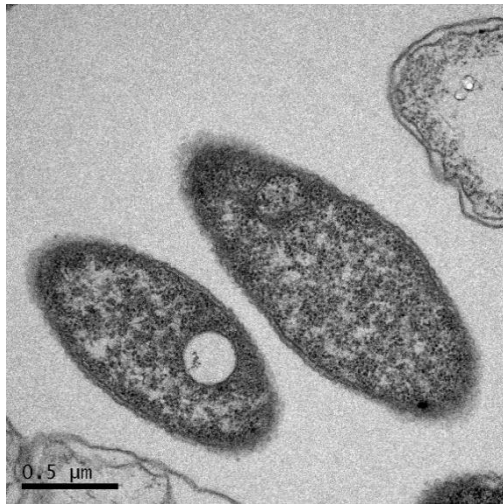


Figure 4.1. TEM of *E. coli* expressing an empty vector control or MamQ.

Transmission electron micrographs of *E. coli* BL21 (DE3) Star cells producing an empty pET3a vector (left column) or MamQ (right column), following an overnight protein induction.

LemA.153



LemA.159

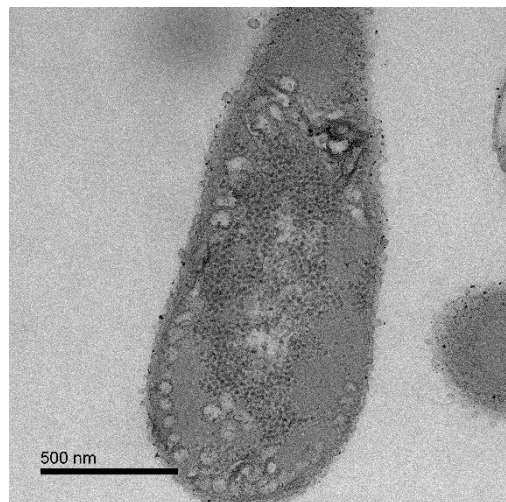
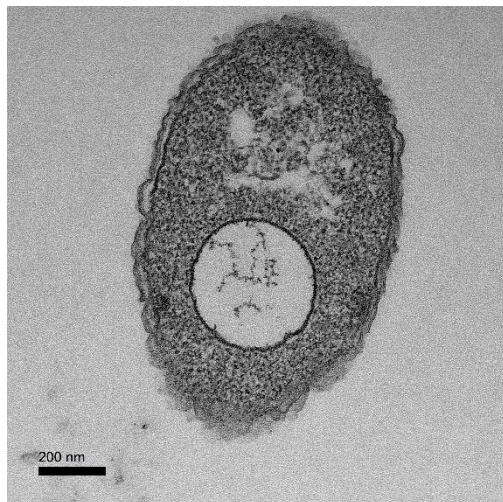
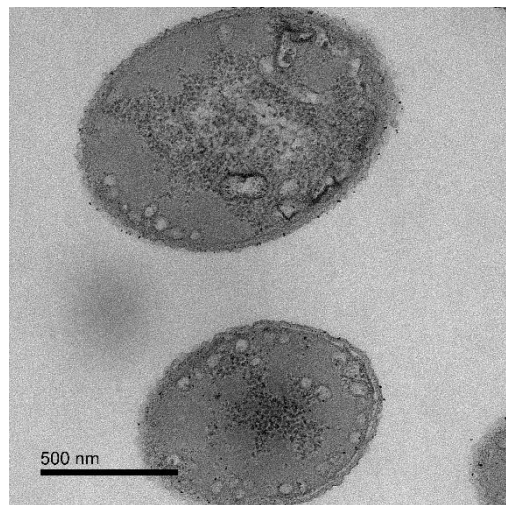
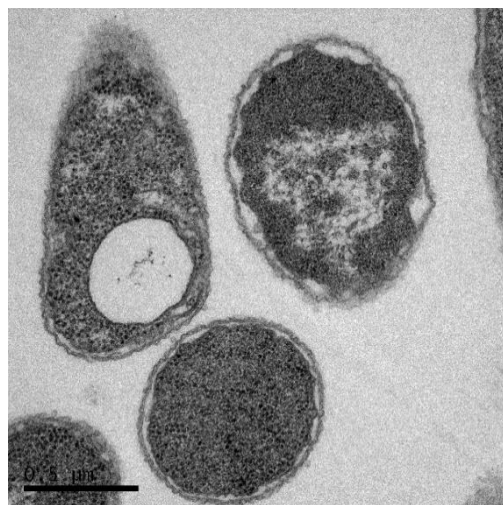
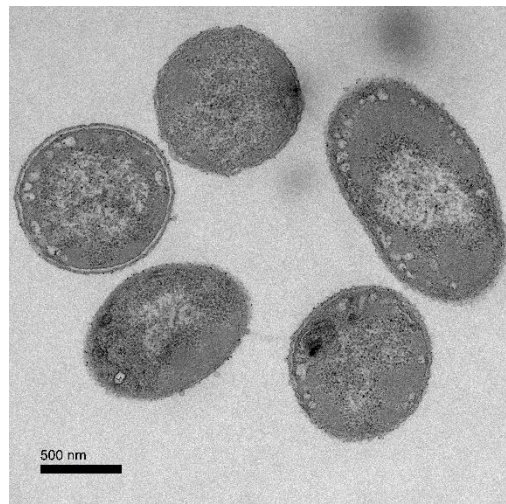


Figure 4.2. TEM of *E. coli* expressing *LemA.153* or *LemA.159*.

Transmission electron micrographs of *E. coli* BL21 (DE3) Star cells producing LemA.153 (left column) or LemA.159 (right column), following an overnight protein induction.

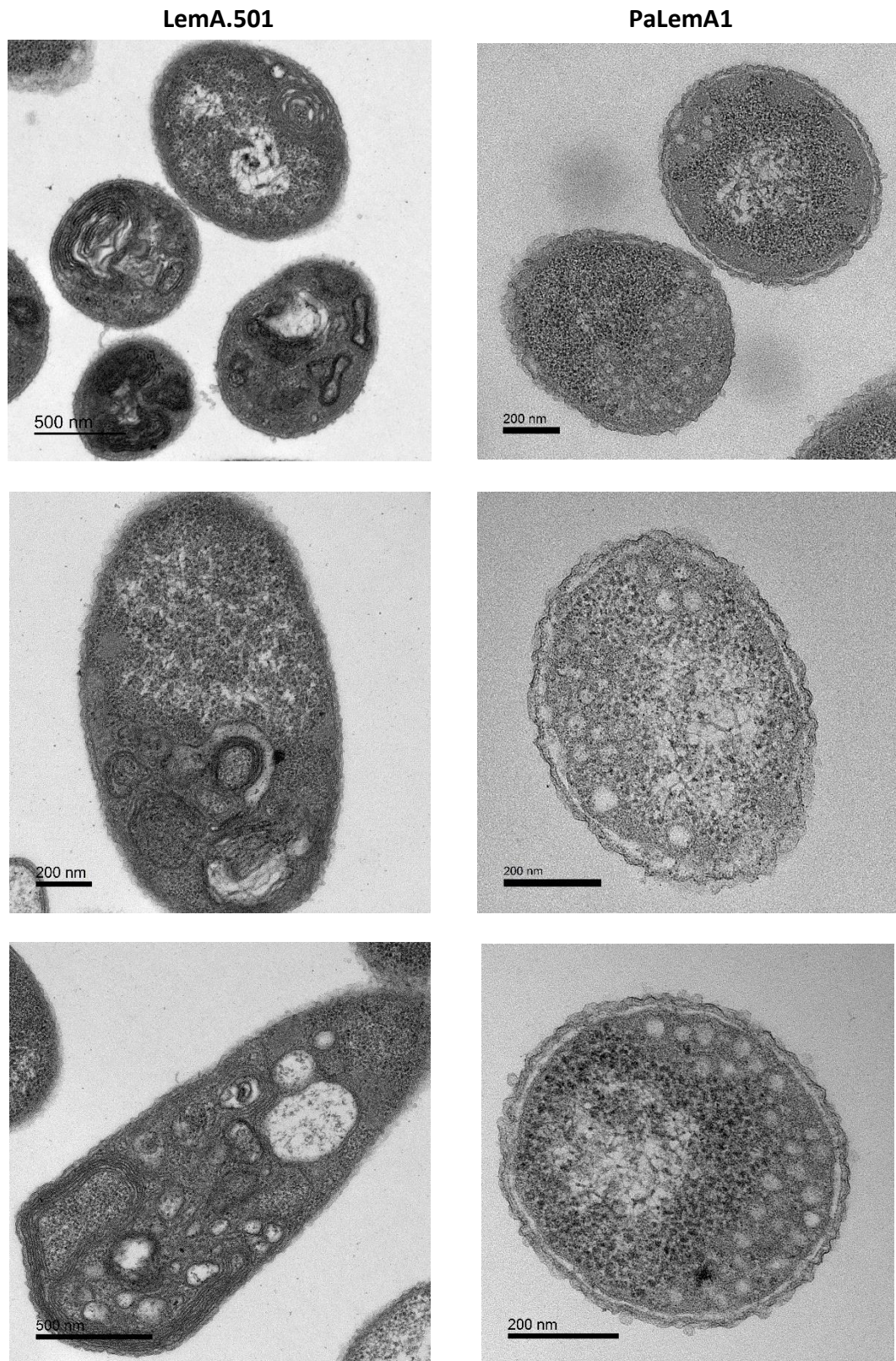


Figure 4.3. TEM of *E. coli* expressing *LemA.501* or *PaLemA1*.

Transmission electron micrographs of *E. coli* BL21 (DE3) Star cells producing LemA.501 (left column) or PaLemA1 (right column), following an overnight protein induction.

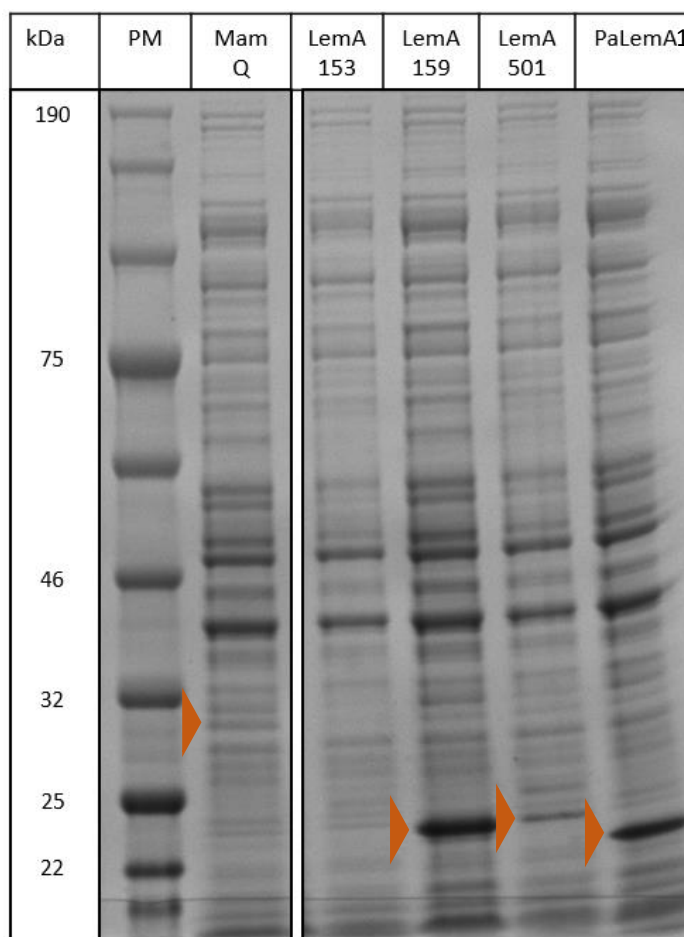


Figure 4.4. SDS-PAGE analysis of *E. coli* producing the chosen LemA proteins.

E. coli BL21 DE3 Star cells expressing MamQ, LemA.153, LemA.159, LemA.501 and PaLemA1. PM refers to the protein marker. **Arrows** indicate observable protein overproduction.

4.2.2 Expressing the transmembrane and the soluble domains of LemA proteins individually

In order to obtain more information about the membrane restructuring properties of the LemA proteins, the TMD and the soluble domains were expressed individually in *E. coli* BL21 (DE3) Star cells. Following overnight protein production, cells were fixed, dehydrated, embedded in resin, sectioned, stained and imaged using TEM. Protein production was analysed using SDS-PAGE. The SDS-PAGE gels were cropped out to remove lanes that were not relevant to this study.

The production of MamQ TMD alone did not seem to restore the phenotypic membrane invaginations that seem characteristic of the full MamQ protein. However, small inclusion bodies, as well as some outer membrane hypervesiculation could be observed in these cells (**Figure 4.5**). The expression of the soluble domain of MamQ, while leading to the production of large inclusion bodies, did also seem to lead to outer membrane vesiculation (**Figure 4.5**). Interestingly, despite successful transformations of *E. coli* DH10 β cells with the construct harbouring LemA.153 TMD, *E. coli* BL21 (DE3) Star cells did not yield any bacterial colonies. This suggests that the production of the short peptide is toxic to the cells. On the other hand, the soluble domain of LemA.153 (**Figure 4.6**) similarly to MamQ (**Figure 4.1**, right column) led to the formation of inclusion bodies, with only a few cells showing large invaginations. These invaginations could represent large vesicles or mesosomes, which are artifacts produced by the chemical fixation techniques during sample preparation.

In the case of LemA.159 both the TMD and the soluble domains led to large inclusion body formation and the hypervesiculation of the outer membrane, when compared with the empty vector control (**Figure 4.7**). It appears that the production of the TMD or the soluble domain alone is not enough to lead to the formation of intracellular vesicles, a phenotype seen when *lemA.159* is expressed (**Figure 4.2**, right column). As inclusion bodies were seen in the LemA.159 TMD and soluble domain samples with no intracellular vesicles observed, it suggests that the full length protein is required for the induction of membrane curvature that is necessary for vesicle formation. Although the molecular mechanism behind the vesicle formation is unclear, it is likely that the LemA.159 protein is integrated into the inner membrane where the topology of the soluble and the transmembrane domains induces a kink in the membrane causing it to bend and pinch off. Alternatively, phospholipid homeostasis could be disrupted by the altered lipid:protein ratio of the IM, leading to an increase in the phospholipid synthesis, resulting in intracellular vesicle formation.

On the other hand, the TMD of LemA.501 led to the formation of large intracellular invaginations which could be representative of mesosomes or vesicles (**Figure 4.8**). The soluble domain of LemA.501 led to large inclusion body formation, which was accompanied by an increase in outer membrane vesiculation, when comparing it visually with the empty vector control. Interestingly, with the expression of *PaLemA1* TMD small intracellular vesicle production was observed around the areas where inclusion bodies formed (**Figure 4.9**). This could suggest that the PaLemA1 TMD may play a big part in the induction of

curvature in the inner membrane. Similarly to the expression of other LemA soluble domains, PaLemA1 led to the formation of large inclusion bodies and the hypervesiculation of the outer membrane (**Figure 4.9**).

SDS-PAGE analysis confirmed the overproduction of all LemA soluble domains, although confirming this for the TMDs, perhaps due to the small size of the peptide proved difficult, with only the LemA.159 TMD appearing visible on the SDS-PAGE gel (**Figure 4.10**).

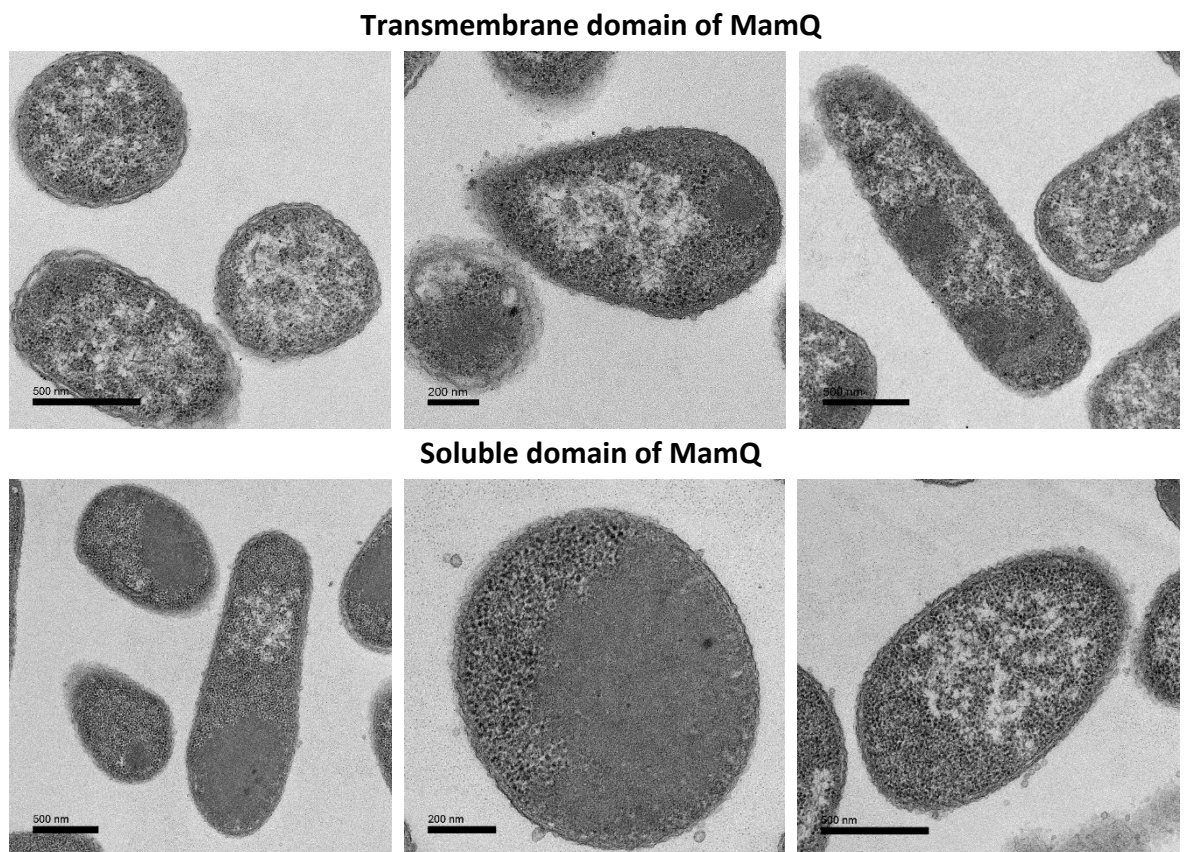


Figure 4.5. TEM of *E. coli* expressing the transmembrane or the soluble domain of MamQ.

Transmission electron micrographs of *E. coli* BL21 (DE3) Star cells producing the transmembrane domain of MamQ or the soluble domain of MamQ following an overnight protein induction.

Soluble domain of LemA.153

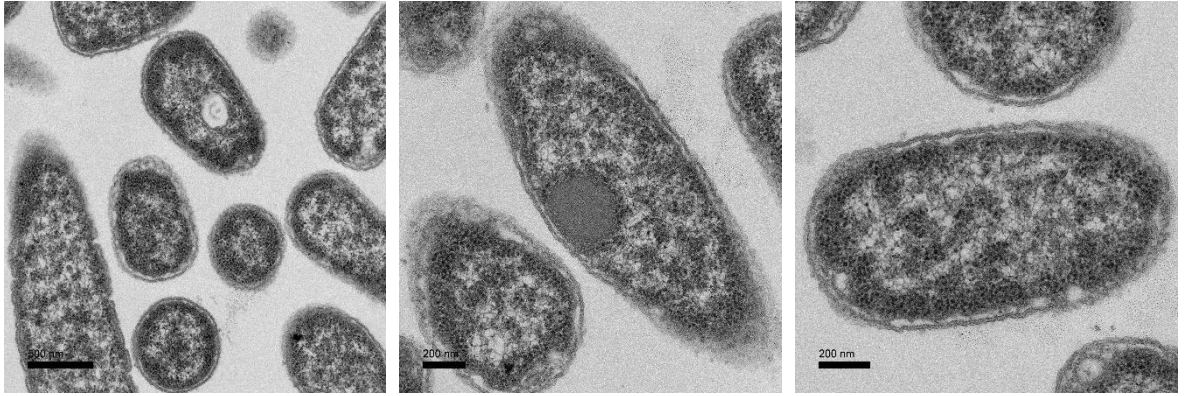
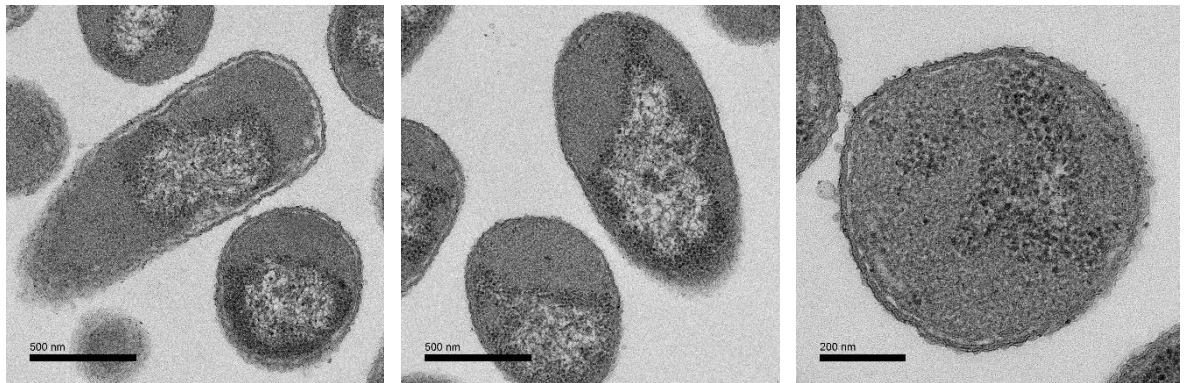


Figure 4.6. TEM of *E. coli* expressing the soluble domain of LemA.153.

Transmission electron micrographs of *E. coli* BL21 (DE3) Star cells producing the soluble domain of LemA.153 following an overnight protein induction.

Transmembrane domain of LemA.159



Soluble domain of LemA.159

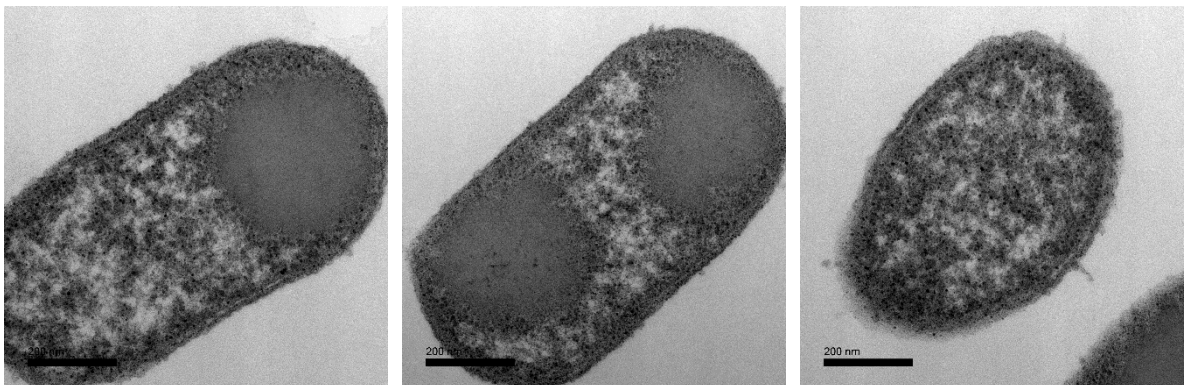
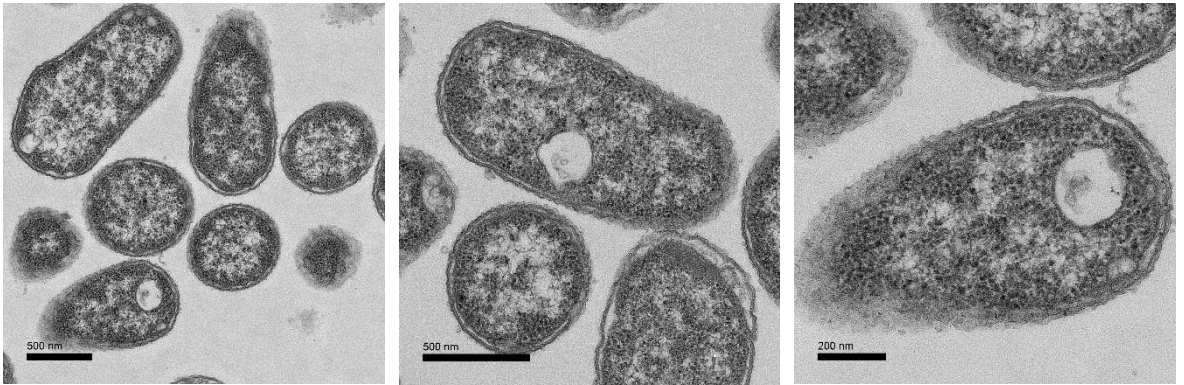


Figure 4.7. TEM of *E. coli* expressing the transmembrane or the soluble domain of LemA.159.

Transmission electron micrographs of *E. coli* BL21 (DE3) Star cells producing the transmembrane domain or the soluble domain of LemA.153 following an overnight protein induction.

Transmembrane domain of LemA.501



Soluble domain of LemA.501

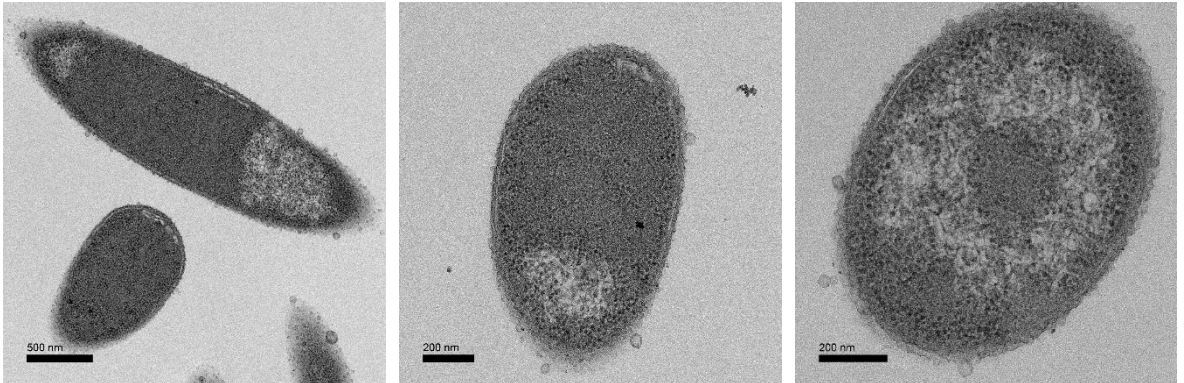
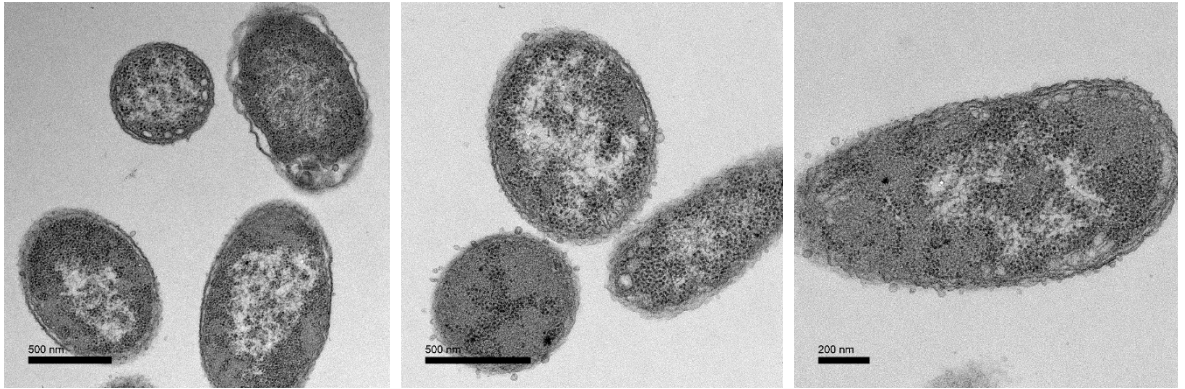


Figure 4.8. TEM of *E. coli* expressing the transmembrane or the soluble domain of LemA.501.

Transmission electron micrographs of *E. coli* BL21 (DE3) Star cells producing the transmembrane domain or the soluble domain of LemA.501 following an overnight protein induction.

Transmembrane domain of PaLemA1



Soluble domain of PaLemA1

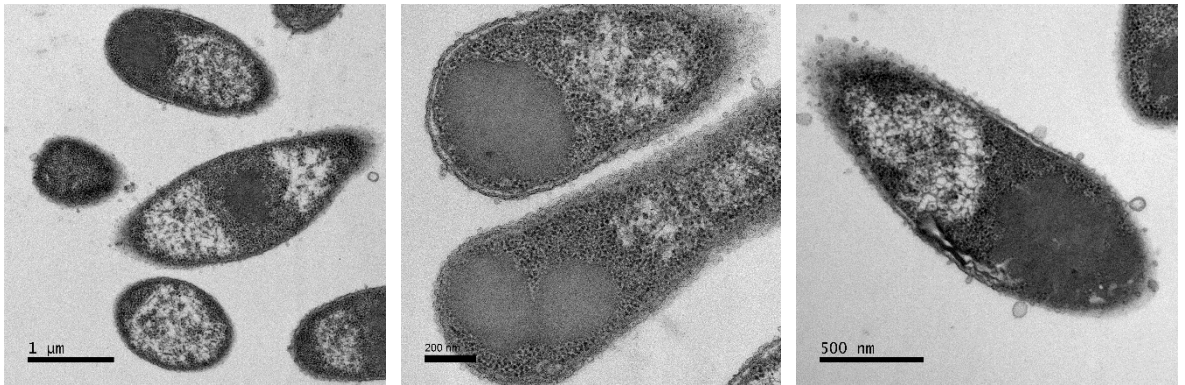


Figure 4.9. TEM of *E. coli* expressing the transmembrane or the soluble domain of PaLemA1.

Transmission electron micrographs of *E. coli* BL21 (DE3) Star cells producing the transmembrane domain or the soluble domain of PaLemA1 following an overnight protein induction.

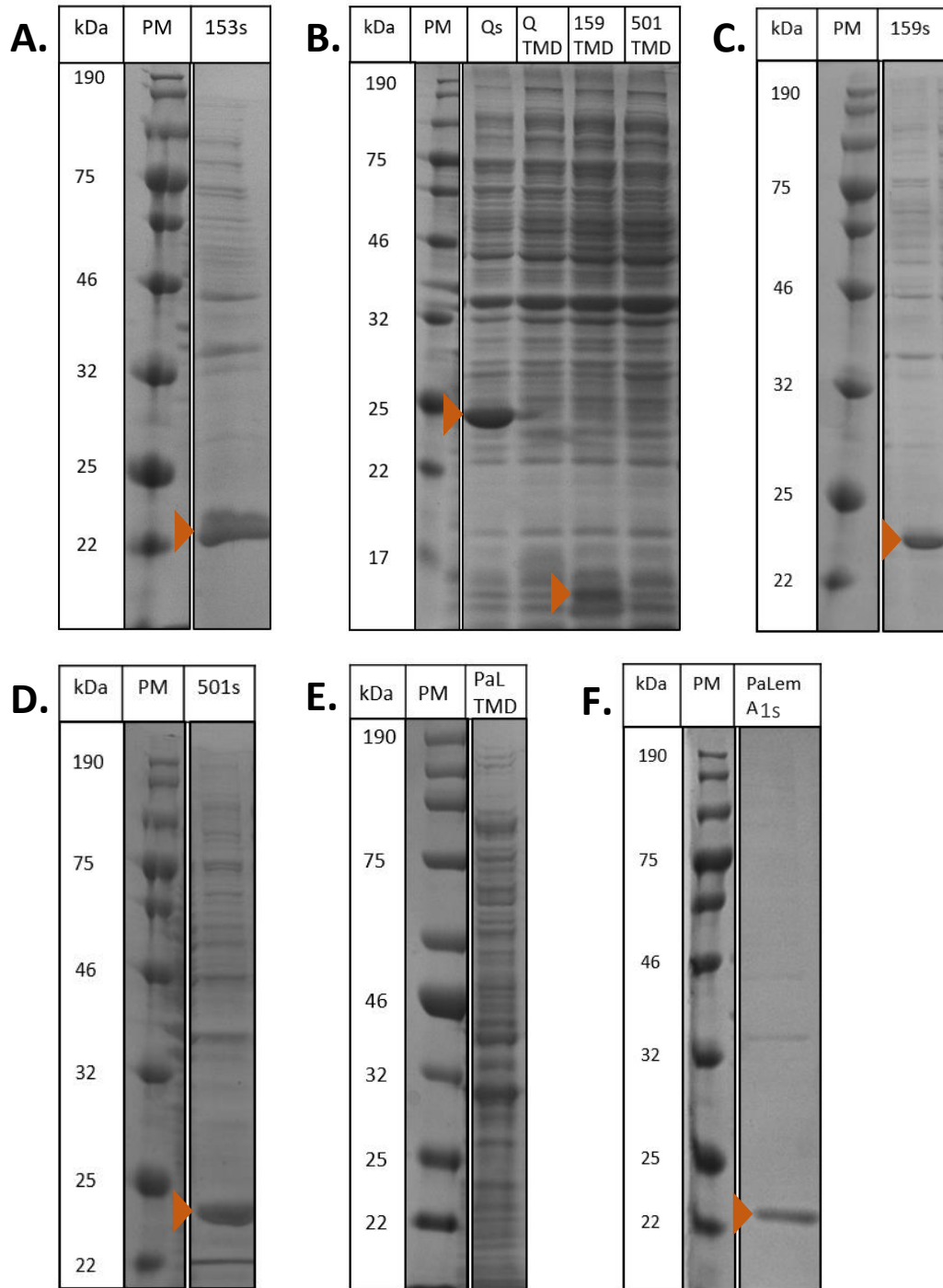


Figure 4.10. SDS-PAGE analysis of *E. coli* expressing the transmembrane domain or the soluble domain of either MamQ, LemA.153, LemA.159, LemA.501 or PaLemA1 proteins. *E. coli* BL21 DE3 Star cells expressing **A:** the soluble domain of LemA.153; **B:** the soluble domain of MamQ (MamQs), the transmembrane domain of MamQ (MamQ TMD), the transmembrane domain of LemA.159 (159 TMD) and the transmembrane domain of LemA.501 (501 TMD); **C:** the soluble domain of LemA.159 (159s); **D:** the soluble domain of LemA.501 (501s); **E:** the transmembrane domain of PaLemA1 (PaL TMD); **F:** the soluble domain of PaLemA1 (PaLemA1s). PM: protein marker. **Arrows** indicate observable protein overexpression.

4.2.3 Generation and expression of LemA hybrid protein

The production of the different LemA proteins, as well as their transmembrane and the soluble domains individually, yielded some interesting results. The formation of intracellular vesicles, as well as the increased vesiculation of the outer membrane suggested that the overproduction of these proteins results in membrane restructuring in *E. coli*. To gather more information about the possible topology of the LemA proteins and to explore whether we could employ protein engineering to selectively produce novel membranous structures, LemA hybrid protein fusions were generated. The LemA hybrids were comprised of mix and matched transmembrane and soluble domains of the selected LemA proteins. The construction of these was achieved by digesting the pET14b vector harbouring the soluble domain and the pET3a vector containing the transmembrane domain with NdeI and SpeI restriction enzymes. The TMDs and the soluble domains were then ligated in a 'mix and match' order so that every possible combination of the LemA hybrids was generated (majority of which were kindly gifted by Dr. R Juodeikis, University of Kent). It is worth noting that this cloning approach introduced a 2 amino acid linker composed of a histidine and a methionine between the TMD and the soluble domain of each LemA hybrid. Cells expressing the different hybrid constructs were analysed by electron microscopy, and constructs of interest which exhibit distinct phenotypes will be discussed in this section.

While the overproduction of the MamQ TMD MamQs hybrid protein was evident following SDS-PAGE analysis (**Figure 4.17**, Lane 1), electron microscopy revealed the presence of small vesicles that appear to remain attached to the inner membrane (**Figure 4.11**, panel A). Approximately 24.5% of cells exhibited this phenotype (**Table 4.2**), which appears to differ to that of the original MamQ protein where larger membrane invaginations were seen (**Figure 4.1**, right column). Interestingly, this is despite there only being a difference of 2 amino acids between the original and the MamQ hybrid sequence. Expression of MamQ TMD LemA.153s resulted in the formation of intracellular compartments that appear to have a defined membrane and a distinctly lighter stained lumen, suggesting that these compartments encase some cellular contents (**Figure 4.11**, panel B). MamQ TMD LemA.501s appeared to cause hypervesiculation of the outer membrane, inclusion body formation as well as some small intracellular vesicle production (**Figure 4.11**, panel C). Similarly, MamQ TMD PaLemA1s also appeared to increase the vesiculation of the outer

membrane (**Figure 4.12**, panel D), though cells also showed signs of disrupted phospholipid homeostasis as ectopic membranes could be seen in the polar regions of the cells.

In the case of LemA.153 TMD LemA.159s (**Figure 4.12**, panel E) and LemA.153 TMD LemA.501s (**Figure 4.12**, panel F) hybrid proteins, cellular debris was seen in the thin cell sections. A large proportion of regions contained lysed cells. However, it is worth noting that while the cellular debris regions of the LemA.153 TMD LemA.159s sample largely contained only the remains of the cellular membranes, the lysed cells from the LemA.153 TMD LemA.501s sample retained small intracellular vesicles in the otherwise empty lysed cells. As small vesicles can be seen in intact cells, it suggests that the vesicle formation was not a direct consequence of cellular lysis, but more likely an event that occurred prior to this as a result of protein production. It is interesting that the commonality between the two constructs is the transmembrane domain of LemA.153, which suggests that the way this domain is inserted into the membrane could disrupt the integrity of the cell. This together with the fact that the LemA.153 TMD construct could not be successfully expressed in *E. coli*, both support the idea that the expression of this domain is likely toxic to the cells.

The production of LemA.159 TMD MamQs (**Figure 4.13**, panel G) and LemA.159 TMD LemA.501s (**Figure 4.13**, panel H) largely resulted in the production of inclusion bodies, while LemA.159 TMD PaLemA1s showed a range of membranous phenotypes (**Figure 4.13**, panel I). Membrane invaginations could be seen inside some cells producing LemA.159 TMD PaLemA1s, however, a relatively large proportion of cells (~65%) contained small intracellular vesicles (**Table 4.2**). These vesicles appeared localised around the inner membrane and were largely surrounded by inclusion bodies, a characteristic phenotype of the LemA.159 protein following its overproduction in *E. coli* (**Figure 4.2**, right column). This finding suggests that the LemA.159 and PaLemA1 proteins may have some structural similarities since both native LemA.159 and PaLemA1 proteins produce intracellular vesicles in *E. coli* (**Figure 4.2**, right column; **Figure 4.3**, right column). Also, since the production of the PaLemA1 soluble domain (**Figure 4.9**) and the LemA.159 transmembrane domain (**Figure 4.7**) individually did not result in vesicle formation, means the presence of both domains is necessary for membrane remodelling.

Expression of the LemA.501 TMD MamQs construct appeared to result in cellular stress, as almost half of the cell population appeared lysed or in the process of lysing (**Figure 4.14**,

panel J). In addition, the cells that remained intact showed an increase in outer membrane vesiculation, though lacked any organised membranous structures. Similarly, LemA.501 TMD LemA.501s production also resulted in cellular lysis (**Figure 4.14**, panel L), though to a lesser extent, while LemA.501 TMD LemA.159s led to the formation of large inclusions bodies (**Figure 4.14**, panel K). This hints towards the possibility that the soluble domain of the protein may play an important role in inducing local membrane curvature. This combined with the introduction of the 2 amino acid linker between the TMD and the soluble domains, specifically in the case of the LemA.501 hybrid protein, indicates that the linker may result in the induction of a large kink in the membrane that is detrimental to cellular integrity. This goes in line with the native LemA.501 protein microscopy analysis (**Figure 4.3**, left column), since cell lysis was not observed in this sample.

Interestingly, the production of PaLemA1 TMD LemA.153s resulted in the formation of tubular structures that did not appear to have a very defined shape (**Figure 4.15**, panel N). In the case of the PaLemA1 hybrid protein, PaLemA1 TMD PaLemA1s, the presence of cytoplasmic tubules was observed (**Figure 4.16**, panel Q), which was a phenotypic deviation from the usually observed intracellular spherical vesicles in the native protein (**Figure 4.3**, right column). It was remarkable that the presence of a 2 amino acid linker between the two protein domains had such a big impact of the resulting cellular phenotype. These tubules appeared to be stemming from the inner membrane and were arranged in an orderly fashion, with 78.9% of cells displaying this phenotype (**Table 4.2**).

Lastly, the PaLemA1 TMD LemA.501s construct led to the formation of intracellular vesicles some of which appeared spherical, but for the most part seemed irregularly shaped (**Figure 4.16**, panel P). On the other hand, PaLemA1 TMD LemA.159s overproduction led to inclusion body formation with some membranous compartments being seen around the inner membrane of the cell (**Figure 4.15**, panel O). In comparison to the other LemA hybrid proteins, those which possessed the PaLemA TMD appeared to retain the ability to form intracellular membranous compartments in combination with different soluble domains. This coupled with the results obtained following the production of the PaLemA1 TMD alone (**Figure 4.9**), suggests that this domain has intrinsic curvature, and after insertion into the membrane is likely able to induce a localised kink in the membrane, a characteristic which favours the formation of intracellular membranous compartments.

Hybrid protein	Molecular weight (kDa)	Percentage of cells
Empty vector control (pET3a)	0	8.2%
MamQ TMD MamQs	30.26	24.5%
MamQ TMD LemA.153s	26.30	63.4%
MamQ TMD LemA.501s	27.56	57.2%
MamQ TMD PaLemA1s	26.40	41.7%
LemA.153 TMD LemA.159s	21.78	24.5%
LemA.153 TMD LemA.501s	23.35	55.3%
LemA.159 TMD MamQs	25.62	54.5%
LemA.159 TMD LemA.501s	22.93	33.7%
LemA.159 TMD PaLemA1s	21.76	65.0%
LemA.501 TMD MamQs	26.23	67.8%
LemA.501 TMD LemA.159s	21.96	72.0%
LemA.501 TMD LemA.501s	23.53	35.6%
LemA.501 TMD PaLemA1s	22.37	33.5%
PaLemA1 TMD LemA.153s	21.22	72.2%
PaLemA1 TMD LemA.159s	20.91	50.5%
PaLemA1 TMD LemA.501s	22.49	68.7%
PaLemA1 TMD PaLemA1s	21.32	78.9%

Table 4.2. Quantitative electron microscopy analysis of LemA hybrid proteins.

Thin sections of *E. coli* cells expressing the LemA hybrid constructs were quantified by counting a total of 300 cells per sample, with the average number of cells displaying a membranous phenotype expressed as a percentage. The empty vector pET3a was used as the control sample.

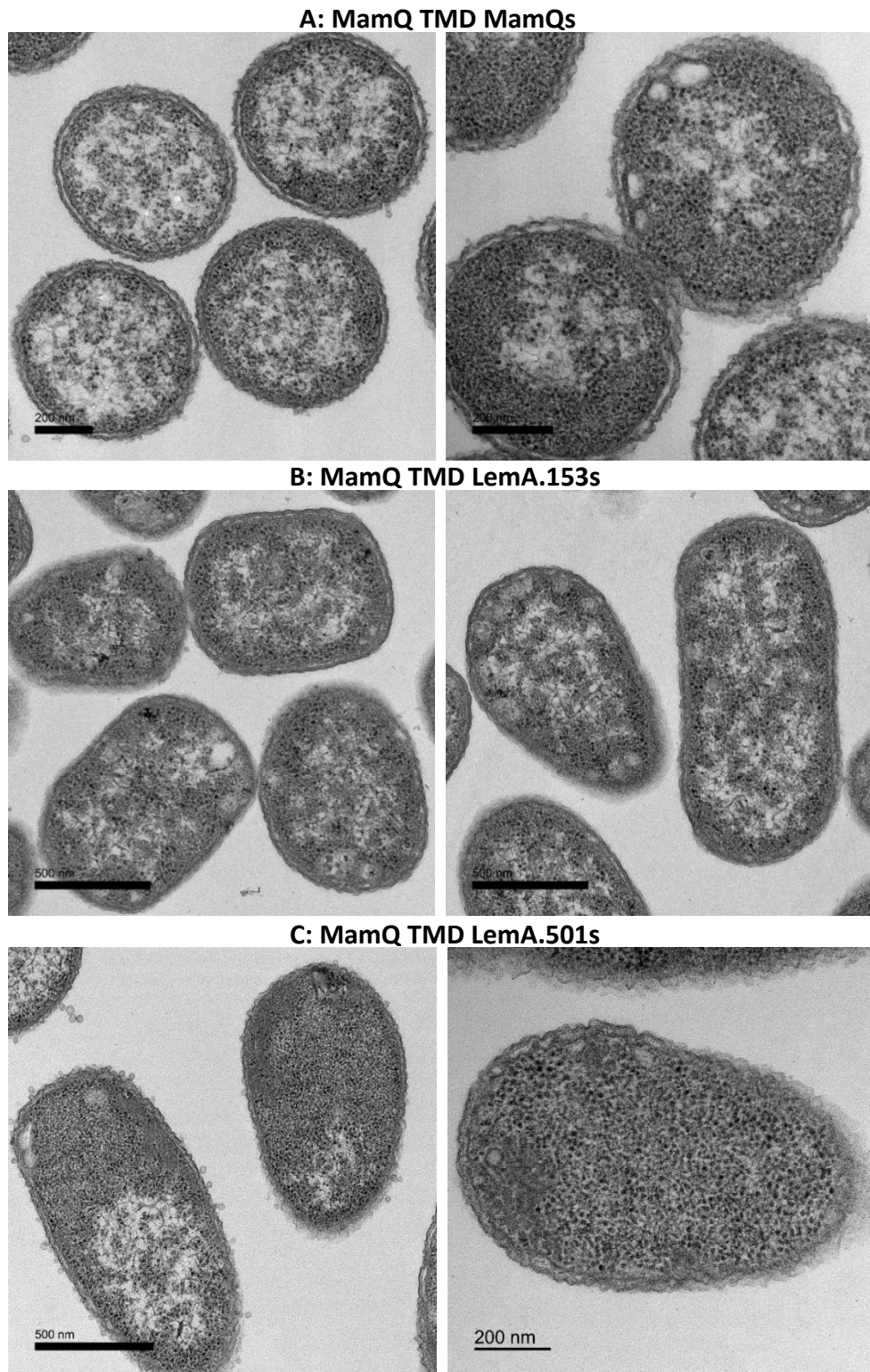
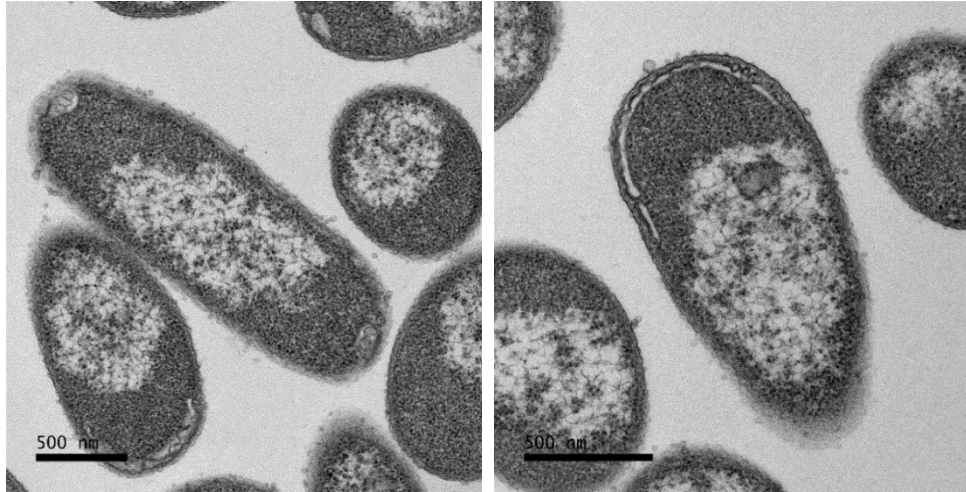


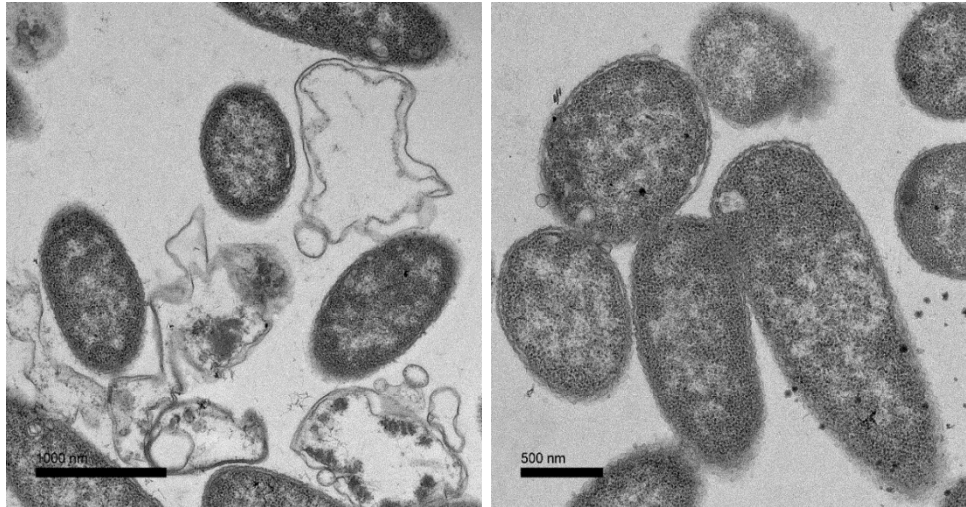
Figure 4.11. TEM of *E. coli* producing LemA hybrid proteins.

Transmission electron micrographs of *E. coli* BL21 (DE3) Star cells producing MamQ TMD together with the soluble domain of MamQ (**A**), MamQ TMD together with the soluble domain of LemA.153 (**B**) and MamQ TMD together with the soluble domain of LemA.501 (**C**).

D: MamQ TMD PaLemA1s



E: LemA.153 TMD LemA.159s



F: LemA.153 TMD LemA.501s

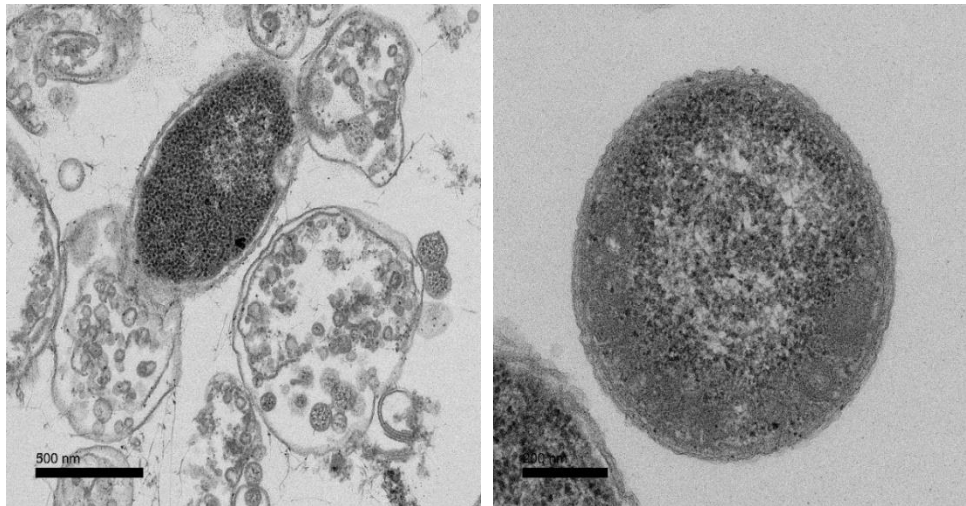
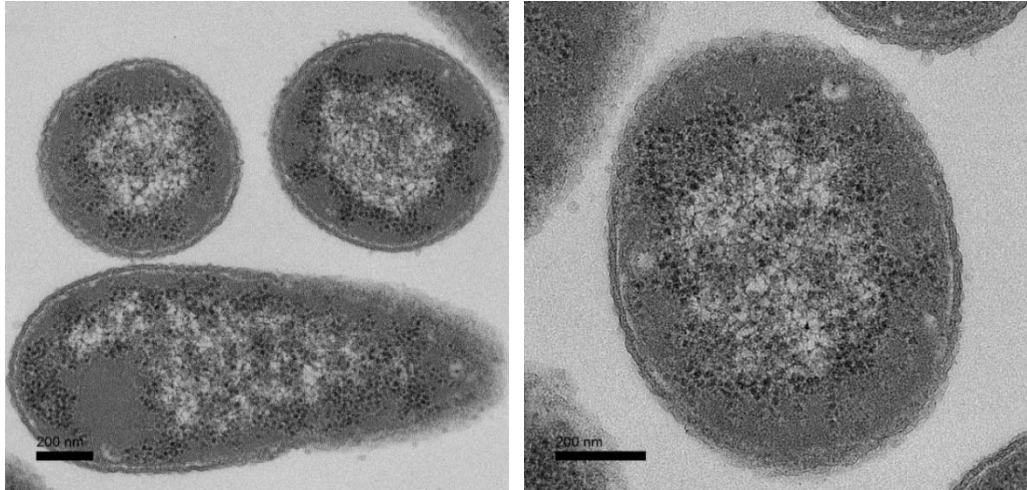


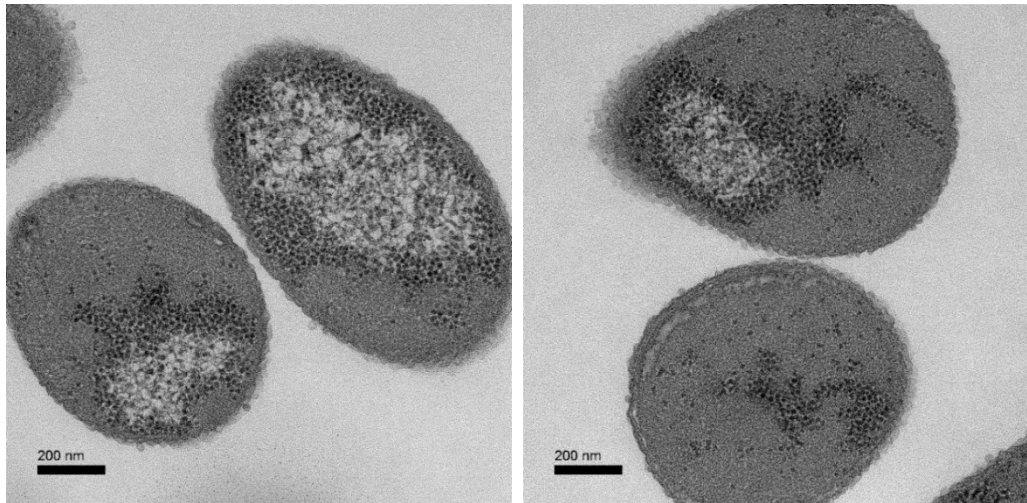
Figure 4.12. TEM of *E. coli* producing LemA hybrid proteins.

Transmission electron micrographs of *E. coli* BL21 (DE3) Star cells producing MamQ TMD together with the soluble domain of PaLemA1 (**D**), LemA.153 TMD together with the soluble domain of LemA.159 (**E**) and LemA.153 TMD together with the soluble domain of LemA.501 (**F**).

G: LemA.159 TMD MamQs



H: LemA.159 TMD LemA.501s



I: LemA.159 TMD PaLemA1s

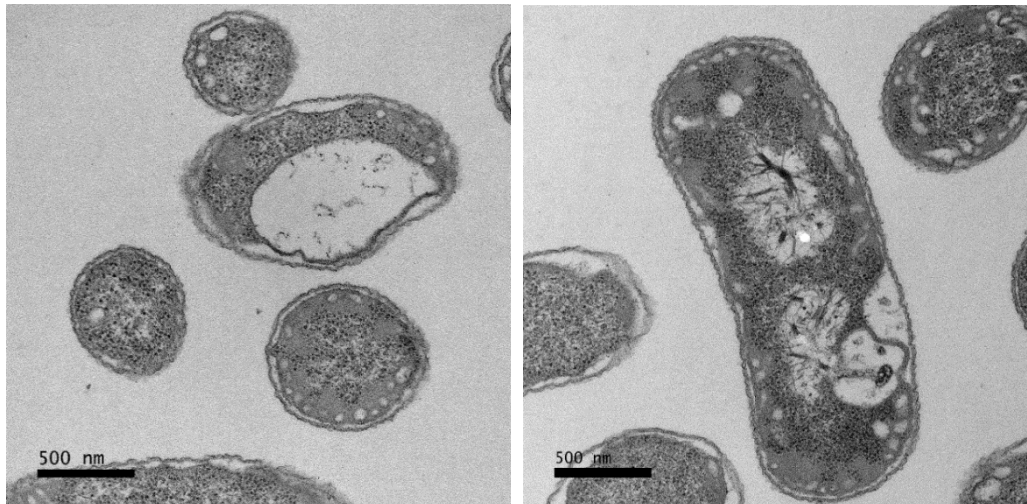
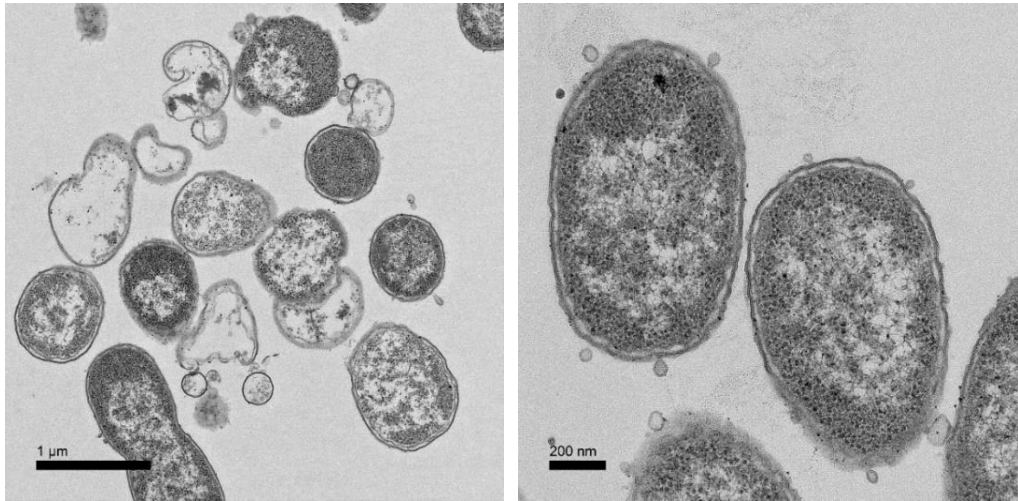


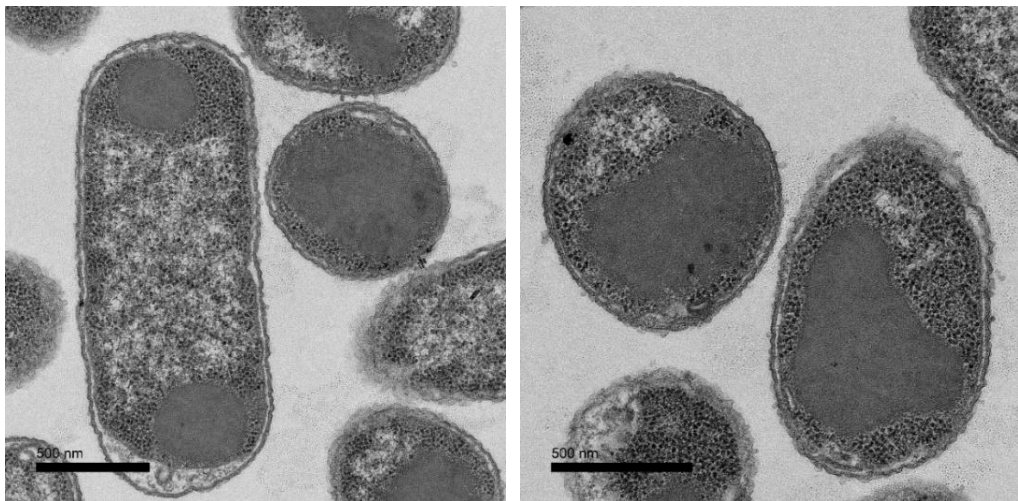
Figure 4.13. TEM of *E. coli* producing LemA hybrid proteins.

Transmission electron micrographs of *E. coli* BL21 (DE3) Star cells producing LemA.159 TMD together with the soluble domain of MamQ (**G**), LemA.159 TMD together with the soluble domain of LemA.501 (**H**) and LemA.159 TMD together with the soluble domain of PaLemA1 (**I**).

J: LemA.501 TMD MamQs



K: LemA.501 TMD LemA.159s



L: LemA.501 TMD LemA.501s

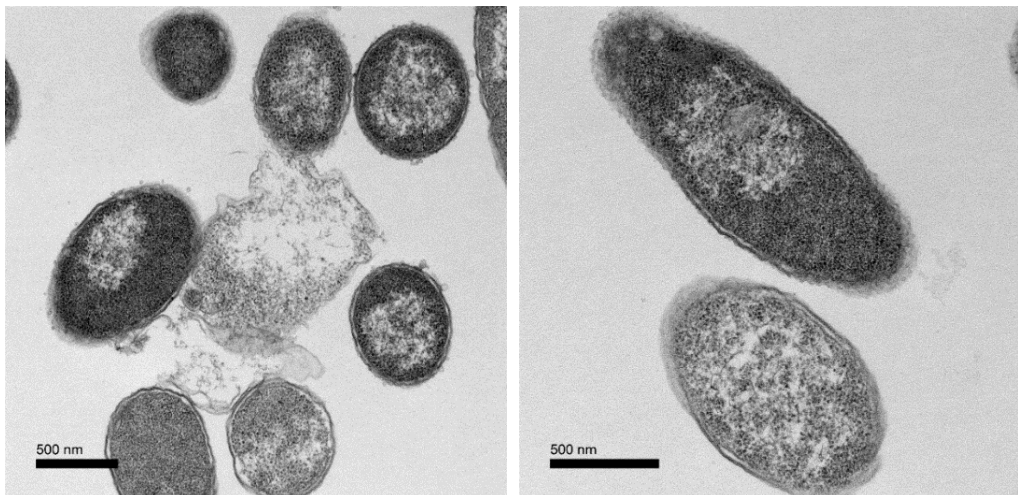
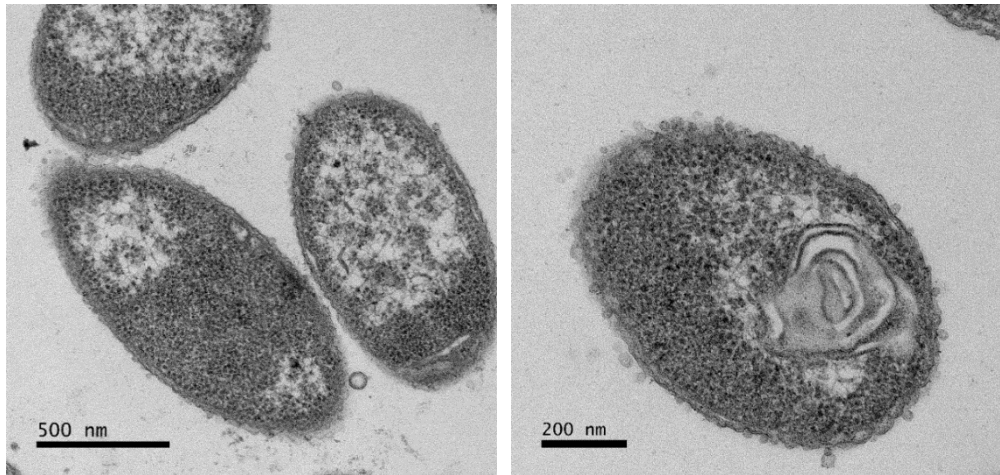


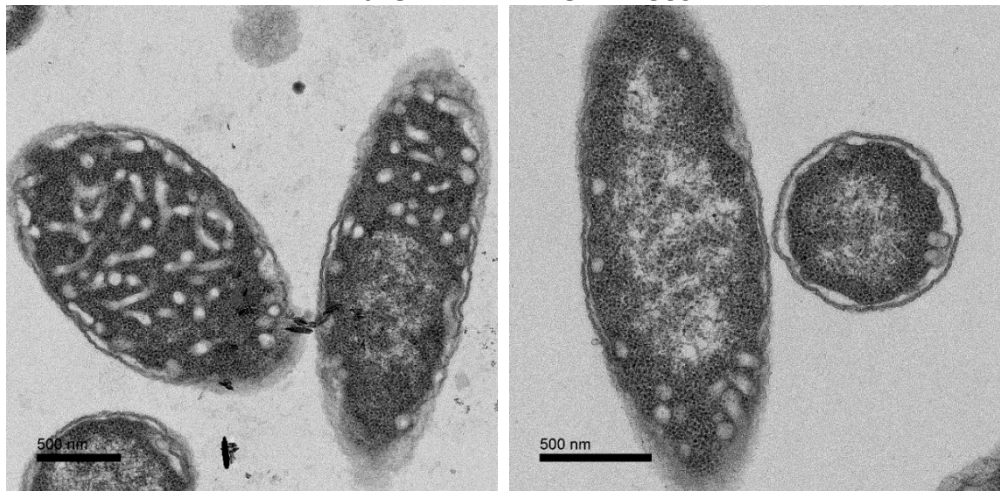
Figure 4.14. TEM of *E. coli* producing LemA hybrid proteins.

Transmission electron micrographs of *E. coli* BL21 (DE3) Star cells producing LemA.501 TMD together with the soluble domain of MamQ (**J**), LemA.501 TMD together with the soluble domain of LemA.159 (**K**) and LemA.501 TMD together with the soluble domain of LemA.501 (**L**).

M: LemA.501 TMD PaLemA1s



N: PaLemA1 TMD LemA.153s



O: PaLemA1 TMD LemA.159s

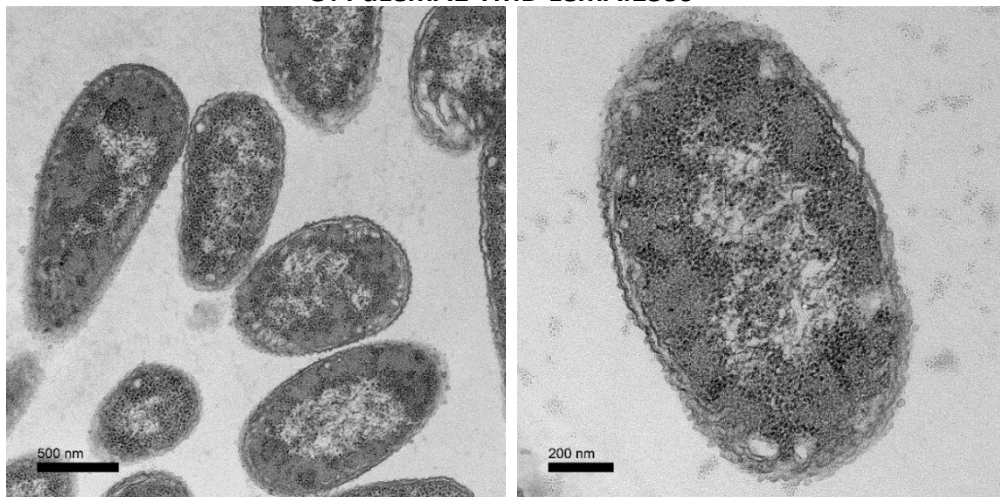
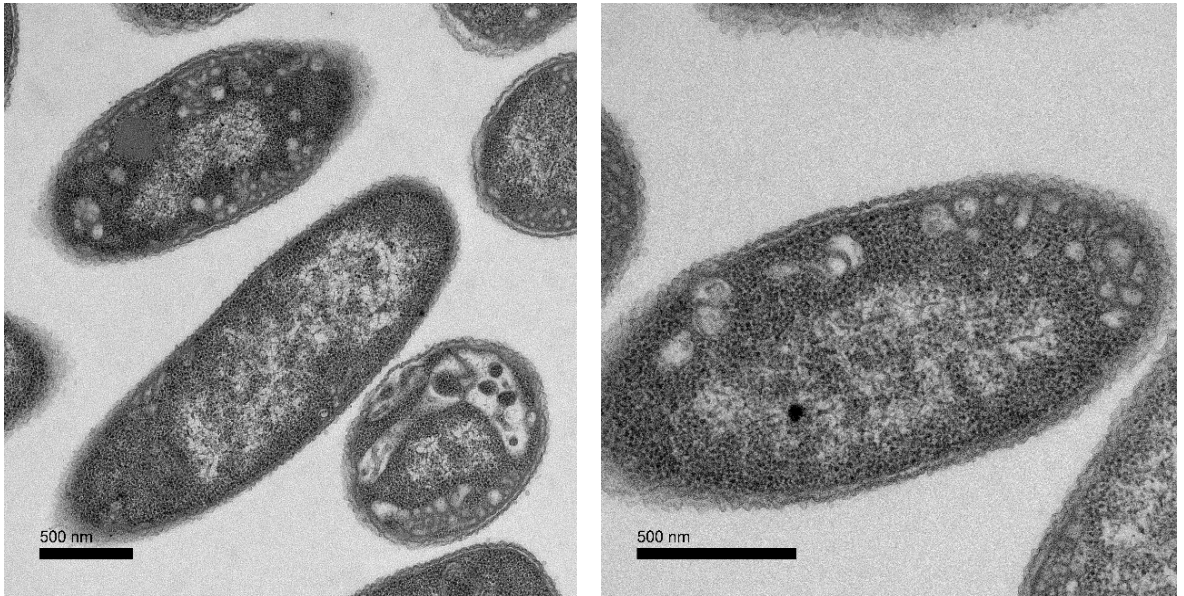


Figure 4.15. TEM of *E. coli* producing LemA hybrid proteins.

Transmission electron micrographs of *E. coli* BL21 (DE3) Star cells producing LemA.501 TMD together with the soluble domain of PaLemA1 (**M**), PaLemA1 TMD together with the soluble domain of LemA.153 (**N**) and PaLemA1 TMD together with the soluble domain of LemA.159 (**O**).

P: PaLemA1 TMD LemA.501s



Q: PaLemA1 TMD PaLemA1s

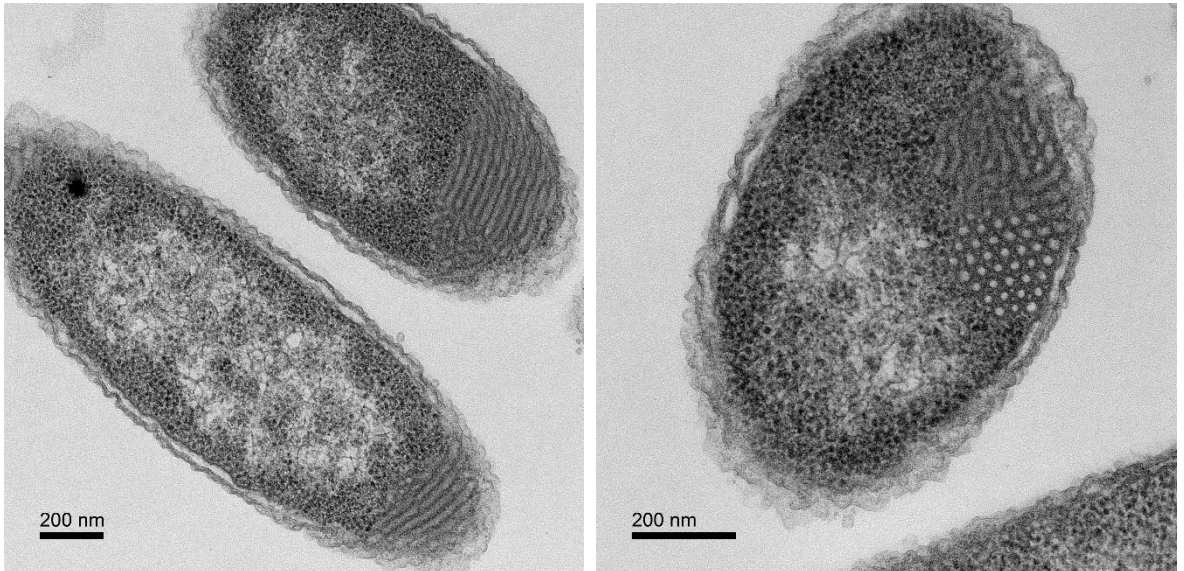


Figure 4.16. TEM of *E. coli* producing LemA hybrid proteins.

Transmission electron micrographs of *E. coli* BL21 (DE3) Star cells producing PaLemA1 TMD together with the soluble domain of LemA.501 (**P**) and PaLemA1 TMD together with the soluble domain of PaLemA1 (**Q**).

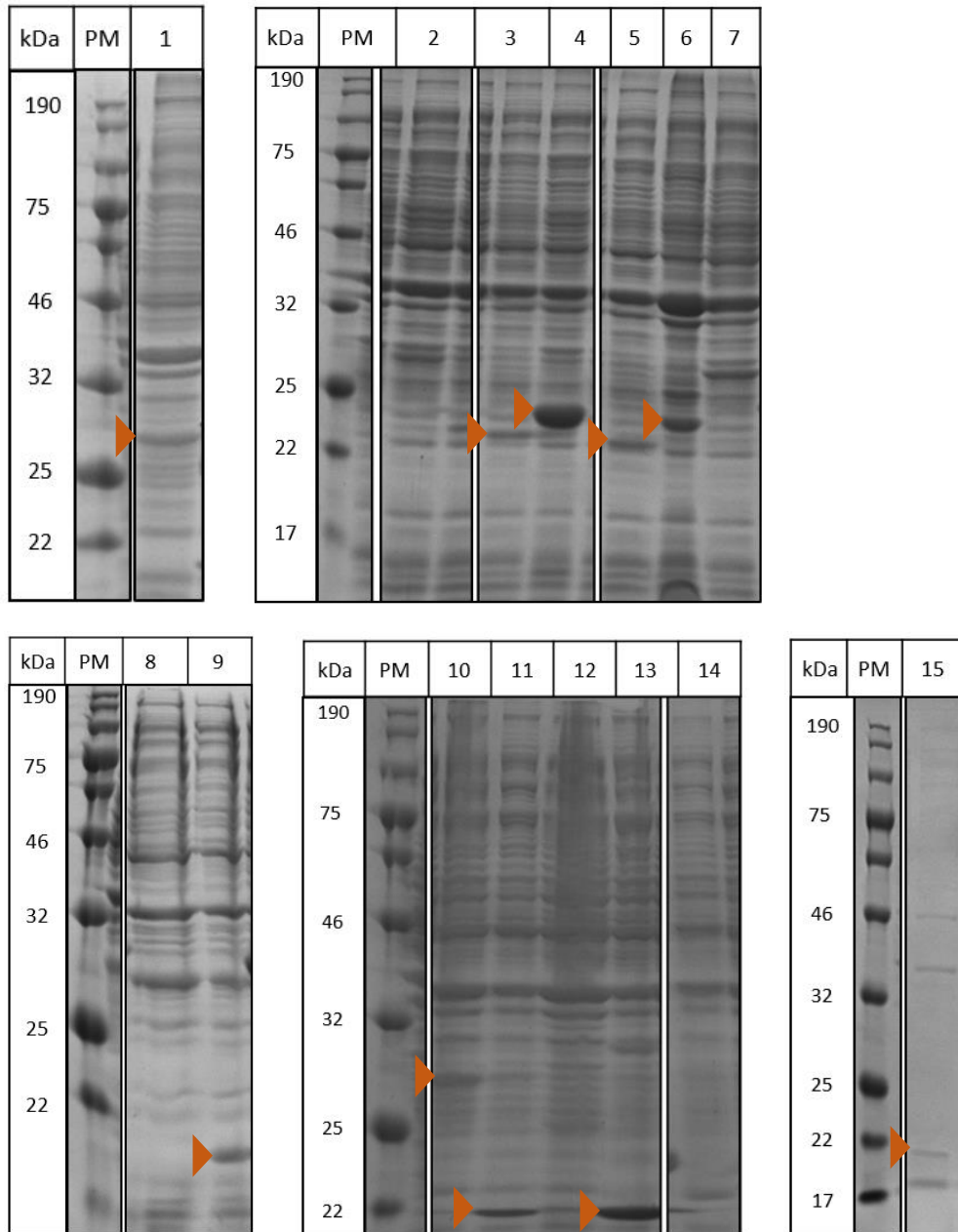


Figure 4.17. SDS-PAGE analysis of *E. coli* expressing the LemA hybrid proteins.

E. coli BL21 DE3 Star cells expressing **1**: MamQ TMD with MamQ soluble domain; **2**: MamQ TMD with LemA.153 soluble domain; **3**: LemA.153 TMD with LemA.501 soluble domain; **4**: LemA.159 TMD with MamQ soluble domain; **5**: LemA.153 TMD with LemA.159 soluble domain; **6**: LemA.501 TMD with MamQ soluble domain; **7**: LemA.501 TMD with LemA.159 soluble domain; **8**: LemA.501 with PaLemA1 soluble domain; **9**: PaLemA1 TMD with PaLemA1 soluble domain; **10**: MamQ TMD with LemA.501 soluble domain; **11**: PaLemA1 TMD with LemA.501 soluble domain; **12**: LemA.501 TMD with LemA.501 soluble domain; **13**: LemA.159 TMD with LemA.501 soluble domain; **14**: PaLemA1 TMD with LemA.153 soluble domain; **15**: LemA.159 TMD with PaLemA1 soluble domain. PM: protein marker.

Arrows indicate observable protein overexpression.

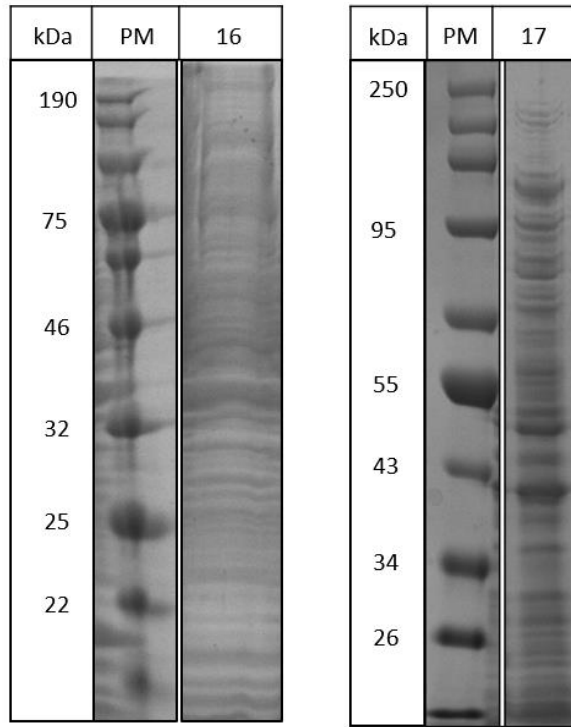


Figure 4.18. SDS-PAGE analysis of *E. coli* expressing the LemA hybrid proteins.

E. coli BL21 DE3 Star cells expressing **16**: MamQ TMD with PaLemA1 soluble domain; **17**: PaLemA1 TMD with LemA.159 soluble domain. PM: protein marker.

4.3 Discussion

In this chapter, the effects of expressing the chosen LemA proteins was explored. In particular, to confirm the previous findings, five LemA proteins of interest were firstly expressed in *E. coli*. Subsequently, taking into account the predicted structure of these proteins, it was decided to express the transmembrane and the soluble domains individually to understand more about the contribution of each domain to the observed membranous phenotype. Lastly, this was followed by the production of different LemA hybrid proteins in *E. coli*. This was done in order to explore the potential of such protein engineering approaches in allowing the selective generation of membranous vesicular structures for specific biotechnological approaches, particularly vaccine production.

The analysis of MamQ, LemA.153, LemA.159, LemA.501 and PaLemA1 proteins (**Figures 4.1, 4.2, 4.4**) confirmed the reproducibility of the previously obtained data (**Figure 1.9**). The membranous phenotypes that were observed in these cells varied according to which of the LemA proteins was produced. This coupled with the fact that the sequence identity of the five LemA proteins was between ~20-40%, means it is probable that each protein plays a different biological role in their respective organisms. It is worth noting that during this study the overproduction of these proteins, apart from LemA.153, was finally demonstrated using SDS-PAGE analysis (**Figure 4.4**). This provided a stronger basis for attributing the phenotypic cellular changes to the production of these LemA proteins in *E. coli*. In support of this are recent studies demonstrating that overexpression of some membrane proteins in *E. coli* can lead to ectopic intracellular membrane production (Jamin *et al.*, 2018). These intracellular membranes have been shown to have a number of different morphologies which include tubules, vesicles as well as poly-membrane bodies. An example of this is the overproduction of the membrane protein, glycosyltransferase MurG, which results in the formation of intracellular vesicles. Interestingly these cells had a higher cardiolipin content when compared to the cells only harbouring the empty vector control. Furthermore, the vesicles were found to be enriched with cardiolipin, suggesting that an interaction between MurG and cardiolipin occurs during vesicle formation (Van den Brink-van der Laan *et al.*, 2003). While it is unclear if the vesicles produced following *LemA.159* and *PaLemA1* overexpression (**Figures 4.2, 4.3**) are enriched with cardiolipin, studies looking into the lipid profile of these cells as well as the purified vesicles, could provide more answers.

It is clear that the generation of such morphologies requires the modification of membrane curvature, especially since such structures have been shown to be enriched with the overproduced membrane protein and cardiolipin. It is not surprising that cardiolipin has been implicated in the formation of membranous compartments, as its conical shape provides intrinsic curvature to the regions of the membrane where it is localised. Moreover, it is negatively charged which allows it to form electrostatic interactions with the basic residues of the neighbouring membrane proteins, further promoting membrane bending (Lin and Weibel, 2016; Royes *et al.*, 2020).

While the membrane protein enrichment is due to the insertion of the protein into the inner membrane, an increase in cardiolipin content could be explained by the impairment of membrane homeostasis sensors. This impairment could be due to a selective interaction between the integrated membrane protein and cardiolipin, causing localised cardiolipin clustering. This in turn could lead to an imbalance of anionic phospholipids in the inner membrane, which would subsequently be detected by the lipid homeostasis sensors, promoting lipid biosynthesis (Mileykovskaya and Dowhan, 2009; Bramkamp and Lopez, 2015; Lin and Weibel, 2016; Beltrán-Heredia *et al.*, 2019). These newly synthesised lipid membranes would permit more membrane protein insertion into the IM while maintaining cellular integrity, thus allowing the production of the membranous compartments to continue.

An alternative to this could be the formation of membrane microdomains composed of the overproduced membrane protein and cardiolipin/PG. This would in turn reduce the accessibility of these lipids to the homeostasis membrane sensors, thus stimulating lipid biosynthesis and promoting ectopic membrane production (Royes *et al.*, 2020). It is also worth considering that the LemA proteins may possess intrinsic curvature, which when integrated into the IM in large numbers could cause the membrane to bend into the cytoplasm. However, the phospholipid homeostasis mechanisms would still likely play a role in the maintenance of the lipid-protein ratio in the IM and promote phospholipid synthesis. It is uncertain whether either of these experimentally demonstrated approaches could explain the production of ectopic membranes and intracellular vesicles following LemA protein overproduction. As such, further work characterising the lipid profile of *E. coli* cells producing the different LemA proteins and structural analysis of these proteins could shed some more light on this matter.

The production of the transmembrane and soluble domains of the five LemA proteins individually led to the formation of inclusion bodies in all of the samples, except LemA.501 TMD (**Figures 4.5, 4.6, 4.7, 4.8, 4.9**). This is not unusual as high levels of recombinant protein expression in *E. coli* often result in the formation of protein aggregates. This is because the quality control system of the bacterium becomes overwhelmed and the partially folded or misfolded protein strands aggregate and form inclusion bodies (Singh *et al.*, 2015; Mathieu *et al.*, 2019). Interestingly, in these cells, an increase in the outer membrane vesiculation was also observed. However, in this case the generation of these BEVs is likely a stress response to the presence of cytoplasmic protein aggregates. This goes in line with the recent studies that have demonstrated the enrichment of such BEVs with aggregated material (Klimentová and Stulík, 2015). Although the molecular mechanisms which result in the packaging and delivery of the aggregated material to the OM remain to be elucidated.

Furthermore, the production of the membrane interacting domains alone was not sufficient to promote membrane curvature in the IM, meaning that additional protein domains are often required. This suggests that the additional protein domains play a major role in inducing highly curved membrane regions capable of modulating the formation of different intracellular structures. Thus, it was fascinating to witness the presence of a small number of intracellular vesicles following PaLemA1 TMD production alone (**Figure 4.8**). This finding could suggest that the transmembrane domain of PaLemA1 may have intrinsic curvature, which when integrated into the IM results in a localised kink in the membrane, leading to vesicle production.

When different LemA hybrids were overproduced in *E. coli* a range of different phenotypes was observed. While eight out of 25 samples did not yield any interesting results, which is likely due to a lack of protein overproduction, the remaining samples had a variety of cellular morphological changes. Namely, when overproduced in *E. coli* the LemA.153 TMD LemA.501s hybrid protein (**Figure 4.12**, panel F) leads to the lysis of a large proportion of cells. Interestingly these lysed cells contained small intracellular vesicles, which appear to have remained intact despite cellular rupture. While some of these vesicles remained attached to the membranes, a large proportion of them appeared to be freely positioned in the empty parts of the remaining cell debris. Although explosive cell lysis has been attributed as one of the mechanisms for the formation of bacterial membrane vesicles, this

seems to be an unlikely explanation for the observed phenotype (Turnbull *et al.*, 2016). This is because the cells which remain intact appear to contain small intracellular vesicles, deeming it probable that the vesicles are formed prior to cell lysis. Furthermore, during explosive cell lysis both the inner and the outer membranes would be expected to be compromised, however, in this sample a large proportion of cells appeared to have the outer membrane intact. It could therefore be likely that cellular integrity becomes compromised at the inner membrane, since the LemA hybrid proteins are likely targeted there. In addition, less of the inner membrane can be seen in the lysed cells. This could be due to a number of reasons, though the most likely causes are likely down to the continued insertion of the hybrid protein and/or disruption of phospholipid homeostasis. When considering the biotechnological applications of such a system, being able to selectively induce cellular lysis after intracellular vesicle production without the use of harsh chemicals or mechanical treatment presents an attractive method for vesicle extraction. This is due to the fact that the aforementioned treatments risk damaging the vesicles themselves.

Following the production of PaLemA TMD LemA.153s (**Figure 4.15**, panel N), tubular structures could be observed in the cytoplasm. These structures appeared to be extending from the inner membrane, though they did not have a clearly defined shape, as some of these tubules appeared bent. As these tubular structures were not seen after the production of the native LemA proteins, it is likely that the combination of these particular transmembrane and soluble domains, together with the two amino acid linker, favoured the extension of the inner membrane inwards to the cytoplasm. Conversely, the overproduction of PaLemA1 TMD PaLemA1s (**Figure 4.16**, panel Q) resulted in the formation of cytoplasmic tubules which were often localised to the polar regions of the cells. Similar tubular extensions have been seen following the overproduction of fumarate reductase and glycerol-3-phosphate acyltransferase in *E. coli*, and in accordance with previous studies, these tubules were seen to be enriched with cardiolipin (Weiner *et al.*, 1984; Wilkison and Bell, 1997). It was fascinating that the introduction of a histidine and a methionine in between the transmembrane and soluble domains of the PaLemA1 protein had such a significant impact on the shape of the vesicles. While it is difficult to pinpoint the exact molecular mechanism for this change in phenotype, it could be that the amino acid linker gives the soluble domain a little more flexibility, preventing it from inducing large bends in the inner membrane. This would favour the extension of the inner membrane into the cytoplasm, rather than promoting the bending and subsequent pinching of the

membrane in the case of spherical vesicle production. Alternatively, it may be that the addition of a positively charged histidine that is closely located to other positively charged residues, promotes a stronger interaction with the negatively charged cardiolipin in the membrane. This could bring about a slight difference in the way the membrane is forced to bend, generating a novel phenotype.

Overall, the production of MamQ, LemA.153, LemA.159, LemA.501 and PaLemA1 seemed to have an effect on the inner membrane of *E. coli* and confirmed the reproducibility of the previously obtained data. Transmembrane domains alone were not sufficient to bring about membranous compartment formation in the bacterium, however, when combined with different soluble domains, produced a range of different phenotypes. As such, it is clear that the LemA protein family are able to restructure the bacterial membrane in many ways. The data presented in this chapter demonstrates the potential of utilising protein engineering approaches in directing the formation of specific membranous organelles, which could be valuable for many biotechnological applications.

Chapter 5

Structural investigations into the *Pseudomonas aeruginosa* PA14 PaLemA1 protein

5.1 Introduction

Membrane proteins represent an important class of macromolecule that have essential functions in a wide range of cellular processes vital for the survival of organisms. These include, but are not limited to, roles in signal and energy transduction, catalysis of chemical reactions and transport of molecules and ions across the membrane.

Often, membrane proteins are composed of multiple protein domains, some of which are hydrophobic and bury themselves within cell membranes, while others are hydrophilic and face the aqueous cytoplasm/periplasm or the cell exterior. Usually, the transmembrane domain of integral membrane proteins has a sequence of approximately 19-23 hydrophobic amino acids that spans the hydrophobic interior of a cell membrane (Yeagle, 2011). In the majority of cases the native topology of membrane proteins is established co-translationally with the assistance of the Sec translocon (Heinrich *et al.*, 2000). Together with the YidC 'insertase', the Sec translocon is thought to usher the transmembrane helices to the membrane core through a lateral opening within its transbilayer pore (Petriman *et al.*, 2018).

Astonishingly, membrane proteins account for 20-30% of all synthesised proteins in all organisms, further signifying their biological importance (Almén *et al.*, 2009). However, despite efforts being made to solve the structures for many of these proteins, only 3% of all solved structures currently account for unique membrane proteins (Moraes and Quigley, 2021). This can be explained by the many caveats associated with structural studies of membrane proteins. In most cases, native membrane proteins have a low cellular abundance which proves insufficient for structural analysis. Consequently, heterologous expression systems often utilise the *E. coli* BL21(DE3) strain together with T7 promoter-based plasmids for the overproduction of membrane proteins (Mathieu *et al.*, 2019). However, in many cases, due to the high level of overexpression, a large proportion of these proteins fail to insert into the membrane leading to inclusion body formation and cellular stress, which may be deleterious to the cell. Subsequently, the isolation of membrane proteins often requires the use of detergents, which allow for the controlled dissociation of the membrane protein from its lipid environment. This step, too, requires detergent optimisation on a case-by-case basis, as efficient protein solubilisation is dependent on many different empirical factors, with many membrane proteins being relatively unstable in detergent micelles (Kalipatnapu and Chattopadhyay, 2005). As a result, progress in

membrane protein structure determination has been slow. However, once sufficient quality and quantities of the membrane protein become available, there are several methods that can be utilised for structural determination, which include X-ray crystallography, NMR and cryo-electron microscopy.

The LemA protein family was shown to promote large scale membrane restructuring, since the overproduction of the LemA proteins in *E. coli* resulted in the formation of various membranous phenotypes (**Figure 1.5**). Particularly, the overproduction of PaLemA1 led to the formation of small intracellular lipid vesicles (**Figure 4.3**), which offers potential for many biotechnological applications, especially in the development of a novel vaccine delivery platform. Bacterial extracellular vesicles currently being used as carriers of specific antigens in vaccine formulations (Holst *et al.*, 2013) largely rely on detergents for the generation of these vesicles. The PaLemA1 directed membrane restructuring therefore may allow for a more targeted approach for the construction of antigen presenting lipid vesicles for vaccine delivery systems. This could be achieved by utilising protein engineering approaches to create chimeric proteins that contain a membrane integrated domain and an adequate antigen, and direct bacterial membrane vesiculation. However, due to our lack of understanding of the molecular mechanisms underpinning PaLemA1 driven vesicle formation, further work is necessary to understand the processes associated with bacterial membrane restructuring. This would allow for a more targeted approach to bacterial cellular redesign.

In general, protein structures can provide a lot of information about a protein of interest, for example its topology, oligomerisation status, and bearing in mind that the shape of the protein determines its interaction with other molecules, with further analysis could provide invaluable information about the function of the protein. Consequently, structural studies were carried out on PaLemA1 in order to gain a greater understanding of the structure-function relationship of this protein.

5.2 Results

5.2.1 Cloning of PaLemA1 with a polyhistidine tag

In order to produce sufficient amounts of the PaLemA1 protein and to simplify the purification process, an appropriate vector had to be constructed. A pET23b vector was chosen to house the construct as it harbours a polyhistidine (His) tag. As the transmembrane domain of the PaLemA1 protein was predicted to be on the N-terminus, a key region for membrane insertion, the PaLemA1 protein was cloned in-frame with the His-tag on the C-terminus. To generate this construct the gene within the pET3a PaLemA1 construct was firstly amplified using the primers harbouring NdeI (forward) and XhoI (reverse) restriction sites, as listed below.

Forward: GATATACATATGAGTCTGACCGCTATCGCTTTCTGGGTTGCCTGCTG

Reverse: GACTCGAGGCCGAACAGGGCCTTGAG

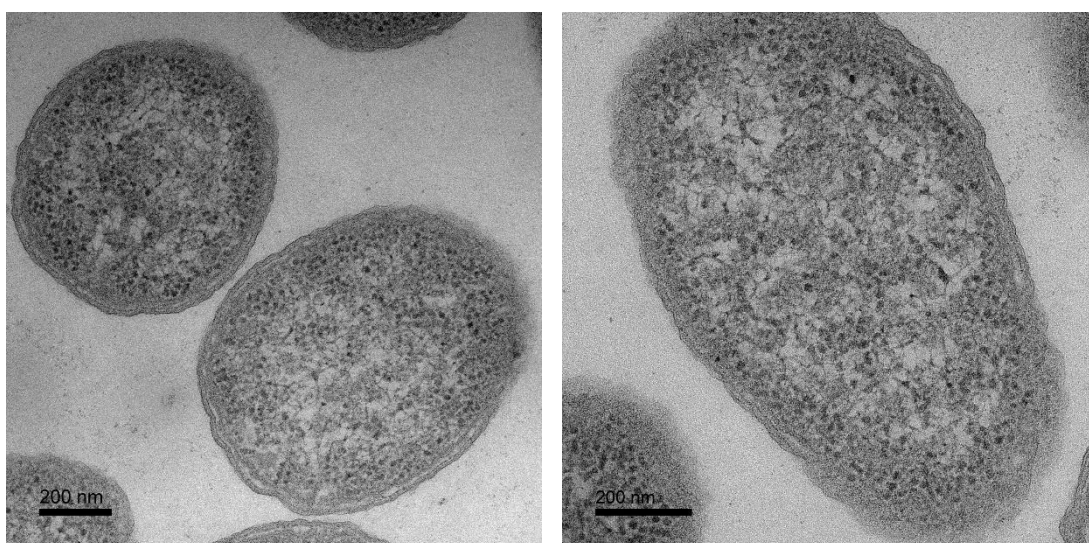
Secondly, a pET23b vector harbouring the MamB protein was used as the source of the pET23b vector after deletion of the *mamB* gene. The pET23b vector harbouring the MamB protein with the ribosome binding site of the pET14b vector, and the *PaLemA1* insert generated as mentioned above, were digested with NdeI and XhoI restriction endonucleases. By doing this the *mamB* gene was removed from the pET23b vector and compatible sticky ends for both the insert and the vector were generated. Following the ligation of the vector and the insert, the successful clones were verified by a restriction digest and sequencing.

5.2.2 Electron microscopy analysis of PaLemA1 with a polyhistidine tag

As the LemA protein family is yet to be characterised, many questions remain unanswered about the molecular functions of these proteins. Consequently, it is difficult to predict whether modifying any LemA protein would affect its function. In order to perform accurate structural studies, the protein is required to assume its native conformation. In the case of PaLemA1, the overproduction of the native protein has been shown to result in the formation of intracellular vesicles, which we believe to be a direct consequence of PaLemA1 integration into the inner membrane. Thus, it is possible to use this as a crude comparative of PaLemA1 functionality when assessing the effects of a His tag on the C-terminus of this protein.

Following the overexpression of the *PaLemA1*-His tagged construct in *E. coli*, the strain was embedded and subject to thin sectioning prior to TEM. An analysis of the thin sections by TEM revealed the presence of intracellular vesicles (**Figure 5.1**, bottom panel). The vesicles appeared characteristic of the PaLemA1 native protein when it is overproduced in *E. coli* (**Figure 3.1**, panels D, E and F). However, it is worth noting that a few larger vesicles were seen inside a small number of cells (**Figure 5.1**, panel C), a feature not observed when PaLemA1 protein is produced alone. This together with the fact that the tag is small in size provides encouraging results that deem it unlikely that the small polyhistidine tag has a drastic affect upon folding of this protein.

Empty vector control



PaLemA1-His

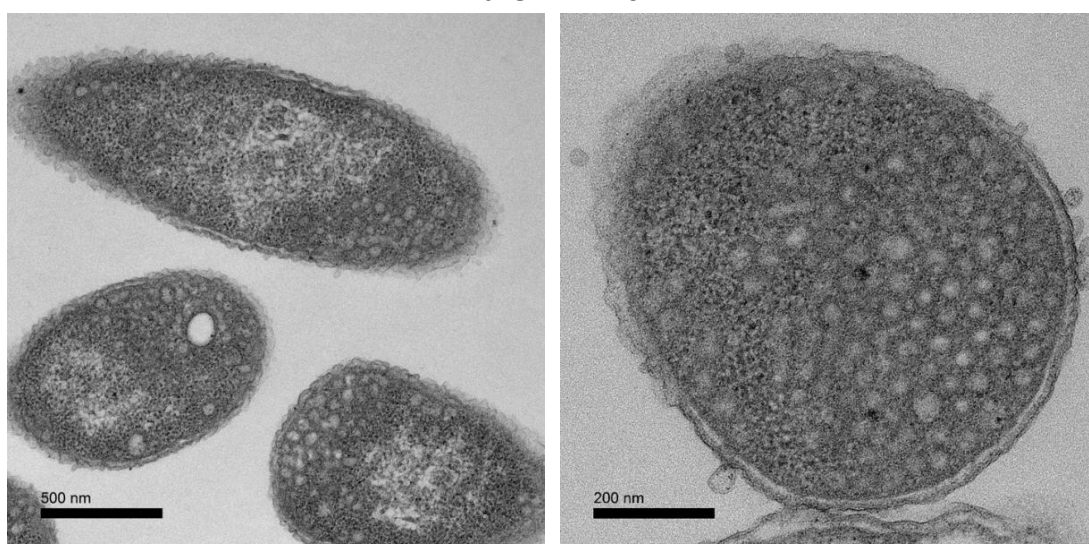


Figure 5.1. TEM of *E. coli* expressing an empty pET23b vector control and *PaLemA1*. Transmission electron micrographs of *E. coli* BL21 (DE3) Star cells producing an empty pET23b vector or PaLemA1. While the control sample (**A**, **B**; top panel) displays typical cellular morphology of *E. coli*, the PaLemA1-His producing sample (**C**, **D**; bottom panel) shows the presence of small intracellular vesicles, as well as some bacterial extracellular vesicle formation.

5.2.3 Initial PaLemA1 purification experiments

Initially, PaLemA1 purification studies were performed to determine the solubility of the protein. To begin with, following the overnight expression of the pET23b PaLemA1-His tagged construct, the *E. coli* cell culture was centrifuged at 4000 rpm for 10 minutes, after which the cells were resuspended in 50 mM Hepes, pH8.0, containing 300 mM NaCl. The cells were sonicated, as described in Section 2.8.2, and differential centrifugation was used to separate the soluble proteins from the insoluble materials. To determine if this had any bearing on PaLemA1 protein recovery, the sonicated cellular lysate was divided between different tubes and centrifuged at either 4000 rpm, 6000 rpm, 8000 rpm, 10,000 rpm, 12,000 rpm and 14,000 rpm for 20 minutes. The soluble fractions were collected and following the addition of Laemmli buffer were boiled for 10 minutes. Similarly, the pellets were resuspended in 50 mM Hepes, pH8.0, containing 300 mM NaCl prior to the addition of Laemmli buffer and subsequent boiling. The samples were analysed using SDS-PAGE.

The results show the overproduction of the PaLemA1-His tagged protein (**Figure 5.2**, lane 1) in the whole cell sample. Following centrifugation of the lysed cells, the protein appears to be largely located in the insoluble fractions, as a distinct band around 23 kDa was seen in these fractions (**Figure 5.2**, lanes 3, 5, 7, 9, 11 and 13). In addition, while a larger protein band appears following the centrifugation of the cellular lysate sample at 4000 rpm around 23 kDa (**Figure 5.2**, lane 3), it is unlikely that this centrifugation speed provides a better protein yield in comparison to the rest of the test conditions. This is because while less of the PaLemA1-His tagged protein appears in the insoluble fractions (**Figure 5.2**, lanes 5, 7, 9, 11 and 13), an increased amount of this protein is not observed in the soluble samples (**Figure 5.2**, lanes 4, 6, 8, 10 and 12), which would be expected. Thus, it seems likely that the sample that was initially loaded onto the gel (**Figure 5.2**, lane 3) contained an inherently higher amount of cellular proteins, as the bands representing other cellular proteins appeared more pronounced in this sample when compared to the others. Due to this, it was decided that subsequent purification experiments were going to utilise the 4000 rpm centrifugal speed for the separation of soluble and insoluble fractions following cellular lysis.

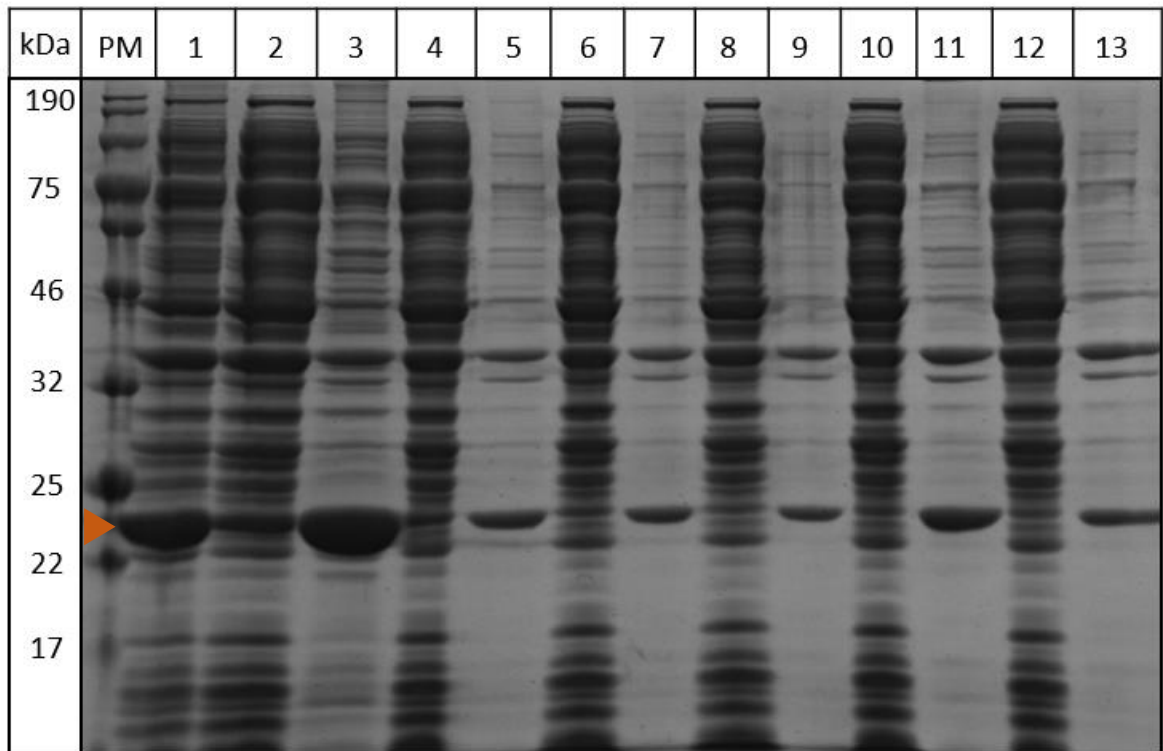


Figure 5.2. SDS-PAGE analysis of *E. coli* overproducing PaLemA1-His tagged protein.

E. coli BL21 DE3 Star cells producing the PaLemA1-His tagged protein (**1**). Following protein production, the cells were lysed via sonication and centrifuged into soluble and insoluble fractions at different speeds. **2**) Soluble fraction centrifuged at 4000 rpm; **3**) Insoluble fraction centrifuged at 4000 rpm; **4**) Soluble fraction centrifuged at 6000 rpm; **5**) Insoluble fraction centrifuged at 6000 rpm; **6**) Soluble fraction centrifuged at 8000 rpm; **7**) Insoluble fraction centrifuged at 8000 rpm; **8**) Soluble fraction centrifuged at 10000 rpm; **9**) Insoluble fraction centrifuged at 10000 rpm; **10**) Soluble fraction centrifuged at 12000 rpm; **11**) Insoluble fraction centrifuged at 12000 rpm; **12**) Soluble fraction centrifuged at 14000 rpm; **13**) Insoluble fraction centrifuged at 14000 rpm. PM: protein marker. **Arrow** indicates observable protein overexpression.

Due to the protein remaining in the insoluble fraction following sonication and centrifugation, it was important to establish a method for solubilising PaLemA1-His protein. This was not surprising, since the protein is predicted to possess a membrane targeting domain, meaning post-sonication the protein likely centrifuges together with the membrane fraction of the cell debris, where it remains attached. Furthermore, any protein located in the cytoplasm would likely be a part of intracellular vesicles and/or inclusion bodies (**Figure 5.1**, panels C and D), which together with SDS-PAGE analysis (**Figure 5.2**)

suggests that unless the PaLemA1-His protein concentration in these vesicles is low, the vesicles likely sediment with the insoluble fraction.

As a result, the detergent n-dodecyl β -d-maltoside (DDM), which is one of the most successful detergents used for the crystallisation of inner membrane proteins, was utilised. To test the solubilisation efficiency of DDM, as well as to compare two different pre-induction temperatures, 28 °C and 37 °C, the PaLemA1-His protein was purified using the Ni-NTA column. To begin with, following culture inoculation, the cells were grown at either 28 °C or 37 °C until the OD₆₀₀ was 0.4-0.8. After which the cells were induced with 100 μ M IPTG and incubated at 19 °C overnight. The PaLemA1-His protein was solubilised as stated in section 2.8.2, except the lysis buffer contained 1 mM EDTA instead of the EDTA-free protease inhibitor, and the concentration of DDM during these initial studies was adjusted to the cell pellet weight. As such, for each gram of the membrane pellet the lysis buffer containing 1% Triton X-100 (v/v), was supplemented with 1.25% DDM (w/v). Following the overnight solubilisation, the PaLemA1-His protein was purified using the IMAC column (section 2.8.3), however, similarly to the lysis buffer, 1 mM of EDTA was added to the purification buffers.

The results of the IMAC column purification were analysed using SDS-PAGE. The presence of a more pronounced protein band corresponding to the PaLemA1-His protein in the insoluble fraction of the 37 °C sample was seen (**Figure 5.3**, panel A, lane 2), when compared to the 28 °C sample (**Figure 5.4**, panel A, lane 2). As both samples were treated exactly the same following biomass sedimentation, including being re-suspended in equal amounts of lysis buffer, means it is likely that this observed difference is due to a higher cell density of the 37 °C sample (**Figure 5.3**). This is supported by the lower OD₆₀₀ absorbance value of 3.18 seen in the 28 °C sample following overnight induction, in comparison to 4.44 seen in the 37 °C sample.

Following the overnight incubation of the resuspended membranes in the lysis buffer with detergents, SDS-PAGE samples were collected for the soluble and insoluble fractions. By looking at the solubilisation profile of both samples (**Figure 5.3**, gel A, lane 3 and **Figure 5.4**, gel A, lane 3), it was evident that a large proportion of the PaLemA1-His protein was successfully solubilised. However, a prominent band was still visible for the insoluble fraction following solubilisation attempt in both samples (**Figure 5.3**, gel A, lane 4 and **Figure 5.4**, gel A, lane 4).

After the loading of the soluble fraction onto the IMAC column, the binding capacity of the PaLemA1-His protein was assessed. From the gel, it was evident that a lot of the protein does not bind to the column since it is seen coming off in the flow-through in both samples (**Figure 5.3**, gel A, lane 5 and **Figure 5.4**, gel A lane 5). This could be due to a number of reasons, with the first being the presence of EDTA, which can chelate the nickel making it dissociate from the Sepharose® beads. In fact, during this particular purification this was observed, as some nickel was being stripped off the column after the loading of the buffers containing EDTA. Secondly, the IMAC column could have become over-saturated with the protein, meaning it had no further capacity to bind more PaLemA1-His. The elution fractions (**Figure 5.3**, gel B and **Figure 5.4**, gel B) of this purification displayed a band around 24 kDa, which represents the PaLemA1-His protein, which was confirmed using western blot analysis, while the band occurring around 22 kDa is likely a degradation product of the PaLemA1-His protein. It is likely that the N-terminus of the protein was degraded in this case, as the C-terminal region of the protein contains the polyhistidine tag which is responsible for the protein binding to the nickel column. Consequently, subsequent cultures intended for purification were grown at 37 °C pre-induction and an EDTA-free protease inhibitor was used in the purification steps to prevent protein degradation.

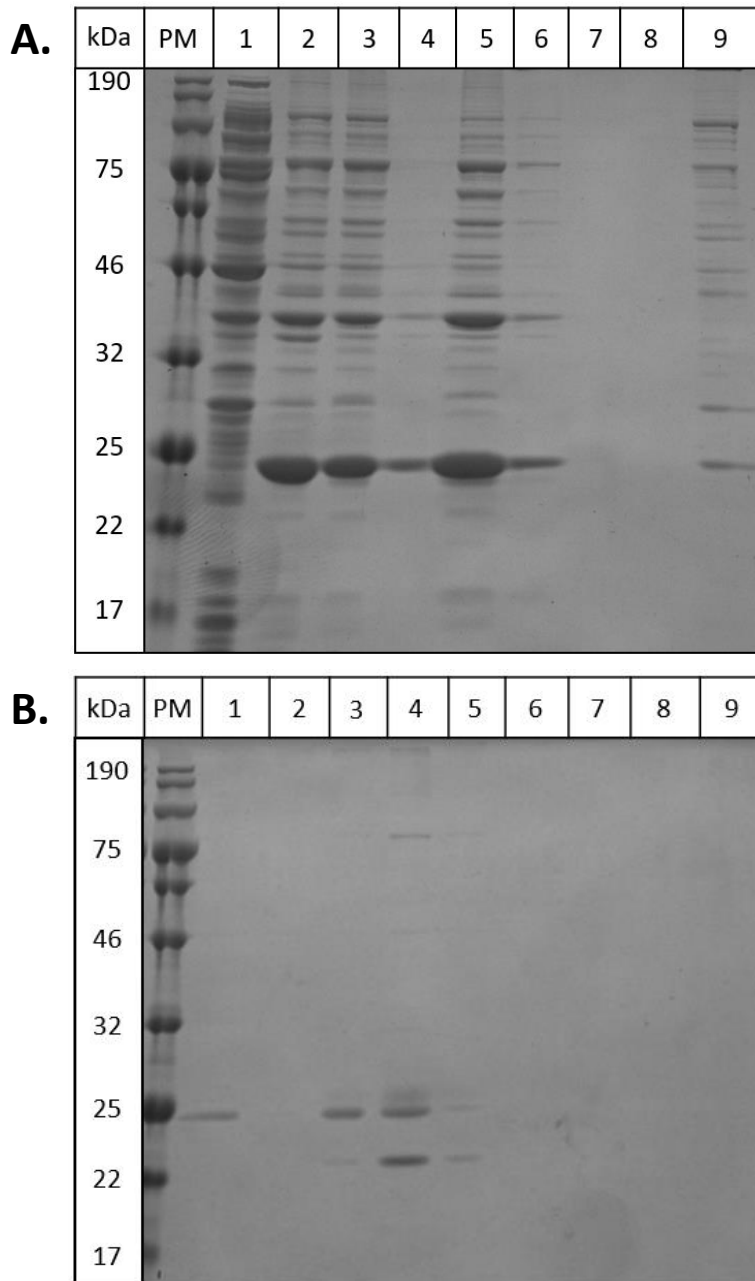


Figure 5.3. SDS-PAGE analysis of the detergent purified PaLemA1-His tagged protein from *E. coli* cells initially grown at 28 °C.

E. coli BL21 DE3 Star cells were grown at 28 °C prior to protein induction, when the cell culture was moved to 19 °C. The PaLemA1-His tagged protein was purified using a Ni-NTA column from *E. coli*. The purification process is detailed in panel **A**, with **1**) showing the soluble fraction post cell sonication; **2**) showing the insoluble fraction post sonication; **3**) soluble fraction after overnight solubilisation in n-dodecyl β -D-maltoside (DDM); **4**) insoluble fraction after overnight solubilisation in DDM; **5**) flowthrough from the Ni-NTA column after loading of the soluble fraction following overnight solubilisation in DDM; **6**) Wash 1; **7**) Wash 2; **8**) Wash 3; **9**) Wash 4. Panel **B** shows elution fractions 1-9, in corresponding lane numbers.

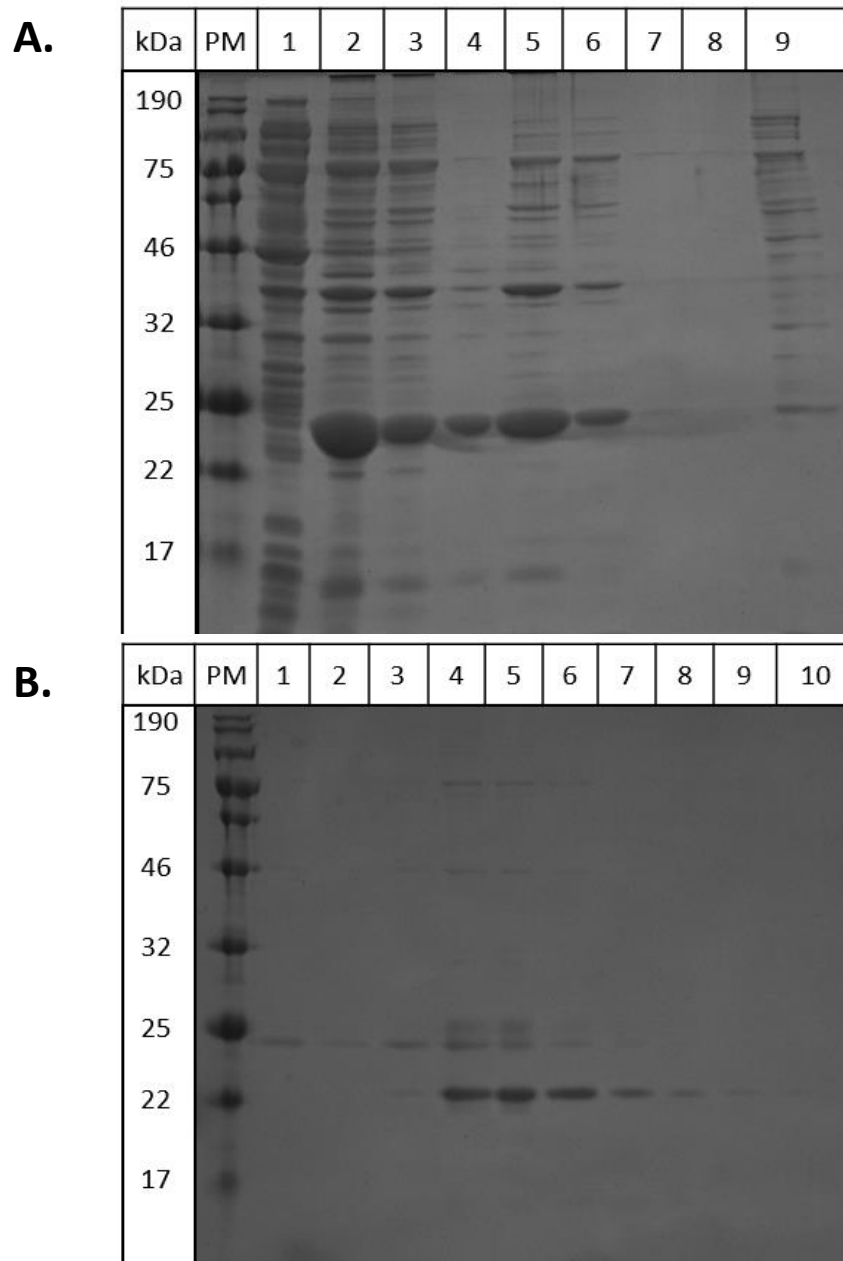


Figure 5.4. SDS-PAGE analysis of the detergent purified PaLemA1-His tagged protein from *E. coli* cells initially grown at 37 °C.

E. coli BL21 DE3 Star cells were grown at 37 °C prior to protein induction, when the cell culture was moved to 19 °C. The PaLemA1-His tagged protein was purified using a Ni-NTA column from *E. coli*. The purification process is detailed in panel **A**, with **1**) showing the soluble fraction post cell sonication; **2**) showing the insoluble fraction post sonication; **3**) soluble fraction after overnight solubilisation in DDM; **4**) insoluble fraction after overnight solubilisation in DDM; **5**) flowthrough from the Ni-NTA column after loading of the soluble fraction following overnight solubilisation in DDM; **6**) Wash 1; **7**) Wash 2; **8**) Wash 3; **9**) Wash 4. Panel **B** shows elution fractions 1-10, in corresponding lane numbers.

The optimisation processes for the purification of PaLemA1-His protein included detergent optimisation, appropriate size exclusion chromatography buffer selection and culture scale-up in order to attain desired protein yields. The final protocol can be found in Sections 2.8.2 and 2.8.3. Although the PaLemA1-His protein was found in the insoluble cell fraction (**Figure 5.5**, Lane 1), following overnight solubilisation in 1% (w/v) DDM and 1% (v/v) Triton X-100, the protein

shows a good solubilisation profile, with the majority of the protein appearing in the soluble fraction following centrifugation (**Figure 5.5**, Lane 4). It is worth noting that after the soluble overnight fraction was loaded onto the Ni-NTA column a large proportion of the protein did not bind to the column (**Figure 5.5**, Lane 5), despite the use of a larger Ni-NTA column. This again could be due to a lack of column capacity for protein binding that could be improved by having a larger volume of the Chelating Sepharose Fast Flow resin. Despite this, the elution fractions still appeared to have a significant amount of purified PaLemA1 (**Figure 5.6**, Panel A). However, co-purification of other cellular proteins also appeared to take place. Due to the requirement of a high purity protein sample for crystallisation work, size exclusion chromatography using the Superdex™ S200 Increase 10/300 column was carried out. While the PaLemA1 protein shows a prominent band following SDS-PAGE analysis (**Figure 5.6**, Panel B, Lanes B5-C1), the presence of fainter bands which could represent dimers, multimers and other contaminants is still observed.

Subsequently, lanes B5-C1 of **Figure 5.6** were collected and concentrated using the Amicon® Ultra-15 10 kDa cut-off centrifugal filter columns, until the protein concentration was approximated to be 12.8 mg/mL. Lipidic cubic phase (LCP) crystallisation technique was used as the method for crystallisation (Section 2.8.9). Despite these efforts, crystals were not obtained using various concentrations of the PACT Premier™, Morpheus®, MemGold2™, MemMeso™, MemGoldMeso (Molecular Dimensions) or the Tris buffer with varying pH and salts crystallisation screens.

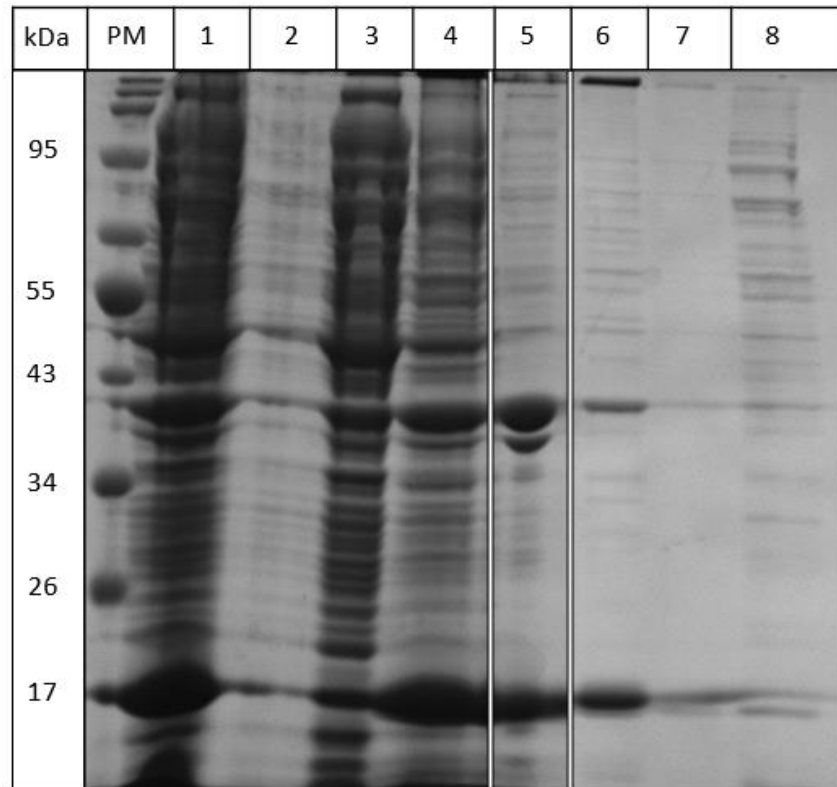


Figure 5.5. SDS-PAGE analysis of the detergent purified PaLemA1-His protein from *E. coli* cells.

The PaLemA1-His tagged protein was purified from BL21 (DE3) Star *E. coli* cells using the Ni-NTA column. The lanes are as described: **1)** showing the insoluble fraction of cell culture; **2)** showing the soluble fraction of cell culture; **3)** insoluble fraction after overnight solubilisation in n-dodecyl β -d-maltoside (DDM); **4)** soluble fraction after overnight solubilisation in DDM; **5)** flowthrough from the Ni-NTA column after loading of the soluble fraction following overnight solubilisation in DDM; **6)** Wash 1; **7)** Wash 2; **8)** Wash 3.

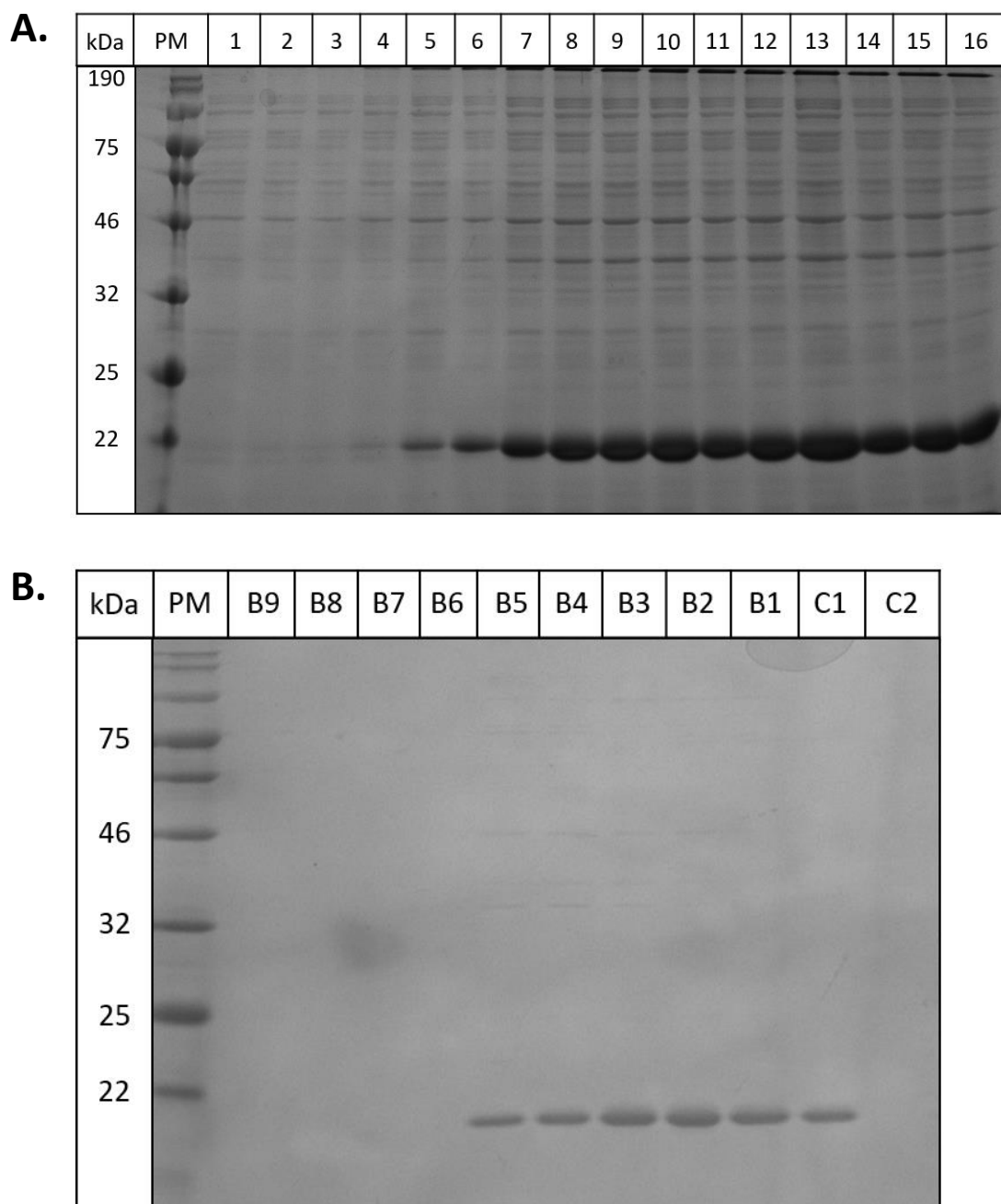


Figure 5.6. SDS-PAGE analysis of the detergent purified PaLemA1-His tagged protein from *E. coli* cells.

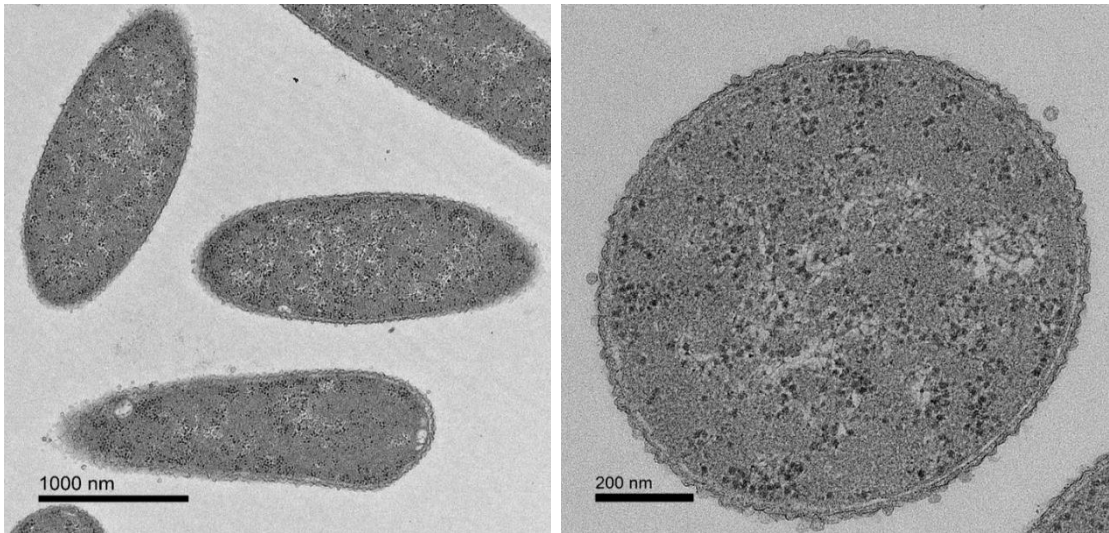
The PaLemA1-His tagged protein was purified from BL21 (DE3) Star *E. coli* cells using the Ni-NTA column. Panel **A** shows the elution fractions 1-16 of PaLemA1, in corresponding lane numbers. Panel **B** displays the purified size exclusion chromatography fractions that were collected using the Superdex™ S200 Increase 10/300 column, with fractions B5-C1 showing the presence of PaLemA1-His protein.

5.2.4 Generation and TEM analysis of PaLemA1-sfGFP fusion protein

Due to the lack of crystal formation following the purification and the set-up of crystallisation screens for the PaLemA1-His protein, a different approach was taken. A fusion construct consisting of PaLemA1 cloned in-frame with a cleavable C-terminal superfolder GFP (sfGFP) tag was generated. The gene for the sfGFP tag (32.29 kDa) was synthesised by Eurofins™ and within the sequence also contained an N-terminal NdeI restriction site and a C-terminal SpeI restriction site, which allowed for its integration into a pET3a vector. The protein sequence of the tag itself consisted of an N-terminal tobacco etch virus (TEV) protease site, followed by the sfGFP and the polyhistidine tag (TEV-sfGFP-His). When cloned in-frame with PaLemA1 this construct allowed for the selective cleavage of the sfGFP-His tag by use of the TEV protease.

Similarly to the pET23b PaLemA1 construct, it was important to compare the effects of the PaLemA1-TEV-sfGFP-His fusion protein on the functionality of the native PaLemA1 protein in *E. coli*. As such, TEM studies were conducted, with the sfGFP fusion tag alone used as the control. While the overproduction of the sfGFP fusion tag alone leads to the formation of amorphous sized inclusion bodies in *E. coli* (**Figure 5.7**, top panel), the PaLemA1-sfGFP construct results in the formation of intracellular vesicles (**Figure 5.7**, bottom panel) when the various strains were analysed by TEM after thin sectioning. These vesicles appeared in regions with inclusion bodies and were of comparative size to those produced following *PaLemA1* overexpression alone. However, it should be noted that the vesicle morphology varied in the longitudinal cell sections where slightly elongated vesicles with less defined membranes could be seen. This suggests that the large sfGFP fusion tag had an effect on the topology of PaLemA1, likely impacting its membrane curvature inducing properties.

sfGFP tag



PaLemA1-sfGFP tag

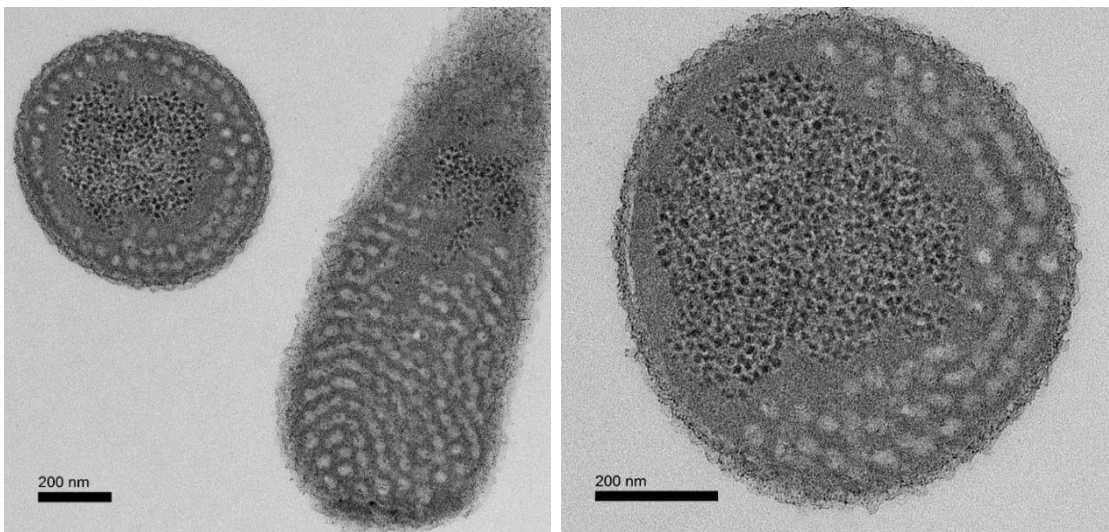


Figure 5.7. TEM of *E. coli* expressing sfGFP and *PaLemA1-sfGFP* constructs.

Transmission electron micrographs of *E. coli* BL21 (DE3) Star cells expressing a pET3a vector encoding either the *sfGFP* tag alone (top panel) or *PaLemA1-sfGFP* tag (bottom panel) construct. The control sample overproducing the *sfGFP* tag alone shows a large proportion of the cells harbouring amorphous inclusion bodies. While the *PaLemA1-sfGFP* fusion protein overproduction results in the formation of intracellular vesicles that appear slightly elongated in the longitudinal sections of cells.

5.2.5 Purification and crystallisation of PaLemA1 using a sfGFP fusion tag

The PaLemA1-sfGFP protein fusion was overproduced in *E. coli* BL21 (DE3) Star cells and solubilised and purified as outlined in Sections 2.8.2 and 2.8.3. Although the whole cell fraction is oversaturated with protein, it is still possible to see significant overproduction of the PaLemA1-sfGFP protein, with a band present around the expected 54 kDa region (**Figure 5.8**, Lane 1). The fusion protein showed a good solubilisation profile following incubation of cell membranes in DDM and Triton X-100 overnight (**Figure 5.8**, Lane 2), although some protein remained insoluble (**Figure 5.8**, Lane 3). As was the case for the PaLemA1-His protein (**Figure 5.5**, Lane 5), the PaLemA1-sfGFP protein over-saturated the Ni-NTA column, as excess protein was seen flowing through the column and was confirmed by SDS-PAGE analysis (**Figure 5.8**, Lane 4). Due to the presence of the sfGFP it was a lot easier to follow the purification process, as such the protein was eluted into a single tube. SDS-PAGE analysis revealed a significant amount of PaLemA1-sfGFP in the elution fraction (**Figure 5.8**, Lane 8).

Subsequently, the purified PaLemA1-sfGFP fusion protein was digested with the TEV protease overnight as described in Section 2.8.4, and a 'reverse' Ni-NTA purification approach was used to separate the digested PaLemA1 protein from the remaining proteins. It was evident that a large proportion of PaLemA1-sfGFP remained undigested following overnight incubation with the TEV protease (**Figure 5.9**, Panel A, Lane 1) as a band around 60 kDa could be seen. While the expected molecular weight of the PaLemA1-sfGFP protein is expected to be around 54 kDa, the appearance of a band at a higher molecular weight is not unusual for membrane proteins. However, the multimerisation of PaLemA1 alone cannot be excluded.

A step-wise gradient of 50 mM (wash 2), 150 mM (wash 3), 250 mM (wash 4) and 400 mM (elution) imidazole in 50 mM Hepes (pH8), 300 mM NaCl buffer was used to elute the digested PaLemA1 protein (**Figure 5.9**, Panel A). This was done because following the loading of the digested sample onto the Ni-NTA column, the flow-through, which was expected to largely contain the PaLemA1 protein alone did not show this result (**Figure 5.9**, Panel A, Lane 2). Furthermore, a subsequent wash with 50 mM Hepes (pH 8) buffer containing 300 mM NaCl (wash 1) alone did not encourage the protein to flow through the column (**Figure 5.9**, Panel A, Lane 3). This could indicate that a possible weak interaction exists between the bound proteins on the nickel column and the digested PaLemA1

protein, as the addition of imidazole into the wash buffers facilitated the elution of PaLemA1 (**Figure 5.9**, Panel A, Lanes 3-6).

Due to the fact that wash 3, wash 4 and the elution fractions each contained a relatively large proportion of PaLemA1 in comparison to other contaminating components (**Figure 5.9**, Panel A, Lanes 4-6), these samples were combined together and concentrated. Size exclusion chromatography was used to further purify the concentrated samples (**Figure 5.9**, Panel B). A large proportion of the digested PaLemA1 (21.05 kDa) can be seen in lanes B4-B2 (**Figure 5.9**, Panel B). It is worth noting that a band occurring around 60 kDa could also be witnessed, though it remains unclear if this represents a PaLemA1 trimer or the undigested PaLemA1-sfGFP protein. The B4-B2 fractions were collected and concentrated to around 30 μ L, with the approximated concentration of the protein being 14.2 mg/mL.

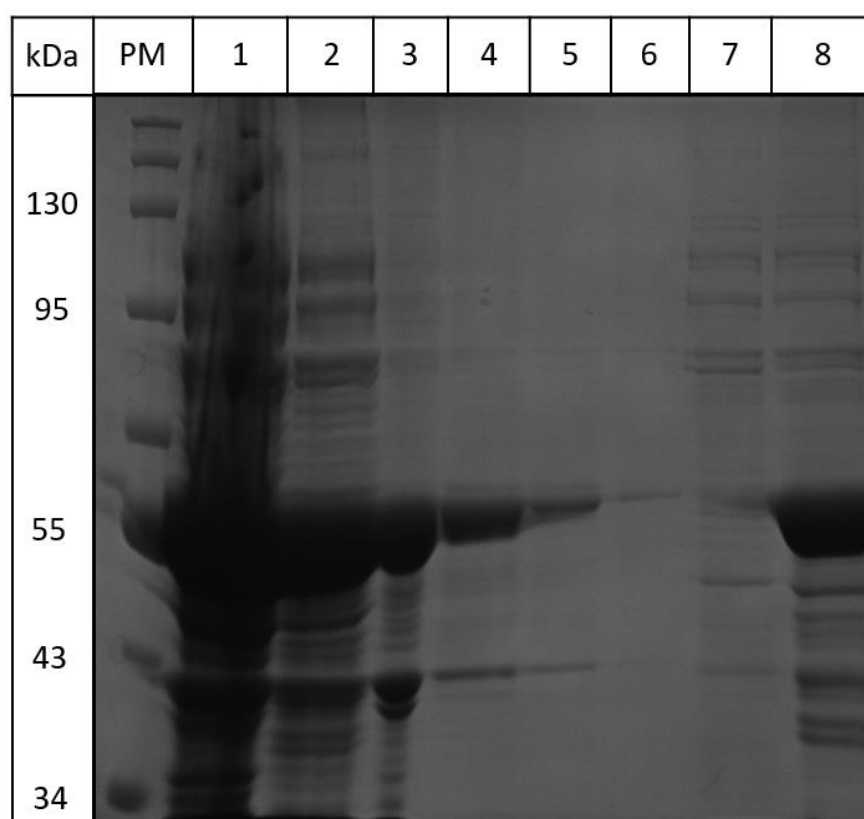


Figure 5.8. SDS-PAGE analysis of the detergent purified PaLemA1-sfGFP fusion protein from *E. coli* cells.

The PaLemA1-sfGFP fusion protein was overproduced and purified in BL21 (DE3) Star *E. coli* cells using the Ni-NTA column. The lanes are as described: **1)** the insoluble fraction containing pelleted cells; **2)** the soluble fraction containing PaLemA1-sfGFP after overnight solubilisation in DDM; **3)** insoluble fraction after cell membranes were solubilised overnight in DDM; **4)** flowthrough from the Ni-NTA column after loading of the soluble protein fraction following overnight solubilisation in DDM; **5)** Wash 1; **6)** Wash 2; **7)** Wash 3; **8)** eluted protein.

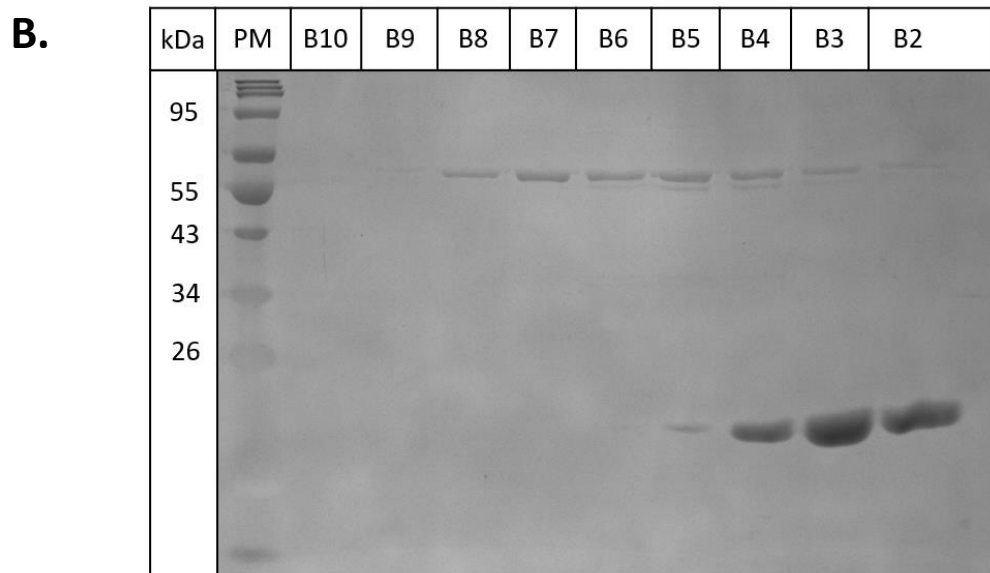
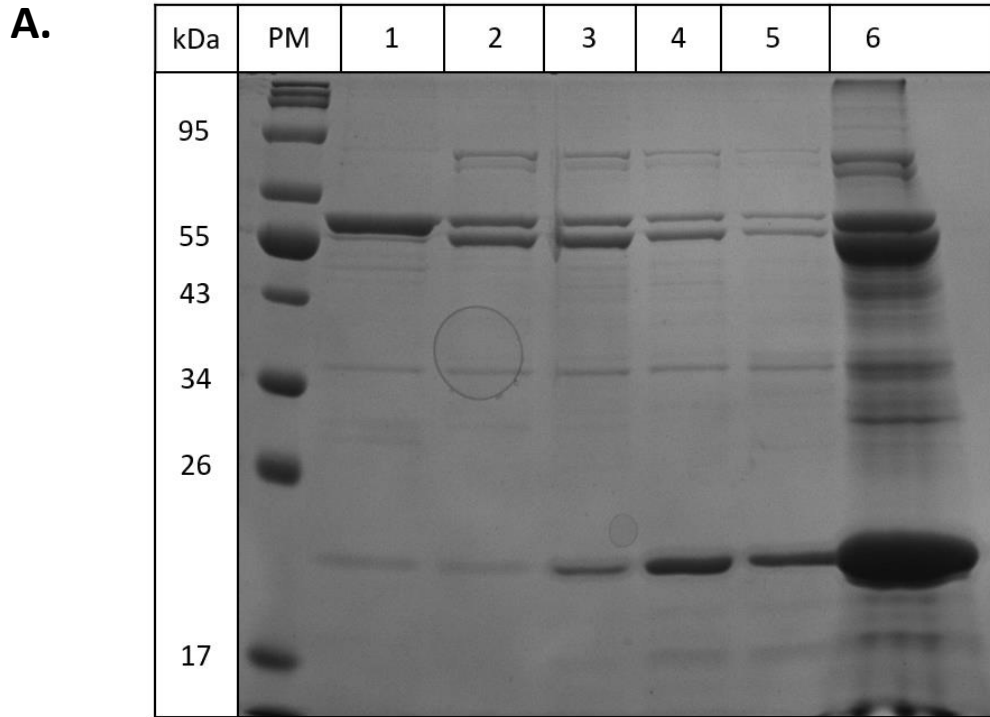


Figure 5.9. SDS-PAGE analysis of the TEV protease cleaved PaLemA1-sfGFP protein and the resulting size exclusion chromatography fractions.

The PaLemA1-sfGFP fusion protein was purified from BL21 (DE3) Star *E. coli* cells using the Ni-NTA column and digested with the TEV protease. Panel **A** shows the results of the proteolytic cleavage reaction between the TEV protease and PaLemA1-sfGFP fusion protein. Lane **1**) shows the digestion profile of PaLemA1-sfGFP protein following overnight incubation of the protein with the TEV protease; Lane **2**) shows the flow-through from the Ni-NTA following the loading of the digested sample onto the column; Lane **3**) Wash 1; Lane **4**) Wash 2; Lane **5**) Wash 3; Lane **6**) Elution. Panel **B** displays the purified size exclusion chromatography fractions that were collected using the Superdex™ S200 Increase 10/300 column, with fractions B5-B2 showing a prominent band corresponding to the PaLemA1 protein (21.05 kDa).

Following the concentration of the purified PaLemA1 sample, the protein was combined with molten monolein in a 2:3 ratio, respectively, using a syringe mixer. The LCP crystallisation screens were set up as stated in Section 2.8.9 using the 96 well Laminex™ plastic sandwich plates, and a range of different conditions were tried as previously discussed in Section 5.2.3. Using a light microscope, the plates were periodically inspected for crystal formation. Initial screening conditions which were 50 mM Tris-HCl, pH 8, 0.2M potassium phosphate monobasic and 50 mM Tris-HCl, pH 8, 0.1M sodium sulphate decahydrate, yielded small protein crystals (**Figure 5.10**). Attempts were made to harvest the crystals using an appropriately sized micro-loop, however, due to the challenging nature of this extraction, the LCP dissolved together with the formed crystals. In order to improve the quality and size of the crystals, the next steps were going to include the optimisation of the pH and salt concentrations around the two successful conditions. Moreover, Diffrax™ plates (Molecular Dimensions) were acquired as these allow for *in situ* X-ray crystallography, removing the need for manual crystal retrieval. Unfortunately, due to the time pressures placed by the current pandemic it was not possible to carry out these next steps.

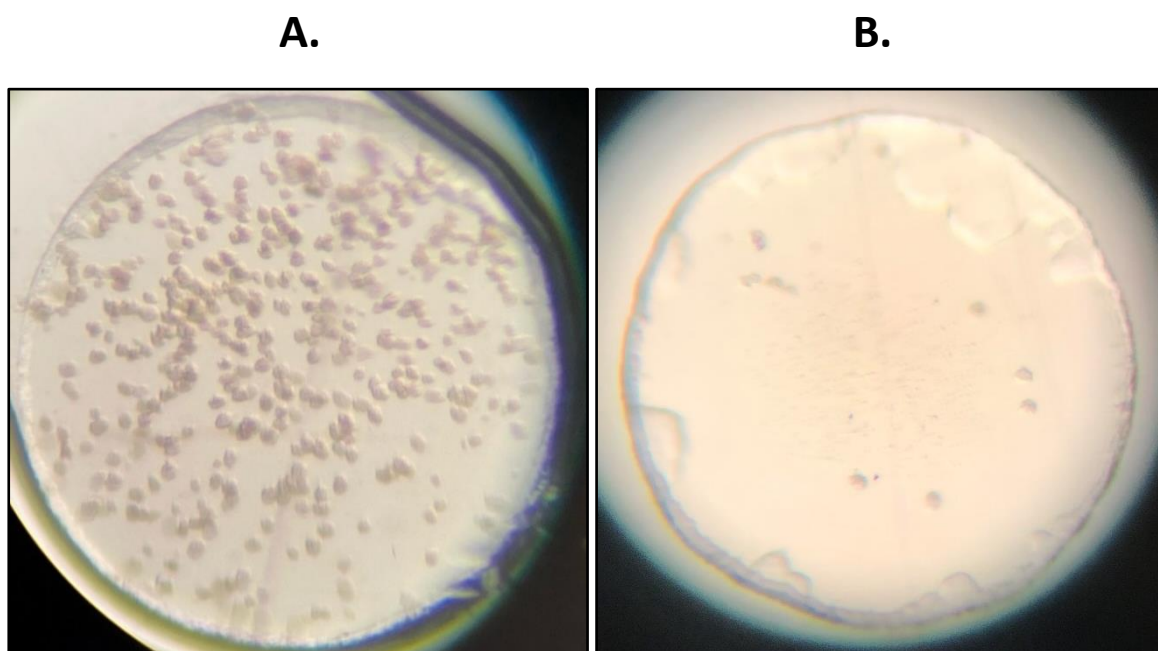


Figure 5.10. PaLemA1 protein crystals formed during LCP crystallisation screening.

The crystals were grown in **A)** 50 mM Tris-HCl, pH8, 0.2M potassium phosphate monobasic screening solution; **B)** 50 mM Tris-HCl, pH8, 0.1M sodium sulphate decahydrate screening solution.

5.2.6 Purification of ^{15}N -labelled PaLemA1-His protein for NMR analysis

The preparation of the ^{15}N -labelled PaLemA1-His protein for NMR analysis was carried out as described in Section 2.8.1. The pET23b PaLemA1 construct (discussed in Section 5.2.1) was used for the transformation of *E. coli* BL21 (DE3) Star cells. The purification of the ^{15}N -labelled PaLemA1-His protein was carried out with the use of the Ni-NTA column (Section 2.8.3), the results of which were later analysed using SDS-PAGE. As the PaLemA1-His protein was observed in the insoluble fraction (**Figure 5.11**, Lane 3) detergent extraction was used in the purification of this protein. Following the incubation of the cell membranes with DDM overnight, a significant amount of PaLemA1-His protein was observed in the soluble fraction of the sample (**Figure 5.11**, Lane 4), which was loaded onto the Ni-NTA column. The 1 mL elution fractions from the purification showed the presence of a band around 22 kDa which was expected for the PaLemA1-His protein (**Figure 5.12**, Lanes 9-24)

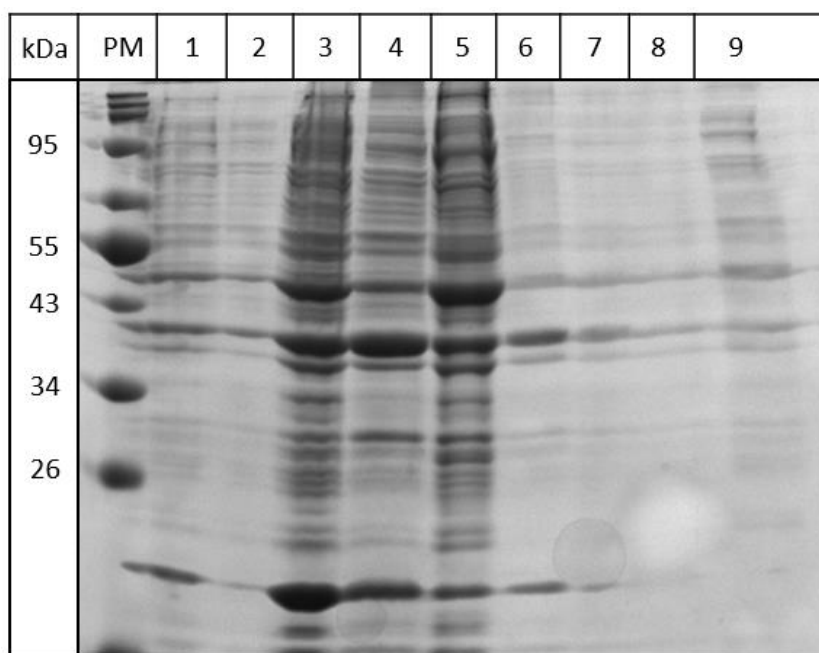


Figure 5.11. SDS-PAGE analysis of the detergent purified PaLemA1-His protein from *E. coli* cells for NMR analysis.

The PaLemA1-His protein was overproduced and purified from BL21 (DE3) Star *E. coli* cells using the Ni-NTA column. The lanes are as described: **1)** whole culture sample after overnight protein induction; **2)** the soluble fraction of cell culture; **3)** the insoluble fraction of cell culture; **4)** the soluble protein fraction following overnight solubilisation in DDM; **5)** the insoluble protein fraction following overnight solubilisation in DDM; **6)** flowthrough from the Ni-NTA column after loading of the soluble protein fraction following overnight solubilisation in DDM; **7)** Wash 1; **8)** Wash 2; **9)** Wash 3.

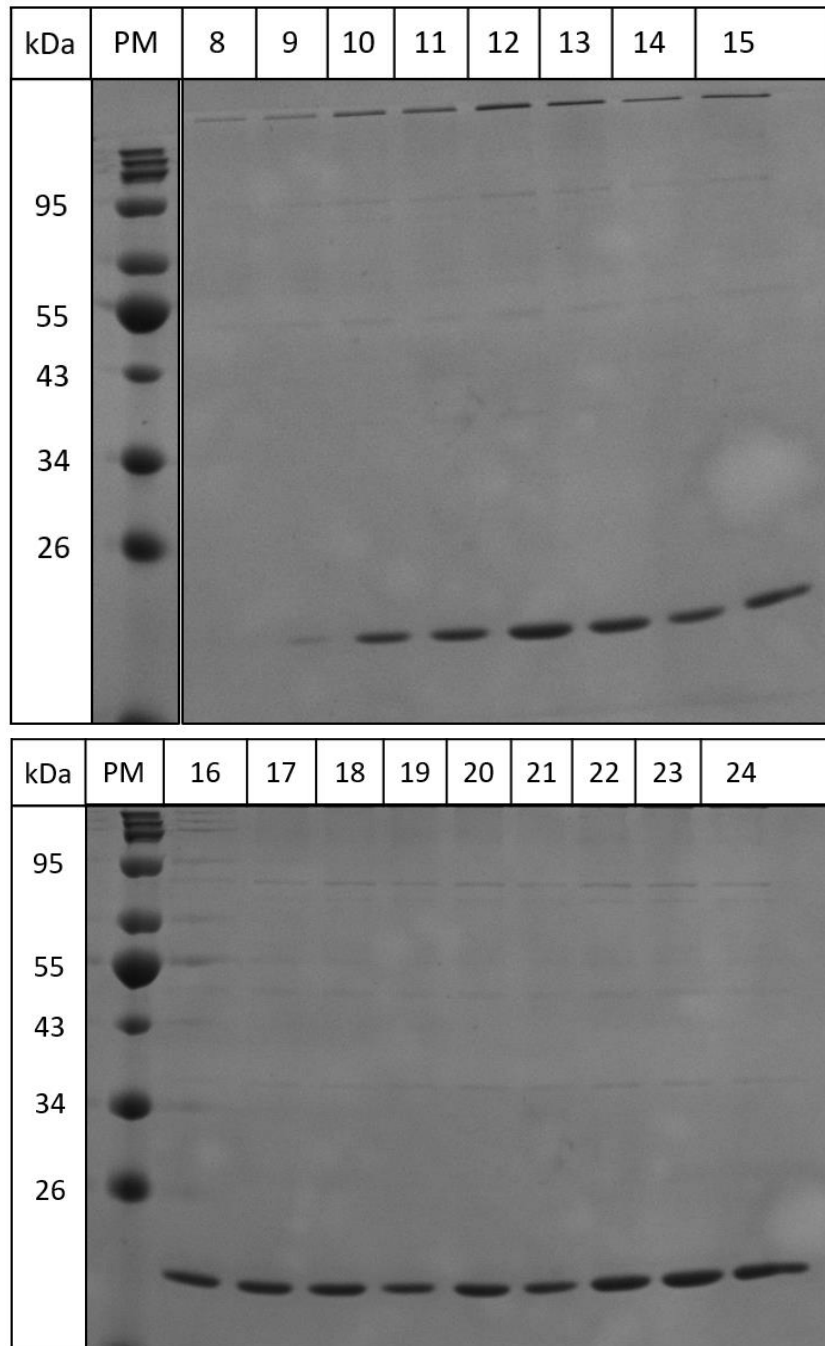


Figure 5.12. SDS-PAGE analysis of the eluted fractions from the purification of PaLemA1-His protein from *E. coli* cells.

The PaLemA1-His protein was overproduced and purified from BL21 (DE3) Star *E. coli* cells using the Ni-NTA column. The lanes represent the elution fractions which were collected following PaLemA1-His purification. In the top panel the intervening lanes 1-7 were cut out as these did not contain any visible PaLemA1-His protein.

The elution fractions (**Figure 5.12**, Lanes 10-24) were then concentrated to 500 μ L prior to being injected into the size exclusion chromatography column. Following this a few faint bands around 40 kDa and 60 kDa could be seen, which could represent contaminating proteins or perhaps multimerisation events of the PaLemA1-His protein. The fractions were collected in 50 mM Hepes buffer (pH 7.4) containing 20 mM NaCl and 0.03% (w/v) DDM, after which the protein fractions corresponding to lanes B6-C1 in **Figure 5.13** were concentrated to 300 μ L prior to NMR analysis. The concentration of the PaLemA1-His protein in the sample was approximately 0.1 mM.

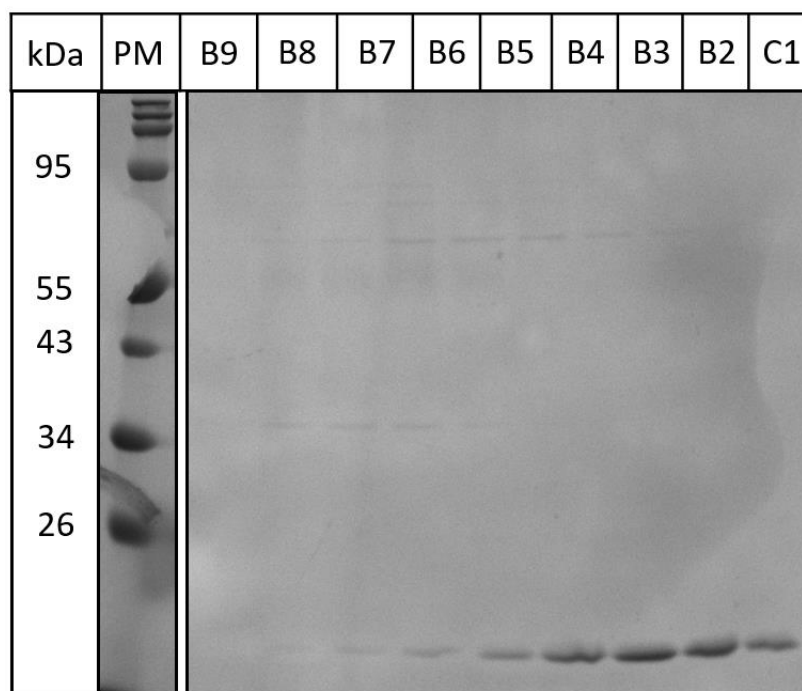


Figure 5.13. SDS-PAGE analysis of the PaLemA1-His protein size exclusion fractions.

The PaLemA1-His protein was overproduced and purified from BL21 (DE3) Star *E. coli* cells using the Ni-NTA column. The lanes represent the protein fractions which were collected using the Superdex™ S200 Increase 10/300 column during size exclusion chromatography. The fractions B6-C1 show a prominent band corresponding to the PaLemA1-His protein (~22 kDa).

5.2.7 Preliminary NMR analysis of ^{15}N -labelled PaLemA1-His protein

$^{15}\text{N}/^1\text{H}$ selective optimized flip angle short transient (SOFAST) heteronuclear single quantum correlation (HSQC) 2D experiment was acquired on the Bruker Avance III spectrometer at 25 °C (**Figure 5.14**). NMR analysis was acquired with the help of Dr. Jose Ortega-Roldan (University of Kent). The distribution of the peaks suggests that the PaLemA1-His protein is in a folded state, however, amino acid assignment could not be carried out as the peaks remained indistinguishable. This is not unexpected due to PaLemA1 being an alpha-helical membrane protein of a large size due to it being solubilised in DDM. The micelles surrounding the protein would significantly affect the size of the molecule and thus the resulting NMR spectra.

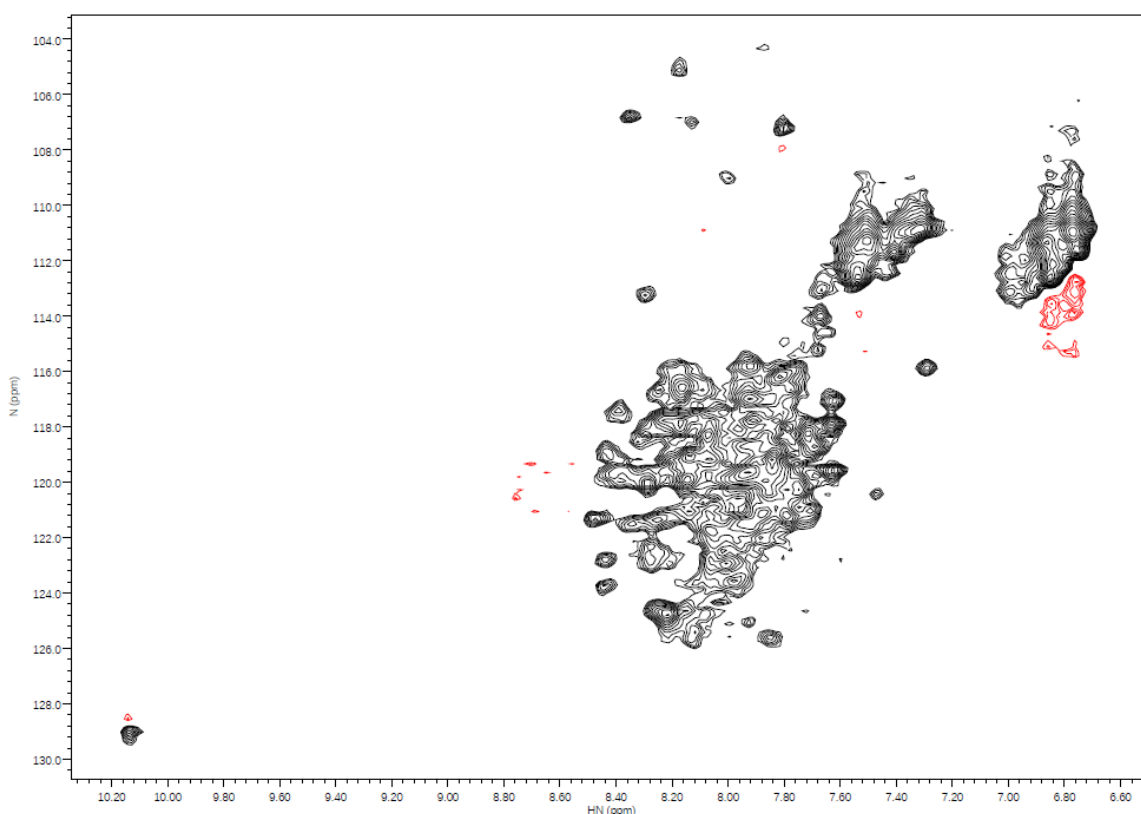


Figure 5.14. $^{15}\text{N}/^1\text{H}$ SOFAST-HSQC spectrum of PaLemA1-His protein at 25 °C.

The relatively close dispersion of the peaks is indicative of the PaLemA1-His protein being in a folded state. The peaks appeared unclear, which prevented any of the peaks from being assigned to particular amino acids. The red peaks refer to negative peaks corresponding to noise.

Further work was conducted which collected $^{15}\text{N}/^1\text{H}$ BEST-transverse relaxation optimized spectroscopy (TROSY)-HSQC spectra, a method which is often used for large biomolecules (**Figure 5.15**). The 2D experiment was acquired as stated in Section 2.8.8 at increasing temperatures of 30, 35 and 40 °C. To ensure protein stability at 40 °C the sample was tested overnight, after which the spectra looked identical, confirming the thermostability of the protein at this temperature. A marginal change in the dispersion of most peaks was observed in comparison to the SOFAST-HSQC spectrum (**Figure 5.14**), with reduced linewidths and increased the spectral resolution being observed. However, amino acid assignments were not attempted in light of the majority of the peaks remaining undistinguishable.

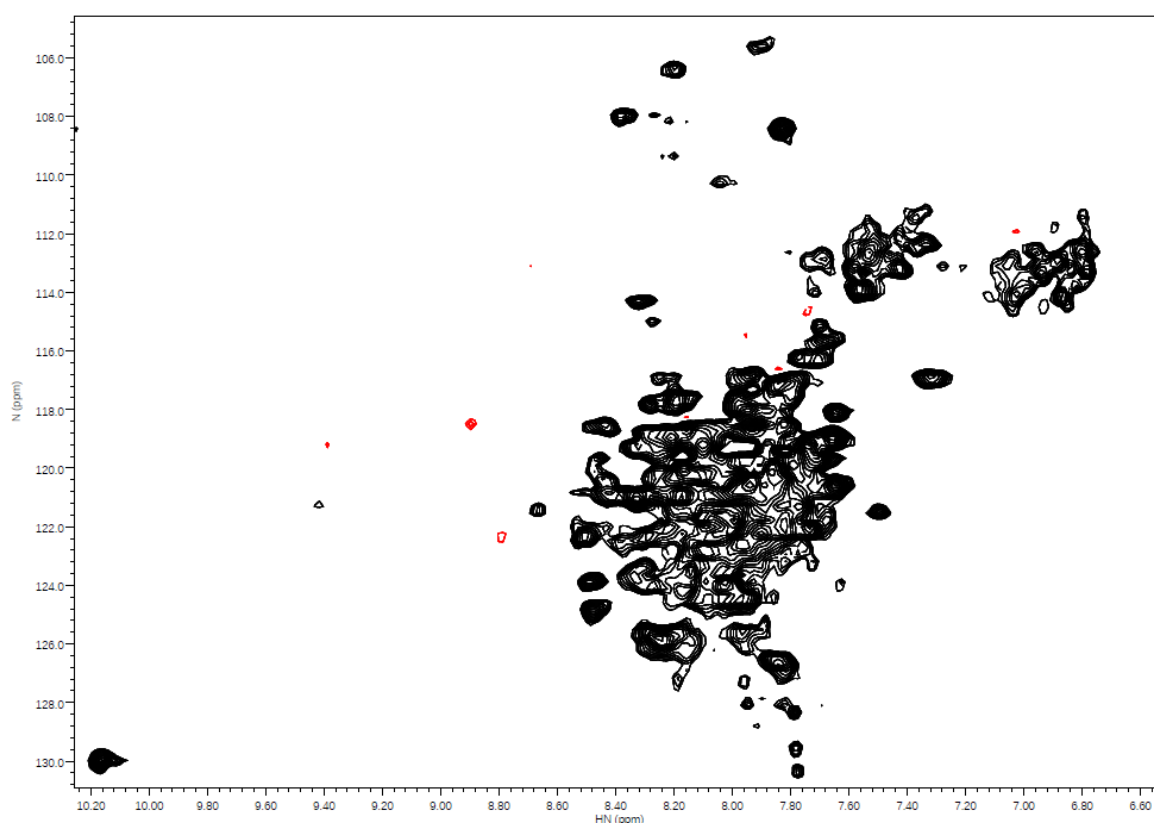


Figure 5.15. $^{15}\text{N}/^1\text{H}$ BEST-TROSY-HSQC spectrum of PaLemA1-His protein at 40 °C.

The 2D spectrum was acquired on a Bruker Avance III spectrometer at a proton frequency of 600MHz using a QCIP cryoprobe after the protein sample was heated to 40 °C. The close dispersion of the amino acid peaks is indicative of the PaLemA1-His protein being in a folded state. However, the peaks remained undistinguishable which prevented any of the peaks from being assigned to particular amino acids. The red peaks refer to negative peaks corresponding to noise.

5.3 Discussion

In this chapter, attempts were made to gather structural information about the *P. aeruginosa* LemA1 protein in order to better understand the structure-function relationship of this protein. Preliminary tests revealed the insoluble nature of PaLemA1 which was expected given that PaLemA1 is predicted to be anchored to the inner bacterial membrane via the transmembrane spanning domain (**Figure 5.2**). As a result, an additional step was added to the purification protocol, which included the solubilisation of the cellular membranes in DDM and Triton X-100 overnight.

In *E. coli* BL21 (DE3) Star cells, the high level of recombinant protein overproduction often makes the newly synthesised polypeptides more prone to aggregation. This can be due to a number of different factors, some of which include the presence hydrophobic stretches in the synthesised polypeptides, which at high concentrations can interact with similar protein regions and lead to protein aggregation (Carrió and Villaverde, 2002). Moreover, the high translation rate of recombinant proteins in *E. coli* often exhausts the bacterial protein quality control system resulting in the formation of inclusion bodies as partially folded and misfolded protein molecules aggregate (Carrió and Villaverde, 2005). Further to this, the microenvironment of *E. coli* may differ to that of the original host in pH, redox potential, osmolarity and folding mechanisms which may render the protein unstable leading to inclusion body formation.

As a result, two different pre-induction temperatures, 28 °C and 37 °C, were studied to understand whether a lower pre-induction temperature could lead to higher PaLemA1-His protein yields. This was done because a lower initial growth temperature would have likely decreased cellular metabolism of *E. coli*, in turn reducing the initial impact associated with the 'leaky' nature of the T7 promoter system during the exponential growth phase. Moreover, the slower metabolic rate of *E. coli* would have likely reduced the rate of protein production following IPTG induction, which may have been beneficial for protein folding and membrane integration due to increased cytoplasmic chaperone availability. Thus, more functional PaLemA1-His protein may have been yielded during the Ni-NTA chromatography purification (**Figures 5.3 and 5.4**) (Gadgil, Kapur and Hu, 2005). Following induction with IPTG overnight, a slight increase in the PaLemA1-His protein yield could be seen in the 37 °C pre-induction culture (**Figure 5.4**), although the statistical significance of

this observation was not quantified. An increase in the protein yield following Ni-NTA column purification could have been due to many factors such as a higher cellular density of the 37 °C pre-induction culture, as the OD₆₀₀ was 4.44 following protein production overnight. In comparison, the 28 °C pre-induction culture had an OD₆₀₀ of 3.18 after overnight induction.

The solubilisation of both the PaLemA1-His and the PaLemA1-sfGFP protein revealed that this step could be further optimised, as some of the protein remained in the insoluble fraction following overnight incubation with DDM and Triton X-100 (**Figures 5.5** and **5.8**, Lane 3). This could be done by investigating the efficacy of other detergents that are widely used for membrane protein solubilisation (Kotov *et al.*, 2019). In addition, it would be beneficial to investigate the time required for the complete solubilisation of the PaLemA1 protein as this could impact end protein yields.

When loading the overnight detergent solubilised fraction onto the Ni-NTA column, a significant proportion of PaLemA1-His and PaLemA1-sfGFP protein were seen flowing through the column (**Figure 5.5**, Lane 5; **Figure 5.8**, Lane 4). Although the size of the Ni-NTA column was increased after initial purification experiments, excess protein was still seen in the flowthrough of each purification. This suggests that a column with an even larger capacity would be needed to bind the excess protein.

The lack of crystal formation following a number of attempts at LCP crystallisation of PaLemA1-His protein could have been due to the presence of the polyhistidine tag, which may have provided the protein with flexibility on the C-terminus, inhibiting crystallisation. Although it is a relatively small sized tag, the stretch of 6 positive residues may hinder protein-protein interactions. This finding is further supported by the crystals formed when using the PaLemA1 protein alone (**Figure 5.10**). The work conducted here has provided a strong basis for future crystallisation studies of PaLemA1 and had time constraints not arisen, this work would have been taken further.

The preliminary NMR work showed some promise, as an increase in temperature coupled with the BEST-TROSY-HSQC experiment provided an improved spectrum with better resolution (**Figure 5.15**). However, due to lower protein yields acquired following PaLemA1 production in M9 media in D₂O, future studies should improve protein concentration by upscaling cell culture to 16 L initially to acquire approximately 0.5 mM worth of protein.

This is because 4 L of cell culture during this study provided about 0.1 mM worth of protein. In addition, it is worth noting that membrane proteins are often found in an oligomeric state, and while this was not confirmed for PaLemA1, it is something that should be investigated in future studies as it could further complicate the acquisition of spectra (Wang *et al.*, 2018). Finally, NMR studies on the soluble domain of PaLemA1 protein alone may also aid in structure determination of this protein and could be further investigated.

Chapter 6

Discussion

6.1 Discussion

The results presented in this thesis reveal a variety of engineered membranous structures generated by overproducing different LemA proteins in the model organism *Escherichia coli*. In particular, the production of intracellular vesicles, tubules, and bacterial extracellular vesicles were observed.

Initially, while the *Pseudomonas aeruginosa* PA14 PaLemA1 protein overproduction in *E. coli* had previously been shown to result in the formation of intracellular lipid vesicles, this was not confirmed by follow up studies. Moreover, genomic analysis of *P. aeruginosa* revealed the presence of a second LemA protein in this organism, PaLemA2, although the predicted structure of this protein was different to that of PaLemA1 in that it did not have a transmembrane domain. Instead, PaLemA2 was predicted to contain an N-terminal lipoprotein signal peptide, which deemed it likely that this protein would be targeted towards the outer membrane of the cell where it could be secreted. Consequently, as the overproduction of the inner membrane targeted PaLemA1 protein led to the production of intracellular vesicles, it was of interest to investigate whether the overproduction of the outer membrane targeted PaLemA2 protein would have an effect on outer membrane vesiculation in *E. coli*. As such a construct harbouring PaLemA2 was made.

Following the expression of both *PalemA1* and *PalemA2* in *E. coli*, TEM analysis revealed the presence of intracellular lipid vesicles. In the case of PaLemA1 the vesicles were small, having an approximate diameter of 50 nm, which was characteristic of the previously observed phenotype. On the other hand, following PaLemA2 overproduction a more diversely sized vesicle population was seen, with small and larger vesicles (some having ~400 nm diameter) being present in the cells. In this sample it was evident that some cells displayed signs of increased membrane lipid biosynthesis as ectopic membranes could be seen inside these cells. This phenotype is commonly observed following the overexpression of some membrane proteins in *E. coli* such as the subunit b of the F₀F₁- ATP synthase and the lipid A disaccharide synthase (Arechaga *et al.*, 2000; Metzger and Raetz, 2009).

To assess the effects of overexpressing *PalemA1* and *PalemA2* genes in *E. coli* SEM analysis was performed. The PaLemA1 sample had a smooth appearing cell envelope whereas the PaLemA2 sample showed signs of vesiculation, where BEVs could be seen blebbing off the OM. This provided some more evidence that this protein may play a role in the restructuring of the outer membrane in its native organism.

Moreover, in comparison to the control, the cells in both samples appeared elongated. While the typical length of an *E. coli* cell is between 1 and 2 μM , on average in both PaLemA1 and PaLemA2 samples the cells appeared to be at least 2 μM . This suggests that there was an inhibition of cell division, which could be due to the hindrance of septum formation by the cytoplasmic membrane invaginations and vesicles. This has previously been seen with the overproduction of the membrane-bound ATP synthase in *E. coli*, which resulted in the production of intracellular vesicles and a variety of membrane invaginations. These cells also appeared elongated and showed signs of inhibited cell division and growth (von Meyenburg, Jørgensen and van Deurs, 1984). However, more work is required to understand the mechanism underlying this cellular elongation.

Interestingly, following the analysis of *P. aeruginosa* strain overexpressing the PaLemA2 protein, the culture filtrates revealed the presence of PaLemA2 outside of the cell, while proteomic analysis of *P. aeruginosa* BEVs following PaLemA2 overproduction demonstrated an enrichment of these vesicles with the protein. Furthermore, SEM analysis of the PaLemA2 *P. aeruginosa* knock-out strain reported a significant decrease in BEV formation (submitted for publication: Juodeikis & Borrero-de Acuna et al., 2021). Together, this further supports the idea that PaLemA2 is targeted to the outer membrane where it can reorganise the membrane and be secreted out of the cell in BEVs.

In contrast to previous studies that were conducted following the overnight production of both PaLemA proteins, time courses were performed to gain a better insight into the temporal formation of the recombinant vesicles in *E. coli*. TEM analysis of cells producing PaLemA1 or PaLemA2 at 0-, 1-, 2-, 4-, 6- and 8-hours post-induction with IPTG was carried out. Although the proportion of control cells displaying a membranous phenotype was relatively high during this study, especially at the 2-hour post-induction time point where 54% of cells showed the presence of intracellular vesicles, this phenotype decreased to 19% at the 8-hour time point. While the membrane vesicles in the control sample appear attached to the inner membrane, their origin remains unclear. However, it is known that as the cells approach stationary phase, the bacteria undergo a range of physiological changes. At the inner bacterial membrane, some extensive remodelling is known to take place, particularly an increase in the amount of phospholipid PE present (Nyström, 2004). A shift in the phospholipid content could perhaps be enough to cause a temporary imbalance of phospholipids in some regions of the inner membrane, resulting in the

formation of the observed membrane invaginations. Although a relatively high proportion of control cells had these intracellular vesicles, on visual examination an average of only a few vesicles were present in these cells. To confirm this, the number of intracellular vesicles present in both the control and the PaLemA1 sample were counted for each time point. A significant difference in the average number of vesicles per cell was seen. While on average the control sample had less than 1 vesicle per cell, the PaLemA1 cells harboured approximately 17 vesicles. In future studies, it would be interesting to evaluate the vesiculation profile of cells which do not harbour a vector. This could provide more information about the presence of intracellular vesicles in empty vector control cells.

Interestingly, prior to protein induction, the formation of intracellular vesicles was observed in the PaLemA1 sample. This is not surprising given the 'leaky' nature of the T7 promoter, and this is further supported by the SDS-PAGE analysis, where the presence of a protein band of corresponding size to PaLemA1 was seen at time point 0. This highlighted that PaLemA1 production is concomitant with intracellular vesicle formation, and likely directly responsible for the creation of these membranous structures.

On the other hand, time-course studies of PaLemA2 production revealed the formation of ectopic intracellular membranes, which appeared to be the dominating phenotype for the first 6 hours of the study. These ectopic membranes were likely a by-product of altered lipid metabolism due to the increased trafficking of PaLemA2 to the periplasm where it could be anchored via a lipid modification to the inner and/or the outer membranes. The disruption of the protein-lipid ratio of either membranes would be enough to stimulate phospholipid biosynthesis in order to counteract this change, thus resulting in excessive membrane proliferation (Jamin *et al.*, 2018). Additionally, it remains unclear how the phenotype progresses from the intracellular ectopic membranes seen during the early stages of protein production, to the increased vesicle formation following 6- and 8-hours post-induction. This possibly could be due to a shift in the proportion of particular phospholipids, such as an increase in cardiolipin which could cluster and form microdomains with the membrane anchored PaLemA2 protein. This would be in support of previous studies that have shown this clustering of cardiolipin with the overproduction of some membrane proteins in *E. coli* (Weiner *et al.*, 1984; Arechaga *et al.*, 2000; Arechaga, 2013). As such, the intrinsic curvature of this lipid and its possible interaction with PaLemA2 may be enough to introduce highly curved membrane regions that could lead to

intracellular vesicle formation. It would therefore be very informative to carry out quantitative lipid analysis on these samples and compare these results to the wild-type strains.

When attempting to analyse the proteins in the PaLemA1 and PaLemA2 operons individually and in various combinations, a range of different membranous phenotypes were observed in *E. coli*. Of particular interest was the PA0538 *P. aeruginosa* protein which is a protein disulphide isomerase (DsbB). Its production in *E. coli* resulted in the mass lysis of a significant proportion of cells. Interestingly, the lysing of cells appeared to lead to vesicle formation. These vesicles were of variable sizes and appeared to contain some cellular components such as ribosomes, meaning they were most likely formed following lysis. Due to the intrinsic curvature possessed by the bacterial membranes, it is likely that the resulting membrane fragments curled and self-annealed, thereby encapsulating the surrounding cellular components. Contrastingly, the cells which remained intact for the most part displayed no membranous phenotype, meaning it was likely that there was a selective pressure against the expression of this particular gene. While it is unclear what precisely led to this phenotype, it could be that the overproduction of DsbB leads to a shift in the redox environment of the cell through excessive oxidative disulphide bond formation. As DsbB would usually be present in a relatively low abundance in *E. coli*, this increase DsbB production would likely be at a detriment to the cell. Alternatively, taking into account that DsbB is a membrane embedded protein with 4 transmembrane domains, its overproduction and subsequent integration into the membrane may compromise cellular integrity resulting in cell lysis.

Similarly, the overproduction of PA0538-PaLemA2 also resulted in a large proportion of cell lysis, though to a lesser extent than PA0538 alone. Additionally, the cells remaining intact showed the presence of ectopic membranes, displaying a shift in the phenotype to the PA0538 production alone. As such, it was interesting to see that the expression of the full PaLemA2 operon in *E. coli* did not result in cell lysis but led to membrane invagination. However, this could be due to the fact that the operon was expressed at very low levels and not enough of the proteins were present to cause cell lysis. This is supported by the SDS-PAGE analysis as the overproduction of the full PaLemA2 operon was not observed. In order to understand more about the possible function of these proteins in their native organism, these genes were subcloned into a *P. aeruginosa* compatible vector for

microscopy studies. However, due to the time limitations as a result of the current pandemic, these studies were not carried out, but remain a subject of interest for future work.

Immunofluorescence studies of stable CHO-S cells expressing PaLemA1 revealed the successful generation of cells harbouring the PaLemA1 construct. Although more than 50% of cells appeared to express this protein at a low level, as indicated by the low fluorescence of these samples, protein overproduction was observed following western blot analysis. While it was hoped that the overproduction of a membrane protein would lead to increased membrane production through an alteration of the lipid metabolism, this was not observed. In fact, apart from a higher number of lysosomal compartments no other observable difference was seen. As these cells intrinsically possess a high level of membrane vesiculation, future experiments would benefit from expressing *PaLemA1* in a different cell line.

To study the effects of producing LemA proteins (MamQ, LemA.153, LemA.159, LemA.501 and PaLemA1) from different microorganisms in *E. coli* and to assess the possibility of utilising protein engineering approaches to direct the formation of different membranous structures, TEM studies were conducted. As the overproduction of different proteins belonging to the LemA family produced a range of membranous phenotypes, some of which varied drastically, it became evident that these proteins may all likely have different functions in their native organisms.

As the sequence analysis of the aforementioned LemA proteins of interest revealed the presence of a transmembrane domain and a soluble domain, it was of interest to see if the expression of the predicted domains individually would have a membranous effect in *E. coli*. While most samples revealed only the presence of inclusion bodies and increased outer membrane vesiculation, the overproduction of the transmembrane domain (TMD) of PaLemA1 resulted in the formation of small intracellular vesicles. This indicated that the TMD of PaLemA1 may have intrinsic curvature which favours membrane bending and subsequent invagination. Consequently, this presents an interesting target for future protein engineering approaches, which could utilise the PaLemA1 TMD as a targeting domain for a number of proteins. For instance, by creating protein fusions consisting of the PaLemA1 TMD and an antigen of interest, could allow for the production of *E. coli* derived intracellular vesicles enriched with a specific antigen for vaccine production.

During the LemA hybrid protein studies, combinations of the PaLemA1 TMD with the soluble domains of either LemA.153, LemA.159, LemA.501 and PaLemA1, led to the formation of different membranous phenotypes. Remarkably, even a 2 amino acid linker in between the TMD and soluble domain of PaLemA1 changed the phenotype of the native protein. As mentioned previously, PaLemA1 produced small intracellular vesicles in *E. coli*, while the overproduction of the hybrid PaLemA1 led to tubule formation in the same host. This indicated that the amino acid sequence that follows the transmembrane domain may play a big role in inducing particular protein topology that affects the behaviour of the neighbouring membranes. Thus, future studies should focus on uncovering the key components of the LemA proteins that are required for membrane restructuring. This could be achieved through manipulation of the residues that follow the transmembrane domain of these proteins. Also, the generation of C-terminally truncated LemA proteins may provide more information about the importance of the soluble domain in membrane reorganisation.

In addition, the overexpression of the LemA.153 TMD LemA.501s construct resulted in the lysis of a large number of cells. These lysed regions contained numerous small membrane vesicles, some of which encapsulated cytoplasmic contents like ribosomes, while others were devoid of this. Some of the intact cells also contained small intracellular vesicles that were found in regions containing inclusion bodies. This suggested that some, if not most, of the vesicles seen in lysed cells may have been produced prior to cell lysis. As mentioned before, current BEV-based vaccine approaches heavily rely upon detergents for the production of the membrane vesicles (Acevedo *et al.*, 2014). However, a dual hybrid protein based system that firstly induces the production of intracellular vesicles and later results in cell lysis could present an alternative approach to membrane vesicle production. To establish if the resulting intracellular vesicles from the LemA.153 TMD LemA.501s sample are enriched with the hybrid protein, the vesicles could be purified and analysed via SDS-PAGE analysis and MALDI-MS.

In order to gain a better understanding about the structure-function relationship of PaLemA1, structural studies were conducted. While preliminary data has shown successful solubilisation of the protein in DDM, a proportion of this protein remained insoluble. Thus, further detergent optimisation may be necessary to increase the solubilisation yield. Moreover, when utilising the PaLemA1-sfGFP protein fusion for the purification of

PaLemA1, the sfGFP tag had to be cleaved prior to protein crystallisation studies. However, the incubation of the fusion protein with TEV protease did not result in the complete proteolytic cleavage of the whole protein population, presenting another area that could further improve the end PaLemA1 protein yield. Nonetheless, in most cases a sufficient amount of protein was obtained. On average the final estimated concentration of PaLemA1 used to set up crystallisation screens ranged between 12-20 mg/ml. During these initial studies two conditions, 50 mM Tris pH 8, 0.1 M sodium sulfate decahydrate and 50 mM Tris pH 8, 0.2 M potassium phosphate monobasic, resulted in the formation of protein crystals. Consequently, it was decided to try and optimise these conditions by varying the pH of the Tris buffer and the concentration of salt. Also, due to the mechanical fragility of the crystals, the Diffrax™ *in situ* crystallisation plates (Molecular Dimensions) were ordered as these would allow for the direct freezing of the crystallisation droplet and data collection without having to handle the crystals. This *in situ* crystallisation method has recently been successfully used to enable X-ray structure determination of the chemokine receptor 2A and holds great promise (Apel *et al.*, 2019). Unfortunately, due to the ramifications of the current SARS-CoV2 pandemic this final optimisation step was not carried out, and continues to be the next stage of this study.

The work discussed in this thesis contributes to the growing field of synthetic biology through the study of novel membrane engineering approaches in *E. coli*. The bacterium itself does not normally produce any intracellular membranous compartments and thus, provides a relatively simplified landscape to work with. Moreover, *E. coli* has unparalleled fast growth kinetics, inexpensive media requirements, and the capacity to produce recombinant proteins at a high level (Sezonov, Joseleau-Petit and D'Ari, 2007). As such it presents itself as an ideal workhorse for the generation of a novel vaccine delivery platform that utilises recombinant intracellular and extracellular vesicles. BEVs produced from a wide range of Gram-negative organisms have shown to be highly immunogenic and present excellent carriers for immunogenic components (Holst *et al.*, 2009). However, currently licensed vaccines utilise BEVs only from the pathogenic strain of interest, thus limiting the implementation of this vaccine delivery system on a wider scale (Claassen *et al.*, 1996). By exploiting protein engineering approaches, a universal system for the production of BEVs and/or intracellular membrane vesicles with targeted protein enrichment, may allow for the generation of efficient, low cost vaccines in *E. coli*.

The work conducted on LemA proteins in this thesis is indicative of the vast potential of these proteins in reorganising the bacterial membranes for the production of specialised membranous compartments. However, further characterisation is required to fully understand the structure-function relationship of these proteins, and the targeting capacity of the LemA proteins in delivering specific antigenic proteins to the intended location. This would allow for a more targeted approach to protein engineering for the development of a universal vaccine delivery platform utilising specialised membrane vesicles derived from *E. coli*.

References

- Acevedo, R. *et al.* (2014) 'Bacterial outer membrane vesicles and vaccine applications', *Frontiers in Immunology*. doi: 10.3389/fimmu.2014.00121.
- Allen, W. J., Phan, G. and Waksman, G. (2009) 'Structural biology of periplasmic chaperones.', *Advances in protein chemistry and structural biology*. doi: 10.1016/s1876-1623(08)78003-9.
- Almén, M. S. *et al.* (2009) 'Mapping the human membrane proteome: A majority of the human membrane proteins can be classified according to function and evolutionary origin', *BMC Biology*. doi: 10.1186/1741-7007-7-50.
- Ampofo, W. K. *et al.* (2012) 'Improving influenza vaccine virus selection Report of a WHO informal consultation held at WHO headquarters, Geneva, Switzerland, 14-16 June 2010', in *Influenza and other Respiratory Viruses*. doi: 10.1111/j.1750-2659.2011.00277.x.
- Apel, A. K. *et al.* (2019) 'Crystal Structure of CC Chemokine Receptor 2A in Complex with an Orthosteric Antagonist Provides Insights for the Design of Selective Antagonists.', *Structure (London, England : 1993)*, 27(3), pp. 427-438.e5. doi: 10.1016/j.str.2018.10.027.
- Arechaga, I. *et al.* (2000) 'Characterisation of new intracellular membranes in *Escherichia coli* accompanying large scale over-production of the b subunit of F1F₀ ATP synthase', *FEBS Letters*. doi: 10.1016/S0014-5793(00)02054-8.
- Arechaga, I. (2013) 'Membrane Invaginations in Bacteria and Mitochondria: Common Features and Evolutionary Scenarios', *Microbial Physiology*, 23(1–2), pp. 13–23. doi: 10.1159/000346515.
- Armour, G. A. and Brewer, G. J. (1990) 'Membrane morphogenesis from cloned fragments of bacteriophage PM2 DNA that contain the *sp6.6* gene', *The FASEB Journal*. doi: 10.1096/fasebj.4.5.2407591.
- Arnold, K. *et al.* (2006) 'The SWISS-MODEL workspace: A web-based environment for protein structure homology modelling', *Bioinformatics*. doi: 10.1093/bioinformatics/bti770.
- Arnold, R. *et al.* (2011) 'Effectiveness of a vaccination programme for an epidemic of meningococcal B in New Zealand', *Vaccine*. doi: 10.1016/j.vaccine.2011.06.120.
- Artaud, C., Kara, L. and Launay, O. (2019) 'Vaccine development: From preclinical studies to phase 1/2 clinical trials', in *Methods in Molecular Biology*. doi: 10.1007/978-1-4939-9550-9_12.
- Authorities, N. R., Introduction, P. and Remarks, G. (2003) *World Health Organization Organisation Mondiale De La Sante Who Guidelines on Nonclinical Evaluation of, Who.Int.*
- Bader, M. *et al.* (1998) 'Reconstitution of a protein disulfide catalytic system', *Journal of Biological Chemistry*. doi: 10.1074/jbc.273.17.10302.
- Barberis, I. *et al.* (2016) 'History and evolution of influenza control through vaccination: From the first monovalent vaccine to universal vaccines', *Journal of Preventive Medicine and Hygiene*. doi: 10.15167/2421-4248/jpmh2016.57.3.642.
- Bärnighausen, T. *et al.* (2014) 'Valuing vaccination', *Proceedings of the National Academy of Sciences of the United States of America*. doi: 10.1073/pnas.1400475111.
- Bartlett, B. L., Pellicane, A. J. and Tyring, S. K. (2009) 'Vaccine immunology', *Dermatologic Therapy*. doi: 10.1111/j.1529-8019.2009.01223.x.
- Beltrán-Heredia, E. *et al.* (2019) 'Membrane curvature induces cardiolipin sorting', *Communications Biology*. doi: 10.1038/s42003-019-0471-x.
- Benn, C. S. *et al.* (2013) 'A Small Jab - A Big Effect: Nonspecific Immunomodulation By Vaccines',

- Trends in Immunology*. doi: 10.1016/j.it.2013.04.004.
- Benz, R. *et al.* (1986) 'Pore formation by LamB of *Escherichia coli* in lipid bilayer membranes', *Journal of Bacteriology*. doi: 10.1128/jb.165.3.978-986.1986.
- Bernaodat, F. *et al.* (2011) 'Heterologous expression of membrane proteins: Choosing the appropriate host', *PLoS ONE*. doi: 10.1371/journal.pone.0029191.
- Bernsel, A. and Daley, D. O. (2009) 'Exploring the inner membrane proteome of *Escherichia coli*: which proteins are eluding detection and why?', *Trends in Microbiology*. doi: 10.1016/j.tim.2009.07.005.
- Bishai, D., Koenig, M. and Ali Khan, M. (2003) 'Measles vaccination improves the equity of health outcomes: Evidence from Bangladesh', *Health Economics*. doi: 10.1002/hec.732.
- Bjune, G. *et al.* (1991) 'Effect of outer membrane vesicle vaccine against group B meningococcal disease in Norway', *The Lancet*. doi: 10.1016/0140-6736(91)91961-S.
- Blaurock, A. E. and Wober, W. (1976) 'Structure of the wall of *Halobacterium halobium* gas vesicles', *Journal of Molecular Biology*. doi: 10.1016/0022-2836(76)90270-9.
- Blum, M. *et al.* (2021) 'The InterPro protein families and domains database: 20 years on', *Nucleic Acids Research*. doi: 10.1093/nar/gkaa977.
- Bonnington, K. E. and Kuehn, M. J. (2014) 'Protein selection and export via outer membrane vesicles', *Biochimica et Biophysica Acta - Molecular Cell Research*. doi: 10.1016/j.bbamcr.2013.12.011.
- Both, G. W. *et al.* (1983) 'Antigenic drift in influenza virus H3 hemagglutinin from 1968 to 1980: multiple evolutionary pathways and sequential amino acid changes at key antigenic sites.', *Journal of Virology*. doi: 10.1128/jvi.48.1.52-60.1983.
- Bramkamp, M. and Lopez, D. (2015) 'Exploring the Existence of Lipid Rafts in Bacteria', *Microbiology and Molecular Biology Reviews*. doi: 10.1128/mubr.00036-14.
- Brantner, C. A. *et al.* (2002) 'Intracellular localization of the particulate methane monooxygenase and methanol dehydrogenase in *Methylomicrobium album* BG8', *Archives of Microbiology*. doi: 10.1007/s00203-002-0426-2.
- Braun, V. and Rehn, K. (1969) 'Chemical Characterization, Spatial Distribution and Function of a Lipoprotein (Murein-Lipoprotein) of the *E. coli* Cell Wall: The Specific Effect of Trypsin on the Membrane Structure', *European Journal of Biochemistry*. doi: 10.1111/j.1432-1033.1969.tb00707.x.
- Van den Brink-van der Laan, E. *et al.* (2003) 'Membrane interaction of the glycosyltransferase MurG: A special role for cardiolipin', *Journal of Bacteriology*. doi: 10.1128/JB.185.13.3773-3779.2003.
- Bruge, J. *et al.* (2004) 'Clinical evaluation of a group B meningococcal N-propionylated polysaccharide conjugate vaccine in adult, male volunteers', *Vaccine*. doi: 10.1016/j.vaccine.2003.10.005.
- Buckland, B. C. (2005) 'The process development challenge for a new vaccine', *Nature Medicine*. doi: 10.1038/nm1218.
- Bury-Moné, S. *et al.* (2009) 'Global analysis of extracytoplasmic stress signaling in *Escherichia coli*', *PLoS Genetics*. doi: 10.1371/journal.pgen.1000651.
- Carranza, G. *et al.* (2017) 'Cardiolipin plays an essential role in the formation of intracellular membranes in *Escherichia coli*', *Biochimica et Biophysica Acta - Biomembranes*. doi: 10.1016/j.bbamem.2017.03.006.

- Carrió, M. M. and Villaverde, A. (2002) 'Construction and deconstruction of bacterial inclusion bodies.', *Journal of biotechnology*, 96(1), pp. 3–12. doi: 10.1016/S0168-1656(02)00032-9.
- Carrió, M. M. and Villaverde, A. (2005) 'Localization of chaperones DnaK and GroEL in bacterial inclusion bodies.', *Journal of bacteriology*, 187(10), pp. 3599–3601. doi: 10.1128/JB.187.10.3599-3601.2005.
- Cartwright, K. *et al.* (1999) 'Immunogenicity and reactogenicity in UK infants of a novel meningococcal vesicle vaccine containing multiple class 1 (PorA) outer membrane proteins', *Vaccine*. doi: 10.1016/S0264-410X(99)00044-4.
- Centers for Disease Control and Prevention (2018) 'Vaccine Effectiveness - How Well Does the Flu Vaccine Work?', *Cdc.Gov*.
- Chen, D. J. *et al.* (2010) 'Delivery of foreign antigens by engineered outer membrane vesicle vaccines', *Proceedings of the National Academy of Sciences of the United States of America*. doi: 10.1073/pnas.0805532107.
- Claassen, I. *et al.* (1996) 'Production, characterization and control of a *Neisseria meningitidis* hexavalent class 1 outer membrane protein containing vesicle vaccine', *Vaccine*. doi: 10.1016/0264-410X(96)00020-5.
- Clifton, L. A. *et al.* (2015) 'Effect of divalent cation removal on the structure of gram-negative bacterial outer membrane models', *Langmuir*. doi: 10.1021/la504407v.
- Corey, L. *et al.* (2020) 'A strategic approach to COVID-19 vaccine R&D', *Science*. doi: 10.1126/science.abc5312.
- Cornejo, E. *et al.* (2016) 'Dynamic remodeling of the magnetosome membrane is triggered by the initiation of biomineralization', *mBio*. doi: 10.1128/mBio.01898-15.
- Cox, M. M. J. and Hollister, J. R. (2009) 'FluBlok, a next generation influenza vaccine manufactured in insect cells', *Biologicals*. doi: 10.1016/j.biologicals.2009.02.014.
- Crommelin, D. J. A. *et al.* (2021) 'Addressing the Cold Reality of mRNA Vaccine Stability', *Journal of Pharmaceutical Sciences*. doi: 10.1016/j.xphs.2020.12.006.
- Cronan, Jr., J. E. and Rock, C. O. (2008) 'Biosynthesis of Membrane Lipids', *EcoSal Plus*. doi: 10.1128/ecosalplus.3.6.4.
- D'Orazio, S. E. F. *et al.* (2003) 'The *Listeria monocytogenes* IemA Gene Product Is Not Required for Intracellular Infection or to Activate fMIGWII-Specific T Cells', *Infection and Immunity*. doi: 10.1128/IAI.71.12.6721-6727.2003.
- Dalbey, R. E. and Kuhn, A. (2012) 'Protein Traffic in Gram-negative bacteria – how exported and secreted proteins find their way', *FEMS Microbiology Reviews*, 36(6), pp. 1023–1045. doi: 10.1111/j.1574-6976.2012.00327.x.
- Dawood, F. S. *et al.* (2020) 'Interim Estimates of 2019–20 Seasonal Influenza Vaccine Effectiveness – United States, February 2020', *MMWR. Morbidity and Mortality Weekly Report*. doi: 10.15585/mmwr.mm6907a1.
- Deogaonkar, R. *et al.* (2012) 'Systematic review of studies evaluating the broader economic impact of vaccination in low and middle income countries', *BMC Public Health*. doi: 10.1186/1471-2458-12-878.
- Dev, I. K. and Ray, P. H. (1984) 'Rapid assay and purification of a unique signal peptidase that processes the prolipoprotein from *Escherichia coli* B', *Journal of Biological Chemistry*. doi: 10.1016/S0021-9258(84)90629-0.
- Devi, S. J. N. *et al.* (1997) 'Preclinical evaluation of group B *Neisseria meningitidis* and *Escherichia*

coli K92 capsular polysaccharide-protein conjugate vaccines in juvenile rhesus monkeys', *Infection and Immunity*. doi: 10.1128/iai.65.3.1045-1052.1997.

Díaz-Mejía, J. J., Babu, M. and Emili, A. (2009) 'Computational and experimental approaches to chart the *Escherichia coli* cell-envelope-associated proteome and interactome', *FEMS Microbiology Reviews*. doi: 10.1111/j.1574-6976.2008.00141.x.

Dou, Z. *et al.* (2008) 'CO₂ fixation kinetics of *Halothiobacillus neapolitanus* mutant carboxysomes lacking carbonic anhydrase suggest the shell acts as a diffusional barrier for CO₂', *Journal of Biological Chemistry*. doi: 10.1074/jbc.M709285200.

Driessen, A. J. M. and Nouwen, N. (2008) 'Protein translocation across the bacterial cytoplasmic membrane', *Annual Review of Biochemistry*. doi: 10.1146/annurev.biochem.77.061606.160747.

Dunkle, L. M. *et al.* (2017) 'Efficacy of Recombinant Influenza Vaccine in Adults 50 Years of Age or Older', *New England Journal of Medicine*. doi: 10.1056/nejmoa1608862.

Ehreth, J. (2003) 'The global value of vaccination', in *Vaccine*. doi: 10.1016/S0264-410X(02)00623-0.

Elhenawy, W. *et al.* (2016) 'LPS remodeling triggers formation of outer membrane vesicles in *salmonella*', *mBio*. doi: 10.1128/mBio.00940-16.

Ellis, T. N. and Kuehn, M. J. (2010) 'Virulence and Immunomodulatory Roles of Bacterial Outer Membrane Vesicles', *Microbiology and Molecular Biology Reviews*. doi: 10.1128/mmbr.00031-09.

Ellis, T. N., Leiman, S. A. and Kuehn, M. J. (2010) 'Naturally produced outer membrane vesicles from *Pseudomonas aeruginosa* elicit a potent innate immune response via combined sensing of both lipopolysaccharide and protein components', *Infection and Immunity*. doi: 10.1128/IAI.00433-10.

Elmes, M. L., Scraba, D. G. and Weiner, J. H. (1986) 'Isolation and characterization of the tubular organelles induced by fumarate reductase overproduction in *Escherichia coli*', *Journal of General Microbiology*. doi: 10.1099/00221287-132-6-1429.

Epand, R. F. *et al.* (2007) 'Cardiolipin Clusters and Membrane Domain Formation Induced by Mitochondrial Proteins', *Journal of Molecular Biology*. doi: 10.1016/j.jmb.2006.10.028.

Eriksson, H. M. *et al.* (2009) 'Massive formation of intracellular membrane vesicles in *Escherichia coli* by a monotopic membrane-bound lipid glycosyltransferase', *Journal of Biological Chemistry*. doi: 10.1074/jbc.M109.021618.

Erridge, C., Bennett-Guerrero, E. and Poxton, I. R. (2002) 'Structure and function of lipopolysaccharides', *Microbes and Infection*. doi: 10.1016/S1286-4579(02)01604-0.

European Medicines Agency (2007) *Guideline on clinical evaluation of new vaccines*. Available at: https://www.ema.europa.eu/en/documents/scientific-guideline/guideline-clinical-evaluation-new-vaccines_en.pdf.

Fahim Halim Khan (2009) *The Elements of Immunology*, Pearson Education.

Fausther-Bovendo, H. and Kobinger, G. P. (2014) 'Pre-existing immunity against Ad vectors: Humoral, cellular, and innate response, what's important?', *Human Vaccines and Immunotherapeutics*. doi: 10.4161/hv.29594.

Fenner, F. (1982) 'A successful eradication campaign. Global eradication of smallpox.', *Reviews of Infectious Diseases*. doi: 10.1093/clinids/4.5.916.

Finne, J., Leinonen, M. and Mäkelä, P. H. (1983) 'Antigenic similarities between brain components and bacteria causing meningitis. Implications for vaccine development and pathogenesis', *The*

Lancet. doi: 10.1016/S0140-6736(83)90340-9.

Fitch, W. M. *et al.* (1997) 'Long term trends in the evolution of H(3) HA1 human influenza type A', *Proceedings of the National Academy of Sciences of the United States of America*. doi: 10.1073/pnas.94.15.7712.

Flannery, B. *et al.* (2004) 'Impact of Childhood Vaccination on Racial Disparities in Invasive *Streptococcus pneumoniae* Infections', *Journal of the American Medical Association*. doi: 10.1001/jama.291.18.2197.

Fotin-Mleczek, M. *et al.* (2011) 'Messenger RNA-based vaccines with dual activity induce balanced TLR-7 dependent adaptive immune responses and provide antitumor activity', *Journal of Immunotherapy*. doi: 10.1097/CJI.0b013e3181f7dbe8.

Fredriksen, J. H. *et al.* (1991) 'Production, characterization and control of MenB-vaccine "folkehelsa": An outer membrane vesicle vaccine against group B meningococcal disease', in *NIPH Annals*.

Fukuda, Y. *et al.* (2006) 'Dynamic analysis of a genomic island in *Magnetospirillum sp.* strain AMB-1 reveals how magnetosome synthesis developed', *FEBS Letters*. doi: 10.1016/j.febslet.2006.01.003.

Gadgil, M., Kapur, V. and Hu, W.-S. (2005) 'Transcriptional response of *Escherichia coli* to temperature shift.', *Biotechnology progress*, 21(3), pp. 689–699. doi: 10.1021/bp049630l.

Garon, J. R., Cochi, S. L. and Orenstein, W. A. (2015) 'The Challenge of Global Poliomyelitis Eradication', *Infectious Disease Clinics of North America*. doi: 10.1016/j.idc.2015.07.003.

Ge, C. *et al.* (2014) 'Membrane remodeling capacity of a vesicle-inducing glycosyltransferase', *FEBS Journal*. doi: 10.1111/febs.12889.

Gerritzen, M. J. H. *et al.* (2017) 'Bioengineering bacterial outer membrane vesicles as vaccine platform', *Biotechnology Advances*. doi: 10.1016/j.biotechadv.2017.05.003.

Giuliani, M. M. *et al.* (2006) 'A universal vaccine for serogroup B meningococcus', *Proceedings of the National Academy of Sciences of the United States of America*. doi: 10.1073/pnas.0603940103.

Goebel, E. M. *et al.* (2008) 'O antigen protects *Bordetella parapertussis* from complement', *Infection and Immunity*. doi: 10.1128/IAI.01629-07.

Goetz, K. B., Pfeleiderer, M. and Schneider, C. K. (2010) 'First-in-human clinical trials with vaccines-what regulators want', *Nature Biotechnology*. doi: 10.1038/nbt0910-910.

Gorby, Y. A., Beveridge, T. J. and Blakemore, R. P. (1988) 'Characterization of the bacterial magnetosome membrane.', *Journal of bacteriology*. doi: 10.1128/jb.170.2.834-841.1988.

Gotschlich, E. C., Goldschneider, I. and Artenstein, M. S. (1969) 'Human immunity to the meningococcus. IV. Immunogenicity of group A and group C meningococcal polysaccharides in human volunteers.', *The Journal of experimental medicine*. doi: 10.1084/jem.129.6.1367.

GOV.UK (2020) *UK authorises Pfizer/BioNTech COVID-19 vaccine*. Available at: <https://www.gov.uk/government/news/uk-authorises-pfizer-biontech-covid-19-vaccine>.

Grass, G. *et al.* (2005) 'FieF (YiiP) from *Escherichia coli* mediates decreased cellular accumulation of iron and relieves iron stress', *Archives of Microbiology*. doi: 10.1007/s00203-004-0739-4.

Grommet, A. B., Feller, M. and Klajn, R. (2020) 'Chemical reactivity under nanoconfinement', *Nature Nanotechnology*. doi: 10.1038/s41565-020-0652-2.

Grünberg, K. *et al.* (2001) 'A Large Gene Cluster Encoding Several Magnetosome Proteins Is

- Conserved in Different Species of Magnetotactic Bacteria', *Applied and Environmental Microbiology*. doi: 10.1128/AEM.67.10.4573-4582.2001.
- Hagan, C. L., Kim, S. and Kahne, D. (2010) 'Reconstitution of outer membrane protein assembly from purified components', *Science*. doi: 10.1126/science.1188919.
- Han, S. (2015) 'Clinical vaccine development', *Clinical and Experimental Vaccine Research*. doi: 10.7774/cevr.2015.4.1.46.
- Hardesty, C., Ferran, C. and DiRienzo, J. M. (1991) 'Plasmid-mediated sucrose metabolism in *Escherichia coli*: Characterization of scrY, the structural gene for a phosphoenolpyruvate-dependent sucrose phosphotransferase system outer membrane porin', *Journal of Bacteriology*. doi: 10.1128/jb.173.2.449-456.1991.
- Harrison, L. H., Trotter, C. L. and Ramsay, M. E. (2009) 'Global epidemiology of meningococcal disease', *Vaccine*. doi: 10.1016/j.vaccine.2009.04.063.
- Hartwig, D. D. *et al.* (2013) 'A prime-boost strategy using the novel vaccine candidate, LemA, protects hamsters against leptospirosis', *Clinical and Vaccine Immunology*. doi: 10.1128/CVI.00034-13.
- Hayashi, S. and Wu, H. C. (1990) 'Lipoproteins in bacteria', *Journal of Bioenergetics and Biomembranes*. doi: 10.1007/BF00763177.
- Hegde, N. R. (2015) 'Cell culture-based influenza vaccines: A necessary and indispensable investment for the future', *Human Vaccines and Immunotherapeutics*. doi: 10.1080/21645515.2015.1016666.
- Von Heijne, G. (1989) 'The structure of signal peptides from bacterial lipoproteins', *Protein Engineering, Design and Selection*. doi: 10.1093/protein/2.7.531.
- Heinrich, S. U. *et al.* (2000) 'The Sec61p complex mediates the integration of a membrane protein by allowing lipid partitioning of the transmembrane domain', *Cell*. doi: 10.1016/S0092-8674(00)00028-3.
- Heinrichs, D. E., Yethon, J. A. and Whitfield, C. (1998) 'Molecular basis for structural diversity in the core regions of the lipopolysaccharides of *Escherichia coli* and *Salmonella enterica*', *Molecular Microbiology*. doi: 10.1046/j.1365-2958.1998.01063.x.
- Heinz, E. and Lithgow, T. (2014) 'A comprehensive analysis of the Omp85/TpsB protein superfamily structural diversity, taxonomic occurrence, and evolution', *Frontiers in Microbiology*. doi: 10.3389/fmicb.2014.00370.
- Hiraoka, S., Matsuzaki, H. and Shibuya, I. (1993) 'Active increase in cardiolipin synthesis in the stationary growth phase and its physiological significance in *Escherichia coli*', *FEBS Letters*. doi: 10.1016/0014-5793(93)80807-7.
- Holst, J. *et al.* (2009) 'Properties and clinical performance of vaccines containing outer membrane vesicles from *Neisseria meningitidis*', *Vaccine*. doi: 10.1016/j.vaccine.2009.04.071.
- Holst, J. *et al.* (2013) 'Vaccines against meningococcal serogroup B disease containing outer membrane vesicles (OMV) Lessons from past programs and implications for the future', *Human Vaccines and Immunotherapeutics*. doi: 10.4161/hv.24129.
- Huang, K. C. and Ramamurthi, K. S. (2010) 'Macromolecules that prefer their membranes curvy: MicroReview', *Molecular Microbiology*. doi: 10.1111/j.1365-2958.2010.07168.x.
- Inouye, S. *et al.* (1983) 'Prolipoprotein signal peptidase of *Escherichia coli* requires a cysteine residue at the cleavage site.', *The EMBO journal*. doi: 10.1002/j.1460-2075.1983.tb01386.x.
- Jafri, R. Z. *et al.* (2013) 'Global epidemiology of invasive meningococcal disease', *Population*

Health Metrics. doi: 10.1186/1478-7954-11-17.

Jamin, N. *et al.* (2018) 'Ectopic neo-formed intracellular membranes in *Escherichia coli*: A response to membrane protein-induced stress involving membrane curvature and domains', *Biomolecules*. doi: 10.3390/biom8030088.

Jogler, C. *et al.* (2009) 'Comparative analysis of magnetosome gene clusters in magnetotactic bacteria provides further evidence for horizontal gene transfer', *Environmental Microbiology*. doi: 10.1111/j.1462-2920.2009.01854.x.

Josefsberg, J. O. and Buckland, B. (2012) 'Vaccine process technology', *Biotechnology and Bioengineering*. doi: 10.1002/bit.24493.

Juodeikis, R. *et al.* (2022) 'LemA directs bacterial membrane restructuring and vesicle formation', *Molecular Microbiology*.

Juodeikis, R. (2016) 'Engineering Membranes in *Escherichia coli*: The Magnetosome, LemA Protein Family and Outer Membrane Vesicles', *Kent Academic Repository*, PhD Thesis, p. Chapter 5.

Juodeikis, R. *et al.* (2020) 'Effect of metabolosome encapsulation peptides on enzyme activity, coaggregation, incorporation, and bacterial microcompartment formation', *MicrobiologyOpen*. doi: 10.1002/mbo3.1010.

Kalipatnapu, S. and Chattopadhyay, A. (2005) 'Membrane protein solubilization: Recent advances and challenges in solubilization of serotonin1A receptors', *IUBMB Life*. doi: 10.1080/15216540500167237.

Kamboj, M. and Sepkowitz, K. A. (2007) 'Risk of Transmission Associated With Live Attenuated Vaccines Given to Healthy Persons Caring for or Residing With an Immunocompromised Patient', *Infection Control & Hospital Epidemiology*. doi: 10.1086/517952.

Kang, S. M. and Compans, R. W. (2009) 'Host responses from innate to adaptive immunity after vaccination: Molecular and cellular events', *Molecules and Cells*. doi: 10.1007/s10059-009-0015-1.

Kaparakis-Liaskos, M. and Ferrero, R. L. (2015) 'Immune modulation by bacterial outer membrane vesicles', *Nature Reviews Immunology*. doi: 10.1038/nri3837.

Kaur, S. P. and Gupta, V. (2020) 'COVID-19 Vaccine: A comprehensive status report', *Virus Research*. doi: 10.1016/j.virusres.2020.198114.

Keller, R. *et al.* (2015) 'The *Escherichia coli* Envelope Stress Sensor CpxA Responds to Changes in Lipid Bilayer Properties', *Biochemistry*. doi: 10.1021/acs.biochem.5b00242.

Kerfeld, C. A. *et al.* (2005) 'Microbiology: Protein structures forming the shell of primitive bacterial organelles', *Science*. doi: 10.1126/science.1113397.

Kerfeld, C. A. *et al.* (2018) 'Bacterial microcompartments', *Nature Reviews Microbiology*. doi: 10.1038/nrmicro.2018.10.

Kim, D. *et al.* (2010) 'DNA vaccine with α -galactosylceramide at prime phase enhances anti-tumor immunity after boosting with antigen-expressing dendritic cells', *Vaccine*. doi: 10.1016/j.vaccine.2010.08.079.

Kim, J. H. *et al.* (2015) 'Gram-negative and Gram-positive bacterial extracellular vesicles', *Seminars in Cell and Developmental Biology*. doi: 10.1016/j.semcdb.2015.02.006.

Kim, J. Y. *et al.* (2008) 'Engineered Bacterial Outer Membrane Vesicles with Enhanced Functionality', *Journal of Molecular Biology*. doi: 10.1016/j.jmb.2008.03.076.

Kim, O. Y. *et al.* (2013) 'Immunization with *Escherichia coli* Outer Membrane Vesicles Protects Bacteria - Induced Lethality via Th1 and Th17 Cell Responses', *The Journal of Immunology*. doi:

10.4049/jimmunol.1200742.

Kim, S. *et al.* (2007) 'Structure and function of an essential component of the outer membrane protein assembly machine', *Science*. doi: 10.1126/science.1143993.

Kirnbauer, R. *et al.* (1992) 'Papillomavirus L1 major capsid protein self-assembles into virus-like particles that are highly immunogenic', *Proceedings of the National Academy of Sciences of the United States of America*. doi: 10.1073/pnas.89.24.12180.

Kis, Z. *et al.* (2019) 'Emerging Technologies for Low-Cost, Rapid Vaccine Manufacture', *Biotechnology Journal*. doi: 10.1002/biot.201800376.

Klimentová, J. and Stulík, J. (2015) 'Methods of isolation and purification of outer membrane vesicles from gram-negative bacteria', *Microbiological Research*. doi: 10.1016/j.micres.2014.09.006.

Koeberling, O., Seubert, A. and Granoff, D. M. (2008) 'Bactericidal antibody responses elicited by a meningococcal outer membrane vesicle vaccine with overexpressed factor H-binding protein and genetically attenuated endotoxin', *Journal of Infectious Diseases*. doi: 10.1086/589308.

Koebnik, R. (1995) 'Proposal for a peptidoglycan-associating alpha-helical motif in the C-terminal regions of some bacterial cell-surface proteins', *Molecular Microbiology*. doi: 10.1111/j.1365-2958.1995.tb02348.x.

Koebnik, R., Locher, K. P. and Van Gelder, P. (2000) 'Structure and function of bacterial outer membrane proteins: Barrels in a nutshell', *Molecular Microbiology*. doi: 10.1046/j.1365-2958.2000.01983.x.

Koff, W. C. *et al.* (2013) 'Accelerating next-generation vaccine development for global disease prevention', *Science*. doi: 10.1126/science.1232910.

Komeili, A. *et al.* (2006) 'Magnetosomes are cell membrane imaginations organized by the actin-like protein MamK', *Science*. doi: 10.1126/science.1123231.

Komeili, A. (2007) 'Molecular mechanisms of magnetosome formation', *Annual Review of Biochemistry*. doi: 10.1146/annurev.biochem.74.082803.133444.

Komeili, A. (2012) 'Molecular mechanisms of compartmentalization and biomineralization in magnetotactic bacteria', *FEMS Microbiology Reviews*. doi: 10.1111/j.1574-6976.2011.00315.x.

Konovalova, A. and Silhavy, T. J. (2015) 'Outer membrane lipoprotein biogenesis: Lol is not the end', *Philosophical Transactions of the Royal Society B: Biological Sciences*. doi: 10.1098/rstb.2015.0030.

Kotov, V. *et al.* (2019) 'High-throughput stability screening for detergent-solubilized membrane proteins', *Scientific Reports*, 9(1), pp. 1–19. doi: 10.1038/s41598-019-46686-8.

Kremer, E. J. (2020) 'Pros and Cons of Adenovirus-Based SARS-CoV-2 Vaccines', *Molecular Therapy*. doi: 10.1016/j.ymthe.2020.10.002.

Krogh, A. *et al.* (2001) 'Predicting transmembrane protein topology with a hidden Markov model: Application to complete genomes', *Journal of Molecular Biology*. doi: 10.1006/jmbi.2000.4315.

Kuehn, M. J. and Kesty, N. C. (2005) 'Bacterial outer membrane vesicles and the host-pathogen interaction', *Genes and Development*. doi: 10.1101/gad.1299905.

Kumar Saha, S. *et al.* (1996) 'A regulatory mechanism for the balanced synthesis of membrane phospholipid species in escherichia coli', *Bioscience, Biotechnology and Biochemistry*. doi: 10.1271/bbb.60.111.

Langley, K. E., Hawrot, E. and Kennedy, E. P. (1982) 'Membrane assembly: Movement of

phosphatidylserine between the cytoplasmic and outer membranes of *Escherichia coli*', *Journal of Bacteriology*.

LaSarre, B. *et al.* (2018) 'Restricted localization of photosynthetic intracytoplasmic membranes (ICMs) in multiple genera of purple nonsulfur bacteria', *mBio*. doi: 10.1128/mBio.00780-18.

Laufer, M., Sanchez-Vegas, C. and Ramos, O. M. (2006) 'Effect of introduction of the pneumococcal conjugate vaccine on drug-resistant *Streptococcus pneumoniae*', *International Pediatrics*. doi: 10.1056/nejmoa051642.

Lee, M. J. *et al.* (2018) 'De novo targeting to the cytoplasmic and luminal side of bacterial microcompartments', *Nature Communications*. doi: 10.1038/s41467-018-05922-x.

Lee, M. J., Palmer, D. J. and Warren, M. J. (2019) 'Biotechnological Advances in Bacterial Microcompartment Technology', *Trends in Biotechnology*. doi: 10.1016/j.tibtech.2018.08.006.

Lefman, J. *et al.* (2004) 'Three-dimensional electron microscopic imaging of membrane invaginations in *Escherichia coli* overproducing the chemotaxis receptor Tsr', *Journal of Bacteriology*. doi: 10.1128/JB.186.15.5052-5061.2004.

Lenz, L. L., Dere, B. and Bevan, M. J. (1996) 'Identification of an H2-M3-Restricted *listeria* epitope: Implications for antigen presentation by M3', *Immunity*. doi: 10.1016/S1074-7613(00)80310-6.

Lerouge, I. and Vanderleyden, J. (2002) 'O-antigen structural variation: Mechanisms and possible roles in animal/plant-microbe interactions', *FEMS Microbiology Reviews*. doi: 10.1016/S0168-6445(01)00070-5.

Levine, M. M. *et al.* (2007) 'Clinical trials of *Shigella* vaccines: Two steps forward and one step back on a long, hard road', *Nature Reviews Microbiology*. doi: 10.1038/nrmicro1662.

Van Der Ley, P. *et al.* (2001) 'Modification of lipid A biosynthesis in *Neisseria meningitidis* lpxL mutants: Influence on lipopolysaccharide structure, toxicity, and adjuvant activity', *Infection and Immunity*. doi: 10.1128/IAI.69.10.5981-5990.2001.

Lin, T. Y. and Weibel, D. B. (2016) 'Organization and function of anionic phospholipids in bacteria', *Applied Microbiology and Biotechnology*. doi: 10.1007/s00253-016-7468-x.

Lin, Y. H. and Machner, M. P. (2017) 'Exploitation of the host cell ubiquitin machinery by microbial effector proteins', *Journal of Cell Science*. doi: 10.1242/jcs.188482.

Lindsay, M. R. *et al.* (2001) 'Cell compartmentalisation in planctomycetes: Novel types of structural organisation for the bacterial cell', *Archives of Microbiology*. doi: 10.1007/s002030100280.

Lindsay, M. R., Webb, R. I. and Fuerst, J. A. (1997) 'Pirellulosomes: A new type of membrane-bounded cell compartment in planctomycete bacteria of the genus *Pirellula*', *Microbiology*. doi: 10.1099/00221287-143-3-739.

Liu, D. (2019) '*Escherichia coli*', in *Encyclopedia of Microbiology*. doi: 10.1016/B978-0-12-801238-3.02291-1.

Loeppke, R. *et al.* (2008) 'The impact of an integrated population health enhancement and disease management program on employee health risk, health conditions, and productivity', *Population Health Management*. doi: 10.1089/pop.2008.0006.

Lohße, A. *et al.* (2014) 'Genetic dissection of the *mamAB* and *mms6* operons reveals a gene set essential for magnetosome biogenesis in *magnetospirillum gryphiswaldense*', *Journal of Bacteriology*. doi: 10.1128/JB.01716-14.

Lopes, A., Vandermeulen, G. and Pr eat, V. (2019) 'Cancer DNA vaccines: current preclinical and clinical developments and future perspectives', *Journal of Experimental and Clinical Cancer*

Research. doi: 10.1186/s13046-019-1154-7.

Louie, K., Chen, Y. C. and Dowhan, W. (1986) 'Substrate-induced membrane association of phosphatidylserine synthase from *Escherichia coli*', *Journal of Bacteriology*. doi: 10.1128/jb.165.3.805-812.1986.

Lycklama A Nijeholt, J. A. and Driessen, A. J. M. (2012) 'The bacterial Sec-translocase: structure and mechanism', *Philosophical transactions of the Royal Society of London. Series B, Biological sciences*, 367(1592), pp. 1016–1028. doi: 10.1098/rstb.2011.0201.

Madigan, M. *et al.* (2008) 'Brock Biology of microorganisms 12th edn', *Int. Microbiol.* doi: 10.2436/im.v11i1.9650.

Makrides, S. C. (1996) 'Strategies for achieving high-level expression of genes in *Escherichia coli*', *Microbiological Reviews*. doi: 10.1128/mmbr.60.3.512-538.1996.

Manini, I. *et al.* (2015) 'Flucelvax (Optaflu) for seasonal influenza', *Expert Review of Vaccines*. doi: 10.1586/14760584.2015.1039520.

Martinon, F. *et al.* (1993) 'Induction of virus-specific cytotoxic T lymphocytes in vivo by liposome-entrapped mRNA', *European Journal of Immunology*. doi: 10.1002/eji.1830230749.

Mashburn, L. M. and Whiteley, M. (2005) 'Membrane vesicles traffic signals and facilitate group activities in a prokaryote', *Nature*. doi: 10.1038/nature03925.

Mathieu, K. *et al.* (2019) 'Functionality of membrane proteins overexpressed and purified from *E. coli* is highly dependent upon the strain', *Scientific Reports*. doi: 10.1038/s41598-019-39382-0.

Matsuyama -i, S., Tajima, T. and Tokuda, H. (1995) 'A novel periplasmic carried protein involved in the sorting and transport of *Escherichia coli* lipoproteins destined for the outer membrane', *EMBO Journal*. doi: 10.1002/j.1460-2075.1995.tb07342.x.

Matsuyama, S. I., Yokota, N. and Tokuda, H. (1997) 'A novel outer membrane lipoprotein, LolB (HemM), involved in the LolA (p20)-dependent localization of lipoproteins to the outer membrane of *Escherichia coli*', *EMBO Journal*. doi: 10.1093/emboj/16.23.6947.

McConnell, M. J. *et al.* (2011) 'Outer membrane vesicles as an acellular vaccine against *Acinetobacter baumannii*', *Vaccine*. doi: 10.1016/j.vaccine.2011.06.001.

McGoldrick, H. M. *et al.* (2005) 'Identification and characterization of a novel vitamin B12 (cobalamin) biosynthetic enzyme (CobZ) from *Rhodobacter capsulatus*, containing flavin, heme, and Fe-S cofactors', *Journal of Biological Chemistry*. doi: 10.1074/jbc.M411884200.

Medina, R. A. *et al.* (2013) 'Glycosylations in the globular head of the hemagglutinin protein modulate the virulence and antigenic properties of the H1N1 influenza viruses', *Science Translational Medicine*. doi: 10.1126/scitranslmed.3005996.

Mena, J. A. and Kamen, A. A. (2011) 'Insect cell technology is a versatile and robust vaccine manufacturing platform', *Expert Review of Vaccines*. doi: 10.1586/erv.11.24.

Metzger, L. E. 4th and Raetz, C. R. H. (2009) 'Purification and characterization of the lipid A disaccharide synthase (LpxB) from *Escherichia coli*, a peripheral membrane protein.', *Biochemistry*, 48(48), pp. 11559–11571. doi: 10.1021/bi901750f.

von Meyenburg, K., Jørgensen, B. B. and van Deurs, B. (1984) 'Physiological and morphological effects of overproduction of membrane-bound ATP synthase in *Escherichia coli* K-12.', *The EMBO journal*, 3(8), pp. 1791–1797.

MHRA (2021) 'MHRA issues new advice, concluding a possible link between COVID-19 Vaccine AstraZeneca and extremely rare, unlikely to occur blood clots'. Available at: <https://www.gov.uk/government/news/mhra-issues-new-advice-concluding-a-possible-link->

between-covid-19-vaccine-astrazeneca-and-extremely-rare-unlikely-to-occur-blood-clots.

Mileykovskaya, E. and Dowhan, W. (2000) 'Visualization of phospholipid domains in *Escherichia coli* by using the cardiolipin-specific fluorescent dye 10-N-nonyl acridine orange', *Journal of Bacteriology*. doi: 10.1128/JB.182.4.1172-1175.2000.

Mileykovskaya, E. and Dowhan, W. (2009) 'Cardiolipin membrane domains in prokaryotes and eukaryotes', *Biochimica et Biophysica Acta - Biomembranes*. doi: 10.1016/j.bbamem.2009.04.003.

Milligan, G. N. and Barrett, A. D. T. (2014) *Vaccinology: An Essential Guide*, *Vaccinology: An Essential Guide*. doi: 10.1002/9781118638033.

Molinaro, A. *et al.* (2015) 'Chemistry of lipid a: At the heart of innate immunity', *Chemistry - A European Journal*. doi: 10.1002/chem.201403923.

Molloy, M. P. *et al.* (2000) 'Proteomic analysis of the *Escherichia coli* outer membrane', *European Journal of Biochemistry*. doi: 10.1046/j.1432-1327.2000.01296.x.

Moraes, I. and Quigley, A. (2021) 'Structural Biology and Structure–Function Relationships of Membrane Proteins', *Biology*. doi: 10.3390/biology10030245.

Muñoz-Gómez, S. A. *et al.* (2017) 'The origin of mitochondrial cristae from alphaproteobacteria', *Molecular Biology and Evolution*. doi: 10.1093/molbev/msw298.

Murat, D. *et al.* (2010) 'Comprehensive genetic dissection of the magnetosome gene island reveals the step-wise assembly of a prokaryotic organelle', *Proceedings of the National Academy of Sciences of the United States of America*. doi: 10.1073/pnas.0914439107.

Nabel, G. J. (2013) 'Designing Tomorrow's Vaccines', *New England Journal of Medicine*. doi: 10.1056/nejmra1204186.

Van Niftrik, L. A. *et al.* (2004) 'The anammoxosome: An intracytoplasmic compartment in anammox bacteria', *FEMS Microbiology Letters*. doi: 10.1016/j.femsle.2004.01.044.

Norheim, G. *et al.* (2012) 'An outer membrane vesicle vaccine for prevention of serogroup A and W-135 meningococcal disease in the African meningitis belt', *Scandinavian Journal of Immunology*. doi: 10.1111/j.1365-3083.2012.02709.x.

Nudelman, H. and Zarivach, R. (2014) 'Structure prediction of magnetosome-associated proteins', *Frontiers in Microbiology*. doi: 10.3389/fmicb.2014.00009.

Nunes, S. F. *et al.* (2014) 'A Synthetic Biology Approach for a Vaccine Platform against Known and Newly Emerging Serotypes of Bluetongue Virus', *Journal of Virology*. doi: 10.1128/jvi.02183-14.

Nyström, T. (2004) 'Stationary-phase physiology.', *Annual review of microbiology*, 58, pp. 161–181. doi: 10.1146/annurev.micro.58.030603.123818.

Okuda, S. and Tokuda, H. (2011) 'Lipoprotein sorting in bacteria', *Annual Review of Microbiology*. doi: 10.1146/annurev-micro-090110-102859.

Oliveira, T. L. *et al.* (2018) 'LemA and Erp Y-like recombinant proteins from *Leptospira interrogans* protect hamsters from challenge using AddaVax™ as adjuvant', *Vaccine*. doi: 10.1016/j.vaccine.2018.03.078.

Oliveira, T. L. *et al.* (2020) 'DNA nanovaccines prepared using LemA antigen protect Golden Syrian hamsters against *Leptospira* lethal infection', *Memorias do Instituto Oswaldo Cruz*. doi: 10.1590/0074-02760190396.

Orskov, F. and Orskov, I. (1992) '*Escherichia coli* serotyping and disease in man and animals', in *Canadian Journal of Microbiology*. doi: 10.1139/m92-115.

- Pace, D. and Pollard, A. J. (2012) 'Meningococcal disease: Clinical presentation and sequelae', *Vaccine*. doi: 10.1016/j.vaccine.2011.12.062.
- Palacios Cruz, M. *et al.* (2021) 'COVID-19, a worldwide public health emergency', *Revista Clinica Espanola*. doi: 10.1016/j.rce.2020.03.001.
- Palsdottir, H. and Hunte, C. (2004) 'Lipids in membrane protein structures', *Biochimica et Biophysica Acta - Biomembranes*. doi: 10.1016/j.bbamem.2004.06.012.
- Papanastasiou, M. *et al.* (2013) 'The *Escherichia coli* peripheral inner membrane proteome', *Molecular and Cellular Proteomics*. doi: 10.1074/mcp.M112.024711.
- Pardee, A. B., Schachman, H. K. and Stanier, R. Y. (1952) 'Chromatophores of *rhodospirillum rubrum*', *Nature*. doi: 10.1038/169282a0.
- Pardi, N. *et al.* (2018) 'Nucleoside-modified mRNA vaccines induce potent T follicular helper and germinal center B cell responses', *Journal of Experimental Medicine*. doi: 10.1084/jem.20171450.
- Parker, H. *et al.* (2010) 'Uptake of *Helicobacter pylori* outer membrane vesicles by gastric epithelial cells', *Infection and Immunity*. doi: 10.1128/IAI.00299-10.
- Peetermans, J. (1992) 'Production, quality control and characterization of an inactivated hepatitis A vaccine', *Vaccine*. doi: 10.1016/0264-410X(92)90557-Z.
- Petriman, N. A. *et al.* (2018) 'The interaction network of the YidC insertase with the SecYEG translocon, SRP and the SRP receptor FtsY', *Scientific Reports*. doi: 10.1038/s41598-017-19019-w.
- Pinos, S. *et al.* (2016) 'Compartmentalization in PVC superphylum: Evolution and impact', *Biology Direct*. doi: 10.1186/S13062-016-0144-3.
- Pirofski, L. A. and Casadevall, A. (1998) 'Use of licensed vaccines for active immunization of the immunocompromised host', *Clinical Microbiology Reviews*. doi: 10.1128/cmr.11.1.1.
- Pliaka, V., Kyriakopoulou, Z. and Markoulatos, P. (2012) 'Risks associated with the use of live-attenuated vaccine poliovirus strains and the strategies for control and eradication of paralytic poliomyelitis', *Expert Review of Vaccines*. doi: 10.1586/erv.12.28.
- Plotkin, S. *et al.* (2017) 'The complexity and cost of vaccine manufacturing – An overview', *Vaccine*. doi: 10.1016/j.vaccine.2017.06.003.
- van der Pol, L., Stork, M. and van der Ley, P. (2015) 'Outer membrane vesicles as platform vaccine technology', *Biotechnology Journal*. doi: 10.1002/biot.201400395.
- Polack, F. P. *et al.* (2020) 'Safety and Efficacy of the BNT162b2 mRNA Covid-19 Vaccine', *New England Journal of Medicine*. doi: 10.1056/nejmoa2034577.
- Price, G. D., Coleman, J. R. and Badger, M. R. (1992) 'Association of carbonic anhydrase activity with carboxysomes isolated from the cyanobacterium *Synechococcus* PCC7942', *Plant Physiology*. doi: 10.1104/pp.100.2.784.
- Price, N. L. *et al.* (2016) 'Glycoengineered Outer Membrane Vesicles: A Novel Platform for Bacterial Vaccines', *Scientific Reports*. doi: 10.1038/srep24931.
- Price, N. L. and Raivio, T. L. (2009) 'Characterization of the Cpx regulon in *Escherichia coli* strain MC4100', *Journal of Bacteriology*. doi: 10.1128/JB.00798-08.
- Probst, J. *et al.* (2006) 'Characterization of the ribonuclease activity on the skin surface', *Genetic Vaccines and Therapy*. doi: 10.1186/1479-0556-4-4.
- Pupo, E. *et al.* (2014) 'Lipopolysaccharide engineering in *Neisseria meningitidis*: Structural analysis of different pentaacyl lipid mutants and comparison of their modified agonist properties',

- Journal of Biological Chemistry*. doi: 10.1074/jbc.M114.554345.
- Que, Y. A. and Moreillon, P. (2014) 'Staphylococcus aureus (Including Staphylococcal Toxic Shock Syndrome)', in *Mandell, Douglas, and Bennett's Principles and Practice of Infectious Diseases*. doi: 10.1016/B978-1-4557-4801-3.00196-X.
- Raetz, C. R. H. *et al.* (2009) 'Discovery of new biosynthetic pathways: The lipid A story', *Journal of Lipid Research*. doi: 10.1194/jlr.R800060-JLR200.
- Raetz, C. R. H. and Dowhan, W. (1990) 'Biosynthesis and function of phospholipids in *Escherichia coli*', *Journal of Biological Chemistry*. doi: 10.1016/S0021-9258(19)40001-X.
- Raetz, C. R. H. and Whitfield, C. (2002) 'Lipopolysaccharide endotoxins', *Annual Review of Biochemistry*. doi: 10.1146/annurev.biochem.71.110601.135414.
- Rahn-Lee, L. *et al.* (2015) 'A Genetic Strategy for Probing the Functional Diversity of Magnetosome Formation', *PLoS Genetics*. doi: 10.1371/journal.pgen.1004811.
- Raivio, T. L., Leblanc, S. K. D. and Price, N. L. (2013) 'The *Escherichia coli* Cpx envelope stress response regulates genes of diverse function that impact antibiotic resistance and membrane integrity', *Journal of Bacteriology*. doi: 10.1128/JB.00105-13.
- Rajaram, S. *et al.* (2020) 'Influenza vaccines: the potential benefits of cell-culture isolation and manufacturing', *Therapeutic Advances in Vaccines and Immunotherapy*. doi: 10.1177/2515135520908121.
- Rappazzo, C. G. *et al.* (2016) 'Recombinant M2e outer membrane vesicle vaccines protect against lethal influenza A challenge in BALB/c mice', *Vaccine*. doi: 10.1016/j.vaccine.2016.01.028.
- Raschdorf, O. *et al.* (2016) 'Genetic and Ultrastructural Analysis Reveals the Key Players and Initial Steps of Bacterial Magnetosome Membrane Biogenesis', *PLoS Genetics*. doi: 10.1371/journal.pgen.1006101.
- Renner, L. D. and Weibel, D. B. (2011) 'Cardiolipin microdomains localize to negatively curved regions of *Escherichia coli* membranes', *Proceedings of the National Academy of Sciences of the United States of America*. doi: 10.1073/pnas.1015757108.
- Rizzitello, A. E., Harper, J. R. and Silhavy, T. J. (2001) 'Genetic evidence for parallel pathways of chaperone activity in the periplasm of *Escherichia coli*', *Journal of Bacteriology*. doi: 10.1128/JB.183.23.6794-6800.2001.
- Roberts, R. *et al.* (2008) 'Outer membrane vesicles as acellular vaccine against *pertussis*', *Vaccine*. doi: 10.1016/j.vaccine.2008.07.004.
- Roier, S. *et al.* (2016) 'A novel mechanism for the biogenesis of outer membrane vesicles in Gram-negative bacteria', *Nature Communications*. doi: 10.1038/ncomms10515.
- Rowlett, V. W. *et al.* (2017) 'The impact of membrane phospholipid alterations in *Escherichia coli* on cellular function', *Journal of Bacteriology*.
- Royes, J. *et al.* (2020) 'Inducible intracellular membranes: Molecular aspects and emerging applications', *Microbial Cell Factories*. doi: 10.1186/s12934-020-01433-x.
- Rubio, A. P. and Eiros, J. M. (2018) 'Cell culture-derived flu vaccine: Present and future', *Human Vaccines and Immunotherapeutics*. doi: 10.1080/21645515.2018.1460297.
- Sacchi, C. T. *et al.* (2000) 'Diversity and prevalence of PorA types in *Neisseria meningitidis* serogroup B in the United States, 1992-1998', *Journal of Infectious Diseases*. doi: 10.1086/315833.
- Sadarangani, M. and Pollard, A. J. (2010) 'Serogroup B meningococcal vaccines-an unfinished story', *The Lancet Infectious Diseases*. doi: 10.1016/S1473-3099(09)70324-X.

- Sankaran, K. and Wu, H. C. (1994) 'Lipid modification of bacterial prolipoprotein. Transfer of diacylglyceryl moiety from phosphatidylglycerol', *Journal of Biological Chemistry*. doi: 10.1016/S0021-9258(17)32077-X.
- Scheel, B. *et al.* (2005) 'Toll-like receptor-dependent activation of several human blood cell types by protamine-condensed mRNA', *European Journal of Immunology*. doi: 10.1002/eji.200425656.
- Schlame, M. *et al.* (1991) 'Molecular species of cardiolipin in relation to other mitochondrial phospholipids: Is there an acyl specificity of the interaction between cardiolipin and the ADP/ATP carrier?', *European Journal of Biochemistry*. doi: 10.1111/j.1432-1033.1991.tb16144.x.
- Schüler, D. (2008) 'Genetics and cell biology of magnetosome formation in magnetotactic bacteria', *FEMS Microbiology Reviews*, 32(4), pp. 654–672. doi: 10.1111/j.1574-6976.2008.00116.x.
- Sezonov, G., Joseleau-Petit, D. and D'Ari, R. (2007) '*Escherichia coli* physiology in Luria-Bertani broth.', *Journal of bacteriology*, 189(23), pp. 8746–8749. doi: 10.1128/JB.01368-07.
- Sharma, O. *et al.* (2020) 'A Review of the Progress and Challenges of Developing a Vaccine for COVID-19', *Frontiers in Immunology*, p. 2413. Available at: <https://www.frontiersin.org/article/10.3389/fimmu.2020.585354>.
- Shively, J. M. *et al.* (1973) 'Functional organelles in prokaryotes: Polyhedral inclusions (carboxysomes) of *Thiobacillus neapolitanus*', *Science*. doi: 10.1126/science.182.4112.584.
- Sierra, G. V. G. *et al.* (1991) 'Vaccine against group B *Neisseria meningitidis*: Protection trial and mass vaccination results in Cuba', in *NIPH Annals*.
- Silhavy, T. J., Kahne, D. and Walker, S. (2010) 'The bacterial cell envelope.', *Cold Spring Harbor perspectives in biology*. doi: 10.1101/cshperspect.a000414.
- Singh, A. *et al.* (2015) 'Protein recovery from inclusion bodies of *Escherichia coli* using mild solubilization process', *Microbial Cell Factories*. doi: 10.1186/s12934-015-0222-8.
- Sinninghe Damsté, J. S. *et al.* (2002) 'Linearly concatenated cyclobutane lipids form a dense bacterial membrane', *Nature*. doi: 10.1038/nature01128.
- Sklar, J. G. *et al.* (2007) 'Lipoprotein SmpA is a component of the YaeT complex that assembles outer membrane proteins in *Escherichia coli*', *Proceedings of the National Academy of Sciences of the United States of America*. doi: 10.1073/pnas.0701579104.
- Small, E. J. *et al.* (2000) 'Immunotherapy of hormone-refractory prostate cancer with antigen-loaded dendritic cells', *Journal of Clinical Oncology*. doi: 10.1200/JCO.2000.18.23.3894.
- Sohrabi, C. *et al.* (2020) 'World Health Organization declares global emergency: A review of the 2019 novel coronavirus (COVID-19)', *International Journal of Surgery*. doi: 10.1016/j.ijssu.2020.02.034.
- Steinhauer, D. A., Domingo, E. and Holland, J. J. (1992) 'Lack of evidence for proofreading mechanisms associated with an RNA virus polymerase', *Gene*. doi: 10.1016/0378-1119(92)90216-C.
- Stevens, R. C. (2000) 'Design of high-throughput methods of protein production for structural biology', *Structure*. doi: 10.1016/S0969-2126(00)00193-3.
- Stevenson, T. C. *et al.* (2018) 'Immunization with outer membrane vesicles displaying conserved surface polysaccharide antigen elicits broadly antimicrobial antibodies', *Proceedings of the National Academy of Sciences of the United States of America*. doi: 10.1073/pnas.1718341115.
- Stock, J. B., Rauch, B. and Roseman, S. (1977) 'Periplasmic space in *Salmonella typhimurium* and *Escherichia coli*', *Journal of Biological Chemistry*. doi: 10.1016/S0021-9258(17)41044-1.

- Stoeger, T., Battich, N. and Pelkmans, L. (2016) 'Passive Noise Filtering by Cellular Compartmentalization', *Cell*. doi: 10.1016/j.cell.2016.02.005.
- Succi, R. C. D. M. and Farhat, C. K. (2006) 'Vaccination in special situations', *Jornal de Pediatria*. doi: 10.2223/JPED.1474.
- Takeda, K. *et al.* (2003) 'Crystal structures of bacterial lipoprotein localization factors, LolA and LolB', *EMBO Journal*. doi: 10.1093/emboj/cdg324.
- Tang, D. C., Devit, M. and Johnston, S. A. (1992) 'Genetic immunization is a simple method for eliciting an immune response', *Nature*. doi: 10.1038/356152a0.
- Tappero, J. W. *et al.* (1999) 'Immunogenicity of 2 serogroup B outer-membrane protein meningococcal vaccines: A randomized controlled trial in Chile', *Journal of the American Medical Association*. doi: 10.1001/jama.281.16.1520.
- Teissié, J. and Zerbib, D. (2018) 'Eradication of bacteria via electropulsion', in *Encyclopedia of Interfacial Chemistry: Surface Science and Electrochemistry*. doi: 10.1016/B978-0-12-409547-2.13455-9.
- Tokunaga, M., Tokunaga, H. and Wu, H. C. (1982) 'Post-translational modification and processing of *Escherichia coli* prolipoprotein in vitro', *Proceedings of the National Academy of Sciences of the United States of America*. doi: 10.1073/pnas.79.7.2255.
- Tripathi, N. K. and Shrivastava, A. (2019) 'Recent Developments in Bioprocessing of Recombinant Proteins: Expression Hosts and Process Development', *Frontiers in Bioengineering and Biotechnology*. doi: 10.3389/fbioe.2019.00420.
- Tsai, Y. *et al.* (2007) 'Structural analysis of CsoS1A and the protein shell of the *Halothiobacillus neapolitanus* carboxysome', *PLoS Biology*, 5(6), pp. 1345–1354. doi: 10.1371/journal.pbio.0050144.
- Tsui, N. B. Y., Ng, E. K. O. and Lo, Y. M. D. (2002) 'Stability of endogenous and added RNA in blood specimens, serum, and plasma', *Clinical Chemistry*. doi: 10.1093/clinchem/48.10.1647.
- Turnbull, L. *et al.* (2016) 'Explosive cell lysis as a mechanism for the biogenesis of bacterial membrane vesicles and biofilms', *Nature Communications*. doi: 10.1038/ncomms11220.
- Uebe, R. *et al.* (2011) 'The cation diffusion facilitator proteins MamB and MamM of *Magnetospirillum gryphiswaldense* have distinct and complex functions, and are involved in magnetite biomineralization and magnetosome membrane assembly', *Molecular Microbiology*. doi: 10.1111/j.1365-2958.2011.07863.x.
- Ullrich, S. *et al.* (2005) 'A hypervariable 130-kilobase genomic region of *Magnetospirillum gryphiswaldense* comprises a magnetosome island which undergoes frequent rearrangements during stationary growth', *Journal of Bacteriology*. doi: 10.1128/JB.187.21.7176-7184.2005.
- United States Food and Drug Administration (2011) *Guidance for industry: General principles for the development of vaccines to protect against global infectious diseases*. Available at: <https://www.fda.gov/media/82306/download>.
- Vollmer, W. and Höltje, J. V. (2001) 'Morphogenesis of *Escherichia coli*', *Current Opinion in Microbiology*. doi: 10.1016/S1369-5274(01)00261-2.
- Voorhout, W. *et al.* (1988) 'Accumulation of LamB-LacZ hybrid proteins in intracytoplasmic membrane-like structures in *Escherichia coli* K12.', *Journal of general microbiology*. doi: 10.1099/00221287-134-3-599.
- Vries, R. D. and Rimmelzwaan, G. F. (2016) 'Viral vector-based influenza vaccines', *Human Vaccines and Immunotherapeutics*. doi: 10.1080/21645515.2016.1210729.

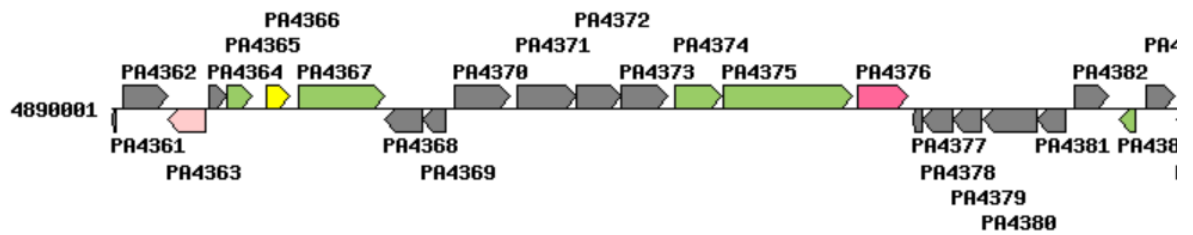
- Wang, Z. *et al.* (2018) 'Comparison of in vitro and in vivo oligomeric states of a wild type and mutant trimeric inner membrane multidrug transporter.', *Biochemistry and biophysics reports*, 16, pp. 122–129. doi: 10.1016/j.bbrep.2018.10.006.
- Wang, Z. *et al.* (2021) 'mRNA vaccine-elicited antibodies to SARS-CoV-2 and circulating variants 2 3', *bioRxiv*.
- Waterbeemd, B. *et al.* (2010) 'Improved OMV vaccine against *Neisseria meningitidis* using genetically engineered strains and a detergent-free purification process', *Vaccine*. doi: 10.1016/j.vaccine.2010.04.082.
- Van De Waterbeemd, B. *et al.* (2013) 'Quantitative proteomics reveals distinct differences in the protein content of outer membrane vesicle vaccines', *Journal of Proteome Research*. doi: 10.1021/pr301208g.
- Watson, D. S., Endsley, A. N. and Huang, L. (2012) 'Design considerations for liposomal vaccines: Influence of formulation parameters on antibody and cell-mediated immune responses to liposome associated antigens', *Vaccine*. doi: 10.1016/j.vaccine.2012.01.070.
- Webb, C. T., Heinz, E. and Lithgow, T. (2012) 'Evolution of the β -barrel assembly machinery', *Trends in Microbiology*. doi: 10.1016/j.tim.2012.08.006.
- Van Weeghel, R. P., Keck, W. and Robillard, G. T. (1990) 'Regulated high-level expression of the mannitol permease of the phosphoenolpyruvate-dependent sugar phosphotransferase system in *Escherichia coli*', *Proceedings of the National Academy of Sciences of the United States of America*. doi: 10.1073/pnas.87.7.2613.
- Wei, C. J. *et al.* (2010) 'Cross-neutralization of 1918 and 2009 influenza viruses: Role of glycans in viral evolution and vaccine design', *Science Translational Medicine*. doi: 10.1126/scitranslmed.3000799.
- Wei, C. J. *et al.* (2020) 'Next-generation influenza vaccines: opportunities and challenges', *Nature Reviews Drug Discovery*. doi: 10.1038/s41573-019-0056-x.
- Weiner, J. H. *et al.* (1984) 'Overproduction of fumarate reductase in *Escherichia coli* induces a novel intracellular lipid-protein organelle', *Journal of Bacteriology*. doi: 10.1128/jb.158.2.590-596.1984.
- WHO (2004) 'Guidelines on clinical evaluation of vaccines: regulatory expectations', *WHO Technical Report*.
- Wilkison, W. O. *et al.* (1986) 'Crystalline arrays of the *Escherichia coli* sn-glycerol-3-phosphate acyltransferase, an integral membrane protein', *Journal of Biological Chemistry*. doi: 10.1016/S0021-9258(18)67608-2.
- Wilkison, W. O. and Bell, R. M. (1997) 'sn-Glycerol-3-phosphate acyltransferase from *Escherichia coli*', *Biochimica et Biophysica Acta - Lipids and Lipid Metabolism*. doi: 10.1016/S0005-2760(97)00099-4.
- Wong, S. *et al.* (2007) 'New Zealand epidemic strain meningococcal B outer membrane vesicle vaccine in children aged 16-24 months', *Pediatric Infectious Disease Journal*. doi: 10.1097/01.inf.0000258697.05341.2c.
- World Health Organization (2007) 'A Description of the Process of Seasonal and H5N1 Influenza Vaccine Virus Selection and Development', *World Health Organization*.
- World Health Organization (WHO) (2012) 'WHO: Weekly epidemiological record Relevé épidémiologique hebdomadaire', *World Health organization Geneva*.
- Wørzner, K. *et al.* (2021) 'Adjuvanted SARS-CoV-2 spike protein elicits neutralizing antibodies and

- CD4 T cell responses after a single immunization in mice', *EBioMedicine*. doi: 10.1016/j.ebiom.2020.103197.
- Wu, X., Smith, T. G. and Rupprecht, C. E. (2011) 'From brain passage to cell adaptation: The road of human rabies vaccine development', *Expert Review of Vaccines*. doi: 10.1586/erv.11.140.
- Wyle, F. A. *et al.* (1972) 'Immunologic response of man to group b meningococcal polysaccharide vaccines', *Journal of Infectious Diseases*. doi: 10.1093/infdis/126.5.514.
- Xu, S. *et al.* (2020) 'mRNA Vaccine Era—Mechanisms, Drug Platform and Clinical Prospection1 Xu, S. *et al.* (2020) mRNA Vaccine Era—Mechanisms, Drug Platform and Clinical Prospection. *Int. J. Mol. Sci.* 21, 6582', *International Journal of Molecular Sciences*.
- Yakushi, T. *et al.* (1998) 'LolA-dependent release of a lipid-modified protein from the inner membrane of *Escherichia coli* requires nucleoside triphosphate', *Journal of Biological Chemistry*. doi: 10.1074/jbc.273.49.32576.
- Yakushi, T. *et al.* (2000) 'A new ABC transporter mediating the detachment of lipid-modified proteins from membranes', *Nature Cell Biology*. doi: 10.1038/35008635.
- Yamaguchi, K., Yu, F. and Inouye, M. (1988) 'A single amino acid determinant of the membrane localization of lipoproteins in *E. coli*', *Cell*. doi: 10.1016/0092-8674(88)90162-6.
- Yashroy, R. (1999) 'A structural model for virulence organellae of gram-negative organisms with reference to *Salmonella* pathogenicity in chicken ileum', *Indian Journal of Poultry Science*.
- Yeagle, P. L. (2011) 'Membrane proteins', in *The Structure of Biological Membranes: Third Edition*. doi: 10.1201/b15106-35.
- Yeates, T. O. *et al.* (2008) 'Protein-based organelles in bacteria: Carboxysomes and related microcompartments', *Nature Reviews Microbiology*. doi: 10.1038/nrmicro1913.
- Zak, E. *et al.* (2001) 'The initial steps of biogenesis of cyanobacterial photosystems occur in plasma membranes', *Proceedings of the National Academy of Sciences of the United States of America*. doi: 10.1073/pnas.241503898.
- Zariri, A. *et al.* (2016) 'Meningococcal outer membrane vesicle composition-dependent activation of the innate immune response', *Infection and Immunity*. doi: 10.1128/IAI.00635-16.
- Zhou, Z. *et al.* (1998) 'Function of *Escherichia coli* MsbA, an essential ABC family transporter, in lipid A and phospholipid biosynthesis', *Journal of Biological Chemistry*. doi: 10.1074/jbc.273.20.12466.
- Zollinger, W. D. *et al.* (1997) 'Bactericidal antibody responses of juvenile rhesus monkeys immunized with group B *Neisseria meningitidis* capsular polysaccharide-protein conjugate vaccines', *Infection and Immunity*. doi: 10.1128/iai.65.3.1053-1060.1997.

Supplementary data

Pseudomonas aeruginosa PA14

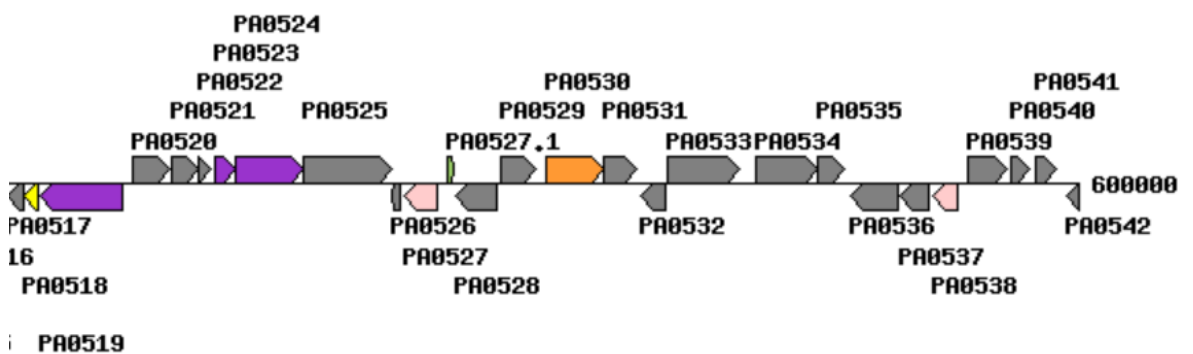
PA4369 (PaLemA1) – hypothetical protein; Pfam: LemA, DUF639



PA4368 - hypothetical protein; Pfam: GIDE, DUF1771, EF-hand_1, DUF5380

Supplementary Figure 1: PaLemA1 operon analysis in *Pseudomonas aeruginosa*

Pseudomonas aeruginosa PA14



PA0538 – Protein dithiol:quinone oxidoreductase; Pfam - DsbB

PA0537 (PaLemA2) – hypothetical protein; Pfam – LemA, PaRep2b

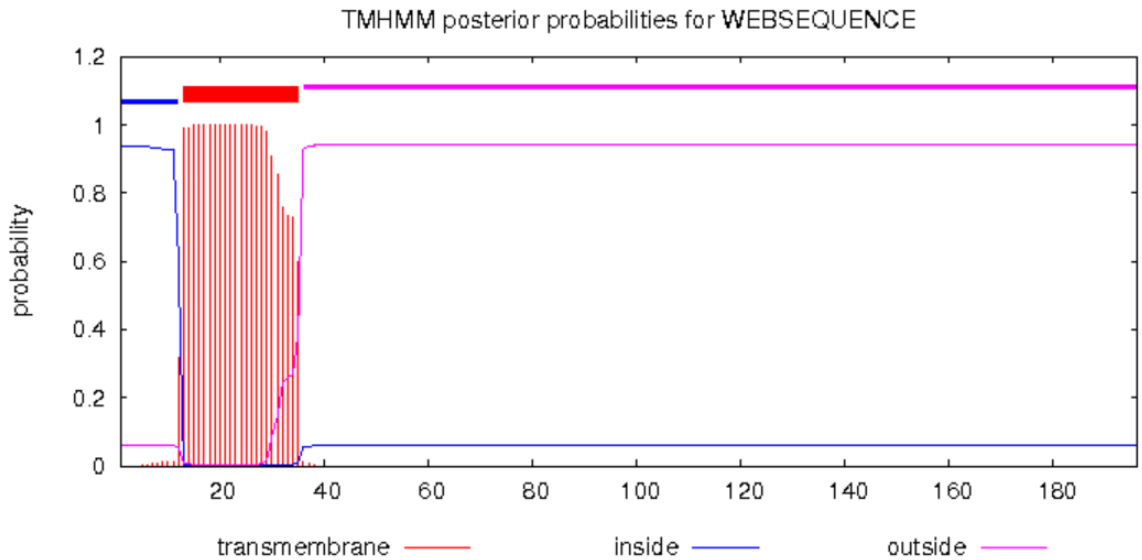
PA0536 – hypothetical protein, Pfam: TPM_phosphatase, MOLO1, BCL9

Supplementary figure 2: PaLemA2 operon analysis in *Pseudomonas aeruginosa*

LemA.153

```

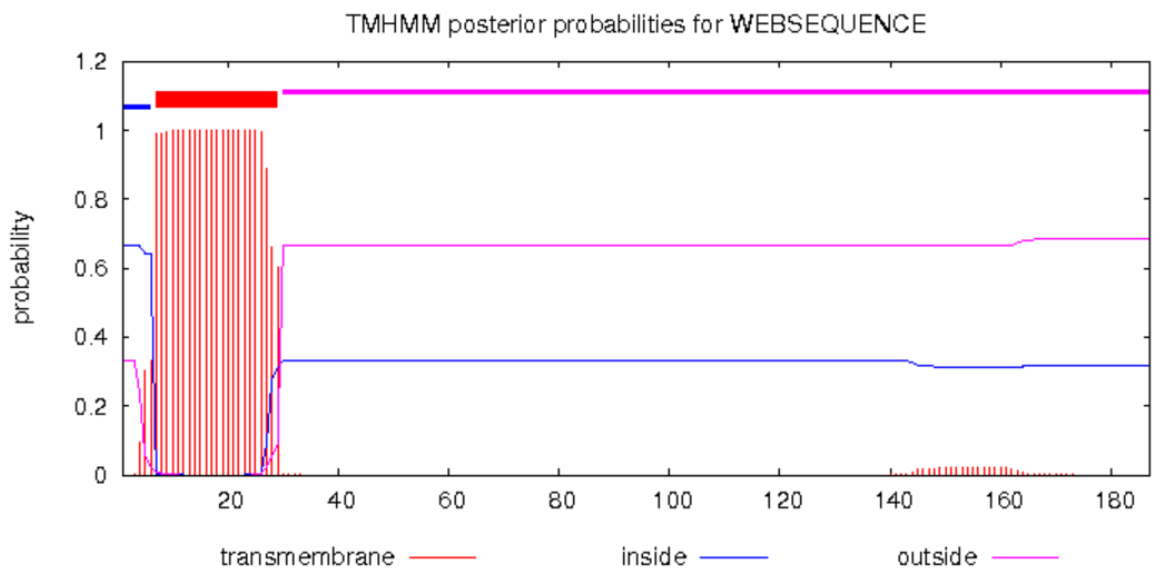
# WEBSEQUENCE Length: 196
# WEBSEQUENCE Number of predicted TMHs: 1
# WEBSEQUENCE Exp number of AAs in TMHs: 21.92126
# WEBSEQUENCE Exp number, first 60 AAs: 21.9209
# WEBSEQUENCE Total prob of N-in: 0.93974
# WEBSEQUENCE POSSIBLE N-term signal sequence
WEBSEQUENCE TMHMM2.0 inside 1 12
WEBSEQUENCE TMHMM2.0 TMhelix 13 35
WEBSEQUENCE TMHMM2.0 outside 36 196
  
```



LemA.159

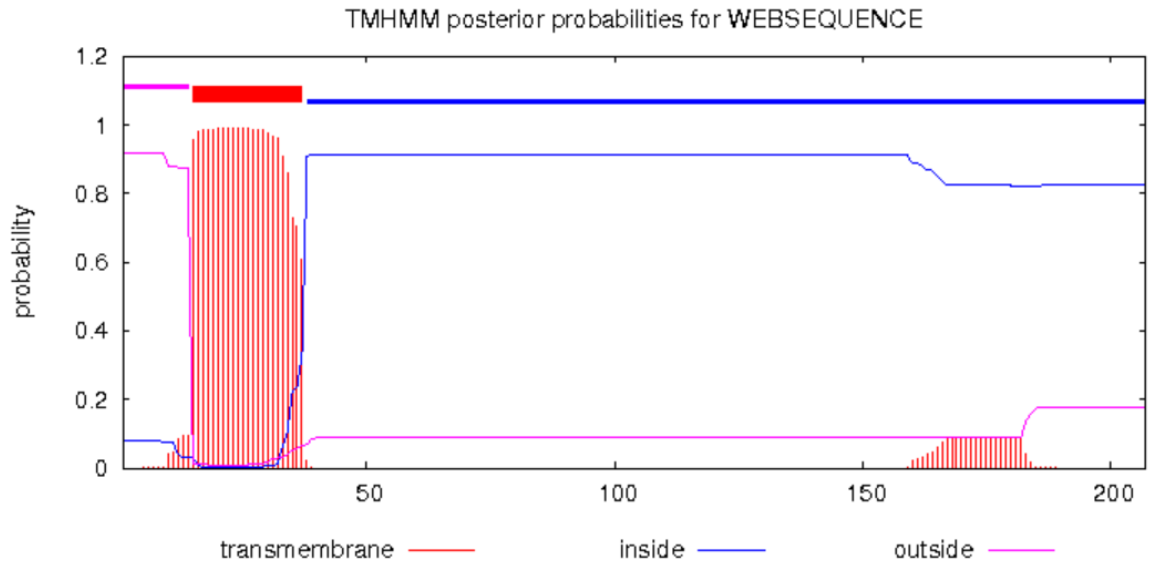
```

# WEBSEQUENCE Length: 187
# WEBSEQUENCE Number of predicted TMHs: 1
# WEBSEQUENCE Exp number of AAs in TMHs: 23.2524
# WEBSEQUENCE Exp number, first 60 AAs: 22.85936
# WEBSEQUENCE Total prob of N-in: 0.66670
# WEBSEQUENCE POSSIBLE N-term signal sequence
WEBSEQUENCE TMHMM2.0 inside 1 6
WEBSEQUENCE TMHMM2.0 TMhelix 7 29
WEBSEQUENCE TMHMM2.0 outside 30 187
  
```



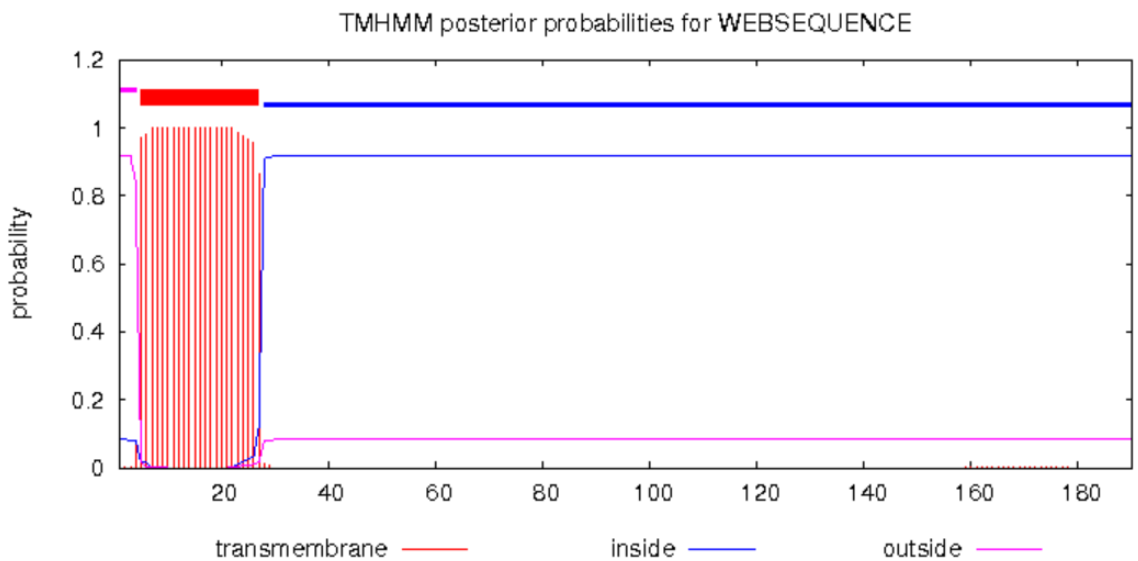
LemA.501

```
# WEBSEQUENCE Length: 207
# WEBSEQUENCE Number of predicted TMHs: 1
# WEBSEQUENCE Exp number of AAs in TMHs: 23.66027
# WEBSEQUENCE Exp number, first 60 AAs: 21.8819
# WEBSEQUENCE Total prob of N-in: 0.07981
# WEBSEQUENCE POSSIBLE N-term signal sequence
WEBSEQUENCE TMHMM2.0 outside 1 14
WEBSEQUENCE TMHMM2.0 TMhelix 15 37
WEBSEQUENCE TMHMM2.0 inside 38 207
```



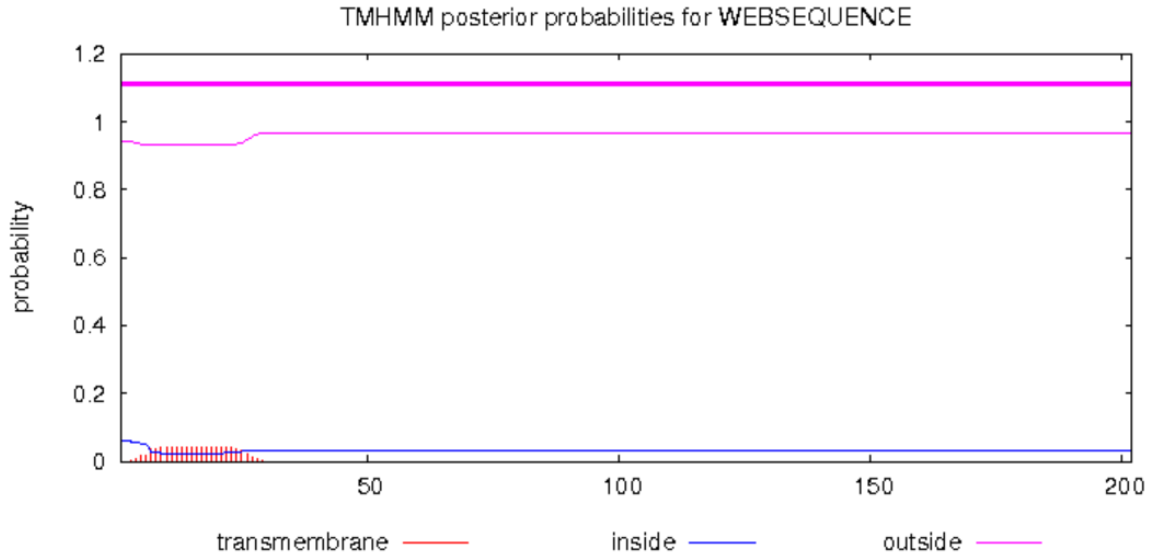
PaLemA1 (PA4369)

```
# WEBSEQUENCE Length: 190
# WEBSEQUENCE Number of predicted TMHs: 1
# WEBSEQUENCE Exp number of AAs in TMHs: 22.80852
# WEBSEQUENCE Exp number, first 60 AAs: 22.79531
# WEBSEQUENCE Total prob of N-in: 0.08361
# WEBSEQUENCE POSSIBLE N-term signal sequence
WEBSEQUENCE TMHMM2.0 outside 1 4
WEBSEQUENCE TMHMM2.0 TMhelix 5 27
WEBSEQUENCE TMHMM2.0 inside 28 190
```



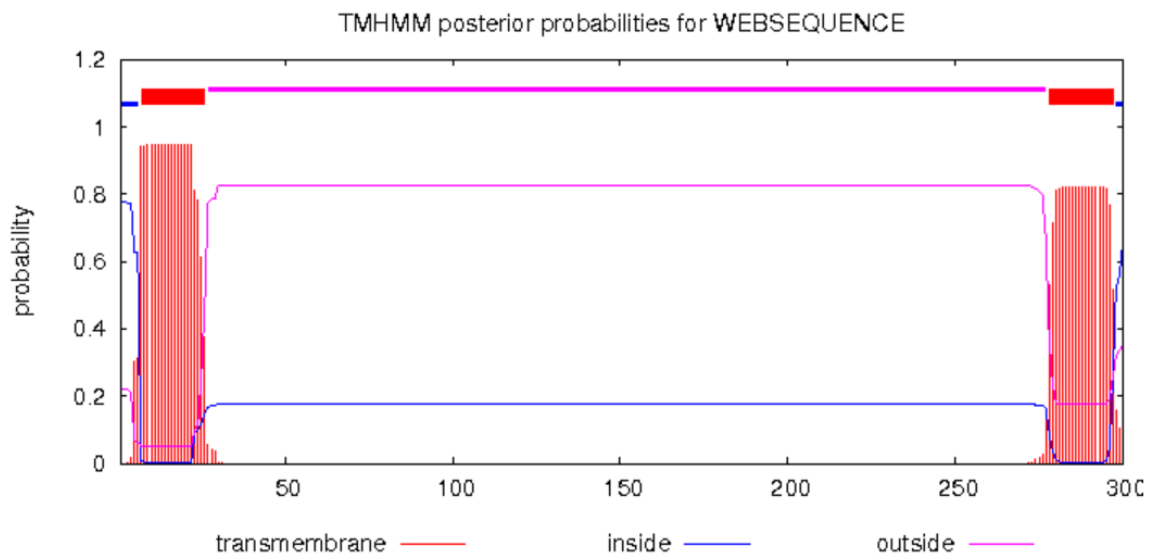
PaLemA2 (PA0537)

```
# WEBSEQUENCE Length: 202
# WEBSEQUENCE Number of predicted TMHs: 0
# WEBSEQUENCE Exp number of AAs in TMHs: 0.866970000000000001
# WEBSEQUENCE Exp number, first 60 AAs: 0.86508
# WEBSEQUENCE Total prob of N-in: 0.05877
WEBSEQUENCE TMHMM2.0 outside 1 202
```



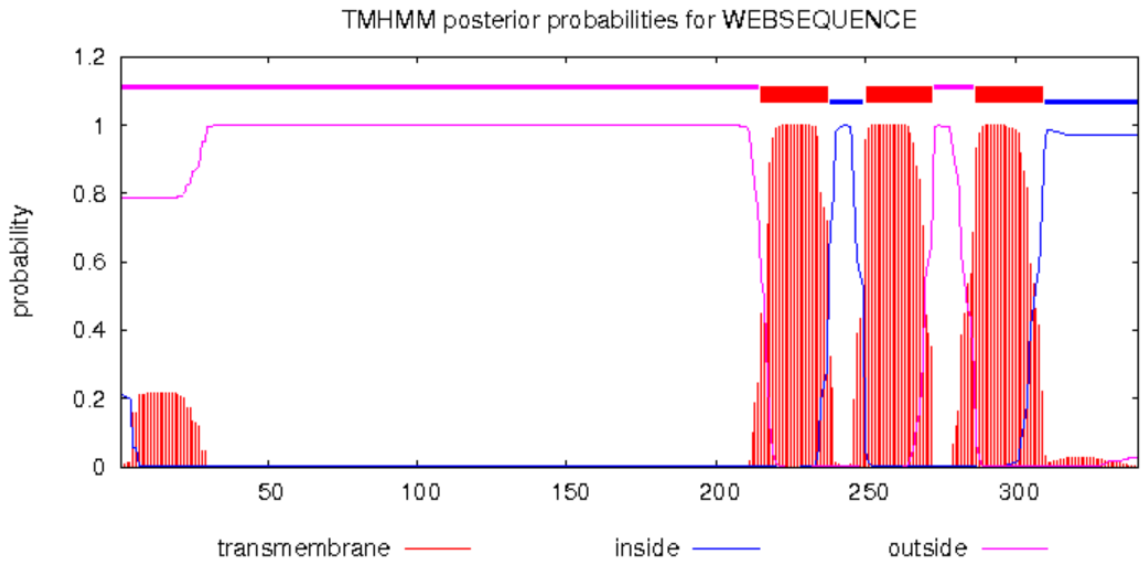
PA4368

```
# WEBSEQUENCE Length: 300
# WEBSEQUENCE Number of predicted TMHs: 2
# WEBSEQUENCE Exp number of AAs in TMHs: 34.60569
# WEBSEQUENCE Exp number, first 60 AAs: 18.49912
# WEBSEQUENCE Total prob of N-in: 0.77761
# WEBSEQUENCE POSSIBLE N-term signal sequence
WEBSEQUENCE TMHMM2.0 inside 1 6
WEBSEQUENCE TMHMM2.0 TMhelix 7 26
WEBSEQUENCE TMHMM2.0 outside 27 277
WEBSEQUENCE TMHMM2.0 TMhelix 278 297
WEBSEQUENCE TMHMM2.0 inside 298 300
```



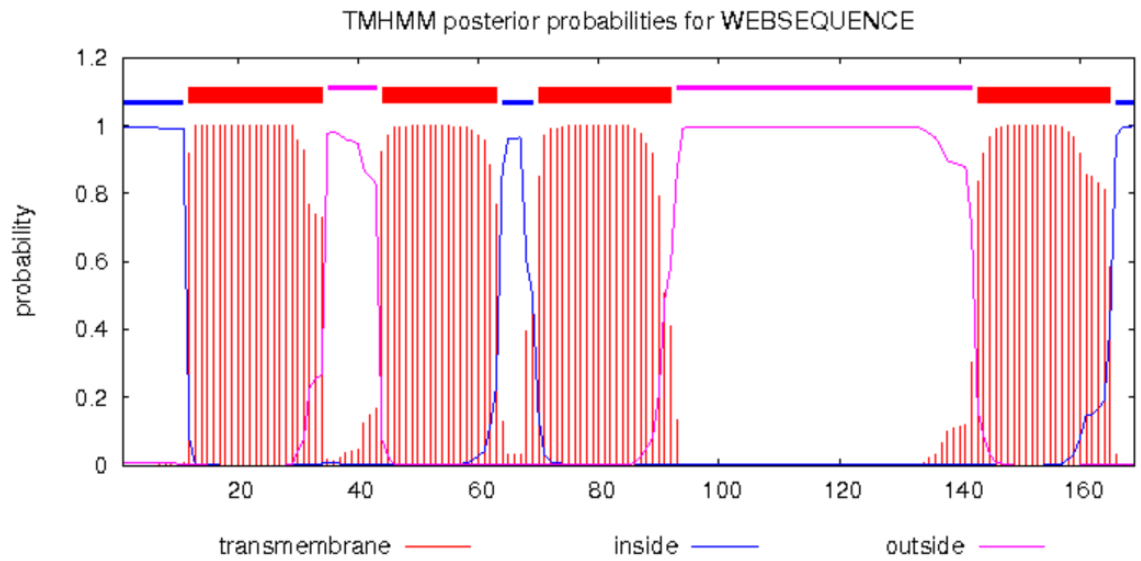
PA0536

```
# WEBSEQUENCE Length: 341
# WEBSEQUENCE Number of predicted TMHs: 3
# WEBSEQUENCE Exp number of AAs in TMHs: 71.57887
# WEBSEQUENCE Exp number, first 60 AAs: 4.55119
# WEBSEQUENCE Total prob of N-in: 0.21405
WEBSEQUENCE TMHMM2.0 outside 1 214
WEBSEQUENCE TMHMM2.0 TMhelix 215 237
WEBSEQUENCE TMHMM2.0 inside 238 249
WEBSEQUENCE TMHMM2.0 TMhelix 250 272
WEBSEQUENCE TMHMM2.0 outside 273 286
WEBSEQUENCE TMHMM2.0 TMhelix 287 309
WEBSEQUENCE TMHMM2.0 inside 310 341
```



PA0538

```
# WEBSEQUENCE Length: 169
# WEBSEQUENCE Number of predicted TMHs: 4
# WEBSEQUENCE Exp number of AAs in TMHs: 87.13432
# WEBSEQUENCE Exp number, first 60 AAs: 39.48645
# WEBSEQUENCE Total prob of N-in: 0.99406
# WEBSEQUENCE POSSIBLE N-term signal sequence
WEBSEQUENCE TMHMM2.0 inside 1 11
WEBSEQUENCE TMHMM2.0 TMhelix 12 34
WEBSEQUENCE TMHMM2.0 outside 35 43
WEBSEQUENCE TMHMM2.0 TMhelix 44 63
WEBSEQUENCE TMHMM2.0 inside 64 69
WEBSEQUENCE TMHMM2.0 TMhelix 70 92
WEBSEQUENCE TMHMM2.0 outside 93 142
WEBSEQUENCE TMHMM2.0 TMhelix 143 165
WEBSEQUENCE TMHMM2.0 inside 166 169
```



Supplementary Figure 3. TMHMM2 predictions for PaLemA1 and PaLemA2 operon proteins.

Cell	CTRL+ T0	CTRL+ T1	CTRL+ T2	CTRL+ T4	CTRL+ T6	CTRL+ T8
1	0	3	0	1	0	2
2	0	2	4	3	0	0
3	0	0	0	0	0	0
4	0	0	0	0	4	1
5	0	3	0	1	0	0
6	0	1	0	2	0	3
7	0	5	1	1	1	0
8	0	10	0	1	1	0
9	0	0	0	0	0	0
10	3	5	6	2	1	1
11	2	0	3	0	0	1
12	0	0	0	0	1	4
13	0	0	4	0	0	0
14	0	1	0	1	4	0
15	1	1	0	0	2	2
16	0	0	4	0	0	1
17	0	1	0	0	1	1
18	0	0	1	0	2	0
19	0	0	7	0	1	0
20	0	0	0	1	3	1
21	0	0	0	0	0	2
22	0	0	0	0	0	0
23	0	4	0	1	1	0
24	1	2	0	2	0	0
25	1	0	0	0	0	4
26	0	0	0	5	1	1
27	2	1	5	0	0	2
28	0	0	3	1	0	0
29	0	1	0	2	3	0
30	1	0	0	0	0	0
31	0	5	0	0	0	1
32	0	1	1	2	0	0
33	0	0	1	0	2	0
34	2	3	1	2	0	4
35	4	5	1	0	2	0
36	0	0	1	1	0	0
37	2	0	0	2	2	1
38	2	0	0	0	0	1
39	0	0	0	3	3	0
40	0	0	0	0	0	0
41	0	5	0	0	0	1
42	1	1	0	0	3	0
43	0	1	4	0	0	0
44	0	0	2	0	1	2
45	1	0	0	1	1	0
46	0	0	0	8	0	0
47	2	0	0	0	3	0
48	1	0	1	0	0	0
49	1	0	0	2	1	1

50	0	0	2	1	3	3
----	---	---	---	---	---	---

Supplementary Table 1. Vesicle counts performed on *E. coli* cells expressing an empty pET3a vector control.

Vesicle counts performed on *E. coli* BL21 (DE3) Star cells expressing an empty vector control over a time course of 8 hours. T0 represents the cells just prior to induction, while T1, T2, T4, T6 and T8 refer to the time points taken after induction. 50 cells were picked at random and assessed for the presence of intracellular vesicles. In the case where such vesicles were found, the number of vesicles inside each cell was counted.

Cell	CTRL+ T0	CTRL+ T1	CTRL+ T2	CTRL+ T4	CTRL+ T6	CTRL+ T8
1	0	2	0	1	0	0
2	0	1	3	0	0	0
3	0	0	0	0	0	0
4	2	1	1	0	0	0
5	0	0	2	0	0	0
6	0	1	0	1	0	0
7	0	0	0	2	1	3
8	0	0	0	0	0	0
9	0	0	1	2	2	0
10	0	1	0	0	1	2
11	2	5	0	0	1	0
12	0	0	0	0	1	0
13	1	0	0	1	0	2
14	0	2	2	1	0	3
15	0	1	3	0	0	0
16	2	3	0	1	0	0
17	0	5	0	1	0	0
18	0	5	0	1	1	5
19	0	1	1	0	0	0
20	0	0	2	0	0	0
21	0	2	0	0	0	0
22	0	2	0	1	0	0
23	0	0	1	0	1	0
24	0	2	0	0	0	0
25	1	1	1	0	0	0
26	0	0	2	0	2	0
27	1	0	0	0	1	0
28	0	3	0	0	0	0
29	0	2	3	0	0	0
30	0	0	0	0	0	0
31	0	2	0	0	2	0
32	0	3	0	0	0	0
33	0	0	0	0	0	0
34	0	4	4	3	0	0
35	0	1	1	0	0	0
36	0	0	0	0	0	1
37	0	1	0	2	1	2
38	0	2	1	0	0	1
39	1	0	0	0	0	1
40	0	0	1	1	0	0
41	0	2	2	0	0	0
42	0	0	0	0	0	0
43	0	0	2	1	0	0
44	0	0	3	0	0	0
45	0	1	2	1	0	0
46	1	4	3	1	0	0
47	1	3	0	1	0	1

48	0	0	0	0	0	0
49	0	2	0	0	3	0
50	3	0	5	0	0	0

Supplementary Table 2. Vesicle counts performed on *E. coli* cells expressing an empty pET3a vector control 2.

Vesicle counts performed on *E. coli* BL21 (DE3) Star cells expressing an empty vector control 2 over a time course of 8 hours. T0 represents the cells just prior to induction, while T1, T2, T4, T6 and T8 refer to the time points taken after induction. 50 cells were picked at random and assessed for the presence of intracellular vesicles. In the case where such vesicles were found, the number of vesicles inside each cell was counted.

Cell	PaLemA1 T0	PaLemA1 T1	PaLemA1 T2	PaLemA1 T4	PaLemA1 T6	PaLemA1 T8
1	0	1	5	0	45	0
2	1	30	3	22	17	5
3	0	0	16	2	18	9
4	0	7	11	25	0	0
5	0	32	20	2	1	7
6	1	56	1	0	13	0
7	11	0	2	5	36	0
8	2	25	45	11	25	9
9	0	32	12	1	4	21
10	6	15	34	2	3	21
11	1	5	15	34	0	10
12	10	9	14	31	4	20
13	12	0	9	69	34	18
14	0	1	46	25	17	0
15	31	0	4	10	30	0
16	1	11	0	41	17	2
17	0	58	6	11	5	7
18	0	3	7	22	1	5
19	0	8	19	8	6	30
20	12	29	2	14	24	0
21	1	18	4	0	3	3
22	0	0	9	0	0	0
23	1	0	29	39	0	17
24	0	43	57	9	2	24
25	0	3	18	1	22	13
26	0	20	44	13	13	14
27	0	36	0	1	34	0
28	8	41	16	4	8	0
29	7	12	5	0	0	0
30	0	31	12	4	0	0
31	1	0	33	5	9	0
32	2	5	25	6	8	1
33	0	19	43	55	37	2
34	3	6	35	7	0	1
35	2	12	23	23	0	6
36	0	5	19	22	6	10
37	0	17	14	46	39	11
38	0	1	0	84	38	0
39	6	3	0	33	22	1
40	0	16	3	19	0	0
41	3	18	62	36	60	41
42	0	9	60	11	13	17
43	1	18	0	28	23	10
44	0	0	0	26	14	24
45	4	7	0	22	59	3
46	0	10	13	0	31	21
47	13	2	1	12	14	0

48	0	26	34	0	40	21
49	0	1	5	11	2	3
50	12	0	9	11	2	31

Supplementary Table 3. Vesicle counts performed on *E. coli* cells expressing PaLemA1.

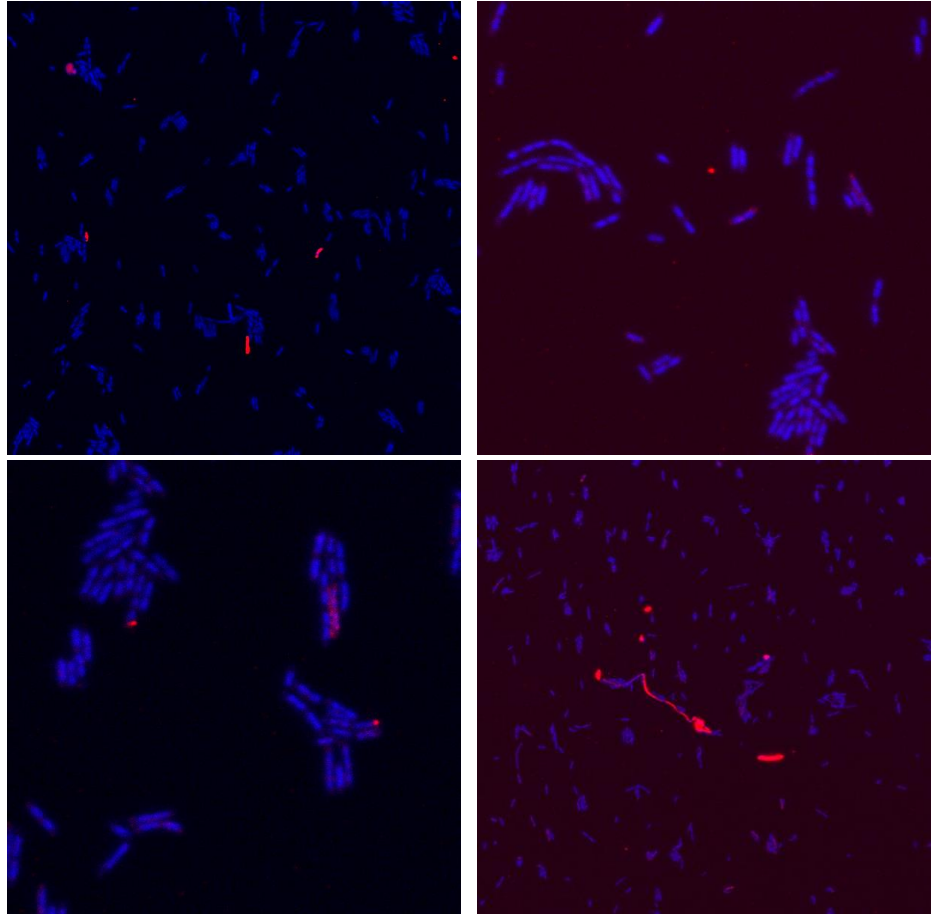
Vesicle counts performed on *E. coli* BL21 (DE3) Star cells expressing PaLemA1 over a time course of 8 hours. T0 represents the cells just prior to induction, while T1, T2, T4, T6 and T8 refer to the time points taken after induction. 50 cells were picked at random and assessed for the presence of intracellular vesicles. In the case where such vesicles were found, the number of vesicles inside each cell was counted.

Cell	PaLemA1 T0	PaLemA1 T1	PaLemA1 T2	PaLemA1 T4	PaLemA1 T6	PaLemA1 T8
1	0	25	45	23	52	25
2	0	9	19	3	10	6
3	4	2	1	27	23	1
4	8	14	74	55	15	14
5	0	44	22	20	10	56
6	1	4	1	27	28	40
7	0	0	2	7	25	10
8	0	4	35	4	38	4
9	1	7	0	35	3	21
10	5	25	22	3	48	8
11	0	20	31	36	30	50
12	12	9	6	38	42	9
13	2	21	33	43	6	11
14	0	42	18	15	14	31
15	0	0	8	2	30	2
16	0	18	17	7	22	39
17	0	22	1	13	28	19
18	0	0	21	0	36	4
19	27	22	21	38	45	20
20	0	0	5	4	2	15
21	0	12	27	7	21	18
22	0	49	24	50	27	16
23	4	38	30	19	4	7
24	1	8	8	16	3	42
25	0	21	0	41	19	16
26	2	27	3	5	52	28
27	0	32	48	11	28	21
28	0	0	42	0	4	4
29	0	11	20	41	32	56
30	0	0	17	32	47	26
31	0	24	17	34	9	0
32	3	9	34	8	15	16
33	1	19	1	35	15	11
34	1	2	1	17	41	42
35	1	18	0	3	15	16
36	11	22	18	13	0	2
37	3	49	39	10	4	9
38	1	25	28	25	2	23
39	1	0	38	14	19	15
40	3	6	25	76	18	11
41	4	0	2	35	34	25
42	0	34	33	5	16	28
43	6	0	22	57	20	14
44	0	51	10	2	3	27
45	0	80	2	51	4	15
46	0	5	0	34	0	78
47	2	1	51	31	5	3

48	0	8	8	7	30	28
49	3	24	8	23	8	1
50	1	29	35	19	20	23

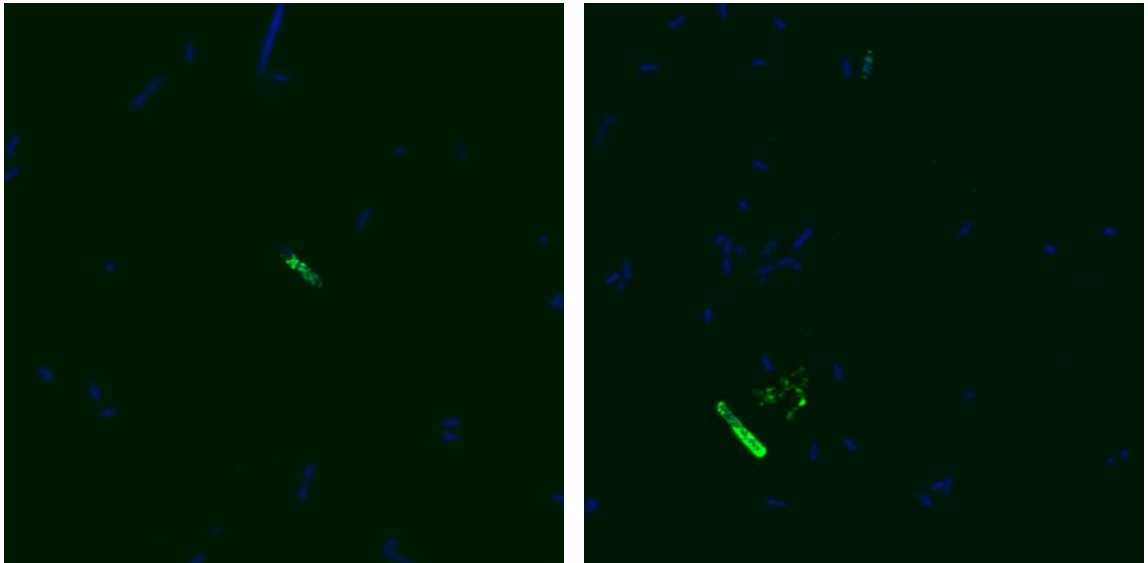
Supplementary Table 4. Vesicle counts performed on *E. coli* cells expressing PaLemA1.

Vesicle counts performed on *E. coli* BL21 (DE3) Star cells expressing PaLemA1 over a time course of 8 hours. T0 represents the cells just prior to induction, while T1, T2, T4, T6 and T8 refer to the time points taken after induction. 50 cells were picked at random and assessed for the presence of intracellular vesicles. In the case where such vesicles were found, the number of vesicles inside each cell was counted.



Supplementary Figure 4. Immunofluorescence staining of *E. coli* cells producing PaLemA1.

Confocal microscopy images of *E. coli* cells producing the PaLemA1 protein following overnight induction. The cells were prepared as mentioned in section 2.9.2. The cells were stained with a primary anti-PaLemA1 and a secondary goat anti-rabbit Alexa 568 antibody (red) + DAPI (blue). The images of cells show only a few cells displaying red fluorescence, which is likely attributed to low primary antibody penetration of the remaining cell population.



Supplementary Figure 5 Immunofluorescence staining of *E. coli* cells producing PaLemA2.

Confocal microscopy images of *E. coli* cells producing the PaLemA2 protein following overnight induction. The cells were prepared as mentioned in section 2.9.2. The cells were stained with a primary anti-PaLemA2 and a secondary goat anti-rabbit Alexa 488 antibody (green) + DAPI (blue). The images of cells show only a few cells displaying green fluorescence, which is likely attributed to low primary antibody penetration of the remaining cell population.